

Distribution Agreement

In presenting this thesis or dissertation as a partial fulfillment of the requirements for an advanced degree from Emory University, I hereby grant to Emory University and its agents the non-exclusive license to archive, make accessible, and display my thesis or dissertation in whole or in part in all forms of media, now or hereafter known, including display on the world wide web. I understand that I may select some access restrictions as part of the online submission of this thesis or dissertation. I retain all ownership rights to the copyright of the thesis or dissertation. I also retain the right to use in future works (such as articles or books) all or part of this thesis or dissertation.

Brandon A. Berryhill

Date

Approval Page

Academic and Applied Considerations of the Population and Evolutionary Dynamics of Bacteria, Antibiotics, and Bacteriophage

By

Brandon A. Berryhill
Doctor of Philosophy

Graduate Division of Biological and Biomedical Sciences
Microbiology and Molecular Genetics

Bruce R. Levin

Advisor

Colleen S. Kraft

Committee Member

Nic M. Vega

Committee Member

Timothy D. Read

Committee Member

Michael H. Woodworth

Committee Member

Accepted:

Kimberly Jacob Arriola, Ph.D, MPH

Dean of the James T. Laney School of Graduate Studies Date

Date

Abstract Cover Page

Academic and Applied Considerations of the Population and Evolutionary Dynamics of Bacteria, Antibiotics, and Bacteriophage

By

**Brandon A. Berryhill
B.S., Emory University, 2020**

Advisor: Bruce R. Levin, Ph.D.

An abstract of
A dissertation submitted to the Faculty of the
James T. Laney School of Graduate Studies of Emory University
in partial fulfillment of the requirements of
Doctor of Philosophy
in Microbiology and Molecular Genetics

2025

Abstract

Academic and Applied Considerations of the Population and Evolutionary Dynamics of Bacteria, Antibiotics, and Bacteriophage

By Brandon A. Berryhill

In 1920, infectious diseases accounted for one in three deaths worldwide. Thanks to advances in treating bacterial infection, particularly the development of antibiotics, this number has declined to one in four globally and one in seven in the Western world. However, the rise of antibiotic resistance threatens to reverse these gains. Given the increase in infections with antibiotic-resistant pathogens, there is a growing need to develop a more comprehensive understanding of antibiotic chemotherapy and other methodologies for preventing and treating diseases. Addressing this challenge requires a deeper understanding of (i) the population and evolutionary dynamics of bacteria under antibiotic treatment and the contribution of the innate immune system, (ii) the potential of alternative therapies such as bacteriophages, (iii) the combined effects of bacteriophages and antibiotics in optimizing treatment outcomes, and (iv) nonpharmacologic strategies to limit pathogen spread. Tremendous progress has been made in these subjects, however the knowledge generated by these findings is primarily molecular and mechanistic. There remains a knowledge gap in these topics, which must be addressed through population and evolutionary dynamic studies.

My dissertation explores these four critical areas using theoretical and experimental approaches with key bacterial pathogens, particularly *Escherichia coli* and *Staphylococcus aureus*, in investigating the population and evolutionary dynamics of antibiotics, bacteriophages, and bacteria. Through a series of studies, my investigations advance our understanding of bacterial infection treatments and the interplay between antimicrobial treatment regimens. Yet, as with all scientific inquiry, each finding raises new questions.

Dissertation Cover Page

**Academic and Applied Considerations of the
Population and Evolutionary Dynamics of
Bacteria, Antibiotics, and Bacteriophage**

By

**Brandon A. Berryhill
B.S., Emory University, 2020**

Advisor: Bruce R. Levin, Ph.D.

A dissertation submitted to the Faculty of the
James T. Laney School of Graduate Studies of Emory University
in partial fulfillment of the requirements of
Doctor of Philosophy
in Microbiology and Molecular Genetics
2025

Acknowledgements

It is said that we are the sum of our experiences, and nowhere is that more evident than in the completion of a Ph.D. This work would not have been possible without my co-authors, to whom I am deeply indebted. I could not have conducted the research without the unwavering support of the administration in the Biology Department at Emory University, especially: Chairman Steve L'Hernault, Tonya Woolcock, Barbara Shannon, Paja Sijacic, Lynn Kenney, Jan Hawes, Sonia Hayden, James Allen, Ann Englert, and Malia Escobar.

I am also incredibly thankful to the wonderful denizens of the O. Wayne Rollins Research Center, including: Ms. Judy, Rob, Abdi Abdi, Jason Chen, LM Bradley, Jacoby Robinson, and Jonathan Owen. During my time with the EcLF (*E. coli* Liberation Front), I had the privilege of working with over 15 amazing undergraduates, each of whom helped shaped me as a mentor. As my own mentor, Bruce Levin, once said, "I hope I didn't mess them up too much!"

To my dear colleagues in the lab—Ingrid McCall, Eduardo Rodríguez-Román, Mohammad Savari, Teresa Gil-Gil, and Alysha Ismail—thank you for your support, collaboration, and friendship. To my committee, I'm grateful for your guidance and encouragement throughout this journey.

A special thank you to my teaching mentor, Arri Eisen. You have fundamentally transformed my teaching approach and multiplied my potential to impact future generations of students. And to my professor and mentor, Bruce, words cannot express my gratitude. I could only hope to be half the scientist and mentor to my future students that you were to me.

I owe much to those who helped shape me before college: my parents, Barry and Felecia Berryhill; my teachers: Mrs. Leah McRae, Mr. Lucas Powell, Mr. Clint Merritt, and Mrs. Amy Patel; my lifelong friends: Allen Barrett, Blake Wojcik, Chris Kegley, Eric Bean, Ethan Rakoff, Gage Bates, Michael Foley, Peter West, Sam Wright, Tommy Cox, Zach Gibby, and Andrew Smith; and, all the friends and colleagues who I have not listed here. To each one of you, I owe more thanks than I could possibly provide in this one page.

Lastly, I dedicate this work to the memory of my late colleagues, Howie Weiss and Tom O'Rourke, whose contributions in science continue to live on.

Table of Contents

Chapter 1. Introduction	1
Chapter 2. What's the Matter with MICs: Bacterial Nutrition, Limiting Resources, and Antibiotic Pharmacodynamics	9
Supporting Information	37
Chapter 3. Theoretical Considerations and Empirical Predictions of the Pharmaco- and Population Dynamics of Heteroresistance	48
Supporting Information	73
Chapter 4. The evolution of heteroresistance via small colony variants in <i>Escherichia coli</i> following long term exposure to bacteriostatic antibiotics	89
Supporting Information	115
Chapter 5. Antibiotic killing of drug-induced bacteriostatic cells	131
Chapter 6. The Future of Phage Therapy in the United States	143
Chapter 7. The book of Lambda doesn't tell us that naturally occurring lysogens of <i>Escherichia coli</i> are likely to be resistant and not only immune to phage coded by their prophage	170
Supporting Information	192
Chapter 8. Enteric Populations of <i>Escherichia coli</i> are Likely to be Resistant to Phages Due to O Antigen Expression	207
Supporting Information	235
Chapter 9. The ecological consequences and evolution of retron-mediated suicide as a way to protect <i>Escherichia coli</i> from being killed by phage	248
Supporting Information	270
Chapter 10. Evaluating the potential efficacy and limitations of a phage for joint antibiotic and phage therapy of <i>Staphylococcus aureus</i> infections	276
Supporting Information	302
Chapter 11. The role of innate immunity, antibiotics, and bacteriophages in the course of bacterial infections and their treatment	325
Supporting Information	351
Chapter 12. Summary and Conclusions	362

Table of Contents Continued

Appendix 1. Using Lambda phages as a proxy for pathogen transmission in hospitals ...	369
Supporting Information	392
Appendix 2. A Bacteriophage-based Validation of a Personal Protective Equipment	
Doffing Procedure to be Used with High Consequence Pathogens	394
Supporting Information	424

Chapter 1

Chapter 1

Introduction

Infectious diseases have long shaped the trajectory of human history. Pandemics have been responsible for the sizeable declines in population, large changes in societal structures, and the development of public health and medical practices (1-3). From the Bubonic Plague to global Cholera outbreaks, the impact of bacterial infectious disease is immeasurable, extending beyond the number of infections or deaths (4, 5).

At the start of the 20th century, infectious diseases accounted for over half of the top ten leading causes of death globally (6). In 1920, nearly one in three deaths worldwide could be attributed to infectious diseases (7). Infections such as tuberculosis, bacterial pneumonia, diphtheria, typhoid fever, and diarrheal diseases were rampant and commonly fatal. The burden of infectious disease mortality and the numerous economic and social sequelae motivated research into microbial pathogens and their treatment.

In the century since, we have witnessed drastic advancements in bacteriology, public health, and medical treatment which, collectively, contributed to a dramatic decline in infectious disease mortality. By the early 21st century, the global mortality rate from infectious diseases had decreased significantly, falling to one in four deaths worldwide and one in seven in Western countries (8). These gains can be attributed to the development of vaccines, improvements in public health, and the employment of effective treatments for common infections.

The reduction in mortality from bacterial infectious diseases is primarily due to the discovery of antibiotics and their subsequent development and widespread use. Since the development of the penicillins and sulfonamides in the early 20th century, the treatment of bacterial infections has fundamentally changed (9). Due to antibiotics, expensive and bespoke treatments such as serum or bacteriophage (phage) therapy were no longer required to have a chance of not succumbing to an infection (the quality and effectiveness of these therapies as employed at the time is questionable) (10, 11). With antibiotics, common infections like syphilis or streptococcal infections were no longer a death sentence (12, 13). The medical and societal impacts of these chemotherapeutics was profound as evidenced by a drastic increase in average lifespan and a shift in the top causes of morbidity and

mortality from infectious diseases to more chronic conditions such as heart disease (14). One could argue that the development of antibiotics was foundational to the development of modern society.

Early efforts to treat bacterial infections were based on non-rigorous, empirical observation. If the application of a therapeutic led to a change in an infection-associated metric such as fever, then the treatment was considered effective (15). One early treatment method which was employed to limited success was phage therapy. Emerging in the 1920s, following the discovery of bacteriophages, the viruses which infect and kill bacteria, by Twort and d'Hérelle the decade prior (16). Though initially promising, phage therapy faced many limitations including the lack of understanding of what phage were and how they functioned. These limitations led to inconsistent results, which were compounded by a failure to publish negative results and a lack of understanding of the published positive results, leading to phage therapy to ultimately fall out of favor around the time of the commercialization of penicillin.

Penicillin, discovered by Alexander Fleming in 1928 but not introduced for widespread use until after refinement by Florey and colleagues in 1941, demonstrated the utility of agents which can kill a broad array of bacteria for the empiric treatment of infectious diseases (17). The success of penicillin ushered in the “Golden Age of Antibiotics” which saw the discovery of over 20 new classes of antibiotics and over one-half of the drugs commonly used today (18). These developments brought about a shift in the treatment of bacterial infections: no longer did we have to identify and culture a causative pathogen to successfully treat an infected individual. This has led to the use of antibiotics in inappropriate cases and the overuse of these drugs.

Parallel with these breakthroughs in chemotherapeutics came an increase in research on the bacterial pathogens themselves. Advances in microbiology revealed the mechanisms by which bacteria interact with hosts, evade immune responses, and cause disease. This research led to the identification of virulence factors, quorum sensing, antibiotic resistance genes, and immune-evasion mechanisms (19). These basic-science advances have facilitated the design of more effective treatments.

Concurrently, non-pharmacologic strategies emerged as tools to mitigate bacterial infections. The application of public health advances such as hand hygiene, sanitation, and infection control protocols in hospitals helped to limit the spread of infectious diseases (20). The development of vaccines against bacteria such as diphtheria,

Haemophilus influenzae, and pneumococcus have underscored the importance of preventative measures alongside therapeutic interventions (21). Together, these strategies have helped abate the looming specter of bacterial infectious diseases.

However, this progress in treating infectious diseases is under increasing threat. Despite the success of antimicrobial chemotherapy, bacterial pathogens continue to evolve. Unlike the previously mentioned bespoke therapies, like serum and phage therapy, antibiotic therapy is fixed. These chemical agents do not evolve and change over time. The emergence and subsequent increase in the frequency of antibiotic-resistant bacteria has become a critical challenge to the health and wellbeing of humans (14). As the effectiveness of our most commonly used antibiotics diminishes, we risk returning to the reality of before the 20th century where a simple streptococcus infection in the throat or a common sexually transmitted disease can mean death. Once easily treatable conditions now have higher rates of treatment failure, prolonged illness, and increased mortality. Infections caused by resistant organisms, such as methicillin-resistant *S. aureus* and carbapenem-resistant *Enterobacteriaceae*, underline the growing difficulties clinicians face in managing what should be routine cases (22). The incredible speed at which resistance can develop and spread is cause for concern. It would be less than one year after the commercialization of penicillin that strains of *Staphylococcus aureus* resistant to this drug were detected first in hospitals and then in the community. By the late 1960s, 80% of both community and hospital acquired *S. aureus* were resistant to penicillin (23). To overcome this problem, an antibiotic which cannot be degraded by the same enzymes as penicillin was developed: methicillin. Within one year MRSA was found in hospitals and by the 1980s MRSA could be found in communities across the world (23). This growing crisis begets further research into the treatment of bacterial infections, the mechanisms of antibiotic resistance, and potential complementary approaches to treat antibiotic-resistant pathogens.

Multidrug-resistant organisms have become increasingly common in both community and healthcare settings, complicating treatment protocols and leading to longer hospital stays, increased mortality, and a greater economic burden (24). The efficacy of antibiotics is not inexhaustible. The widespread, repeated, and indiscriminate use of these agents has mediated the evolution of resistance and increase in frequency of antibiotic-resistant bacteria, rendering antibiotics less effective and in some cases entirely obsolete.

As the frequency of infections with multidrug-resistant bacteria continues to rise globally, the imperative to reevaluate therapeutic regimens becomes more pressing. Efforts to mitigate resistance must extend beyond the discovery of new antibiotics—a venture which is proving more and more difficult—and include a complete redesign of the regimens used to treat bacterial infections (25). Drug choice, dosing strategies, and the use of complementary treatments such as phage all play a role in shaping resistance dynamics and require further understanding to optimize treatment (26-28).

This dissertation is founded on the recognition that addressing antibiotic resistance requires not only molecular and mechanistic insights but also a broader investigation into the population and evolutionary dynamics of bacteria under treatment. The complexity of bacterial responses to antibiotics and the interactions with the host's immune response, environmental conditions, and complementary therapies such as phage demands investigation at the population level. The integration of ecological and evolutionary perspectives into antimicrobial research is paramount and enables the development of more sustainable treatments.

To that end, this dissertation investigates four areas at the intersection of microbiology, evolutionary biology, ecology, and clinical science. First, I explore how sub-inhibitory concentrations of antibiotics influence the population dynamics of bacteria and how environmental factors, such as nutrient availability, modulate the pharmacodynamics of treatment. Second, I examine antibiotic heteroresistance from a purely theoretical perspective, modeling both progressive and direct generation of resistant subpopulations and their implications for treatment responses. Third, I investigate the evolutionary consequences of long-term exposure to bacteriostatic antibiotics and find, unexpectedly, that heteroresistance evolves. Fourth, I identify the specific conditions under which synergistic effects may arise from the joint use of bacteriostatic and bactericidal antibiotics.

Following these considerations of antibiotic-based therapy, the dissertation transitions to an analysis of phage ecology and evolution and phage therapy. This section begins with a historical overview of phage therapy and a critical assessment of its current state, including the scientific, clinical, and regulatory changes needed to enhance its applicability. Second, I explore a central ecological question regarding the evolutionary advantage of phage being virulent (purely lytic) rather than temperate, finding that prophage-carrying bacteria are often

resistant/refractory rather than immune to infection by the cognate phages. Third, I examine the potential role of fecal microbiota transplantation (FMT) as an inadvertent form of phage therapy, with the surprising finding that Gram-negative bacteria in the gut microbiome display broad resistance to phages due to expression of the O-antigen. Fourth, I investigate a bacterial defense mechanism in which infected cells self-destruct to prevent phage proliferation with a focus on the population and evolutionary implications of such a system. Fifth, I explore a seemingly ideal phage for treating *Staphylococcus* infections and evaluate its interactions with antibiotic agents. Finally, I characterize and demonstrate the suitability of *Galleria mellonella* as an *in vivo* model system for quantitatively studying the combined effects of antibiotics, phages, and the innate immune system on infection dynamics. In the appendix, I give consideration to the use of phages as proxies for infectious agents in developing nonpharmacologic prevention strategies.

As this dissertation will demonstrate, the fight against bacterial infections is no longer solely a matter of drug discovery, but of understanding the broader ecological and evolutionary dynamics that govern treatment outcomes. Addressing the challenges posed by antimicrobial resistance requires many approaches: experimental biology, mathematical modeling, and tool development. Together, these studies contribute to a more complete understanding of the treatment of bacterial infections.

References

1. S. Sampath *et al.*, Pandemics Throughout the History. *Cureus* **13**, e18136 (2021).
2. R. Jedwab, A. M. Khan, J. Russ, E. D. Zaveri, Epidemics, pandemics, and social conflict: Lessons from the past and possible scenarios for COVID-19. *World Dev* **147**, 105629 (2021).
3. A. Casadevall, Pandemics past, present, and future: progress and persistent risks. *J Clin Invest* **134** (2024).
4. G. Alfani, B. Marco, M. and Fochesato, Pandemics and socio-economic status. Evidence from the plague of 1630 in northern Italy. *Population Studies* **78**, 21-42 (2024).
5. W. B. Greenough, 3rd, The human, societal, and scientific legacy of cholera. *J Clin Invest* **113**, 334-339 (2004).
6. Anonymous, Control of infectious diseases. *MMWR Morb Mortal Wkly Rep* **48**, 621-629 (1999).
7. Anonymous, The World Health report 1996--fighting disease, fostering development. *World Health Forum* **18**, 1-8 (1997).
8. C. M. Michaud, Global Burden of Infectious Diseases. *Encyclopedia of Microbiology* 10.1016/b978-012373944-5.00185-1, 444-454 (2009).
9. M. I. Hutchings, A. W. Truman, B. Wilkinson, Antibiotics: past, present and future. *Current Opinion in Microbiology* **51**, 72-80 (2019).
10. A. Glatman-Freedman, A. Casadevall, Serum therapy for tuberculosis revisited: reappraisal of the role of antibody-mediated immunity against Mycobacterium tuberculosis. *Clin Microbiol Rev* **11**, 514-532 (1998).
11. P. T. Fowoyo, Phage Therapy: Clinical Applications, Efficacy, and Implementation Hurdles. *The Open Microbiology Journal* **18** (2024).
12. L. Ekselius, B. Gerdin, A. Vahlquist, The Syphilis Pandemic Prior to Penicillin: Origin, Health Issues, Cultural Representation and Ethical Challenges. *Acta Derm Venereol* **104**, adv34879 (2024).

13. Anonymous, in *Streptococcus pyogenes: Basic Biology to Clinical Manifestations*, J. J. Ferretti, D. L. Stevens, V. A. Fischetti, Eds. (University of Oklahoma Health Sciences Center. © The University of Oklahoma Health Sciences Center., Oklahoma City (OK), 2016).
14. C. L. Ventola, The antibiotic resistance crisis: part 1: causes and threats. *P t* **40**, 277-283 (2015).
15. W. C. Summers, The strange history of phage therapy. *Bacteriophage* **2**, 130-133 (2012).
16. V. H. Aswani, S. K. Shukla, An Early History of Phage Therapy in the United States: Is it Time to Reconsider? *Clin Med Res* **19**, 82-89 (2021).
17. R. Gaynes, The Discovery of Penicillin—New Insights After More Than 75 Years of Clinical Use. *Emerg Infect Dis* **23**, 849-853 (2017).
18. R. I. Aminov, A brief history of the antibiotic era: lessons learned and challenges for the future. *Front Microbiol* **1**, 134 (2010).
19. B. Alberts *et al.*, *Molecular Biology of the Cell 4th Edition: International Student Edition* (Routledge, 2002).
20. H. Institute of Medicine Committee for the Study of the Future of Public, in *The Future of Public Health*. (National Academies Press (US). Copyright© 1988 by the National Academy of Sciences., Washington (DC), 1988), 10.17226/1091.
21. A. Osterloh, Vaccination against Bacterial Infections: Challenges, Progress, and New Approaches with a Focus on Intracellular Bacteria. *Vaccines (Basel)* **10** (2022).
22. S. DonkorEric, S. CodjoeFrancis.
23. F. D. Lowy, Antimicrobial resistance: the example of *Staphylococcus aureus*. *J Clin Invest* **111**, 1265-1273 (2003).
24. J. Davies, D. Davies, Origins and evolution of antibiotic resistance. *Microbiol Mol Biol Rev* **74**, 417-433 (2010).
25. L. L. Silver, Challenges of antibacterial discovery. *Clin Microbiol Rev* **24**, 71-109 (2011).
26. S. K. Olofsson, O. Cars, Optimizing Drug Exposure to Minimize Selection of Antibiotic Resistance. *Clinical Infectious Diseases* **45**, S129-S136 (2007).

27. B. R. Levin, M. J. Bonten, Cycling antibiotics may not be good for your health. *Proc Natl Acad Sci U S A* **101**, 13101-13102 (2004).
28. X. Li *et al.*, A combination therapy of Phages and Antibiotics: Two is better than one. *Int J Biol Sci* **17**, 3573-3582 (2021).

Chapter 2

Chapter 2

What's the Matter with MICs: Bacterial Nutrition, Limiting Resources, and Antibiotic Pharmacodynamics

Reprinted from: Berryhill BA, Gil-Gil T, Manuel JA, Smith AP, Margollis E, Baquero F, Levin BR. 2023.

What's the Matter with MICs: Bacterial Nutrition, Limiting Resources, and Antibiotic Pharmacodynamics.

Microbiology Spectrum. <https://doi.org/10.1128/spectrum.04091-22>

Abstract

The MIC of an antibiotic required to prevent replication is used both as a measure of the susceptibility/resistance of bacteria to that drug and as the single pharmacodynamic parameter for the rational design of antibiotic treatment regimes. MICs are experimentally estimated *in vitro* under conditions optimal for the action of the antibiotic. However, bacteria rarely grow in these optimal conditions. Using a mathematical model of the pharmacodynamics of antibiotics, we make predictions about the nutrient dependency of bacterial growth in the presence of antibiotics. We test these predictions with experiments in broth and a glucose-limited minimal media with *Escherichia coli* and eight different antibiotics. Our experiments question the sufficiency of using MICs and simple pharmacodynamic functions as measures of the pharmacodynamics of antibiotics under the nutritional conditions of infected tissues. To an extent that varies among drugs: (i) the estimated MICs obtained in rich media are greater than those estimated in minimal media; (ii) exposure to these drugs increases the time before logarithmic growth starts, their lag; and (iii) the stationary-phase density of *E. coli* populations declines with greater sub-MIC antibiotic concentrations. We postulate a mechanism to account for the relationship between sub-MICs of antibiotics and these growth parameters. This study is limited to a single bacterial strain and two types of culture media with different nutritive content. These limitations aside, the results of our study clearly question the use of MIC as the unique pharmacodynamic parameter to develop therapeutically oriented protocols.

Introduction

Fundamental to the rational, as opposed to purely empirical design of antibiotic treatment regimens are the bacterial-dependent pharmacodynamics, PD [1-3], and host-dependent pharmacokinetics, PK [1, 2, 4], and their relationship known as PK/PD indices. The PKs of antibiotics are measured from the changes in concentrations of the drug in the serum of treated hosts, often utilizing uninfected volunteers [5, 6]. Although different measures of PK of the antibiotic are employed for PK/PD indices [7], most commonly a single measure of the PD of the antibiotic and its target bacteria are employed. This measure is the minimum concentration of the antibiotic necessary to prevent the replication of the bacteria, the Minimum Inhibitory Concentration [8].

MICs are measured *in vitro*, most commonly by two-times serial dilution of the antibiotic [9, 10]. In this method, bacteria are inoculated into a rich media at a density of 5×10^5 cells per mL and the antibiotic is added at a high concentration to a single culture. The cultures are serially diluted by a factor of two and incubated for a defined period of time. At this time, the optical densities of the antibiotic-exposed cultures are estimated by eye, looking for the well where turbidity drastically decreases [11]. The antibiotic concentration at which this sharp decrease in turbidity is seen is called the MIC. This method tends to have a lower throughput than what is needed for clinical laboratories, thus other standardized, machine-based protocols are used for estimating MICs. Though, these methods such as the VITEK [12, 13] are also based on optical density, and work by comparing the growth of a known isolate to an unknown isolate. Non-optical density-based methods do exist, such as E-Tests [14, 15].

It has been shown that the value of the MIC estimated for antibiotic and bacteria pairs are critically dependent on the density of bacteria exposed to the antibiotics when starting MIC estimation experiments [16]. In this investigation we use mathematical models to explore the relationship between the richness of the media and concentration of a limiting resource, on the pharmacodynamics of antibiotics and bacteria. Using *Escherichia coli* growing in a highly buffered glucose-limited minimal medium and Lysogeny Broth (LB) we explore the fit of these models to the pharmacodynamics of antibiotics of eight different classes.

The results of our study show how different factors affect the MIC estimation as determined by standard procedures and question the sufficiency and validity of this pivotal parameter to provide a quantitatively accurate picture of the pharmacodynamics of antibiotics and bacteria [17]. We demonstrate that: i) The PD of antibiotics are critically dependent on the media used, (ii) exposure to sub-MIC concentrations of antibiotics increases the time before bacteria start to grow, (iii) exposure to sub-MIC concentrations of antibiotics decreases the growth rate of these bacteria in proportion to the concentration of the drug, (iv) the stationary phase density to which the bacteria grow is inversely related to the concentration of antibiotics, (v) sub-MIC concentrations of antibiotics increase the nutrient requirements of the treated bacteria. We discuss the implications of these PD results to the design and evaluation of antibiotic treatment protocols.

Results

A generalized model of the pharmacodynamics of antibiotics and bacteria and its predictions

For our model of the pharmacodynamics of antibiotics and bacteria we combine Hill functions [16] with a resource-limited growth model [18]. In accord with this extended model, the hourly rate of growth of the bacteria is defined with respect to the concentration of the antibiotic (A $\mu\text{g}/\text{mL}$) and the limiting resource (r $\mu\text{g}/\text{mL}$) as shown in Equation 1.

$$\Pi(A, r) = v_{max} - \left[\frac{(v_{max} - v_{min}) \cdot \left(\frac{A}{MIC}\right)^K}{\left(\frac{A}{MIC}\right)^K - \left(\frac{v_{min}}{v_{max}}\right)} \right] \cdot \psi(r) \quad \text{Eq. 1}$$

The parameter v_{MAX} is the maximum rate of growth per cell per hour of the bacteria in the absence of the antibiotic, where $v_{MAX} > 0$. v_{MIN} is the minimum growth rate per cell per hour of the bacteria in the presence of the antibiotic, $v_{MIN} < 0$. MIC is the minimum inhibitory concentration in $\mu\text{g}/\text{mL}$ of the antibiotic. K is a shape parameter that determines the acuteness of the $\pi(A, r)$ function, the greater the value of K the more acute. $\psi(r)$, defined in Equation 2, expresses the relationship between the rate of growth of the bacteria and the concentration of the limiting resource, r . The parameter k in $\mu\text{g}/\text{mL}$ is the Monod constant which is the concentration of the resource when the growth rate in the absence of antibiotics is half of its maximum value, v_{MAX} .

$$\psi(r) = \frac{r}{(r+k)} \quad \text{Eq. 2}$$

To explore the relationship between antibiotic concentration, limiting resource concentration, and bacterial density, we present three coupled differential equations based on the Hill functions.

$$\frac{dN}{dt} = \Pi(A, r) \cdot N \quad \text{Eq. 3}$$

$$\frac{dr}{dt} = -e \cdot \Pi(A, r) \cdot N \quad \text{Eq. 4}$$

$$\frac{dA}{dt} = -da \cdot A \quad \text{Eq. 5}$$

$\Pi(A,r)$ is the Hill function designated rate of growth or death of the bacteria when the concentration of the antibiotic is A and the resource is r (Eq. 3). The conversion efficiency, e μg , is the amount of the limiting resource needed to produce a new cell (Eq. 4). The parameter d_a is the hourly rate of decline in the concentration of the antibiotic (Eq. 5).

In Figure 1A and 1B we illustrate the predicted relationship between the concentration of the antibiotic and the rates of growth and death of bacteria in an environment with an indefinite amount of resource, $\psi(r)=1.0$, for a bacteriostatic (Condition I), weakly bactericidal (Condition II), and strongly bactericidal (Condition III) antibiotic based on different Hill function parameters. Other than indicating the minimum concentration of the antibiotic that prevents growth, the MIC of an antibiotic provides no information about the dynamics, rate of growth, or rate of death of the bacteria. Antibiotics with the same MIC can be bacteriostatic (Figure 1A Condition I) or they can be bactericidal (Figure 1A Condition II and Condition III). Moreover, the rate of growth of bacteria exposed to sub-MIC concentrations of bacteriostatic antibiotics (Figure 1B Condition I) would be greater than bacteria exposed to highly bactericidal antibiotics (Figure 1B Condition III).

In Figure 2 we follow theoretical changes in the density of bacteria exposed to different concentrations of a strongly bactericidal antibiotic as predicted by our model (Equations 1-5). Under these conditions, the model predicts that the density achieved by the bacterial population is the same at all concentrations of the antibiotic below MIC. Stated another way, the theory predicts that the reduction in growth rate due to the presence of the antibiotic only increases the time before the population reaches stationary phase.

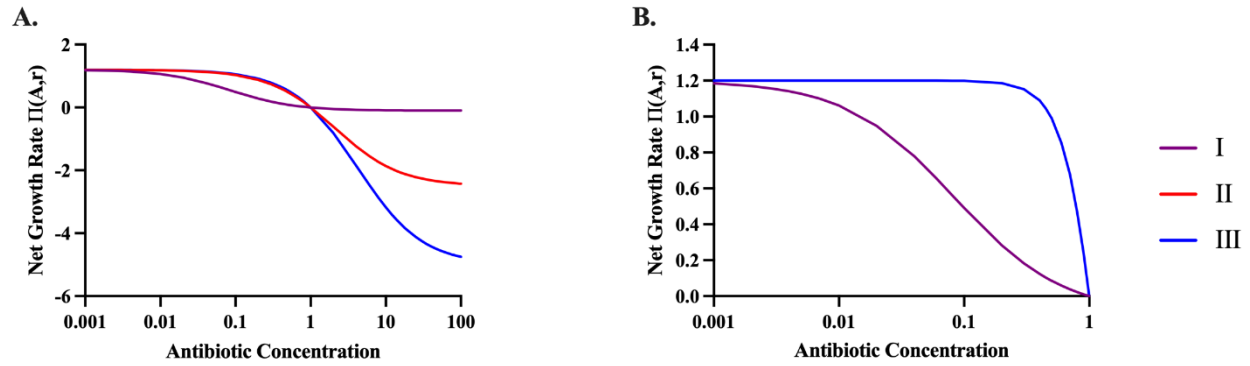


Figure 1. Predicted growth rates of antibiotic-exposed bacteria. To illustrate the properties of this model, we explore three different parameters sets I, II, and III. Condition I represents a bacteriostatic antibiotic ($v_{MIN} = -0.0001$). Condition II represents a weakly bactericidal antibiotic ($v_{MIN} = -2.5$). Condition III represents a strong bactericidal antibiotic ($v_{MIN} = -5.0$). Parameters used for these simulations are $e = 5 \times 10^{-7}$ $\mu\text{g}/\text{per cell}$, $v_{MAX} = 1.2$ per cell per hour, $K=1$, $k=1$, $\text{MIC}=1.0$. **(A)** and **(B)** The relationship between the concentration of an antibiotic and the rates of growth and death of bacteria $\pi(A, r)$ anticipated by the pharmacodynamic function for the described values of the Hill function parameters (Equation 1). In these figures the population is not limited by the resource $\psi(r)=1.0$. **(A)** All concentrations, **(B)** Sub-MIC concentrations of the antibiotic.

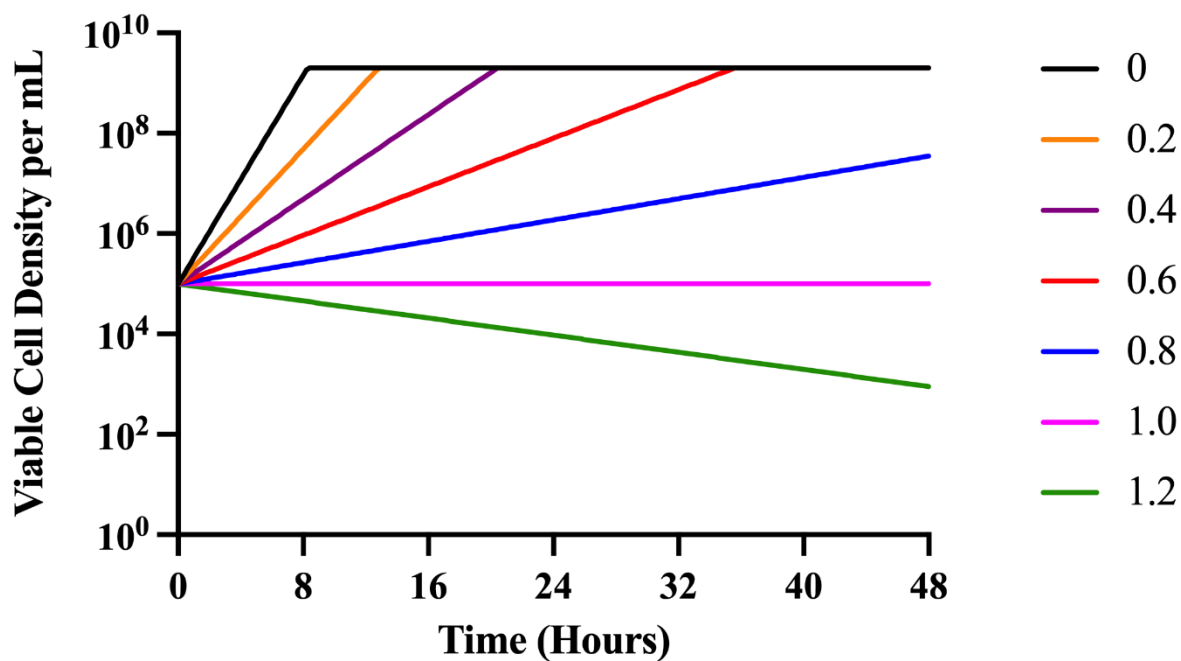


Figure 2. Predicted changes in density of antibiotic-exposed bacteria. To illustrate the properties of this model, we explore only the strong bactericidal antibiotic condition (Condition III). Condition III represents a strong bactericidal antibiotic with $v_{MIN} = -5.0$. Parameters used for these simulations are $e=5 \times 10^{-7}$ $\mu\text{g}/\text{per cell}$, $v_{MAX} = 1.2$ per cell per hour, $K=1$, $k=1$, $\text{MIC}=1.0$. Changes in the viable density of bacteria anticipated from the Hill function model for different concentrations of the antibiotic, respectively 0 to 1.2 times MIC. In these numerical solutions to equations 2-4, we assume the concentration of the limiting resource (r) is 1000 when the bacteria are first introduced to the antibiotic and the concentration of the antibiotic does not decay, $da=0$.

Experimental exploration of MIC as the primary PD parameter

Minimum Inhibitory Concentrations

We open our experimental exploration of the pharmacodynamics of antibiotics and bacteria with a consideration of the relationship between the experimentally estimated MICs of antibiotics with *E. coli* MG1655 growing in LB, Davis Minimal (minimal) medium with 1000 μ g/mL glucose, and Mueller-Hinton (MH) (Table 1).

Table 1. Experimentally estimated MICs of *E. coli* MG1655 for eight antibiotics in LB, glucose-limited minimal medium, and MH.

Antibiotic	LB MIC (μ g/mL)	Minimal MIC (μ g/mL)	MH MIC (μ g/mL)
AZM	25	6.25	6.25
CIP	0.03	0.03	0.03
TET	2.5	0.8	2.5
FOF	37.5	25	37.5
GEN	12	0.75	3
RIF	25	12.5	25
CHL	6.25	6.25	6.25
CRO	0.05	0.03	0.05

For ciprofloxacin (CIP), fosfomicin (FOS), chloramphenicol (CHL), rifampin (RIF), and ceftriaxone (CRO) the MICs in broth and minimal medium are equal or nearly so. For azithromycin (AZM), gentamicin (GEN), and tetracycline (TET) the MICs in broth are substantially greater than that in glucose-limited minimal medium. In the case of MH, all the MICs are the same as in LB with the exception of GEN and AZM which are notably higher in LB. In supplemental Table 1, we show the MICs with minimal medium with different carbon sources. Notably, the MICs of certain drugs such as azithromycin, fosfomicin, and ceftriaxone are lower in alternative carbon sources than they are in glucose. The values presented for the MICs of these drugs were chosen as the first concentration at which the optical density declined substantially approached that of the media. As shown in supplemental figure S1, sub-MIC concentrations in most antibiotics lead to a decrease in the optical density in proportion to the drug concentration, an effect we call MIC ooze, that is to say, there is not one clear MIC as the OD decreases stepwise across several wells, rather than precipitously.

Growth dynamics at sub-MIC concentrations of eight antibiotics in LB and minimal media.

In Figure 3 and Figure 4 we follow the changes in optical density of *E. coli* MG1655 exposed to different antibiotics in LB and minimal media, respectively. A detailed comparison of the parameters estimated from this analysis (maximum growth rate, length of the lag phase, and maximum optical density) are available in Supplemental figures Fig S2 and Fig S5, Fig S3 and Fig S6, and Fig S4 and Fig S7, respectively.

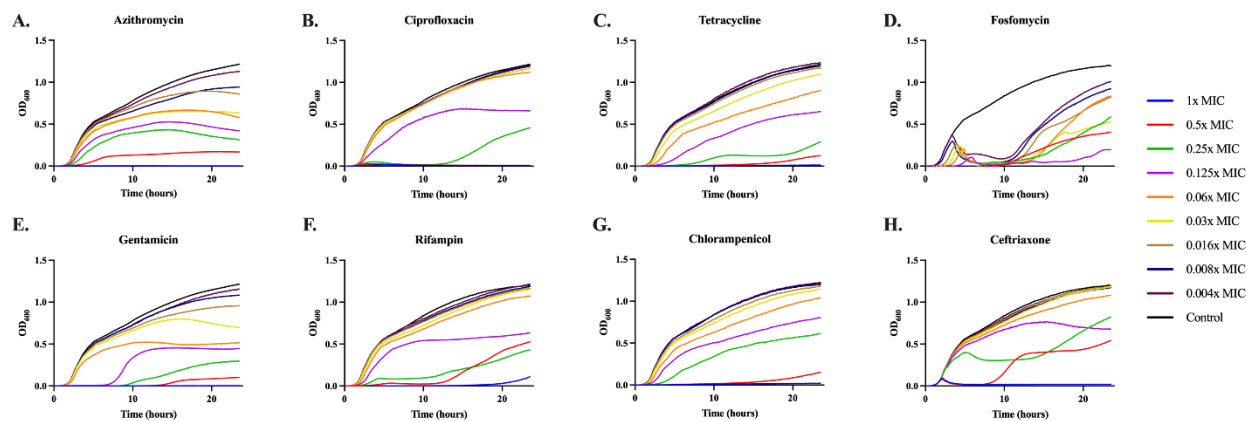


Figure 3. Growth dynamics in LB. Changes in optical density (600nm) of *E. coli* MG1655 exposed to different sub-MIC concentrations of eight antibiotics for 24 hours in LB. Lines are representative of the average of five technical replicas and normalized to the time zero optical density. Each concentration is shown as a fraction of the MIC for the noted drug (Table 1): 1x (blue), 0.5x (red), 0.25x (green), 0.125x (purple), 0.06x (orange), 0.03x (yellow), 0.016x (brown), 0.008x (dark blue), 0.004x (dark purple), and a no drug control (black).

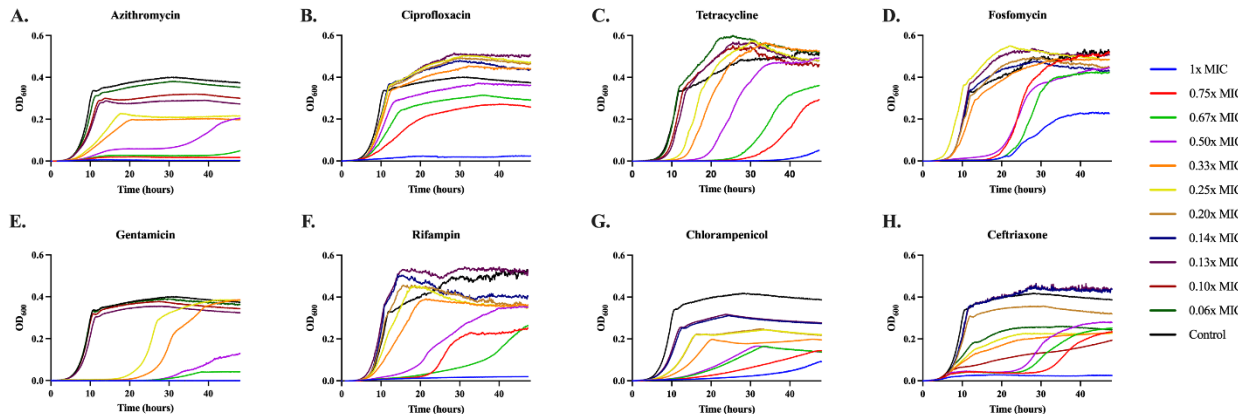


Figure 4. Growth dynamics in minimal medium. Changes in optical density (600nm) of *E. coli* MG1655 exposed to different sub-MIC concentrations of eight antibiotics for 48 hours in glucose-limited minimal medium. Lines are representative of the average of five technical replicas and normalized to the time zero optical density. Each concentration is shown as a fraction of the MIC for the noted drug (Table 1): 1x (blue), 0.75x (red), 0.67x (green), 0.50x (purple), 0.33x (orange), 0.25x (yellow), 0.20x (brown), 0.14x (dark blue), 0.13x (dark purple), 0.10x (dark red), 0.06x (dark green), and a no drug control (black).

The dynamics of change in optical densities of MG1655 vary among the drugs in both broth and minimal medium. For all eight antibiotics, these dynamic data indicate concentration-dependent variation in the time before the populations start to grow, the rate of growth, and the density achieved at 24 hours for LB and 48 hours for the minimal medium.

In Figure S2 and S5 we plot the relationship between the estimated maximum growth rates as a function of sub-MIC concentration of the antibiotics in LB (Fig S2) and minimal (Fig S5). With the exception of fosfomycin in both media, the max rate of growth increases with the declining concentration of antibiotic. The observation that higher concentrations of the antibiotics would be reducing the growth rate of the bacteria to an extent greater than at lower concentrations is anticipated and central to the use of the pharmacodynamic Hill functions.

In Figure S3 and S6, we plot the amount of time required before the optical density exceeds 0.020, the relative lag for different concentrations of the antibiotics in LB and minimal medium, respectively. In both media, there

is a concentration dependent increase in the lag time, with higher concentrations of the drug leading to longer lag times.

The optical density at 24 hours in LB and 48 hours in minimal DM are presented in Figure S4 and S7, respectively. In both media, for all of the antibiotics the maximum optical density increases with the decline in the concentration of the antibiotic. This decrease in the maximum optical density is associated with a decrease in the viable colony forming units (CFU) of these cultures (Figure S8).

Consistently across all three testing conditions, fosfomycin, gentamicin, and rifampin have high variability between replicates. This high variability can be explained by the emergence of resistance. For fosfomycin and rifampin resistances emerge independently across replicas as shown in Figure S9 and S10. For fosfomycin an increase in MIC of over 11-fold was seen between pre- and post- antibiotic exposed cultures, while for rifampin an increase of 35 times was seen. This rapid selection for fosfomycin resistance is well known as it has been shown that there is a large inoculum density effect when performing MICs with this drug [19]. When MG1655 was exposed to gentamicin, a large number of small colony variants were recovered. One possibility is that the exposure to the drug during LB double dilution rapidly selects for a resistant minority population. As a test of this, we performed an E-Test on MG1655 with gentamicin and found the MIC to be 24 times lower by E-Test as compared to double dilution, a result we believe to be consistent with heteroresistance. All three resistances are observed as a stable increase in MIC.

Consumption of a limited resource in sub-MIC treated cultures

The association between the concentration of the drug and the final optical density of each culture (Figures 3 and 4) is striking and inconsistent with the predictions of Figure 2. In accord with the model, we would expect drug concentration to simply increase the amount of time needed to reach stationary phase, but not to impact the level of stationary phase. This is clearly not the case. One possibility is that when exposed to the drugs, the bacteria become less efficient in the consumption of resource. The utilization of glucose limited minimal media allows for direct measurement of the glucose level (Figure 5) and in accord with the above hypothesis, we would expect there to be no excess glucose after 48 hours of bacterial growth. Our results are consistent with this

hypothesis. At super-MIC concentrations of the drugs, we see low to no consumption of the glucose, while at sub-MIC concentrations we see consumption of almost all the limiting resource. With the exception of ceftriaxone, which at super-MIC concentrations consumes a large amount of glucose.

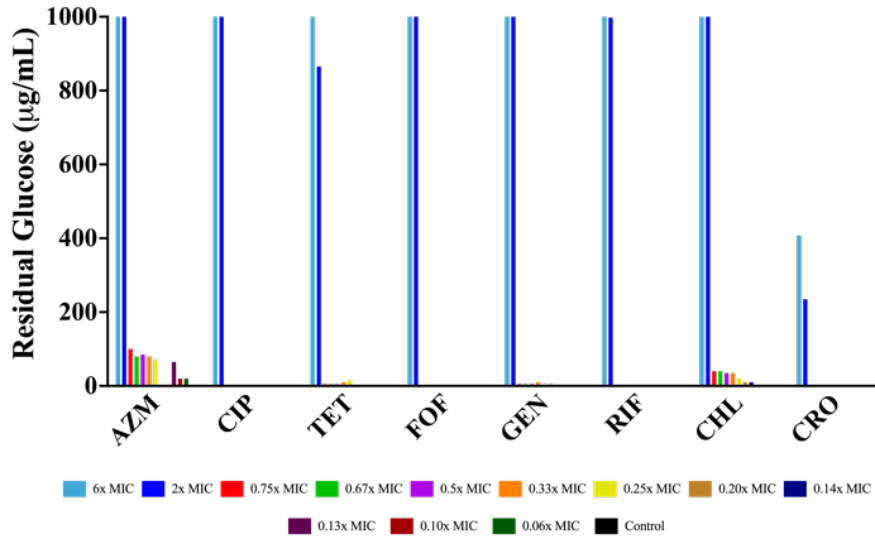


Figure 5. Final Glucose Concentrations. Amount of glucose ($\mu\text{g/mL}$) in each culture of *E. coli* MG1655 exposed to different super- and sub-MIC concentrations of eight antibiotics after 48 hours of incubation in glucose-limited minimal medium.

Antibiotic dependent resource consumption

In accord with Figure 2, the stationary phase densities of bacteria exposed to sub-MIC concentrations of antibiotics should be independent of the concentration of the drug. That is clearly not the case as the stationary phase density declines with the concentration of the antibiotic (Figures S4 and S7). One possible explanation is that in addition to reducing the rate of growth of the *E. coli*, the antibiotic increases the amount of resource necessary to produce a new cell [17]. As such, we have updated Equation 4 to make resource consumption dependent on the concentration of the antibiotic (Eq. 6). By modifying the resource uptake equation, we get:

$$\frac{dr}{dxt} = (-e + C \cdot A) \cdot \prod(A, r) \cdot N \quad \text{Eq. 6}$$

where C is a constant that determines the extent to which e is increased. In Figure 6 we illustrate the changes in density predicted by this updated model. As shown in Figure 3 and 4, sub-MIC concentrations of antibiotics are able to decrease the stationary phase density achieved.

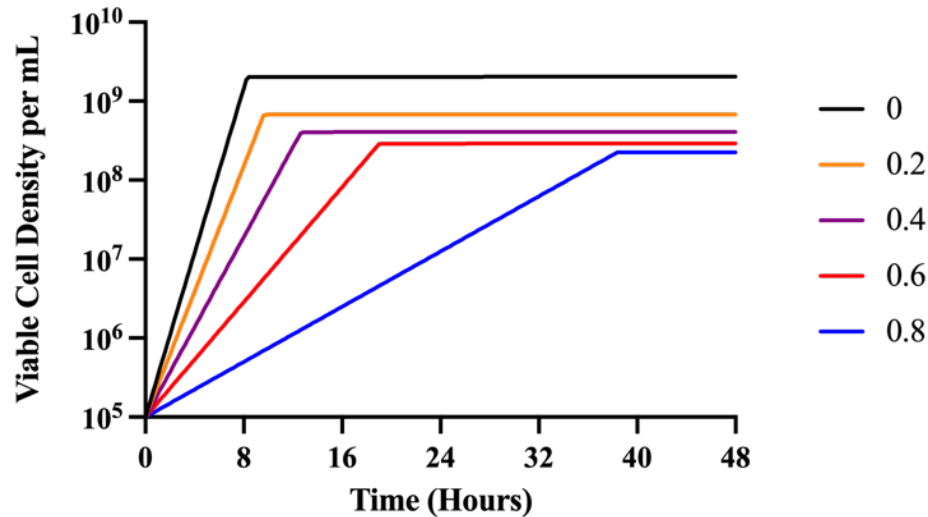


Figure 6. Predicted changes in density of antibiotic-exposed bacteria with antibiotic-dependent resource consumption. To illustrate the properties of this model, we explore only the strong bactericidal antibiotic condition (Condition III). Condition III represents a strong bactericidal antibiotic with $v_{MIN} = -5.0$. Parameters used for these simulations are $e=5 \times 10^{-7}$ $\mu\text{g}/\text{per cell}$, $v_{MAX} = 1.2$ per cell per hour, $K=1$, $k=1$, $\text{MIC}=1.0$. Changes in the viable density of bacteria anticipated from the Hill function model for different concentrations of the antibiotic, respectively 0 to 0.8 times MIC. In these numerical solutions, we assume the concentration of the limiting resource (r) is 1000 when the bacteria are first introduced to the antibiotic and the concentration of the antibiotic does not decay, $d_a=0$, and that $C= 5 \times 10^{-6}$.

Rates of antibiotic-dependent growth and mortality

To explore the relationship between the concentration of the antibiotic and the rates of growth and death of *E. coli* MG1655, we performed time-kill experiments. Overnight cultures of the bacteria in LB (Figure 7) or minimal medium (Figure 8) were mixed with different concentrations of the antibiotics above and below the

MIC for the drugs in the noted media. Viable cell densities (CFUs) of the cultures were estimated at different times.

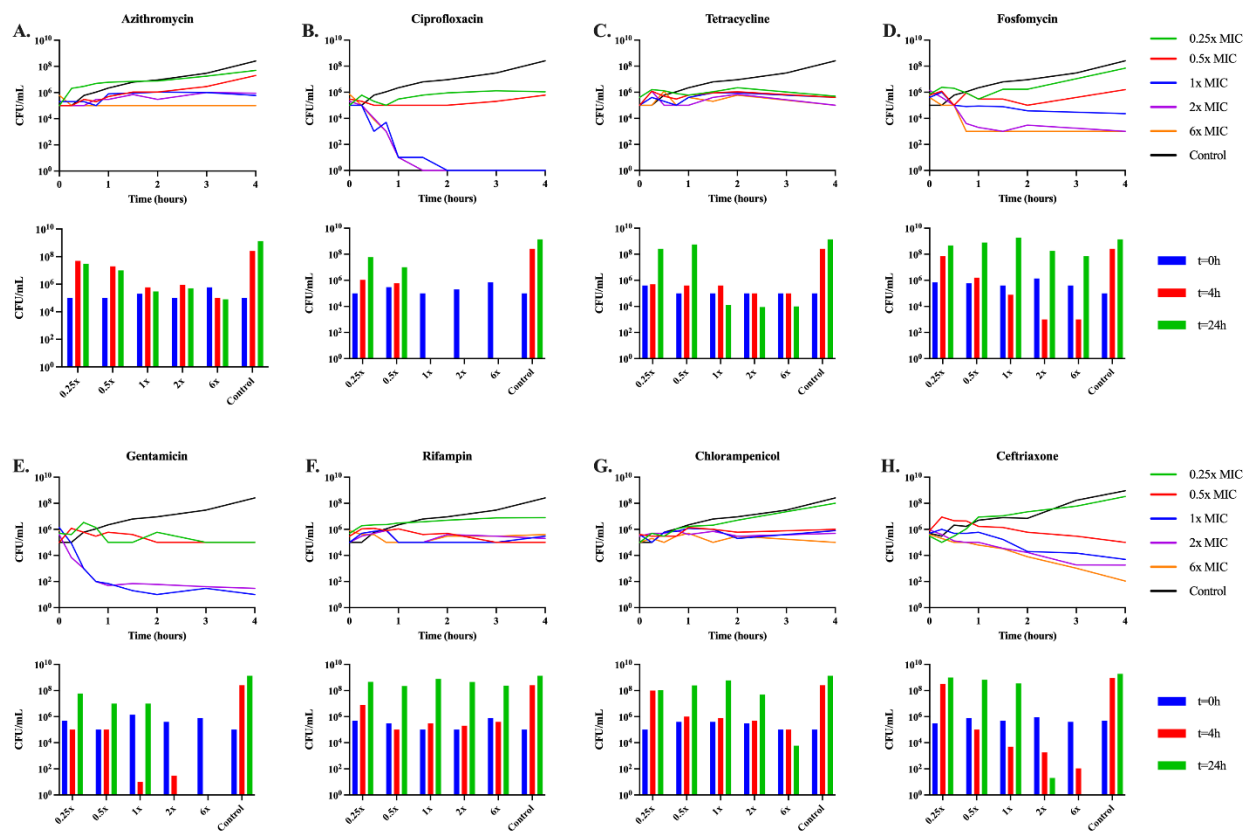


Figure 7. LB time-kills. Changes in viable cell density of *E. coli* MG1655 exposed to sub- and super- MIC concentrations of the eight antibiotics in broth for 24 hours. Shown for each panel in the line graph are changes in the viable cell density over a four-hour period, shown in the bar graph is the viable cell density at 0, 4, and 24 hours. (A) Azithromycin (B) Ciprofloxacin (C) Tetracycline (D) Fosfomycin (E) Gentamicin (F) Rifampin (G) Chloramphenicol (H) Ceftriaxone.

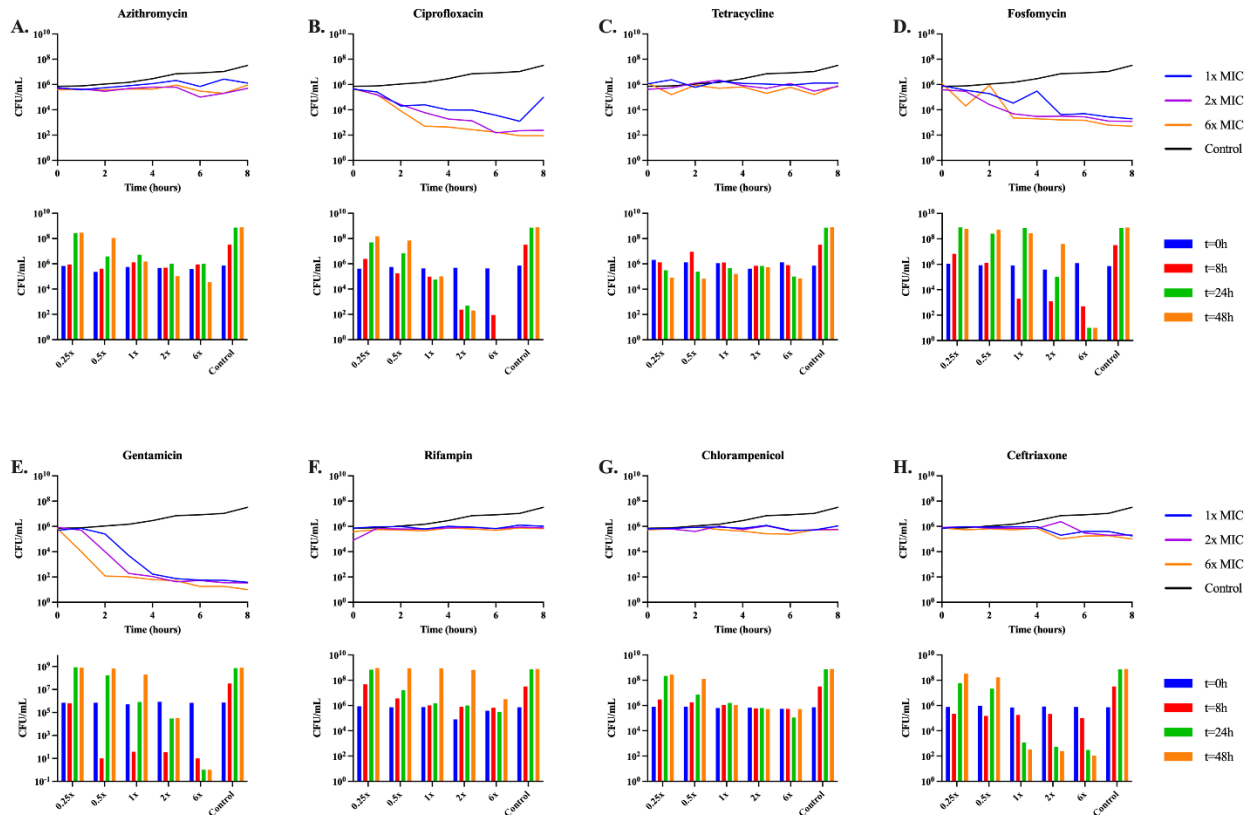


Figure 8. Minimal medium time-kills. Changes in viable cell density of *E. coli* MG1655 exposed to sub- and super- MIC concentrations of the eight antibiotics in minimal for 48 hours. Shown for each panel in the line graph are changes in the viable cell density over a four-hour period, shown in the bar graph is the viable cell density at 0, 8, 24, and 48 hours. Sub-MIC concentrations of the antibiotics are not shown, as over eight hours there was no change in CFUs in any of the cultures. (A) Azithromycin (B) Ciprofloxacin (C) Tetracycline (D) Fosfomicin (E) Gentamicin (F) Rifampin (G) Chloramphenicol (H) Ceftriaxone.

In both LB and minimal medium, the bacteriostatic drugs (azithromycin, tetracycline, and chloramphenicol) suppress growth of the bacteria at super-MIC concentrations. In both media ciprofloxacin, gentamicin, and ceftriaxone appear highly bactericidal, though ceftriaxone does not kill at all in the first eight hours in minimal media. Rifampin and fosfomicin are both complicated by the emergence of genotypic resistance. Rifampin appears static for the first several hours in both media, but the bacteria end up growing to the level of the control by 24 and 48 hours respectively. Fosfomicin kills the *E. coli* for the first several hours, but by the end

of the experiments, the bacterial densities are similar to that of the antibiotic free control. As we obtain qualitatively similar results in both the LB and highly buffered minimal medium, we find it unlikely that changes in pH would account for the results shown in LB. Also, as we see bacterial density suppression at 48 hours, the drugs are likely not decaying to a sufficient degree to allow for the bacteria to overcome the drug effects.

Discussion

The diagnosis of the most frequent diseases and protocols for their treatment are commonly based on relatively few estimated parameters like cholesterol levels, blood pressure, white cell counts, and glucose concentrations. In the case of antibiotic treatment, this parametric reductionism is in the application of the minimum concentration of the antibiotic required to prevent the replication of the bacteria presumed to be responsible for the infection, the MIC. As the unique measure of the pharmacodynamics, MICs are employed as both a measure of the susceptibility of the bacteria to the drug and for the design of dosing regimens for treatment of infections with those bacteria [8, 20]. Under *in vivo* conditions, the local bacterial concentration at the site of infection, the replication rate, the available nutrients, the antibiotic concentration, and the effect of immune response are highly heterogeneous in time and space. In addition, under *in vivo* conditions within tissues, most bacteria are likely exposed to sub-MIC concentrations of drugs derived to an antibiotic gradient, and not to the drug concentration present in the serum [21]. A single, simple test will be insufficient to cover these diverse and changing conditions. Efforts to design culture media mimicking the tissue environment, referred to by Ersoy *et al.* as the “fundamental flaw in the paradigm for antimicrobial susceptibility testing” [22], could slightly improve the *in vitro/in vivo* correlation, but these medias cannot evade the inconvenience of environmental heterogeneity [23-28]. Our approach is evaluating the effects of nutrients and limiting resources on MIC. Glucose is likely not the main carbon source for *E. coli* in the host [29], but limitations *in vitro* of glucose or other carbon sources mimic the effect of shortage of other possible nutrients. The results of this study with eight antibiotics and *E. coli* illustrate the limitations of MICs for these purposes and also those of more comprehensive measures of the PD of antibiotics, such as Hill functions [30].

MICs are officially estimated with low densities of bacteria introduced into rich media, most commonly broths such as LB or Mueller-Hinton [14, 31]. Our results demonstrate that estimates of this parameter for azithromycin, tetracycline, and gentamicin obtained in highly buffered glucose-limited minimal medium are markedly lower than those estimated in broth. We have also shown that carbon source plays a large role in the determination of the MIC, particularly for azithromycin and fosfomicin. This is an indication that both nutrient limitation and choice of nutrient plays a large role in the determination of MIC [17, 32]. It is to be noted that

nutrient limitation and antibiotic action might both influence the bacterial stringent response, where (p)ppGpp “alarmone” levels lead to slower growth of the bacteria and effectively generate persister cells [33, 34]. These population heterogeneities, reflected in our work, reveal a major limitation in the method for estimating MIC. Most notably, this singular pharmacodynamic parameter inherently cannot account for the possibility of rapid emergence of antibiotic resistance.

In addition to MICs, pharmacodynamic Hill functions provide information about the relationship between the concentration of the antibiotic and the dynamics and rates of growth of bacteria exposed to the drug [30]. The parameters of Hill functions are estimated from the antibiotic concentration-dependent growth rates of the bacteria with the assumption being that these drugs only act by modifying these rates and do not take into account changes in any other bacterial growth parameters [30]. The results of this and previous studies [35] question the validity of this assumption.

Our original model, a modification of the Hill functions which allows for resource consumption, predicts that if at sub-MIC concentrations all antibiotics did was to reduce the growth rate of the exposed bacteria, their populations would achieve the same stationary phase densities but do so at times that increase with the concentration of the antibiotic. To an extent that varies among drugs, sub-MIC concentrations of antibiotics increase the time before the bacteria start to grow, the lag. This effect is most prominent among drugs that alter cellular metabolism. Antibiotics slowing metabolic processes likely slow development of cellular structures, as all structural elements of the cell will derive from glucose metabolism, which would be seen as an increase in the lag time. Also unanticipated by our model extending the Hill functions is that the maximum density to which the bacteria grow is dependent on the antibiotic concentration. Though, our updated model, which varies the conversion efficiency of glucose with an increasing concentration of an antibiotic, can account for these effects.

One possible explanation for why sub-MIC concentrations of antibiotics lower the densities to which the exposed populations of bacteria grow is that these drugs reduce the efficacy of use of the limiting resource. Stated another way, the bacteria exposed to sub-inhibitory antibiotic concentrations require more resource for

replication. The effect of antibiotics on bacterial nutritional efficiency can explain this result. Certainly, antibiotic exposure decreases the metabolic flux, in that there is a waste of intracellular metabolites that are synthesized but not integrated into metabolic pathways. For instance, exposure to chloramphenicol and rifampin results in an accumulation of amino acids, nucleotides, and lipids [36]. Similarly, beta-lactam exposure induces a futile cycle of cell wall synthesis and degradation, which depletes cellular resources [37]. There is also emerging evidence that sub-MIC concentrations of antibiotics can influence non-essential tRNA and RNA modifications, leading to unnecessary energy expenditures [38]. Such energetic waste should be compensated by the consumption of nutrients that do not necessarily contribute to the net growth rate.

Consistent with this hypothesis at sub-MIC concentrations, all of the antibiotic treated cultures fail to grow up to the glucose-limited density of the controls, but yet all of the glucose is utilized in that no or very little free glucose is detectable. While, at super-MIC concentrations the bacterial densities are suppressed, and a substantial amount of free glucose remains. As a departure from this trend, the cultures treated with super-MIC concentrations of ceftriaxone use more free glucose than the cultures treated with super-MIC concentrations of the other drugs, but yet a large amount of glucose is still present. It has not escaped our notice that based on Figure 8 this beta-lactam over the first eight hours appears very similar to the bacteriostatic drugs. Could it be that in these first few hours, the growth rate is equal to the death rate [39] so that these bacteria are still utilizing the free glucose? Alternatively, ceftriaxone is known to produce filaments due to PBP3 inhibition, could it be that these multicellular filaments have an increased surface/volume ratio (favoring glucose uptake) and perhaps an increased metabolic requirement when compared to their ancestor cells?

We are confident that the results of the experiments performed here are broadly replicable across antibiotic drug classes and media type (rich versus minimal) but recognize there are caveats to consider. Firstly, that our study was performed with just one laboratory strain of *E. coli*, MG1655. Secondly, the study was also conducted with only two media. One of which was Lysogeny Broth which we used to represent nutrient rich conditions, though MICs for clinical purposes are officially performed in Mueller-Hinton. We postulate our choice of strain and media will not change the observed phenomena qualitatively. That said, we do anticipate changing strains

or media will quantitatively change the results observed here. More specifically, we expect the MICs obtained will depend on both the bacterial strain and media.

Advancement in the way we measure and understand pharmacodynamics should have therapeutic implications. Our main difficulty is the heterogeneity of the microecological conditions at the site of infection (such as immunological factors, nutritional deficiencies, local pH or oxygen availability, access of the drugs, or protein binding). Factors which are difficult or impossible to reproduce under *in-vitro* conditions. In laboratory tests, the most used PD parameter, the MIC, certainly allows for the comparison of antibiotic susceptibility between two isolates of the same species under identical *in vitro* conditions. However, MIC is an insufficient PD marker for several reasons. Firstly, the antibiotic effect at subinhibitory concentrations is not considered. Secondly, this parameter does not tell us anything about the susceptibility of a given organism at different cell densities. Thirdly, it tells us nothing about changes in growth parameters such as the effect on lag, average growth rate, final density, or overall rate of drug-mediated killing. Lastly, MIC indicates nothing about post-antibiotic effects, resistance, persistence, or heteroresistance. All these pharmacodynamic dimensions change the effect of antibiotics *in vivo* as the concentration of the drug changes over time, as predicted by the PK. Without understanding these effects, the operative linkage of PK/PD is insufficient to obtain robust predictions about antibiotic efficacy. When MIC is used as the sole PD parameter, this insufficiency is even more apparent. Most PK/PD approaches look at one of three PK parameters: either maximum concentration of the antibiotic to MIC, drug exposure to MIC (which is to say area under the curve to MIC), or the time that the drug concentration is above the MIC [40]. Most importantly, the development of novel antibiotics should consider these PD complexities and adopt a non-reductive approach which is not simply limited to MIC. An antibiotic should be more effective than another as shown by a holistic superiority-test, considering multiple parameters for PD. These tests should take into account: the effect of the density of the starting bacterial population, the effectiveness of the drug on bacteria in different stages of growth, the ability to reduce bacterial growth rate, increase lag time, and decrease final population size, as well as decrease the number of persisters. Optimally, all these advantages would also reduce the length of treatment, the emergence of antibiotic resistance, and the recurrent infections, as well as the possibility of transmission of

pathogens to other hosts. However, the usual microbiological PD tests in drug development do not include these calculations, benefits which would go unrecognized by using an only-MIC-focused approach.

Materials and Methods

Numerical solutions (simulations)– For our numerical analysis of the equations presented (equations 1-6), we used Berkeley Madonna, using parameters in the ranges estimated for *E. coli*. Copies of the Berkeley Madonna program used for these simulations are available at www.eclf.net.

Growth media– LB broth (244620) was obtained from BD. The DM (Davis Minimal) minimal base without dextrose (15758-500G-F) was obtained from Sigma Aldrich (7 g/l dipotassium phosphate, 2 g/l monopotassium phosphate, 0.5 g/l sodium citrate, 0.1 g/l magnesium sulfate, 1 g/l ammonium sulfate). MH broth (M391-500g) was obtained from HiMedia. Glucose (41095-5000) was obtained from Acros, Succinic Acid (S-2378) was obtained from Sigma Aldrich, Lactose (L3750) was obtained from Sigma Aldrich, Maltose (M2250) was obtained from Sigma Aldrich, Glycerol (G7757) was obtained from Honeywell and Fructose (161355000) was obtained from ACROS Organics. LB agar (244510) for plates was obtained from BD.

Bacterial strains– *E. coli* MG1655 was obtained from the Levin Lab Bacterial collection. This Whole Genome Shotgun project has been deposited at DDBJ/ENA/GenBank under the accession JAQIDJ000000000. The version described in this paper is version JAQIDJ010000000.

Antibiotics– Ciprofloxacin (A4556) was obtained from AppliChem Panreac, Tetracycline (T17000) was obtained from Research Products International, Fosfomycin (P5396) was obtained from Sigma Aldrich, Chloramphenicol (23660) was obtained from USB, Rifampin (BP2679-1) was obtained from Fisher BioReagents, Ceftriaxone (C5793) was obtained from Sigma Aldrich, Azithromycin (3771) was obtained from TOCRIS and Gentamicin (BP918-1) was obtained from Fisher BioReagents.

Sampling bacterial densities– The densities of bacteria were estimated by serial dilution in 0.85% saline and plating. The total density of bacteria was estimated on Lysogeny Broth (LB) plates with 1.6% agar.

Growth rate estimation– Exponential growth rates were estimated from changes in optical density (OD₆₀₀) in a Bioscreen C. For this, 24-hours stationary phase cultures were diluted in LB or glucose-limited liquid media to an initial density of approximately 10⁵ cells per mL. Five replicas were made for each estimate by adding 300µl of the suspensions to the wells of the Bioscreen plates. The plates were incubated at 37°C and shaken continuously. Estimates of the OD (600nm) were made every five minutes for 24 hours in LB and 48 hours in

glucose-limited medium. Normalization, replicate means and error, growth rate, lag and maximum OD were found using a novel R Bioscreen C analysis tool accessible at https://josheclf.shinyapps.io/bioscreen_app.

Sequencing and analyses– Bacterial DNA was extracted using Promega’s (Wisconsin, USA) Wizard Genomics DNA Purification Kit (Cat# A1120) using the manufacturer’s protocol. The extracted DNA was quantified on ThermoFisher’s NanoDrop OneC microvolume spectrophotometer (Cat# ND-ONEW). Samples were sent to the Microbial Genome Sequencing Center in Pittsburgh, Pennsylvania, USA, for whole genome sequencing on the Illumina NextSeq 2000 platform. Analysis of FASTAQ files received from the Microbial Genome Sequencing Center were analyzed using Geneious Prime version 2022.0.1.

Minimum inhibitory concentrations– Antibiotic MICs were estimated using a 2-fold microdilution procedure as described in [41].

Antibiotic time-kills– For these experiments, overnight cultures of *E. coli* MG1655 were added to LB broth or DM 1000 µg/mL glucose liquid media at an initial density of approximately 10^5 cells per mL, followed by 1 h incubation at 37°C and shaken continuously. After incubation, antibiotics were added at the concentrations indicated in Figures 4 and 5 and the initial densities of the cultures were estimated. The cultures with the antibiotics were incubated for 24 h in LB media and 48 h in DM glucose and estimates of the viable cell densities were made at 15 min, 30 min, 45 min, 1 h, 1.5 h, 2 h, 3 h, 4 h and 24 h for LB cultures and 1 h, 2 h, 3 h, 4 h, 5 h, 6 h, 7 h, 8 h, 24 h and 48 h for the DM glucose liquid media cultures.

Glucose assay– Glucose concentration was measured by the dinitrosalicylic colorimetric method as described in [42].

Acknowledgements

We would like to thank Danielle Steed, Michael Woodworth, and Ahmed Babiker for their discussions of the clinical implications and relevance of this work. We would also like to thank Nic Vega, Ingrid McCall, Gene and Dean Ween, and the other members of the Levin Lab.

BRL would like to thank the US National Institute of General Medical Sciences for their funding support via R35 GM 136407 and the US National Institute of Allergy and Infectious Diseases for their funding support via U19 AI 158080-02. As well as the Emory Antibiotic Resistance Center.

TGG would like to thank the US Fulbright Program and the Spanish Government FPI fellowship for their funding support.

Data Availability Statement

All the data generated are available in this manuscript and its supporting supplemental material.

References

1. Andes, D., et al., *Application of pharmacokinetics and pharmacodynamics to antimicrobial therapy of respiratory tract infections*. Clin Lab Med, 2004. **24**(2): p. 477-502.
2. Craig, W.A. and D. Andes, *Pharmacokinetics and pharmacodynamics of antibiotics in otitis media*. Pediatric Infectious Disease Journal, 1996. **15**(3): p. 255-9.
3. Velkov, T., et al., *PK/PD models in antibacterial development*. Curr Opin Microbiol, 2013. **16**(5): p. 573-9.
4. Frimodt-Moller, N., *How predictive is PK/PD for antibacterial agents?* Int J Antimicrob Agents, 2002. **19**(4): p. 333-9.
5. Levison, M.E. and J.H. Levison, *Pharmacokinetics and pharmacodynamics of antibacterial agents*. Infect Dis Clin North Am, 2009. **23**(4): p. 791-815, vii.
6. Rawson, T.M., et al., *Exploring the Pharmacokinetics of Phenoxyethylpenicillin (Penicillin-V) in Adults: A Healthy Volunteer Study*. Open Forum Infectious Diseases, 2021. **8**(12).
7. Khan, D.D., L.E. Friberg, and E.I. Nielsen, *A pharmacokinetic-pharmacodynamic (PKPD) model based on in vitro time-kill data predicts the in vivo PK/PD index of colistin*. Journal of Antimicrobial Chemotherapy, 2016. **71**(7): p. 1881-1884.
8. Landersdorfer, C.B. and R.L. Nation, *Limitations of Antibiotic MIC-Based PK-PD Metrics: Looking Back to Move Forward*. Front Pharmacol, 2021. **12**: p. 770518.
9. Lorian, V., *Antibiotics in Laboratory Medicine*. 2005: Lippincott Williams & Wilkins.
10. Kowalska-Krochmal, B. and R. Dudek-Wicher, *The Minimum Inhibitory Concentration of Antibiotics: Methods, Interpretation, Clinical Relevance*. Pathogens, 2021. **10**(2).
11. Wikler, M.A., *Methods for dilution antimicrobial susceptibility tests for bacteria that grow aerobically: approved standard*. Clsi (Nccls), 2006. **26**: p. M7-A7.

12. Ling, T.K., Z.K. Liu, and A.F. Cheng, *Evaluation of the VITEK 2 system for rapid direct identification and susceptibility testing of gram-negative bacilli from positive blood cultures*. J Clin Microbiol, 2003. **41**(10): p. 4705-7.
13. Bobenchik, A.M., et al., *Performance of Vitek 2 for antimicrobial susceptibility testing of Enterobacteriaceae with Vitek 2 (2009 FDA) and 2014 CLSI breakpoints*. J Clin Microbiol, 2015. **53**(3): p. 816-23.
14. Colombo, A.L., et al., *Comparison of Etest and National Committee for Clinical Laboratory Standards broth microdilution method for azole antifungal susceptibility testing*. J Clin Microbiol, 1995. **33**(3): p. 535-40.
15. Amsler, K., et al., *Comparison of Broth Microdilution, Agar Dilution, and Etest for Susceptibility Testing of Doripenem against Gram-Negative and Gram-Positive Pathogens*. Journal of Clinical Microbiology, 2010. **48**(9): p. 3353-3357.
16. Udekwa, K.I., et al., *Functional relationship between bacterial cell density and the efficacy of antibiotics*. J Antimicrob Chemother, 2009. **63**(4): p. 745-57.
17. Stokes, J.M., et al., *Bacterial Metabolism and Antibiotic Efficacy*. Cell Metab, 2019. **30**(2): p. 251-259.
18. Monod, J., *THE GROWTH OF BACTERIAL CULTURES*. Annual Review of Microbiology, 1949. **3**(1): p. 371-394.
19. Ballesterro-Téllez, M., et al., *Role of inoculum and mutant frequency on fosfomycin MIC discrepancies by agar dilution and broth microdilution methods in Enterobacteriaceae*. Clinical Microbiology and Infection, 2017. **23**(5): p. 325-331.
20. Benkova, M., O. Soukup, and J. Marek, *Antimicrobial susceptibility testing: currently used methods and devices and the near future in clinical practice*. Journal of Applied Microbiology, 2020. **129**(4): p. 806-822.
21. Baquero, F. and M.C. Negri, *Selective compartments for resistant microorganisms in antibiotic gradients*. Bioessays, 1997. **19**(8): p. 731-6.
22. Ersoy, S.C., et al., *Correcting a Fundamental Flaw in the Paradigm for Antimicrobial Susceptibility Testing*. EBioMedicine, 2017. **20**: p. 173-181.

23. Luna, B., et al., *A nutrient-limited screen unmasks rifabutin hyperactivity for extensively drug-resistant Acinetobacter baumannii*. Nat Microbiol, 2020. **5**(9): p. 1134-1143.
24. Lee, B., et al., *In Vitro Activity of Rifabutin and Rifampin against Antibiotic-Resistant Acinetobacter baumannii, Escherichia coli, Staphylococcus aureus, Pseudomonas aeruginosa, and Klebsiella pneumoniae*. mSphere, 2021. **6**(6): p. e0092021.
25. Cheng, J., et al., *Synergistic Rifabutin and Colistin Reduce Emergence of Resistance When Treating Acinetobacter baumannii*. Antimicrob Agents Chemother, 2021. **65**(4).
26. Farha, M.A., et al., *Overcoming Acquired and Native Macrolide Resistance with Bicarbonate*. ACS Infect Dis, 2020. **6**(10): p. 2709-2718.
27. Farha, M.A., et al., *Bicarbonate Alters Bacterial Susceptibility to Antibiotics by Targeting the Proton Motive Force*. ACS Infect Dis, 2018. **4**(3): p. 382-390.
28. Dillon, N., et al., *Surprising synergy of dual translation inhibition vs. Acinetobacter baumannii and other multidrug-resistant bacterial pathogens*. EBioMedicine, 2019. **46**: p. 193-201.
29. Brown, S.A., K.L. Palmer, and M. Whiteley, *Revisiting the host as a growth medium*. Nat Rev Microbiol, 2008. **6**(9): p. 657-66.
30. Regoes, R.R., et al., *Pharmacodynamic functions: a multiparameter approach to the design of antibiotic treatment regimens*. Antimicrob Agents Chemother, 2004. **48**(10): p. 3670-6.
31. Leclercq, R., et al., *EUCAST expert rules in antimicrobial susceptibility testing*. Clin Microbiol Infect, 2013. **19**(2): p. 141-60.
32. Allison, K.R., M.P. Brynildsen, and J.J. Collins, *Metabolite-enabled eradication of bacterial persisters by aminoglycosides*. Nature, 2011. **473**(7346): p. 216-20.
33. McCall, I.C., et al., *Antibiotic Killing of Diversely Generated Populations of Nonreplicating Bacteria*. Antimicrob Agents Chemother, 2019. **63**(7).

34. Ro, C., M. Cashel, and L. Fernández-Coll, *The secondary messenger ppGpp interferes with cAMP-CRP regulon by promoting CRP acetylation in Escherichia coli*. PLoS One, 2021. **16**(10): p. e0259067.
35. Atkinson, B.A., L. Amaral, and J.A. Washington, *Sublethal Concentrations of Antibiotics, Effects on Bacteria and the Immune System*. CRC Critical Reviews in Microbiology, 1982. **9**(2): p. 101-138.
36. Lobritz, M.A., et al., *Antibiotic efficacy is linked to bacterial cellular respiration*. Proc Natl Acad Sci U S A, 2015. **112**(27): p. 8173-80.
37. Cho, H., T. Uehara, and T.G. Bernhardt, *Beta-lactam antibiotics induce a lethal malfunctioning of the bacterial cell wall synthesis machinery*. Cell, 2014. **159**(6): p. 1300-11.
38. Babosan, A., et al., *Non-essential tRNA and rRNA modifications impact the bacterial response to sub-MIC antibiotic stress*. bioRxiv, 2022: p. 2022.02.06.479318.
39. Ratiu, I.A., et al., *Temporal influence of different antibiotics onto the inhibition of Escherichia coli bacterium grown in different media*. Analytical Biochemistry, 2019. **585**: p. 113407.
40. Eyer, R.F. and K. Shvets, *Clinical Pharmacology of Antibiotics*. Clin J Am Soc Nephrol, 2019. **14**(7): p. 1080-1090.
41. Jorgensen, J.H. and M.J. Ferraro, *Antimicrobial susceptibility testing: a review of general principles and contemporary practices*. Clin Infect Dis, 2009. **49**(11): p. 1749-55.
42. Miller, G.L., *Use of dinitrosalicylic acid reagent for determination of reducing sugar*. Analytical chemistry, 1959. **31**(3): p. 426-428.

Supporting Information

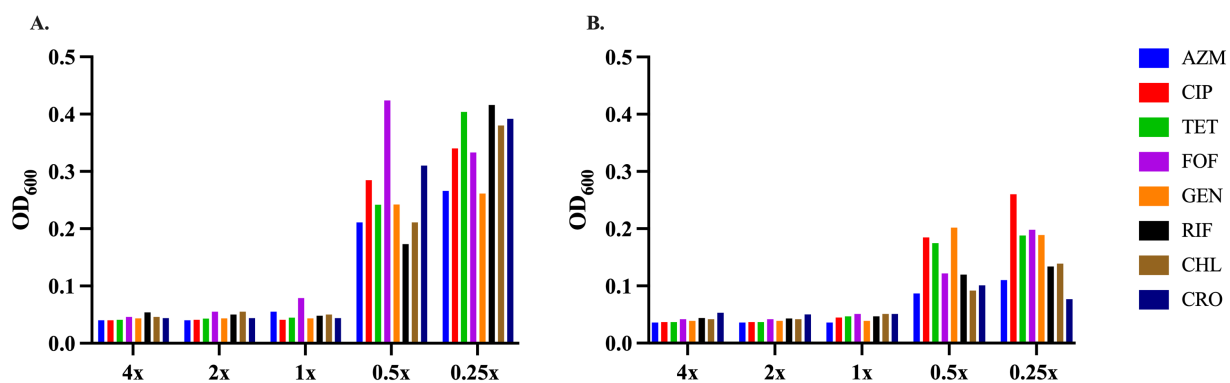


Fig. S1. MIC ooze. Antibiotic MICs were performed using a 2-fold microdilution procedure and after 24 hours in (A) LB and 48 h in (B) glucose-limited minimal medium the final optical density (OD_{600nm}) was measured at different concentrations of antibiotic.

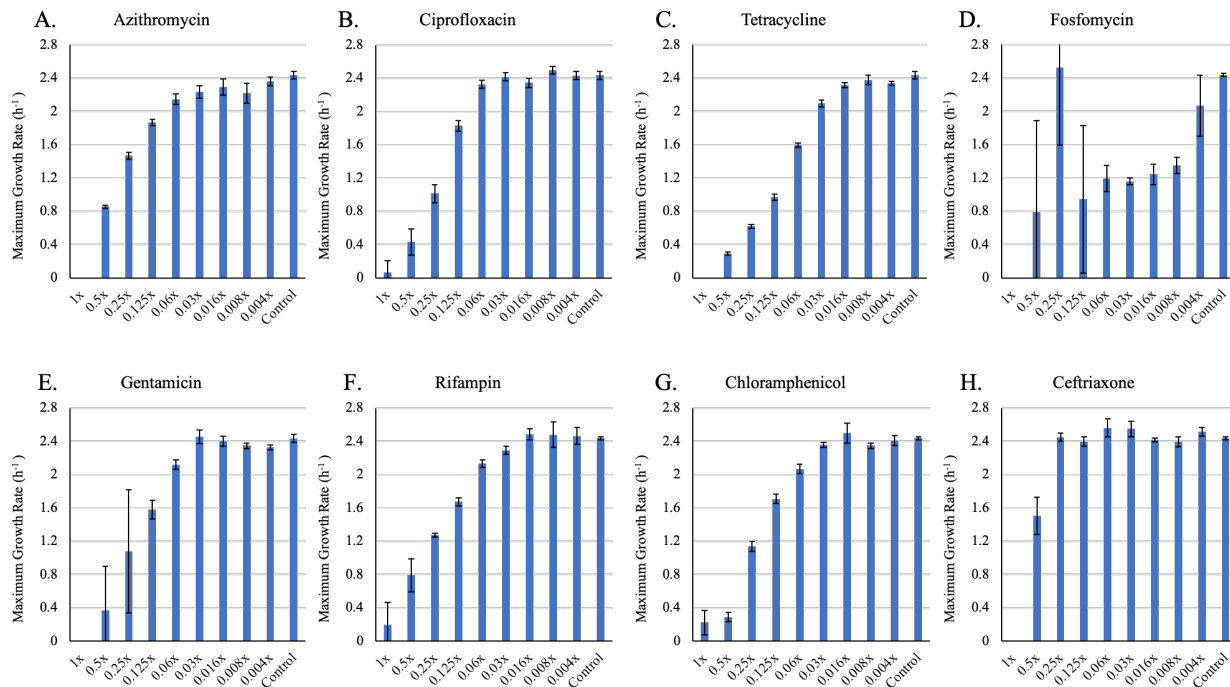


Fig. S2. Changes in maximum growth rate (v_{MAX}) of *E. coli* MG1655 exposed to different sub-MIC concentrations of eight antibiotics for 24 hours in LB. Bars are representative of the average of five technical replicas. Each concentration is shown as a fraction of the MIC for the noted drug (A) Azithromycin (B) Ciprofloxacin (C) Tetracycline (D) Fosfomycin (E) Gentamicin (F) Rifampin (G) Chloramphenicol (H) Ceftriaxone.

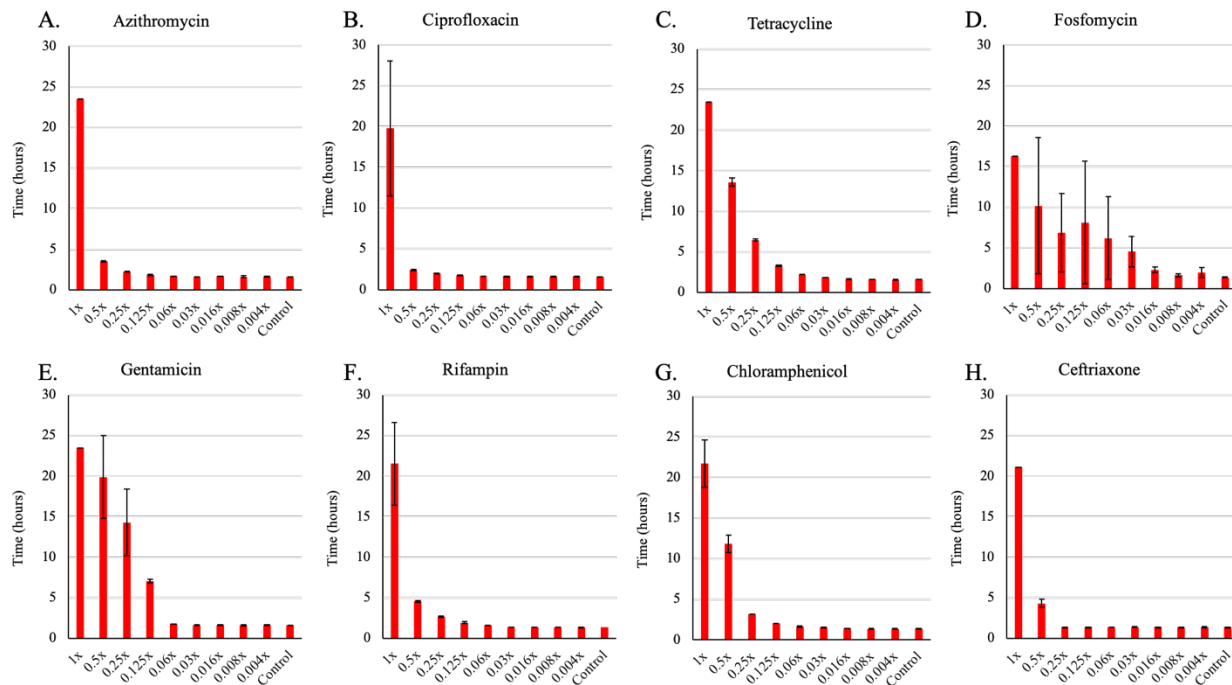


Fig. S3. Changes in the time before the bacteria start to grow (lag) of *E. coli* MG1655 exposed to different sub-MIC concentrations of eight antibiotics for 24 hours in LB. Bars are representative of the average of five technical replicas. Each concentration is shown as a fraction of the MIC for the noted drug (**A**) Azithromycin (**B**) Ciprofloxacin (**C**) Tetracycline (**D**) Fosfomycin (**E**) Gentamicin (**F**) Rifampin (**G**) Chloramphenicol (**H**) Ceftriaxone.

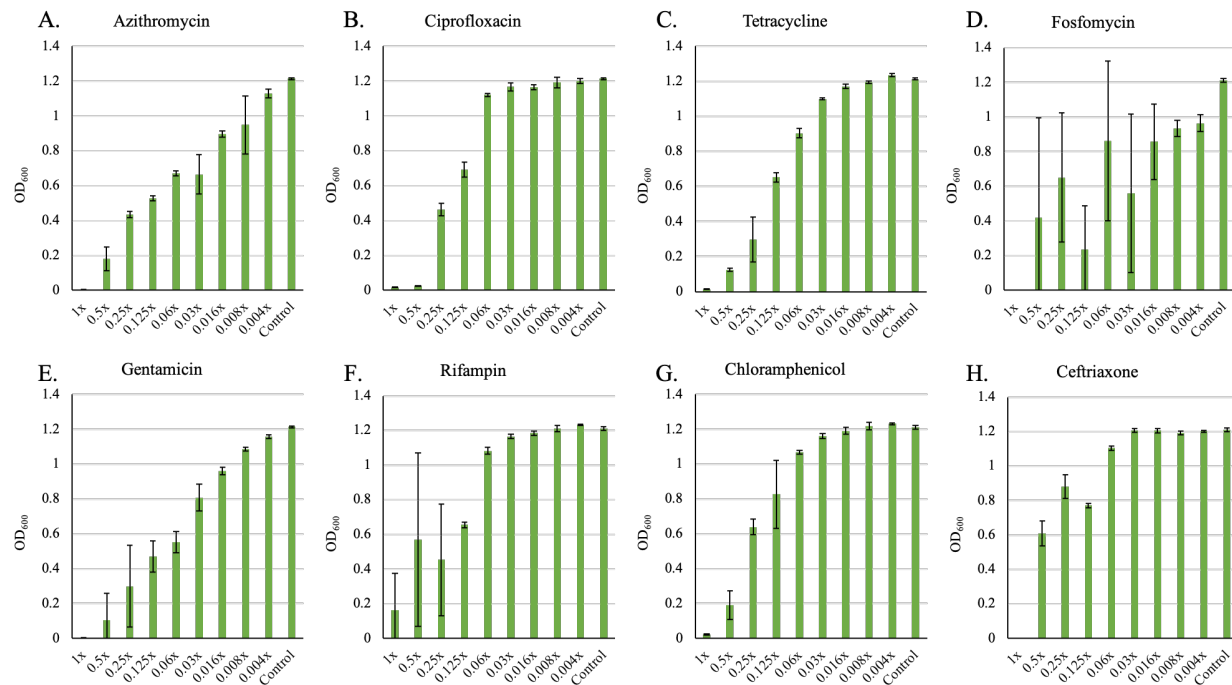


Fig. S4. Changes in the maximum optical density (OD 600nm) of *E. coli* MG1655 exposed to different sub-MIC concentrations of eight antibiotics for 24 hours in LB. Bars are representative of the average of five technical replicas. Each concentration is shown as a fraction of the MIC for the noted drug (**A**) Azithromycin (**B**) Ciprofloxacin (**C**) Tetracycline (**D**) Fosfomycin (**E**) Gentamicin (**F**) Rifampin (**G**) Chloramphenicol (**H**) Ceftriaxone.

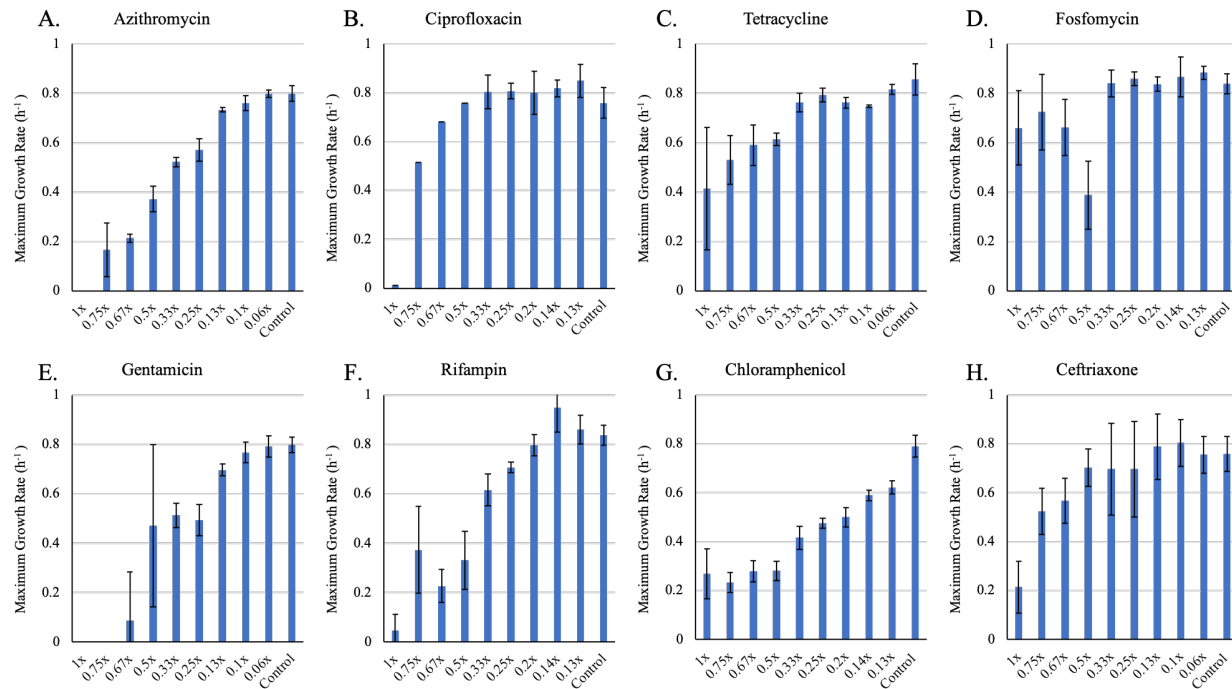


Fig. S5. Changes in maximum growth rate (v_{MAX}) of *E. coli* MG1655 exposed to different sub-MIC concentrations of eight antibiotics for 48 hours in glucose-limited minimal medium. Bars are representative of the average of five technical replicas. Each concentration is shown as a fraction of the MIC for the noted drug (A) Azithromycin (B) Ciprofloxacin (C) Tetracycline (D) Fosfomycin (E) Gentamicin (F) Rifampin (G) Chloramphenicol (H) Ceftriaxone.

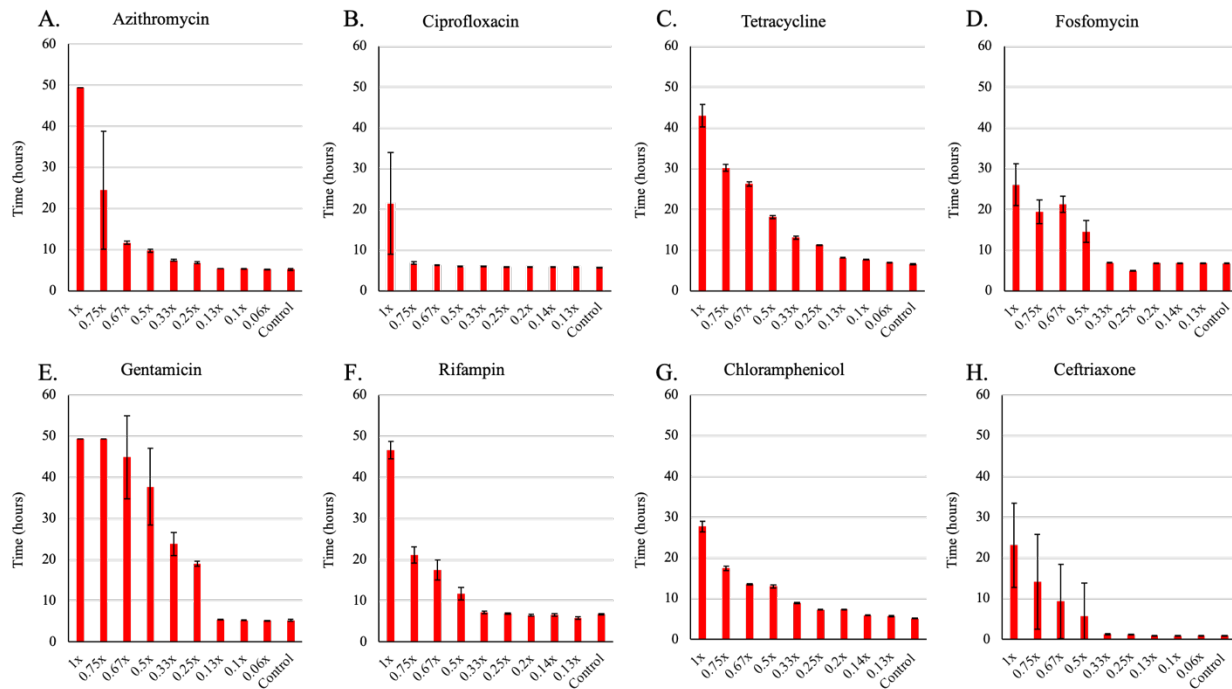


Fig. S6. Changes in the time before the bacteria start to grow (lag) of *E. coli* MG1655 exposed to different sub-MIC concentrations of eight antibiotics for 48 hours in glucose-limited minimal medium. Bars are representative of the average of five technical replicas. Each concentration is shown as a fraction of the MIC for the noted drug **(A)** Azithromycin **(B)** Ciprofloxacin **(C)** Tetracycline **(D)** Fosfomycin **(E)** Gentamicin **(F)** Rifampin **(G)** Chloramphenicol **(H)** Ceftriaxone.

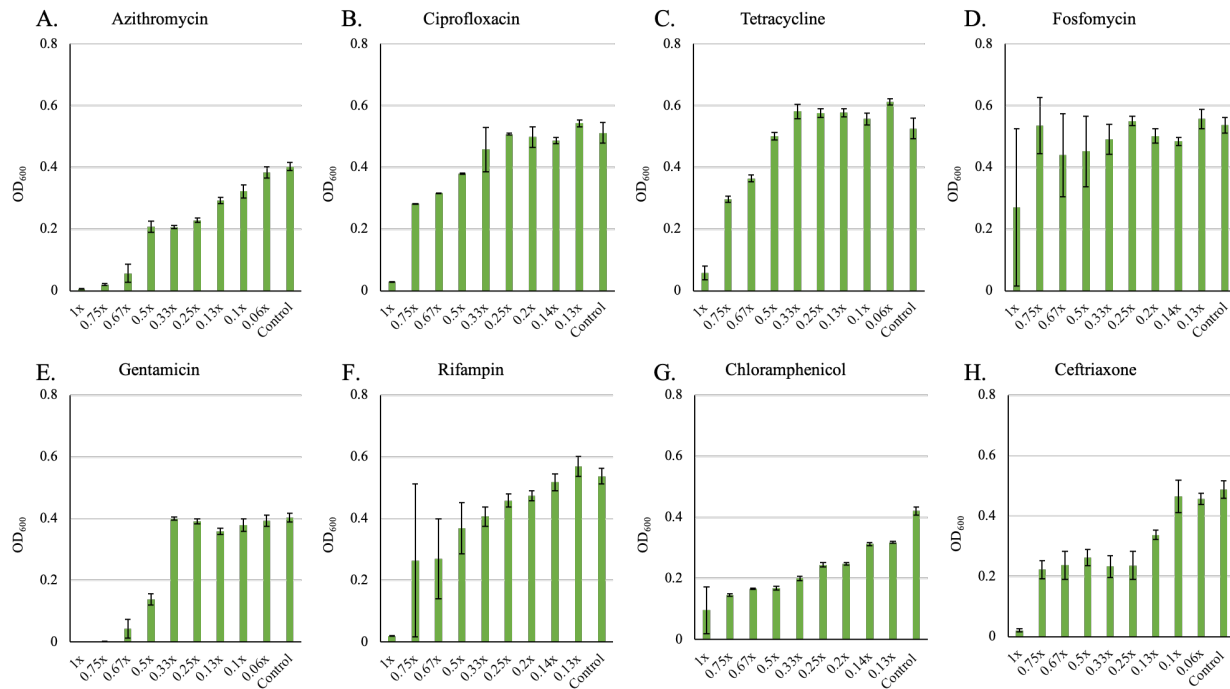


Fig. S7. Changes in the maximum optical density (OD 600nm) of *E. coli* MG1655 exposed to different sub-MIC concentrations of eight antibiotics for 48 hours in glucose-limited minimal medium. Bars are representative of the average of five technical replicas. Each concentration is shown as a fraction of the MIC for the noted drug **(A)** Azithromycin **(B)** Ciprofloxacin **(C)** Tetracycline **(D)** Fosfomycin **(E)** Gentamicin **(F)** Rifampin **(G)** Chloramphenicol **(H)** Ceftriaxone.

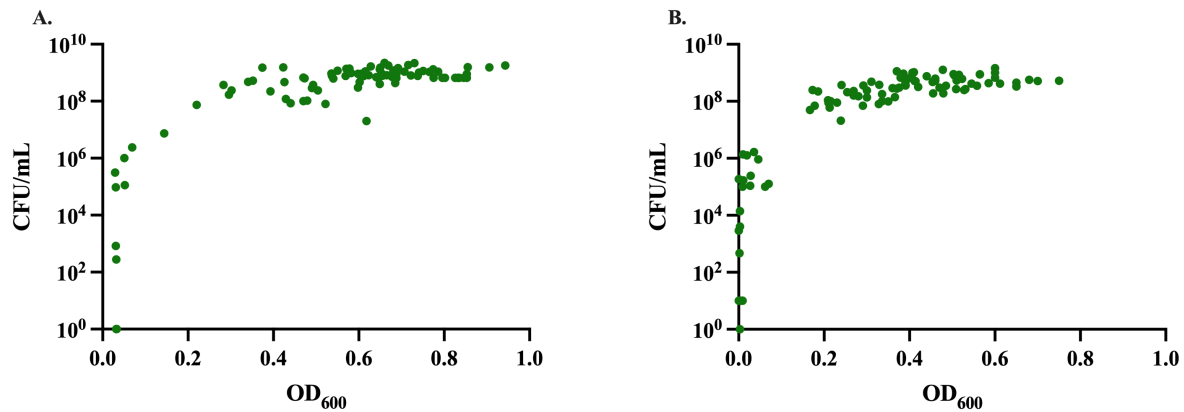


Fig. S8. Relation between optical density and viable colony forming units (CFU) of *E. coli* MG1655 cultures exposed to sub- and super- MIC concentrations of the eight antibiotics in (A) LB after 24 hours and in (B) glucose-limited medium after 48 hours of incubation.

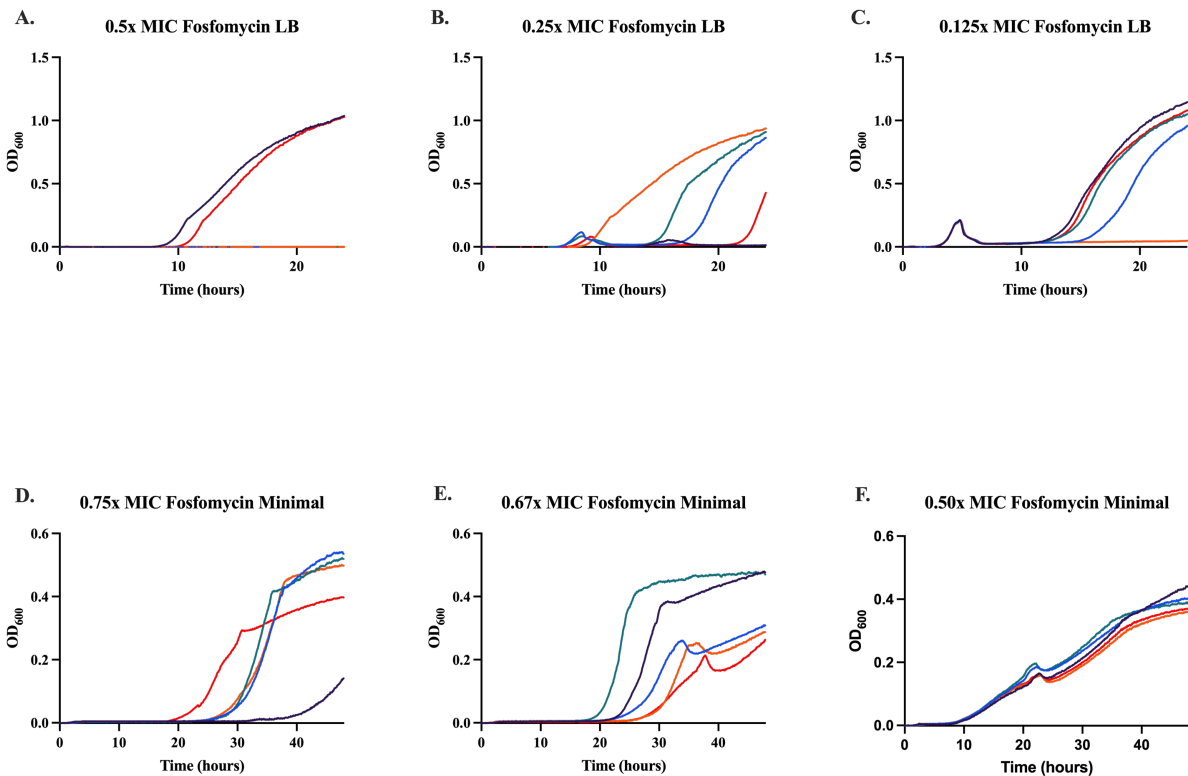


Figure S9. Growth dynamics in LB and glucose-limited medium at different fosfomycin concentrations. Changes in optical density (600nm) of *E. coli* MG1655 exposed to different fosfomycin concentrations for 24 hours in LB and 48 h in glucose-limited medium. Lines are representative of one technical replica and normalized to the time zero optical density. Individual replicate curves show how resistance came up at different fosfomycin concentrations.

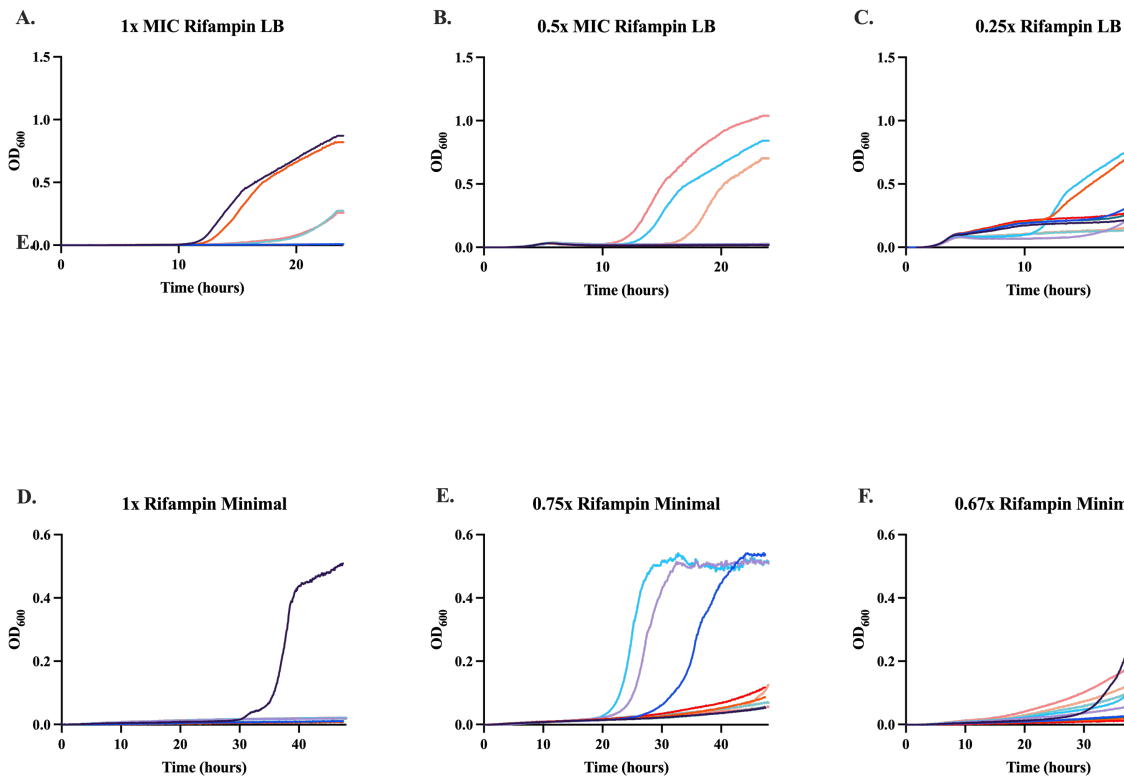


Figure S10. Growth dynamics in LB and glucose-limited medium at different rifampin concentrations.

Changes in optical density (600nm) of *E. coli* MG1655 exposed to different rifampin concentrations for 24 hours in LB and 48 h in glucose-limited medium. Lines are representative of one technical replica and normalized to the time zero optical density. Individual replicate curves show how resistance came up at different rifampin concentrations.

Table S1. Estimated MICs of *E. coli* MG1655 for eight antibiotics in limited minimal medium with different carbon sources

Antibiotic	MIC ($\mu\text{g}/\text{mL}$)					
	Glucose	Succinate	Lactose	Maltose	Glycerol	Fructose
AZM	6.25	1.56	3.13	3.13	1.56	3.13
CIP	0.03	0.03	0.016	0.016	0.016	0.016
TET	0.8	0.8	0.8	0.8	0.8	0.8
FOF	25	3.125	12.5	12.5	25	12.5
GEN	0.75	0.37	0.75	0.37	0.37	0.37
RIF	12.5	12.5	12.5	12.5	12.5	12.5
CHL	6.25	6.25	6.25	6.25	3.13	6.25
CRO	0.03	0.006	0.03	0.012	0.03	0.012

Chapter 3

Chapter 3

Theoretical Considerations and Empirical Predictions of the Pharmacology and Population Dynamics of Heteroresistance

Reprinted from: B.R. Levin, B.A. Berryhill, T. Gil-Gil, J.A. Manuel, A.P. Smith, J.E. Choby, D.I. Andersson, D.S. Weiss, F. Baquero, Theoretical considerations and empirical predictions of the pharmacology and population dynamics of heteroresistance, *Proc. Natl. Acad. Sci. U.S.A.*

Abstract

Antibiotics are considered one of the most important contributions to clinical medicine in the last 100 years. Due to the use and overuse of these drugs, there have been increasing frequencies of infections with resistant pathogens. One form of resistance, heteroresistance, is particularly problematic; pathogens appear sensitive to a drug by common susceptibility tests. However, upon exposure to the antibiotic, resistance rapidly ascends, and treatment fails. To quantitatively explore the processes contributing to the emergence and ascent of resistance during treatment and the waning of resistance following cessation of treatment, we develop two distinct mathematical and computer-simulations models of heteroresistance. In our analysis of the properties of these models, we consider the factors that determine the response to antibiotic-mediated selection. In one model, heteroresistance is progressive, with each resistant state sequentially generating a higher resistance level. In the other model, heteroresistance is non-progressive, with a susceptible population directly generating populations with different resistance levels. The conditions where resistance will ascend in the progressive model are narrower than those of the non-progressive model. The rates of reversion from the resistant to the sensitive states are critically dependent on the transition rates and the fitness cost of resistance. Our results demonstrate that the standard test used to identify heteroresistance is insufficient. The predictions of our models are consistent with empirical results. Our results demand a reevaluation of the definition and criteria employed to identify heteroresistance. We recommend the definition of heteroresistance should include a consideration of the rate of return to susceptibility.

Introduction

Pathogens resistant to existing antibiotics are a significant and increasing source of morbidity and mortality for humans and domestic animals (1, 2). Fundamental to the effective treatment of bacterial infections is choosing an antibiotic to which the pathogen is susceptible. The level of susceptibility is readily estimated by culture methods, both through automation via BioMerieux's VITEK and similar devices (3-6), as well as by non-automated methods such as disk diffusion and Epsilon-diffusion tests (7, 8). By these methods, bacteria are classified as susceptible, intermediate, or resistant according to the international consensus guidelines from the Clinical and Laboratory Standards Institute (CLSI) and the European Committee on Antimicrobial Susceptibility Testing (EUCAST). These categorical descriptions determine whether an antibiotic will or will not be used for treatment. If an isolate appears susceptible to an antibiotic by these criteria, the drug would be presumed to be effective in treating infections with that pathogen. These *in vitro* susceptibility estimates are not sufficient as measures of antibiotic susceptibility if the treated bacteria are heteroresistant to that drug.

A population of bacteria which is heteroresistant often appears susceptible to an antibiotic as assessed by the standard methods described above, but quickly becomes resistant upon confrontation with that drug due to the selection for and ascent of minority resistant populations. Heteroresistance (HR) is typically defined in an operational manner by the presence of one or more sub-populations at a frequency greater than 10^{-7} with a resistance level that crosses the breakpoint at or greater than 8 times the susceptible main population (9). The canonical test for the presence of these sub-populations, and thus for HR, is a Population Analysis Profile (PAP) test (10, 11). This protocol tests for bacterial growth at different concentrations of an antibiotic, thus revealing the presence or absence of resistant sub-populations.

HR is clinically and epidemiology problematic due to the inherent instability of resistance. Within short order of the removal of the antibiotic, heteroresistant populations once again appear susceptible to the treating antibiotic by conventional testing procedures. This effect is most profound when considering the transmission of heteroresistant populations between individuals. Patients with heteroresistant infections transmit these

seemingly antibiotic-susceptible bacteria to other patients, who may then fail treatment with the drug for which the bacteria are HR. This instability of resistance is intrinsic to HR but is not currently part of the definition and thus is considered in few reports of HR (12).

In this report, we develop and analyze the properties of two mathematical and computer-simulation models that represent two extreme cases of HR, which we call progressive and non-progressive. Using these models, we explore the pharmaco- and population dynamic processes responsible for HR and the factors which contribute to the instability of HR. The parameters of these models can be estimated, and the hypotheses generated therefrom tested and rejected *in vitro* and *in vivo*.

Results

Models of Heteroresistance

We open this consideration of the pharmaco- and population dynamics of HR with a description of the two mathematical models employed. For both models of HR, we assume a Hill function for the relationship between the concentration of the antibiotic, the concentration of the limiting resource, and the rates of growth and death of the bacteria, known as the pharmacodynamics (13-15).

Pharmacodynamics:

In accord with the Hill function, the net growth of bacteria exposed to a given antibiotic concentration is given by Equation 1.

$$\Pi_i(r, A) = \left(v_{MAXi} - \frac{\left[(v_{MAXi} - v_{MINi}) \cdot \left(\frac{A}{MIC_i} \right)^{\kappa_i} \right]}{\left(\frac{A}{MIC_i} \right)^{\kappa_i} - \left(\frac{v_{MINi}}{v_{MAXi}} \right)} \right) \cdot \psi(r)$$

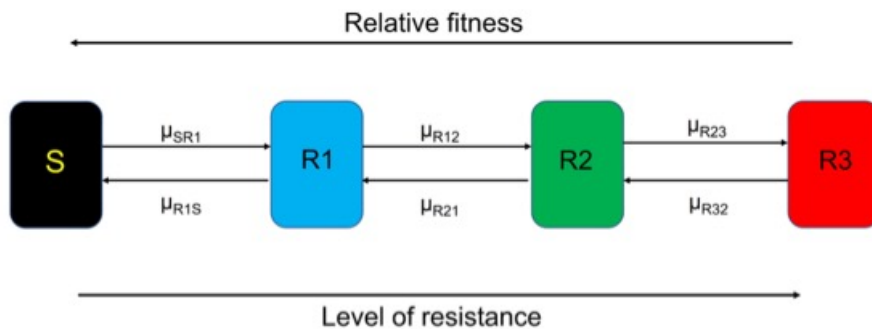
Equation 1

Where A in $\mu\text{g}/\text{mL}$ is the antibiotic concentration and r in $\mu\text{g}/\text{mL}$ is the concentration of the resource which limits the growth of the population. v_{MAXi} is the maximum growth rate in cells per hour of the bacteria of state i , where $v_{MAXi} > 0$. v_{MINi} is the minimum growth rate per cell per hour, which is the maximum death rate when exposed to the antibiotic, where $v_{MINi} < 0$. MIC_i (which is > 0) is the minimum inhibitory concentration of the antibiotic for the bacteria of state i in $\mu\text{g}/\text{mL}$. κ_i is the Hill coefficient for bacteria of state i . The greater the value of κ_i , the more acute the function. The Monod function (15), $\psi(r) = \frac{r}{(r+k)}$, is the rate of growth in the absence of the antibiotic, where k is the resource concentration in $\mu\text{g}/\text{mL}$ when the growth rate is half of its maximum value. $\psi(r)$ measures the physiological state of the bacteria; as the resource concentration declines the cells grow slower. We show in Supplemental Figure 1 the Hill functions for four different bacterial populations with varying MICs and maximum growth rates.

Diagrams of the Heteroresistance Models:

The two models of heteroresistance used here are depicted in Figure 1. In the progressive model (Figure 1A) the increasingly resistant states are generated by a transition from a less resistant state to a more resistant state, and the more resistant states generate the less resistant states sequentially. In the non-progressive model (Figure 1B) the different resistant states are generated directly by a transition from the susceptible state, and the more resistant states transition directly back to the most sensitive state.

A



B

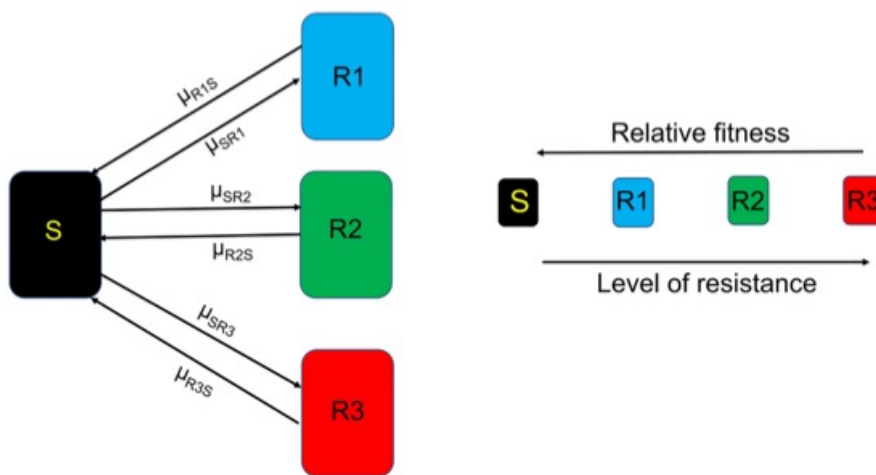


Figure 1. Diagram of the two models of HR. S (black) is the most antibiotic-sensitive state and the state with the highest fitness. We assume the level of antibiotic resistance increases as the fitness decreases from state R1 (blue) to R2 (green) to R3 (red). Transitions occur between states at potentially different rates of μ (where μ_{ij} is the transition from i to j). Panel A is a diagram of the progressive model and panel B is a diagram of the non-progressive model.

The Progressive Model:

In this model (Figure 1A), the bacteria transition between four different states: sensitive, S, and increasingly resistant, R1, R2, R3, which are the designations and densities in cells per mL of bacteria of these different states. The total number of cells in a state is given by the product of the density of the state and the total volume, Vol. Cells of the S state transition to R1, R1 transitions to R2, and R2 transitions to R3 at rates μ_{SR1} , μ_{R1R2} , and μ_{R2R3} per cell per hour, respectively. Cells of resistant states progressively transition to the less resistant states, R3 to R2, R2 to R1, and R1 to S, with rates μ_{R3R2} , μ_{R2R1} , and μ_{R1S} per cell per hour. We simulate these transitions with a Monte Carlo process to account for the stochasticity that occurs during cell division related to either gene amplification or a point mutation at a specific locus due to the polymerase error rate (16). In this Monte Carlo process, a pseudo-random number x ($0 \leq x \leq 1$) is generated from a rectangular distribution (17). If x is less than the product of the total number of cells in the generating state, the transition rate (μ), the Monod function ($\psi(r)$), and the step size (dt) of the Euler method (18) employed for solving differential equation, then $1/(dt*Vol)$ cells are added to the recipient population and removed from the generating population. In the equations below, the transition of cells due to this process is expressed as MIJ , e.g. MR1S for transitions from R1 to S and MR21 for transitions from R2 to R1. For example, if S is 10^5 , μ_{SR1} is 10^{-7} , dt is 10^{-4} , Vol is 1, and $x < S*\mu_{SR1}*dt*Vol*\psi(r)$, which in this case is $10^{-6}*\psi(r)$, then $1/(dt*Vol)$ cells are removed from the S population and added to the R1 population, which in this case would mean that MSR1 is 10^4 cells. Practically, when MSR1 is plugged into the differential equations below, it means that for any given step of the Euler method from t to $t+dt$ we add $(1/(dt*Vol))*dt$ cells, so here there would be one cell added. In this model the assumption that there are 1 sensitive and 3 resistant states is arbitrary, but in reality there could be more or fewer states depending on the mechanism of HR. In the simulations presented in the main text, we assume the transition rates between states are equal in both directions and between states. We also assume that the transitions between states slows down with the decline in the physiological state of the cells in direct proportion to $\psi(r)$. With these definitions, assumptions, and the parameters defined and presented in Supplemental Table 1, the rates of change in the densities of the different populations are given by,

$$\frac{dr}{dt} = -e \cdot \psi(r) \cdot \underbrace{(v_S \cdot S + v_1 \cdot R1 + v_2 \cdot R2 + v_3 \cdot R3)}_{\text{Rate of consumption of the limiting resource}} \quad \text{Equation 2}$$

$$\frac{dS}{dt} = \underbrace{S \cdot \Pi_S(r, A)}_{\text{Growth of } S} + \underbrace{MR1S - MSR1}_{\text{Monte Carlo Transitions}} \quad \text{Equation 3}$$

$$\frac{dR1}{dt} = \underbrace{R1 \cdot \Pi_{R1}(r, A)}_{\text{Growth of } R1} + \underbrace{MSR1 + MR21 - MR12 - MR1S}_{\text{Monte Carlo Transitions}} \quad \text{Equation 4}$$

$$\frac{dR2}{dt} = \underbrace{R2 \cdot \Pi_{R2}(r, A)}_{\text{Growth of } R2} + \underbrace{MR12 + MR32 - MR21 - MR23}_{\text{Monte Carlo Transitions}} \quad \text{Equation 5}$$

$$\frac{dR3}{dt} = \underbrace{R3 \cdot \Pi_{R3}(r, A)}_{\text{Growth of } R3} + \underbrace{MR23 - MR32}_{\text{Monte Carlo Transitions}} \quad \text{Equation 6}$$

The Non-progressive Model:

In this model (Figure 1B) all the resistant states, R1, R2, and R3 are derived from the susceptible state and, by transition, return directly to the susceptible state, S. The rates of transition from state S are respectively μ_{SR1} , μ_{SR2} , and μ_{SR3} per cell per hour. The rates of return to the susceptible state are μ_{R1S} , μ_{R2S} , and μ_{R3S} per cell per hour. The transitions between states are via a Monte Carlo process (16), using a routine like that for the progressive model. When transients from S to the different R states are generated (MSR1, MSR2, and MSR3), $1/(dt \cdot \text{Vol})$ are added to the R1, R2 and R3 populations and are removed from the S population. When transients from the R1, R2, and R3 populations are generated (MR1S, MR2S and MR3S), $1/(dt \cdot \text{Vol})$ are added to the S population and removed from the R1, R2, and R3 populations, respectively. Here, the primary assumption is that all resistant states are derived from and transition back to the sensitive state and we continue to assume there are four states with equal transition rates between them. With these definitions, assumptions, and the parameters defined and presented in Supplemental Table 1 the rates of change in the densities of the different populations are given by:

$$\frac{dr}{dt} = -e \cdot \psi(r) \cdot \underbrace{(v_S \cdot S + v_1 \cdot R1 + v_2 \cdot R2 + v_3 \cdot R3)}_{\text{Rate of consumption of the limiting resource}} \quad \text{Equation 7}$$

$$\frac{dS}{dt} = \underbrace{S \cdot \Pi_S(r, A)}_{\text{Growth of } S} - \underbrace{MSR1 - MSR2 - MSR3 + MR1S + MR2S + MR3S}_{\text{Monte Carlo Transitions}} \quad \text{Equation 8}$$

$$\frac{dR1}{dt} = \underbrace{R1 \cdot \Pi_{R1}(r, A)}_{\text{Growth of } R1} + \underbrace{MSR1 - MR1S}_{\text{Monte Carlo Transitions}} \quad \text{Equation 9}$$

$$\frac{dR2}{dt} = \underbrace{R2 \cdot \Pi_{R2}(r, A)}_{\text{Growth of } R2} + \underbrace{MSR2 - MR2S}_{\text{Monte Carlo Transitions}} \quad \text{Equation 10}$$

$$\frac{dR3}{dt} = \underbrace{R3 \cdot \Pi_{R3}(r, A)}_{\text{Growth of } R3} + \underbrace{MSR3 - MR3S}_{\text{Monte Carlo Transitions}} \quad \text{Equation 11}$$

Simulated Population Dynamics of Heteroresistance

Here we consider the population dynamics of heteroresistance with the distributions of the different resistant states generated from single cells grown up to full densities for the progressive and non-progressive models with four transition rates (Figure 2). We further consider a greater range of transition rates for the non-progressive model to determine the minimum rate for which we generate sufficiently large minority populations in Supplemental Figure 2A-C.

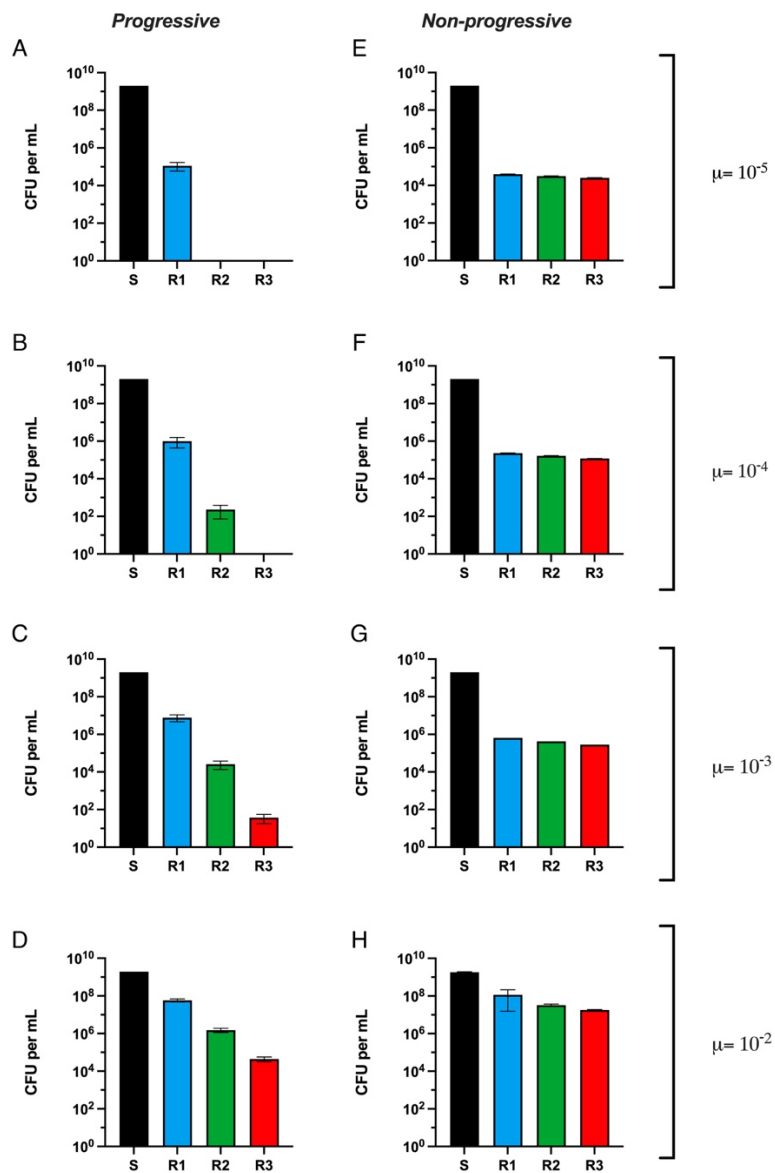


Figure 2. Distribution of stationary phase densities when grown up from a single cell of S. Shown on the left (A, B, C, and D) are the means and standard deviations of the stationary phase densities of the S (black), R1 (blue), R2 (green), and R3 (red) populations from five independent runs with the progressive model with different transition rates, $\mu=10^{-5}$, 10^{-4} , 10^{-3} , and 10^{-2} per cell per hour for A, B, C, and D, respectively. On the right, E, F, G, and H are the corresponding distributions for runs made with the non-progressive model with these respective transition rates.

For the progressive model, only in the runs with the highest transition rates, $\mu=10^{-2}$ and $\mu=10^{-3}$ per cell per hour, is the subpopulation with the highest resistance level, R3, present. A very different situation obtains for the non-progressive model, as at every transition rate the R3 population is present. We also consider the effect that the relative fitness cost of each state has on these stationary phase densities (Supplemental Figure 3) and find modest differences in these distributions.

Using these same parameters for both models, another difference can be seen between the progressive and non-progressive models in the Population Analysis Profile (PAP) tests of each (Figure 3). For these PAP tests, we calculate the ratio of the number of cells generated at a particular antibiotic concentration compared to the number of cells present when there is no antibiotic ($N(A)/N(0)$) for 0, 1, 2, 4, 8, and 16 times the MIC of the susceptible population.

The PAP test results anticipated from the progressive model are very different than those anticipated from the non-progressive model, two extreme HR cases. The presence of four sub-populations with different MICs is apparent from the PAP test of the progressive model with the parameters considered. For the non-progressive model, the differences in the relative densities of the sub-populations are too low to be detected by a PAP test performed in the lab. In general, the plateaus shown in Figure 3 A and B are sharper and more dramatic than would be seen in the lab. This is a consequence of having only three resistant states. Moreover, using the standard HR criteria of having a sub-population with an MIC of >8 times at a frequency of at least 10^{-7} , the progressive model only meets these criteria at high transition rates (exceeding 10^{-4}). On the other hand, the non-progressive model meets these criteria at transition rates as low as 10^{-7} (Supplemental Figure 2D).

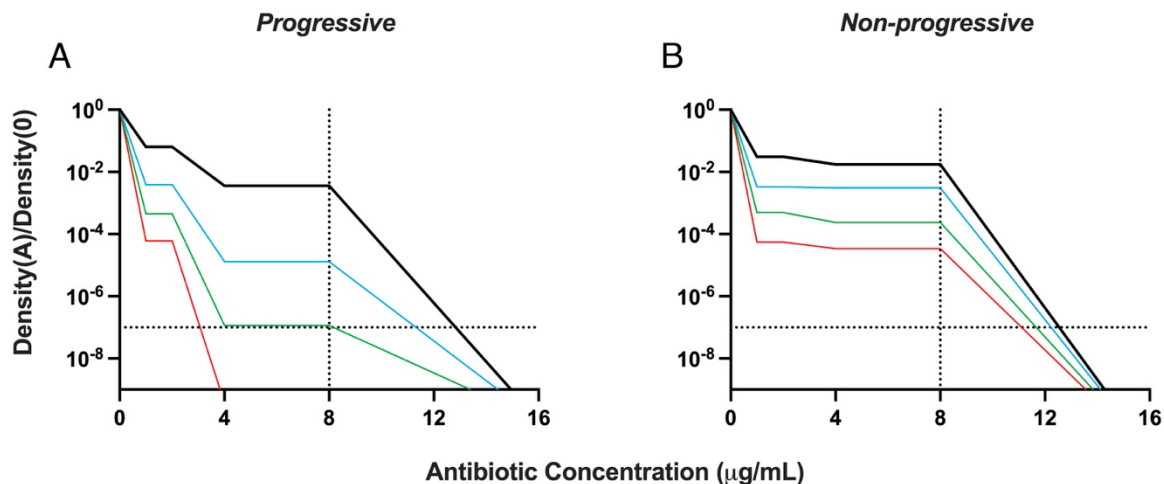


Figure 3. Population Analysis Profile (PAP) tests. The ratio of the density of the number of bacteria surviving at an antibiotic concentration relative to that surviving in the absence of the antibiotic for different transition rates. Black $\mu=10^{-2}$, blue $\mu=10^{-3}$, green $\mu=10^{-4}$, and red $\mu=10^{-5}$ per cell per hour. Panel A is the PAP test using the progressive model and Panel B is the PAP test using the non-progressive model.

To explore how these models differ in their response to antibiotic treatment, we follow the changes in the densities and MICs of heteroresistant populations exposed to two antibiotic concentrations (5 $\mu\text{g}/\text{mL}$ and 10 $\mu\text{g}/\text{mL}$ corresponding to 5x and 10x the MIC of the susceptible population) when $\mu=10^{-2}$ and $\mu=10^{-5}$ per cell per hour (Supplemental Figure 4). We initiate these simulations with 1/100 of the stationary phase densities of the different states anticipated from the heteroresistant populations depicted in Figure 2D and A and Figure 2H and E for the progressive and non-progressive models of heteroresistance, respectively. In Supplemental Figure 5, we consider the effect that the fitness cost of resistance has on these dynamics and find the effect modest at best, just slowing the response time to the antibiotic.

There are apparent differences in the bacterial response to antibiotics between the progressive and non-progressive models of HR. For both models, when $\mu=10^{-2}$ per cell per hour, the R3 population comes to dominate and the MIC increases to the maximum (15 $\mu\text{g}/\text{mL}$), though with the higher concentration of the drug, it takes longer for the R3 population to become dominant. With the lower transition rate of $\mu=10^{-5}$ per cell per hour, at 5 $\mu\text{g}/\text{mL}$ of antibiotic the R2 population comes to dominate in the progressive model and the

R3 population remains minor. At this same transition rate and at 10 $\mu\text{g}/\text{mL}$, resistance does not evolve, and the bacterial populations are lost. In both cases, the MIC does increase but does not go to the maximum value. For these conditions, in the non-progressive model, sub-populations are always able to respond to the antibiotic and are never eliminated.

Upon removal of the antibiotic, the heteroresistant bacterial population reverts to the sensitive state. This reversion is the case for both the progressive and non-progressive models of HR considered here. To illustrate this and elucidate the relative contributions of the rates of transition between states and the fitness cost of resistance (as measured by the growth rates) to the dynamics and the time needed to restore susceptibility, we use serial transfer forms of the progressive and non-progressive versions of the HR models. In these simulations, the populations are grown for 24 hours, diluted by a factor of 100, and fresh resources added. In Figure 4, we present the results of simulations of the changes in the densities of the susceptible and resistant populations as well as the change in average MIC in serial transfer following the removal of the antibiotics. These serial transfer simulations were initiated with 10^7 bacteria per mL of the highest resistance level, R3. We consider two major conditions: one where the fitness cost of resistance is high and another where the fitness cost of resistance is low. In the supplemental materials we consider the dynamics of reversion when a set of even higher fitness costs are used (Supplemental Figure 6).

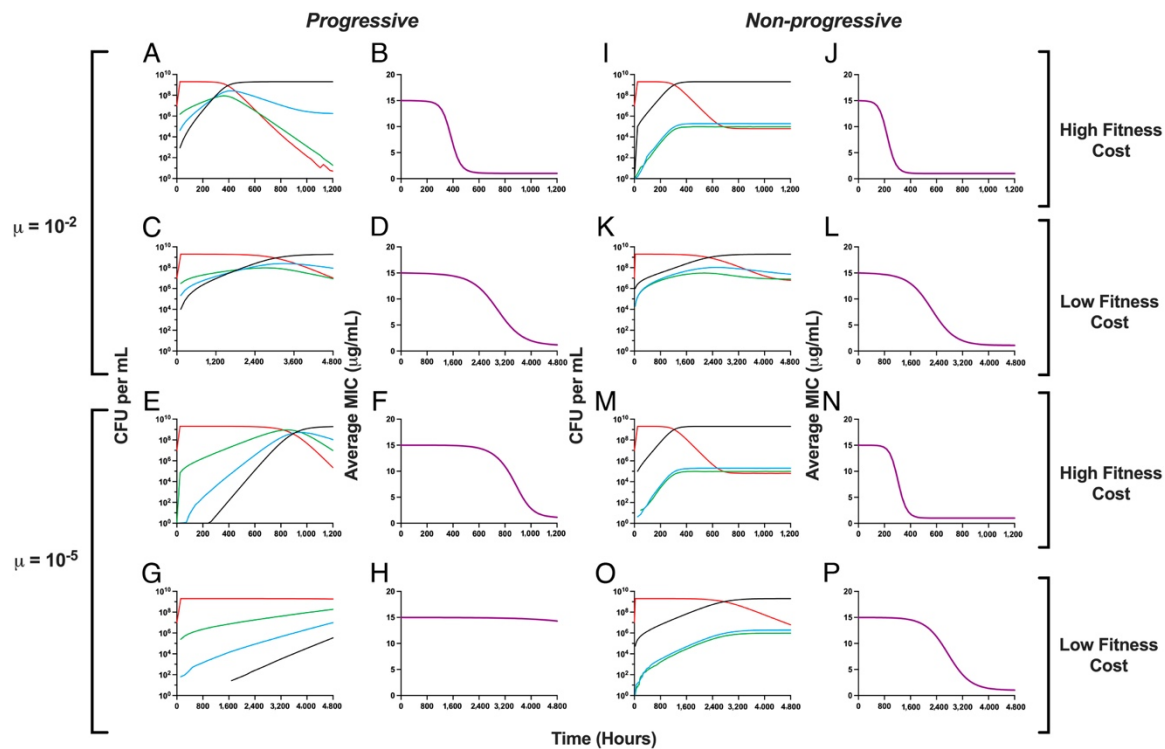


Figure 4. Response of the two heteroresistant models to the removal of antibiotics. Changes in the densities of the susceptible and resistant populations in the absence of the antibiotic and changes in the average MIC. S (black), R1 (blue), R2 (green), and R3 (red). Simulations with the high fitness cost were run for 1200 hours (50 days), while simulations with the low fitness cost were run for 4800 hours (200 days).

In the absence of antibiotics, the populations become increasingly dominated by more susceptible populations for both the progressive and non-progressive models of HR. This change in the composition of the populations is also reflected in a decline in the average MIC, approaching the level of the susceptible population. With the same fitness parameter and transition rates between states, μ , the rate of return to the susceptible state is greater for the non-progressive model than the progressive model. For both models, the rate of return to the sensitive state is proportional to the transition rate between states, μ , and the relative fitness cost of resistance. Notably, the new apparent equilibria obtained for both models differ substantially. In the progressive model, the most resistant populations are in continuous decline and will ultimately be lost or nearly so, while in the non-progressive model, all resistant populations are present at roughly equal frequency and appear to be in

equilibrium. Of note is the vast difference in the time needed for the susceptible population to come to dominate; we list these times in Supplemental Table 2.

Discussion

To elucidate the factors that govern the response of heteroresistant populations to antibiotics, we use mathematical and computer-simulation models to explore quantitatively: i) the factors responsible for generating the distribution of resistant sub-populations, ii) the response of heteroresistant populations to different concentrations of antibiotics, and iii) the amount of time required for an antibiotic-resistant heteroresistant population to become susceptible again when the treating antibiotic is removed.

We consider two models of heteroresistance (HR), which we call progressive and non-progressive. In both models, there are one or more sub-populations with different levels of resistance. In the progressive model, the more susceptible state transitions sequentially to the more resistant states, which in turn transition back to the less resistant states in the same sequence. In the non-progressive model, the susceptible population transitions directly to all the resistant states from the susceptible state before transitioning back directly to the susceptible state. In both models, the transition rates between states and the relative fitness cost of being resistant determine the distribution of the resistant populations in the absence of and in response to antibiotics.

The difference in the distribution of resistant states between these models with the parameters used is apparent with a Population Analysis Profile (PAP) test. With the progressive model, there are different resistance levels with distinct relative densities, which decline as the concentration of the antibiotic increases. With the non-progressive model, although there are multiple sub-populations with different levels of resistance, they likely would not appear as separate populations in a PAP test. The PAP test of the non-progressive HR looks more like that which would obtain with only two resistance levels, sensitive and resistant. However, the PAP tests are insufficient to differentiate the two models of HR, as there are conditions where non-progressive HR would look progressive (Supplemental Figure 7).

The models are also distinct in how they respond to antibiotics. In the progressive model, if the drug concentration is above the MIC of any of the sub-populations and the transition rate is low, the most resistant population can fail to emerge and ascend; this is true even though the drug concentration is still less than the MIC of the most resistant population. With the non-progressive model, the highest level of resistance will always emerge, no matter the transition rate. There are also differences in the population dynamics of each

model when the antibiotics are removed. In the progressive model, the average MIC will return to that of the most susceptible population, and the most resistant populations will be lost. In contrast, in the non-progressive model, the average MIC will not decrease to that of the most susceptible population, and all the resistant sub-populations will remain present. One implication of this is when confronted with antibiotics, a heteroresistant population which is non-progressive will respond to the drugs more consistently and more rapidly than a progressive heteroresistant population.

The standard for detecting and defining a strain as heteroresistant is the PAP test which requires sub-populations to be more frequent than 10^{-7} and to have an MIC $>8x$ that of the susceptible main population (9). These tests are cumbersome, costly, and are unlikely to be performed in clinical microbiology labs. Most critically, our results demonstrate that the PAP test is not sufficient to detect HR. There are conditions with the progressive and non-progressive models where populations would fail to meet the criteria set by the PAP test but would still survive confrontation with high doses of antibiotics – a false negative (Supplemental Figure 2D). There are also conditions where stable resistance would meet the HR criteria set by the PAP test – a false positive (Supplemental Figure 8). The resistance that occurs in Supplemental Figure 8 is a canonical point mutation in *rpoB* which does not have a fitness cost and will not revert (19). Moreover, there are conditions that would be called HR despite requiring thousands of hours to return to a sensitive MIC. These results point to both a failing of the PAP test and to the insufficiency of the operational definition of HR. To address the definitional issue, we recommend revisiting this operational definition to include the rate at which the MIC of potentially heteroresistant strains return to a susceptible MIC as proposed in our model to better capture the underlying biology of HR (12). This is especially important, as the epidemiological risk of HR is the rapid return to a seemingly sensitive state, and as demonstrated experimentally, this can happen in less than 50 generations for certain types of HR (12, 20, 21).

At this juncture, it is not clear how important HR is clinically even though animal experiments (22, 23) and some clinical studies suggest that it can increase the risk of persistent bacteremia, lead to longer hospital stays, and increase mortality (12). We argue that within a single infected individual, the distinction between the emergence of stable resistance and HR is manifest in the risk of treatment failure. With both mechanisms,

antibiotics can select for the ascent of resistant sub-populations which will result in reduced treatment efficacy or even treatment failure, likely leading clinicians to change the treating drug in both cases. This risk of treatment failure is probabilistic in HR, as it is in stable resistance, due to other factors not considered here such as the host's immune system, the compartmental heterogeneity and the chronicity of infection, the total density of infecting bacteria, and the local antibiotic concentrations. Due to the combination of these factors, treatment of a heteroresistant strain with a drug for which it is HR, will not necessarily lead to treatment failure. One distinction between HR and stable resistance is the rapid reversion of a heteroresistant population from a resistant to a susceptible state. This reversion has an additional clinical implication when considering infection transmission between individuals. Should an individual be infected with bacteria that are stably resistant to a drug, that resistance would appear on an assay such as the VITEK, and the drug for which they are resistant would not be used. If that individual is infected with heteroresistant bacteria, it would initially appear sensitive to a treating drug, but resistance could rapidly ascend. Then if that individual passes the infection on to another individual, due to the transient nature of HR, that infection would once again appear susceptible to the drug and once again the wrong drug would be chosen to treat the infection.

Although this study is purely theoretical, the parameters used in these models can be estimated experimentally with different species of bacteria and antibiotics of different classes. The hypotheses generated herein can be tested *in vitro* and, most importantly, can be rejected. There exists evidence supporting these two classes of HR, primarily in the form of PAP tests of known heteroresistant strains as exemplified by data shown in Supplemental Figure 9. A key objective for future experimental work is to determine how the actual mechanisms that can generate an unstable heteroresistant phenotype relate to these theoretical models. At present, we know of two main mechanisms that can generate HR: (i) alterations in copy number of resistance genes or their regulators by either tandem amplifications and/or alterations in plasmid copy number (12, 20, 24, 25), and (ii) regular point mutations that occur at a high frequency (20, 26-28). It is likely that mutational HR is best described by the non-progressive model where instability and reversion to susceptibility is driven by compensatory mutations that concomitantly reduce the fitness costs of the resistance mutations and lead to the loss of resistance (29-31). For gene amplification mechanisms it is less clear which theoretical model best

describes their behavior since these mechanisms could have properties compatible with either model alone or a combination of the two, depending on the actual mechanism by which the amplifications are formed and lost. Further experimental work is needed to clarify these points. Finally, an unstable and transient resistant minority population could potentially also be generated by other types of mechanisms than those presently identified, including inducible resistances, epigenetic changes, and gene conversion events (32).

While our models are agnostic to mechanism and to the underlying bacteria and antibiotic, ultimately, we are interested in and believe our results have clinical implications for the design and implementation of antibiotic treatment regimens. For example, in bacteria such as *E. coli*, *K. pneumoniae*, *A. baumannii* and *S. aureus* mutations in genes involved in, for example, electron transport, cell wall biosynthesis and two-component regulatory systems can lead to resistance to colistin, gentamicin, oxacillin, daptomycin and teichoplanin (18, 24-26, 33). These types of mutations, which are difficult to detect under the standard susceptibility testing conditions, could lead to the rapid emergence of resistance *in vivo* — which would be a type of non-progressive HR. Progressive heteroresistance also necessarily starts by single events which are not detectable in antibiotic susceptibility testing, but only reach clinically relevant levels of resistance after several events, as seen with stepwise gene amplifications of various genes conferring resistance to b-lactams, aminoglycosides, colistin and tetracyclines (24-26, 30). The impact of the reversion rate to the treatment of infected individuals is difficult to evaluate in acute infections. However, the importance of the reversion rate is critical for understanding the level of antibiotic resistance. In the supplemental text and Supplemental Table 3, we provide examples of mechanisms across several drug classes that have been shown to or could hypothetically generate a HR phenotype, predict which model of HR would most accurately pertain, and discuss further clinical implications.

There are, of course, caveats to consider with our models. Firstly, our models are not mechanistic and do not consider the genetic basis of progressive versus non-progressive HR and, as mentioned above, there are likely cases where certain mechanisms (e.g. gene amplification) could look either progressive, non-progressive, or somewhere in between depending on their specific mechanistic properties. Secondly, our models only include three resistant states, and these resistant states either do not transition between each other (non-progressive)

or transition sequentially (progressive) – two extreme cases. Lastly, as with all pharmacodynamic studies, some elements have been neglected from these models, as mentioned previously, the host's immune system and the compartmental heterogeneity of infection such as biofilms and abscesses, as well as variation in local antibiotic concentrations, all of which prohibit *in vitro* models and studies from making solid clinical predictions. All in all, a clear next step would be to test these predictions *in vitro* and then move to an *in vivo* model system. Crucially, we need to develop an understanding of how the definition of HR matches with the clinical implications, specifically considering the frequency and MIC cutoffs previously defined.

Materials and Methods

Numerical Solutions (Simulations): For our numerical analysis of the coupled, ordered differential equations presented (Equations 2-11) we used Berkeley Madonna with the parameters presented in Supplemental Table 1. Copies of the Berkeley Madonna programs used for these simulations are available at www.eclf.net. In the analysis of our simulations, to calculate average MIC we take a weighted average of the MIC of each population.

Bacteria: *Enterobacter cloacae* Mu208 is a carbapenem-resistant isolate collected by the Georgia Emerging Infections Program Multi-site Gram-negative Surveillance Initiative and described previously (23). *Burkholderia cepacia* complex isolate JC8 is a cystic fibrosis patient isolate collected by the Georgia Emerging Infections Program Multi-site Gram-negative Surveillance Initiative. *Escherichia coli* MG1655 was obtained from the Levin Lab's bacterial collection.

Rifampin Population Analysis Profile tests: Single colonies of *E. coli* MG1655 were inoculated into 10 mL lysogeny broth (BD, USA, Product #244610) and grown overnight at 37°C with shaking. Cultures were serially diluted in saline and all dilutions (10^0 to 10^{-7}) plated on LB agar plates (BD, USA, Product #244510) containing 0, 1, 2, 4, 8, and 16 times the MIC of rifampin (Thermo Fisher, USA, Product #J60836.03). Plates were grown at 37°C for 48 hours before the density of surviving colonies was estimated.

Burkholderia and *Enterobacter* Population Analysis Profile tests: Single colonies of *B. cepacia* complex isolate JC8 and *E. cloacae* Mu208 were inoculated into 1.5 mL Mueller-Hinton broth (BD, USA, Product #275730) and cultures were grown overnight at 37°C with shaking. Cultures were serially diluted in phosphate-buffered saline and 10 μ L of each dilution was spotted on Mueller-Hinton agar (BD, USA, Product #225250) plates containing 0, 0.125, 0.25, 0.5, 1, 2, and 4 times the breakpoint concentration of each antibiotic. Antibiotics used were ticarcillin disodium (BioVision, USA, Product #B1536) with clavulanate potassium salt (Cayman Chemical Company, USA, Product #19456), amikacin sulfate (AstaTech, USA, Product # 40003), colistin sulfate salt (Sigma-Aldrich, USA, Product # C4461), and fosfomycin disodium salt (TCI America, USA, Product # F0889). For Mu208 on fosfomycin, broth and agar included 25 μ g/mL glucose-6-phosphate (Sigma-Aldrich, USA, Product #10127647001). Plates were maintained at 37°C overnight for Mu208 and for 36-60 hours for JC8.

Acknowledgements

We thank Dr. Danielle Steed for her discussion of the clinical implications of this manuscript. The authors would also like to thank Jason Chen, generally.

Funding Sources

BRL, DIA, and DSW thank the U.S. National Institute of General Medical Sciences for their funding support via R35GM136407, the U.S. National Institute of Allergy and Infectious Diseases for their funding support via U19AI158080-02, and the Emory University Antibiotic Resistance Center. FB acknowledges the support of CIBERESP (CB06/02/0053) from the Carlos III Institute of Health of Spain. The funding sources had no role in the design of this study and will not have any role during its execution, analysis, interpretation of the data, or drafting of this report. The content is solely the responsibility of the authors and do not necessarily represent the official views of the National Institutes of Health nor those of the Carlos III Institute of Health of Spain.

Data Availability

The Berkeley Madonna programs used for these simulations are available at ECLF.net. All data are presented in this article or its supplementary materials.

References

1. B. Bengtsson, C. Greko, Antibiotic resistance--consequences for animal health, welfare, and food production. *Ups J Med Sci* **119**, 96-102 (2014).
2. C. J. L. Murray *et al.*, Global burden of bacterial antimicrobial resistance in 2019: a systematic analysis. *The Lancet* **399**, 629-655 (2022).
3. A. P. MacGowan, R. Wise, Establishing MIC breakpoints and the interpretation of in vitro susceptibility tests. *J Antimicrob Chemother* **48 Suppl 1**, 17-28 (2001).
4. R. Humphries, A. M. Bobenchik, J. A. Hindler, A. N. Schuetz, Overview of Changes to the Clinical and Laboratory Standards Institute Performance Standards for Antimicrobial Susceptibility Testing, M100, 31st Edition. *J Clin Microbiol* **59**, e0021321 (2021).
5. M. Bardelli *et al.*, A side-by-side comparison of the performance and time-and-motion data of VITEK MS. *Eur J Clin Microbiol Infect Dis* **41**, 1115-1125 (2022).
6. Anonymous, Comité de l'Antibiogramme de la Société Française de Microbiologie report 2003. *Int J Antimicrob Agents* **21**, 364-391 (2003).
7. H. M. Ericsson, J. C. Sherris, Antibiotic sensitivity testing. Report of an international collaborative study. *Acta Pathol Microbiol Scand B Microbiol Immunol* **217**, Suppl 217:211+ (1971).
8. D. F. Brown, L. Brown, Evaluation of the E test, a novel method of quantifying antimicrobial activity. *J Antimicrob Chemother* **27**, 185-190 (1991).
9. M. E. Falagas, G. C. Makris, G. Dimopoulos, D. K. Matthaiou, Heteroresistance: a concern of increasing clinical significance? *Clin Microbiol Infect* **14**, 101-104 (2008).
10. K. Hiramatsu *et al.*, Dissemination in Japanese hospitals of strains of *Staphylococcus aureus* heterogeneously resistant to vancomycin. *Lancet* **350**, 1670-1673 (1997).
11. O. M. El-Halfawy, M. A. Valvano, Antimicrobial heteroresistance: an emerging field in need of clarity. *Clinical microbiology reviews* **28**, 191-207 (2015).

12. D. I. Andersson, H. Nicoloff, K. Hjort, Mechanisms and clinical relevance of bacterial heteroresistance. *Nature Reviews Microbiology* **17**, 479-496 (2019).
13. R. R. Regoes *et al.*, Pharmacodynamic functions: a multiparameter approach to the design of antibiotic treatment regimens. *Antimicrobial agents and chemotherapy* **48**, 3670-3676 (2004).
14. B. A. Berryhill *et al.*, What's the Matter with MICs: Bacterial Nutrition, Limiting Resources, and Antibiotic Pharmacodynamics. *Microbiology Spectrum*, e04091-04022 (2023).
15. J. Monod, The growth of bacterial cultures. *Annual review of microbiology* **3**, 371-394 (1949).
16. N. Metropolis, S. Ulam, The Monte Carlo Method. *Journal of the American Statistical Association* **44**, 335-341 (1949).
17. J. E. Gentle, *Random Number Generation and Monte Carlo Methods* (Springer, 1998).
18. G. Wanner, E. Hairer, *Solving ordinary differential equations II* (Springer Berlin Heidelberg New York, 1996), vol. 375.
19. M. G. Reynolds, Compensatory Evolution in Rifampin-Resistant Escherichia coli. *Genetics* **156**, 1471-1481 (2000).
20. H. Nicoloff, K. Hjort, B. R. Levin, D. I. Andersson, The high prevalence of antibiotic heteroresistance in pathogenic bacteria is mainly caused by gene amplification. *Nature Microbiology* **4**, 504-514 (2019).
21. C. Pereira, J. Larsson, K. Hjort, J. Elf, D. I. Andersson, The highly dynamic nature of bacterial heteroresistance impairs its clinical detection. *Communications Biology* **4**, 521 (2021).
22. V. I. Band *et al.*, Carbapenem-Resistant Klebsiella pneumoniae Exhibiting Clinically Undetected Colistin Heteroresistance Leads to Treatment Failure in a Murine Model of Infection. *mBio* **9** (2018).
23. V. I. Band *et al.*, Antibiotic combinations that exploit heteroresistance to multiple drugs effectively control infection. *Nat Microbiol* **4**, 1627-1635 (2019).

24. K. Hjort, H. Nicoloff, D. I. Andersson, Unstable tandem gene amplification generates heteroresistance (variation in resistance within a population) to colistin in *Salmonella enterica*. *Mol Microbiol* **102**, 274-289 (2016).
25. S. E. Anderson, E. X. Sherman, D. S. Weiss, P. N. Rather, Aminoglycoside Heteroresistance in *Acinetobacter baumannii* AB5075. *mSphere* **3** (2018).
26. Y. Charretier *et al.*, Colistin Heteroresistance and Involvement of the PmrAB Regulatory System in *Acinetobacter baumannii*. *Antimicrob Agents Chemother* **62** (2018).
27. T. Halaby *et al.*, Genomic Characterization of Colistin Heteroresistance in *Klebsiella pneumoniae* during a Nosocomial Outbreak. *Antimicrob Agents Chemother* **60**, 6837-6843 (2016).
28. A. Jayol, P. Nordmann, A. Brink, L. Poirel, Heteroresistance to colistin in *Klebsiella pneumoniae* associated with alterations in the PhoPQ regulatory system. *Antimicrob Agents Chemother* **59**, 2780-2784 (2015).
29. D. I. Andersson, B. R. Levin, The biological cost of antibiotic resistance. *Curr Opin Microbiol* **2**, 489-493 (1999).
30. D. I. Andersson, D. Hughes, Antibiotic resistance and its cost: is it possible to reverse resistance? *Nat Rev Microbiol* **8**, 260-271 (2010).
31. R. C. Allen, J. Engelstädter, S. Bonhoeffer, B. A. McDonald, A. R. Hall, Reversing resistance: different routes and common themes across pathogens. *Proc Biol Sci* **284** (2017).
32. V. G. Meka *et al.*, Reversion to susceptibility in a linezolid-resistant clinical isolate of *Staphylococcus aureus*. *J Antimicrob Chemother* **54**, 818-820 (2004).
33. S. Heidarian, A. Guliaev, H. Nicoloff, K. Hjort, D. I. Andersson, High prevalence of heteroresistance in *Staphylococcus aureus* is caused by a multitude of mutations in core genes. *PLoS Biology* **22**, e3002457 (2024).

Supporting Information

Supporting Information Text

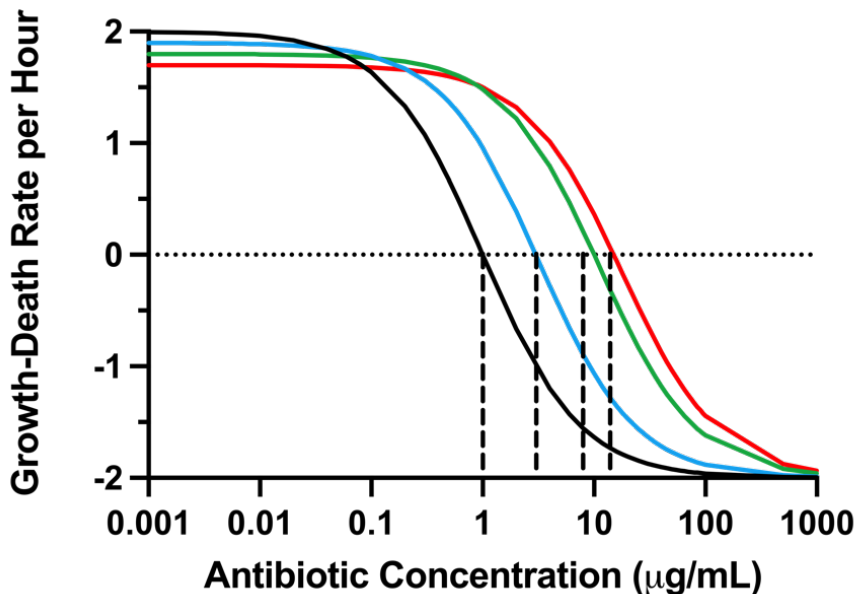
By definition, a heteroresistant strain of bacteria contains one or more resistant sub-populations at a high frequency (greater than 10^{-7}) and with an MIC at least 8x higher than the dominant, susceptible population. For non-progressive HR, all resistant subpopulations emerge by transition directly from the susceptible population. In the progressive model of HR, several sequential transitional steps are required to generate the most resistant population. These resistant subpopulations grow in the presence of the antibiotic, making this phenomenon distinct from persistence. Therefore, HR could have a greater clinical impact on antibiotic treatment than persistence. In most cases, HR remains under-detected by routine susceptibility testing. In Supplemental Table 2 we present examples of genes and mechanisms by which HR may emerge for eleven different classes of antibiotics. It should be noted that the response of one bacteria to one antibiotic could fit both the progressive and non-progressive HR models (Supplemental Figures 5 and 7).

As predicted by our simulated PAP tests and observed in previous data, the frequency of some heteroresistant sub-populations are below the 10^{-7} frequency. Though these strains may be below the definitional threshold, they are still of clinical interest, since the absolute number of cells in some infection sites can easily surpass 10^7 cells.

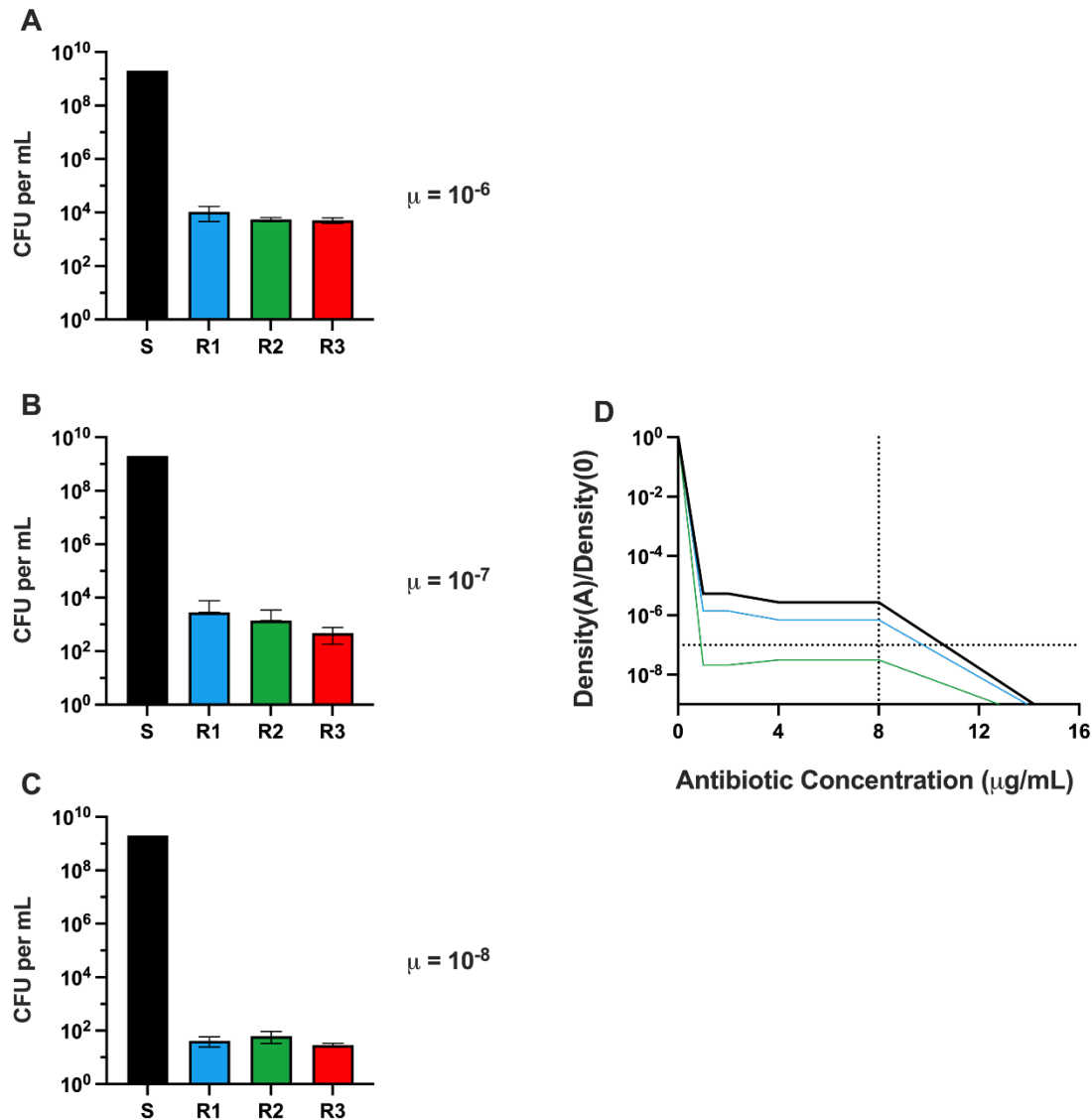
In principle, the transition rate both to and from resistance in both models would depend on the mechanism, underlying fitness cost of being resistant, and frequency of fitness cost compensatory mutations. In Supplemental Table 2, we consider the potential rates both to and from resistance based on mechanism and fitness cost.

The difference in mechanism and transition rates leads us to propose different antibiotic treatment regimens to deal with either progressive or non-progressive heteroresistant infections. For an infection with a non-progressive heteroresistant bacteria, wherein a resistant sub-population could rapidly replace the sensitive population, we suggest frequent (optimally, daily) surveillance of the susceptibility of the bacteria. After a successful therapy, in the case of relapse, susceptibility may be rapidly restored and the same antibiotic could be reconsidered for therapy. We, of course, recommend ensuring that susceptibility has been restored before

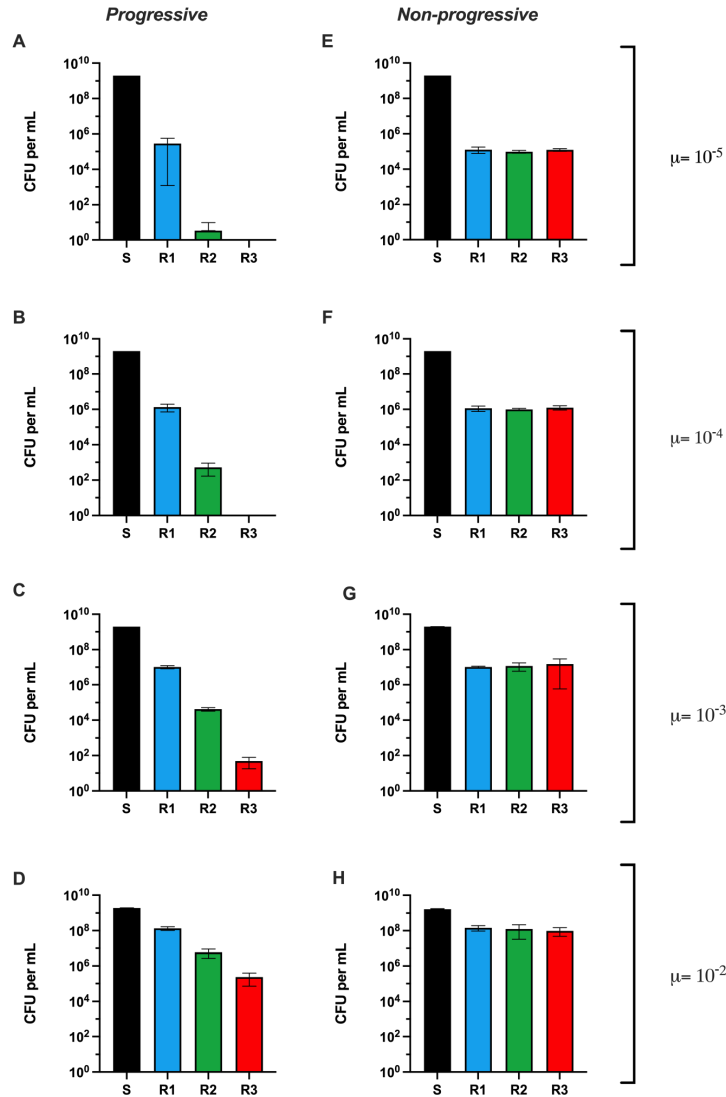
reusing the same antibiotic. For an infection with a progressive heteroresistant bacteria, it is critical to prevent the evolution of the first resistant state. This may be done by increasing the dose of the antibiotic. In the case of progressive HR, susceptibility testing need not be done as frequently as with the non-progressive bacteria. Should treatment fail and the infection relapse, the same antibiotic should not be used as the transition from resistant to sensitive is expected to take a longer time than in the case of a non-progressive heteroresistant infection. In general, if an infecting bacteria is shown to be heteroresistant, antibiotic combinations should always be considered, especially in high-risk patients.



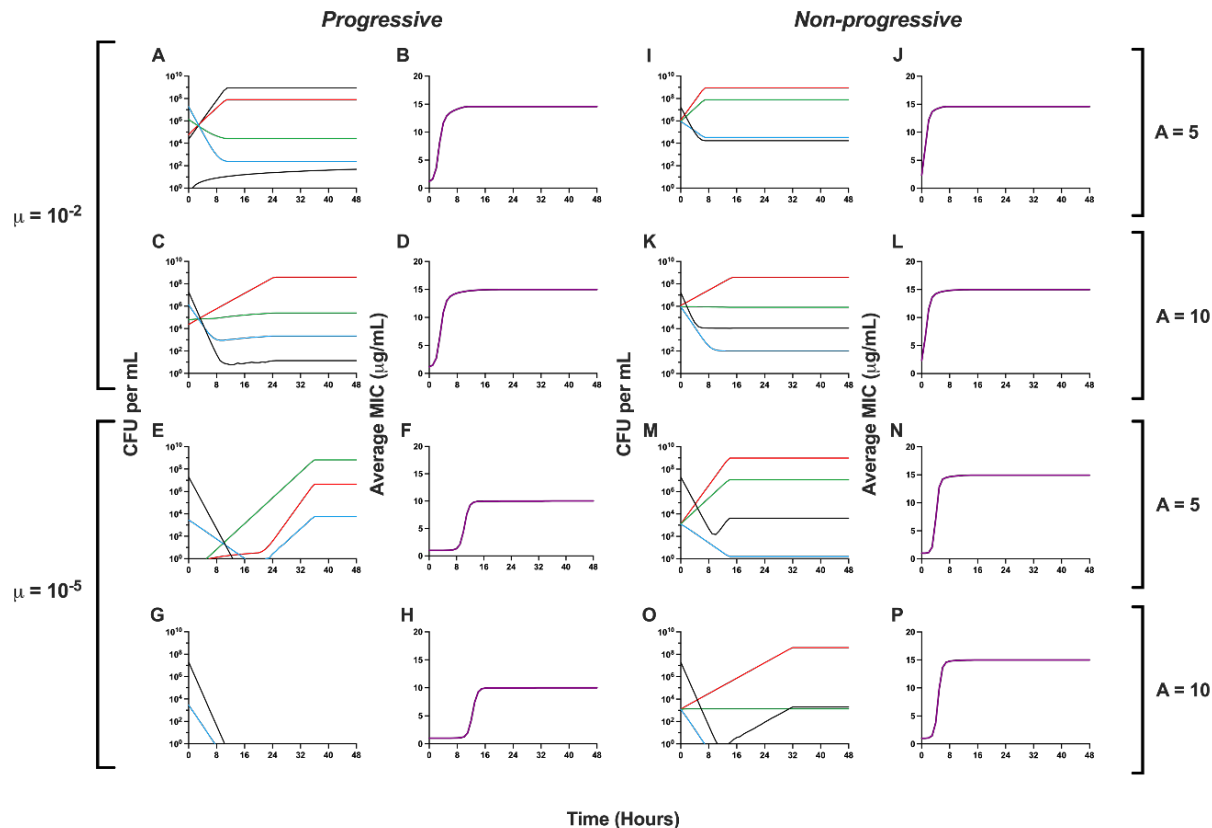
Supplemental Figure 1. Hill function pharmacodynamics. The relationship between the antibiotic concentration and the rate of growth and death of the bacteria. The four bacterial populations, S (black), R1 (blue), R2 (green), and R3 (red) differ in their maximum growth rates, $v_S = 2.0$, $v_{R1} = 1.9$, $v_{R2} = 1.8$, $v_{R3} = 1.7$ per cell per hour, respectively. These bacteria also differ in the resistance levels as measured by their respective MICs, $MIC_S = 1.0$, $MIC_{R1} = 3.0$, $MIC_{R2} = 8.0$, $MIC_{R3} = 15.0$ $\mu\text{g/mL}$, respectively. All the bacteria have the same negative growth rate, $v_{MIN} = -2.0$ per cell per hour and the same Hill coefficient, $\kappa = 1.0$. For the depicted pharmacodynamics, we assume that there is no limitation in the concentration of the resource.



Supplemental Figure 2. Non-Progressive model with low transition rates. (A-C) The distribution of stationary phase densities when grown up from a single cell of S with three different transition rates. A: $\mu=10^{-6}$, B: $\mu=10^{-7}$, C: $\mu=10^{-8}$. (D) A corresponding PAP test when $\mu=10^{-6}$ (Black), $\mu=10^{-7}$ (Blue), and $\mu=10^{-8}$ (Green). Parameters used in this figure: maximum growth rates, $v_S=2.0$, $v_{R1}=1.9$, $v_{R2}=1.8$, $v_{R3}=1.7$ per cell per hour, $MIC_S=1.0$, $MIC_{R1}=3.0$, $MIC_{R2}=10.0$, and $MIC_{R3}=15$ $\mu\text{g/mL}$. S (black), R1(blue), R2 (green), R3 (red).

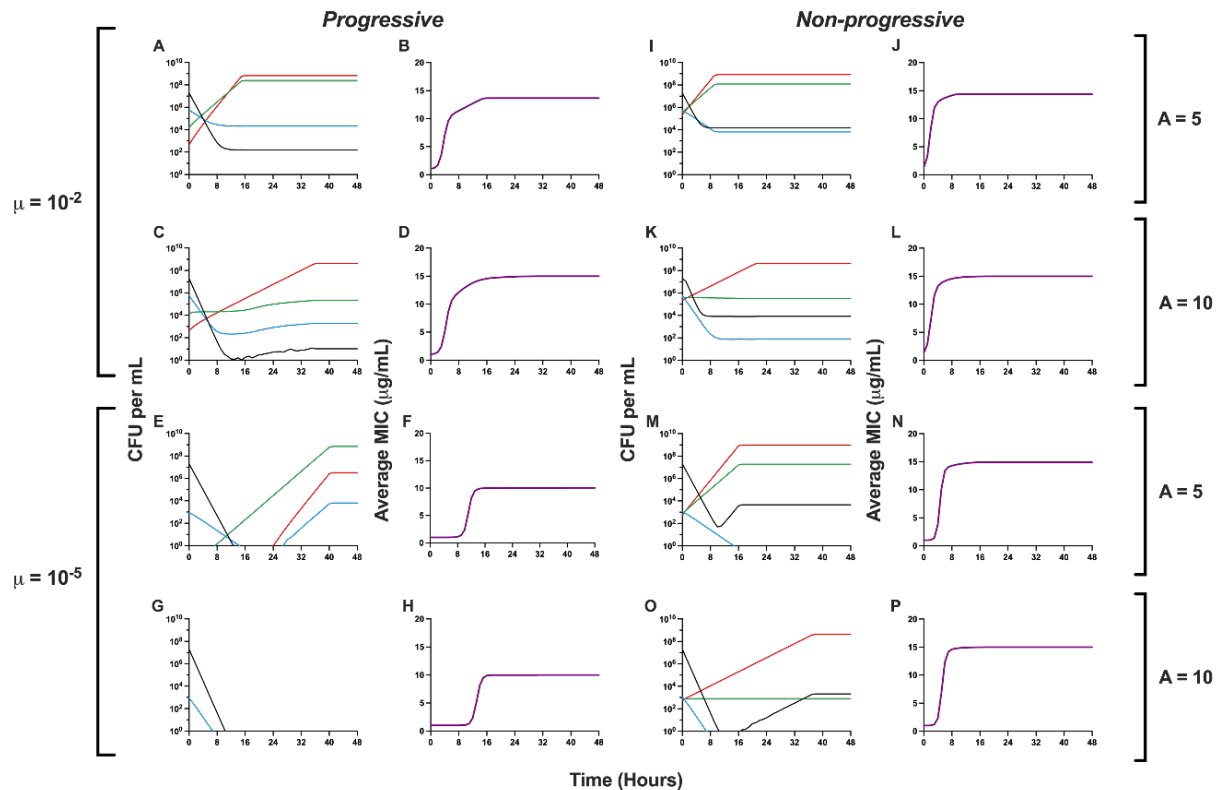


Supplemental Figure 3. Distribution of stationary phase densities with grown up from a single S cell with a low fitness cost. Shown on the left (A, B, C, and D) are the means and standard deviations of the stationary phase densities of the S (black), R1 (blue), R2 (green), and R3 (red) subpopulations from five independent runs with the progressive model with different transition rates, $\mu=10^{-5}$, 10^{-4} , 10^{-3} , and 10^{-2} per cell per hour for A, B, C, and D, respectively. On the right (E, F, G, and H) are the corresponding distributions for runs made with the non-progressive model with these respective transition rates. Unlike in the main body, this figure assumes a low fitness cost with maximum growth rates, $v_S=2.0$, $v_{R1}=1.99$, $v_{R2}=1.98$, and $v_{R3}=1.97$ per cell per hour.

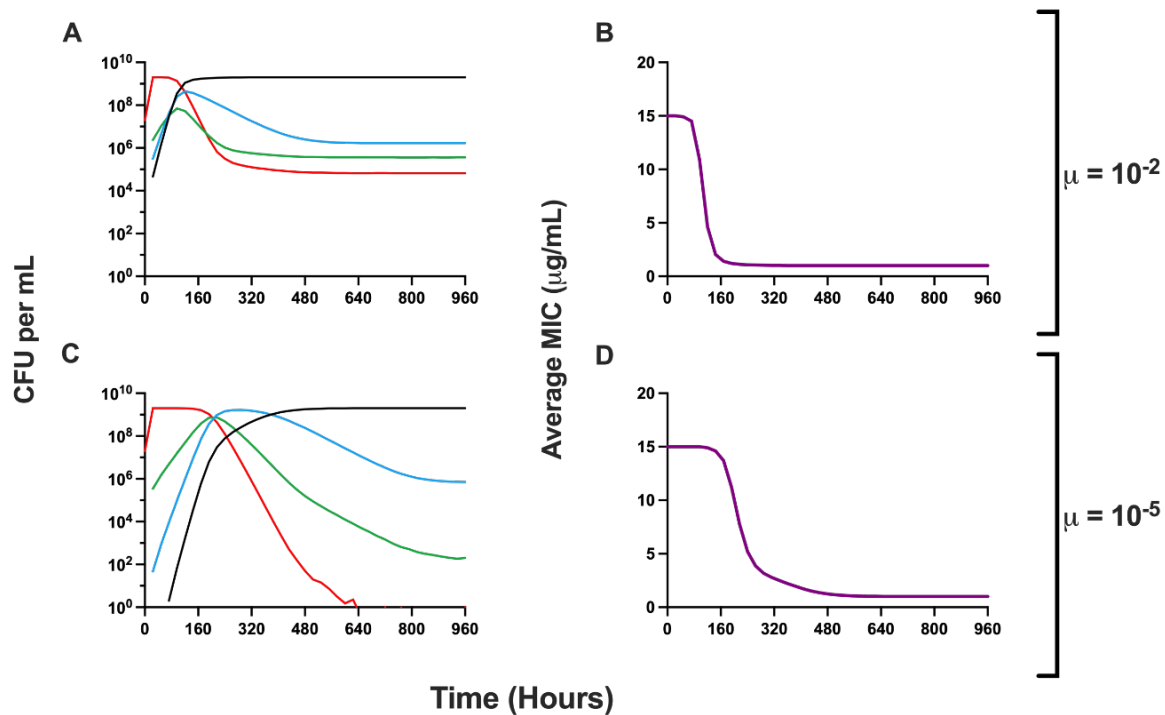


Supplemental Figure 4. Response of heteroresistant populations to two concentrations of antibiotics.

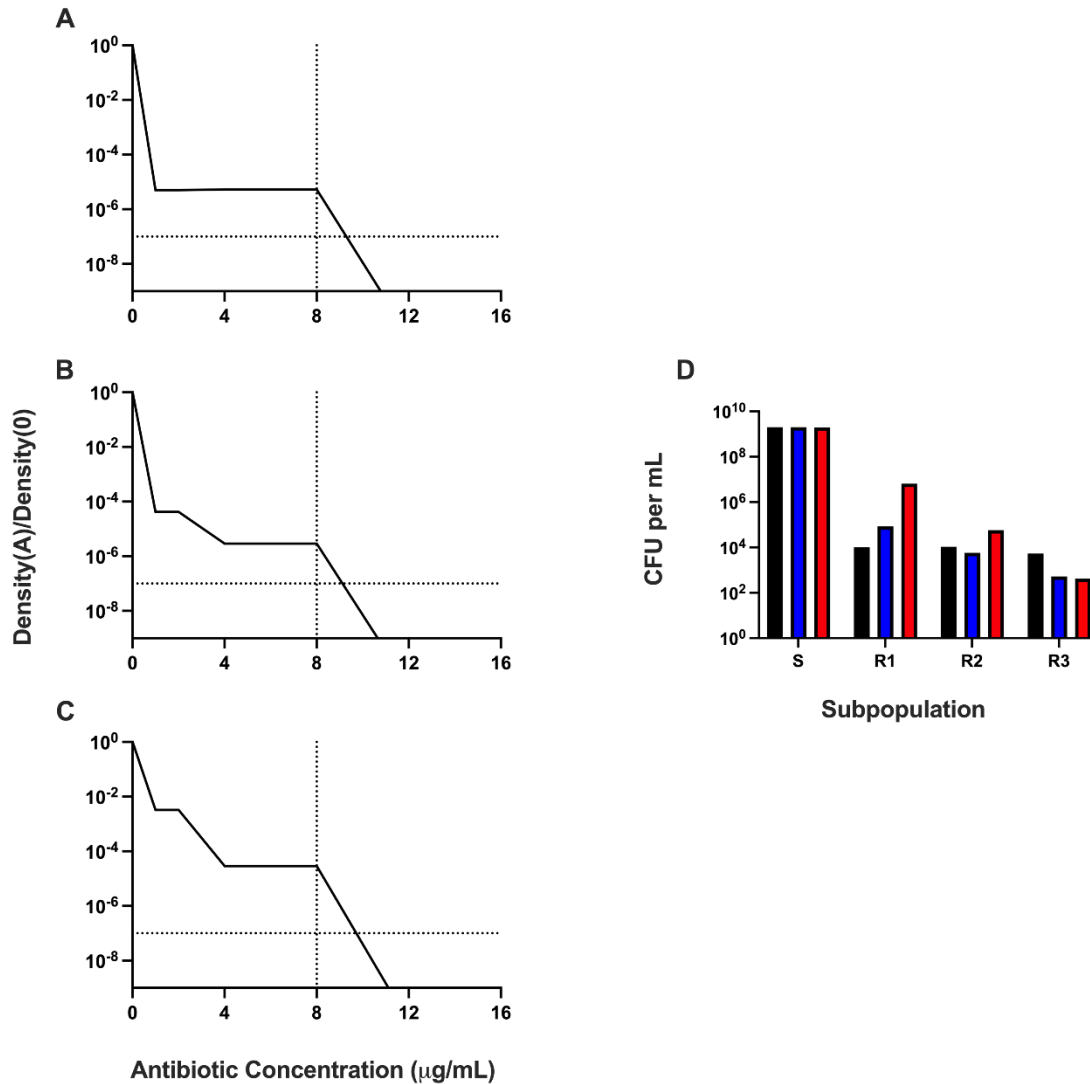
Changes in the densities of the susceptible and the different resistant populations and the average MIC where $\mu=10^{-2}$ or $\mu=10^{-5}$ per cell per hour when exposed to either 5 $\mu\text{g}/\text{mL}$ or 10 $\mu\text{g}/\text{mL}$ (5x and 10x the MIC of the susceptible main population) of the antibiotic. S (black), R1 (blue), R2 (green), and R3 (red). The initial densities for the progressive and non-progressive simulations are 1/100 of the densities presented in Figure 3D and A and Figure 3H and E respectively with the given transition rate.



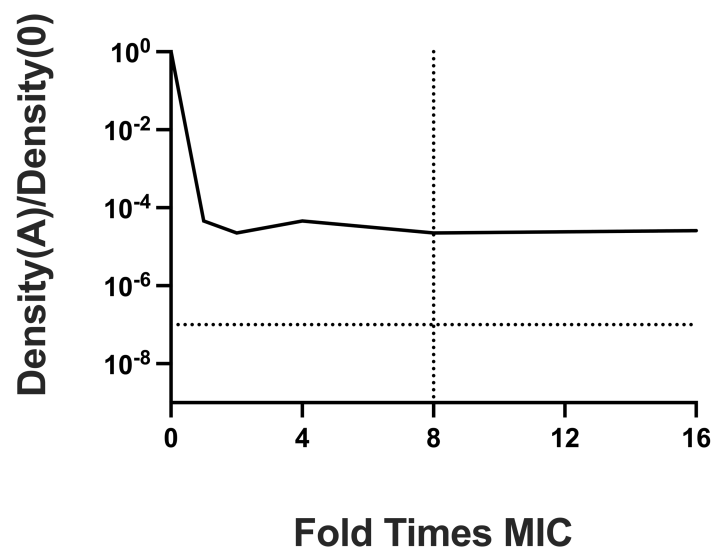
Supplemental Figure 5. Response of heteroresistant populations to different concentrations of antibiotics with a low fitness cost. Changes in the densities of the sensitive and different resistant populations and the average MIC where $\mu=10^{-2}$ or $\mu=10^{-5}$ per cell per hour when exposed to either 5 $\mu\text{g}/\text{mL}$ or 10 $\mu\text{g}/\text{mL}$ of the antibiotic. S (black), R1 (blue), R2 (green), and R3 (red). Low fitness cost maximum growth rates, $v_S=2.0$, $v_{R1}=1.99$, $v_{R2}=1.98$, and $v_{R3}=1.97$ per cell per hour.



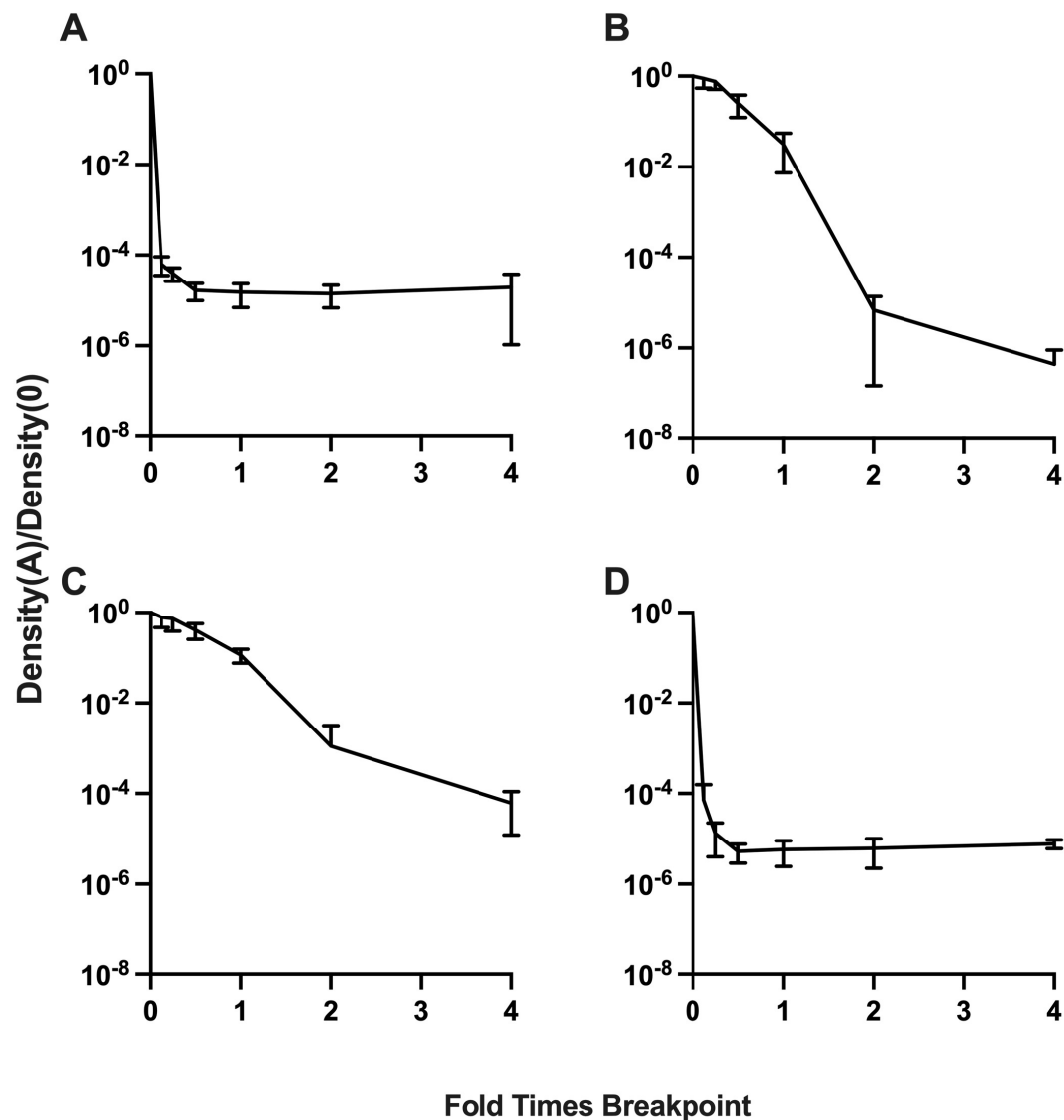
Supplement Figure 6. Response of the two heteroresistant models to the removal of antibiotics with a very high fitness cost. Changes in the densities of the susceptible and resistant populations in the absence of the antibiotic and changes in the average MIC. S (black), R1 (blue), R2 (green), and R3 (red). Simulations with the very high fitness cost were run for 500 hours (approximately 20 days). The return to sensitive when $\mu=10^{-2}$ occurs at 110 hours (approximately 5 days) and when $\mu=10^{-5}$ it takes 370 hours (approximately 15 days).



Supplemental Figure 7. Population analysis profiles for the non-progressive model with different transition rates between states. (A) PAP test with transition rates $\mu=10^{-6}$ per cell per hour. (B) PAP test with transition rates $\mu_{SR1}=\mu_{R1S}=10^{-5}$, $\mu_{SR2}=\mu_{R2S}=10^{-6}$, and $\mu_{SR3}=\mu_{R3S}=10^{-7}$ per cell per hour. (C) PAP test with transition rates $\mu_{SR1}=\mu_{R1S}=10^{-3}$, $\mu_{SR2}=\mu_{R2S}=10^{-5}$, and $\mu_{SR3}=\mu_{R3S}=10^{-7}$ per cell per hour. (D) Distribution of stationary phase densities when grown up from a single cell of S with the transition rates from panel A (black), panel B (blue), and panel C (red). Parameters used in these simulations: maximum growth rates, $v_S=2.0$, $v_{R1}=1.9$, $v_{R2}=1.8$, $v_{R3}=1.7$ per cell per hour, $MIC_S=1.0$, $MIC_{R1}=3.0$, $MIC_{R2}=10.0$, and $MIC_{R3}=15$ $\mu\text{g/mL}$.



Supplemental Figure 8. Population Analysis Profiles of *Escherichia coli* with rifampin result in false positives. *E. coli* MG1655 stable resistant mutants appearing heteroresistant to rifampin.



Supplemental Figure 9. Empirical population analysis profiles. (A) *Burkholderia cepacia* JC8 complex heteroresistant to ticarcillin/clavulanate. (B) *B. cepacia* JC8 complex heteroresistant to amikacin. (C) *Enterobacter cloacae* Mu208 heteroresistant to fosfomycin. (D) *E. cloacae* Mu208 heteroresistant to colistin. Shown are means and standard deviations for each PAP test. Breakpoints used were: 128/2 $\mu\text{g}/\text{mL}$ ticarcillin/clavulanate, 64 $\mu\text{g}/\text{mL}$ amikacin, 256 $\mu\text{g}/\text{mL}$ fosfomycin, and 4 $\mu\text{g}/\text{mL}$ colistin.

Supplemental Table 1. Parameters used in the simulations

Parameter	Definition and Dimensions	Values
$V_s, V_{R1}, V_{R2}, V_{R3}$	Maximum growth rates (per cell/hr)	Very high High Low
		2.0, 1.7, 1.5, 1.2 2.0, 1.9, 1.8, 1.7 2.0, 1.99, 1.98, 1.97
μ_x	Transition rates (per cell/hr)	$10^{-2}, 10^{-3}, \dots, 10^{-8}$
V_{MIN}	Minimum growth/death rates (per cell/hr)	-2.0
k	Hill coefficient	1.0
$MIC_s, MIC_{R1}, MIC_{R2}, MIC_{R3}$	MIC ($\mu\text{g/mL}$)	1.0, 3.0, 10.0, 15.0
k	Monod constant	1.0
e	Resource conversion efficiency (μg)	5×10^{-7}
C	Maximum resource ($\mu\text{g/mL}$)	1000
A	Antibiotic concentration ($\mu\text{g/mL}$)	0, 5, 10
r	Resource concentration at a given time (μg)	$0 \leq r \leq 1000$

Supplemental Table 2. Time for the heteroresistant populations to return to sensitivity

Condition (Panel of Figure 4)	Approximate time in hours (days) before the sensitive population dominates
Progressive Model	
A	400 (16.7 days)
C	3000 (125 days)
E	900 (37.5 days)
G	8000 (333 days)
Non-progressive Model	
I	250 (10.4 days)
K	2400 (100 days)
M	300 (12.5 days)
O	2800 (117 days)

Supplemental Table 3. Examples (1-2) of non-progressive and progressive heteroresistance in different antibiotic classes

Antibiotic Class	Non-progressive HR	Progressive HR	Transition to Resistance	Transition to Susceptibility
Quinolones	<i>gyrA</i> mutations (nalidixic acid)	<i>gyrA</i> mutations (fluoroquinolones) <i>gyrA</i> + <i>parC</i> mutations (fluoroquinolones) <i>gyrA</i> and efflux pumps amplifications (nalidixic acid)	Fast	Slow, but fast in amplification
Aminoglycosides	<i>rpsL</i> mutations (streptomycin) <i>16S rRNA</i> A1402G mutation (kanamycin, gentamicin, and spectinomycin)	<i>aadB</i> amplifications <i>aac(3)IId</i> amplifications	Fast	Slow, but fast when either RpsL K43T compensatory mutation occurs for streptomycin or in amplification events
Beta-lactams	Penicillin binding proteins (PBPs) Outer membrane porin <i>oprD</i> (carbapenems) Inducible hyperexpression or de-repression of <i>ampC</i>	Beta-lactamases <i>bla</i> TEM-1, TEM-10, and TEM-12 mutations Beta-lactamase amplification PBPs mutations <i>oprD</i> mutations in combination with efflux pump mutations (carbapenems)	Fast	Fast or slow, depending on associated fitness cost
Macrolides	<i>23S rRNA</i> mutations L4, L22 ribosomal mutations	Overproduction or mutations in efflux pumps Progressive predominance of L4, L22 mutated ribosomes	Fast with low rRNA copy number	Fast due to high fitness cost
Rifampin	<i>rpoB</i> mutations		Fast	Fast due to <i>tufA</i> or <i>rpoB</i> Y526H compensatory mutations
Trimethoprim	<i>folA</i> mutations	Stepwise <i>folA</i> mutations	Fast	Slow
Linezolid		Single nucleotide transversion in <i>23S rRNA</i> (typically G2576) leading to recombination with other copies of the gene (gene conversion)	Slow	Fast
Fusidic acid	<i>fusA</i> mutations		Fast	Fast

Antibiotic Class	Non-progressive HR	Progressive HR	Transition to Resistance	Transition to Susceptibility
Lipo and glycopeptides		Mutations in <i>mprF</i> , <i>yycFG</i> operon and genes encoding subunits of RNA polymerase Amplification of <i>pmrD</i> , regulating genes encoding proteins that modify lipid A	Slow	Fast due to high fitness cost
Mupirocin	<i>ileS</i> mutations	Consecutive mutations in <i>ileS</i>	Fast	Slow
Fosfomycin	Mutations in <i>murA</i> , <i>ubpT</i> , and <i>glpT</i>		Fast (in the absence of glucose-6 phosphate)	Fast
Tigecycline Tetracyclines		Overproduction of efflux pumps AcrAB-TolC, OqxAB, and MacAB Sequential mutations in <i>ramR</i> , <i>lon</i> , and <i>rpsJ</i> Amplification of <i>tet(A)</i>	Fast	Fast

Supporting Information References

1. F. Baquero *et al.*, Evolutionary Pathways and Trajectories in Antibiotic Resistance. *Rev Clin Microbiol*, 34(4):e0005019 (2021).
2. C. Pereira *et al.*, The highly dynamic nature of bacterial heteroresistance impairs its clinical detection. *Communications Biology*, 4(1), 521 (2021).

Chapter 4

Chapter 4

The evolution of heteroresistance via small colony variants in *Escherichia coli* following long term exposure to bacteriostatic antibiotics

Reprinted from: Gil-Gil, T., Berryhill, B.A., Manuel, J.A. *et al.* The evolution of heteroresistance via small colony variants in *Escherichia coli* following long term exposure to bacteriostatic antibiotics. *Nat Commun* **15**, 7936 (2024). <https://doi.org/10.1038/s41467-024-52166-z>

Abstract

Traditionally, bacteriostatic antibiotics are agents able to arrest bacterial growth. Despite being traditionally viewed as unable to kill bacterial cells, when they are used clinically the outcome of these drugs is frequently as effective as when a bactericidal drug is used. We explore the dynamics of *Escherichia coli* after exposure to two ribosome-targeting bacteriostatic antibiotics, chloramphenicol and azithromycin, for thirty days. The results of our experiments provide evidence that bacteria exposed to these drugs replicate, evolve, and generate a sub-population of small colony variants (SCVs) which are resistant to multiple drugs. These SCVs contribute to the evolution of heteroresistance and rapidly revert to a susceptible state once the antibiotic is removed. Stated another way, exposure to bacteriostatic drugs selects for the evolution of heteroresistance in populations previously lacking this trait. More generally, our results question the definition of bacteriostasis as populations exposed to bacteriostatic drugs are replicating despite the lack of net growth.

Introduction

Antibiotics can be broadly classified as being bactericidal or bacteriostatic based on whether they kill bacteria or simply arrest their growth ¹. However, it is known that at high drug concentrations bacteriostatic drugs can and do kill bacteria. Intuitively, it would make sense to treat an infection with drugs that readily kill the infecting bacteria, the bactericidal drugs, and thereby eliminate the reliance on the host's immune system to clear the infection, as would be the case with bacteriostatic antibiotics. For this reason, bacteriostatic drugs have been considered "weaker" than bactericidal drugs and are not recommended for the treatment of severe infections or infections in immunodeficient patients ^{2,3}.

This distinction between bactericidal and bacteriostatic drugs is manifest in quantitative experimental studies of the pharmacodynamics (PD) of antibiotics and bacteria. These studies focus on the rates and dynamics of the drug's ability to kill exposed populations of bacteria ⁴⁻⁷. Many of the studies concerning why antibiotics fail to control bacterial infections have focused on phenomena solely belonging to bactericidal antibiotics such as persistence and tolerance, that is the ability to survive exposure to high concentrations of an antibiotic of a subpopulation or the whole bacterial population, respectively ^{6,8-10}. These traits are qualities only associated with bactericidal drugs: the bacteriostatic drugs do not kill, and consequently the minority surviving or slower-dying populations are not revealed. With much of the clinical application of antibiotics focusing on bactericidal drugs and the majority of the research on the PD of antibiotics and bacteria also focusing on bactericidal drugs, PD research on bacteriostatic drugs has been relatively neglected.

However, in recent years, clinicians have given less importance to the antibiotic's ability to kill bacteria *in vitro* and instead have focused on the outcome of treatment with these drugs. By this criterion, in many cases bacteriostatic antibiotics are as effective as bactericidal even in severe infections, with the possible exception of immunosuppressed patients ^{2,11}. The increase in use of bacteriostatic antibiotics could reduce the selection pressure for resistance to bactericidal agents used in these critical infections. However, the shift to using bacteriostatic antibiotics requires the development of quantitative measures of the PD of antibiotics that arrest

the growth of, rather than kill, bacteria ¹². One cannot solely characterize the PD of bacteriostatic antibiotics by the minimum concentration required to prevent the replication of exposed bacteria, the MIC ¹³. Furthermore, the evolution of genomic resistance for these agents is rare and the resistant traits tolerance or persistence that occur in bactericidal antibiotics are difficult to define and perhaps impossible to detect with these bacteriostatic agents ^{14,15}. This raises questions about the population and evolutionary dynamics of bacteria confronted with these drugs. If the bacteria exposed to bacteriostatic antibiotics are not replicating, one would not expect them to evolve. Therefore, more considerations of the pharmaco-, population, and evolutionary dynamics of bacteriostatic antibiotics are needed both academically and clinically.

In this study, we explore the pharmaco-, population, and evolutionary dynamics of *Escherichia coli* exposed to two bacteriostatic antibiotics of different classes, chloramphenicol (CHL) and azithromycin (AZM), over 30 days. While resistance did evolve over the 30 days, we did not detect any previously described resistance mechanisms, which include antibiotic efflux, decrease in membrane permeability, or antibiotic inactivation for CHL ¹⁶; nor the overproduction of efflux pumps or mutations in genes encoding the 23S rRNA subunit for AZM ¹⁷. The results of our experiments provide evidence that: (i) long-term exposure to these ribosome-targeting bacteriostatic antibiotics does not change the net density of exposed populations, (ii) despite the fact that the population's net density does not change, bacteria exposed to these drugs replicate, evolve, and generate small colony variants, and (iii) the selective pressure mediated by these drugs favors the evolution of heteroresistant populations, i.e. the emergence of resistant minority populations, in a strain previously lacking this trait.

Results

Long Term Exposure to Bacteriostatic Antibiotics

We begin our investigation into the effects of long-term exposure to ribosome-targeting bacteriostatic drugs by evaluating the impact that these agents have on bacterial survival over 30 days. We exposed four independent cultures of $\sim 10^5$ CFU/mL of *E. coli* MG1655 in glucose-limited minimal media to super-MIC (Minimum Inhibitory Concentration) concentrations of CHL and AZM for 30 days without transferring or diluting (Figure 1). One thousand $\mu\text{g}/\text{mL}$ of glucose was used since this concentration allows cultures to grow to maximum stationary densities while avoiding nutrient limitation. The MIC of CHL and AZM with MG1655 were estimated by broth microdilution in this glucose-limited minimal media and found to be 6.25 $\mu\text{g}/\text{mL}$ for both drugs¹³. Super-MIC concentrations of each drug that were shown to be bacteriostatic with minimal killing and/or growth were used in the experiment (Supplementary Figure 1). Cultures exposed to these drugs were sampled every 5 days. We observed that over the course of the experiment, the control cultures containing no drugs reached their maximum stationary phase density of approximately 10^9 CFU/mL and then went down by approximately two logs over the course of 30 days, while the densities in the cultures containing the drugs remained stable, with at most a half-log change in density in the drug-treated populations. Notably, in drug-treated cultures where the bacteria were not lost, two distinct colony morphologies emerged. The colonies were either similar to the ancestral wild-type *E. coli* or were much smaller bacterial colonies, small colony variants (SCVs). This evolution occurred while under strong selective pressure from these drugs. There was no change in colony size in the drug-free controls, with a limit of detection of 10^{-3} SCVs per colony of the ancestral population. These SCVs started to emerge at day 10 of the long-term experiment in cultures exposed to CHL and at day 15 in cultures exposed to AZM. Their frequency increased from 2-5% when they were first observed in the presence of both antibiotics to 10-44% in CHL and 10-50% in AZM by day 30. To assess the maintenance of the activity of the antibiotics after 30 days, bacteria resistant to the antibiotic in each culture was added at approximately 10^6 CFU/mL and over the course of 24 hours each culture grew approximately three orders of magnitude; while when the susceptible, wild-type *E. coli* strain was added to these 30 days supernatants it was not able to increase in density (Supplementary Figure 2). This residual growth indicates that at 30 days the

antibiotic is still at a super-MIC concentration and thereby is the limiting factor for growth in the long term experiments. Moreover, 0- and 30-day supernatants were filtered, and the amount of antibiotic present tested through a disk diffusion assay. The diameter of both time points was 1 cm for the CHL and 2.8 cm for the AZM supernatants confirming the stability of both antibiotics during the long term experiments.

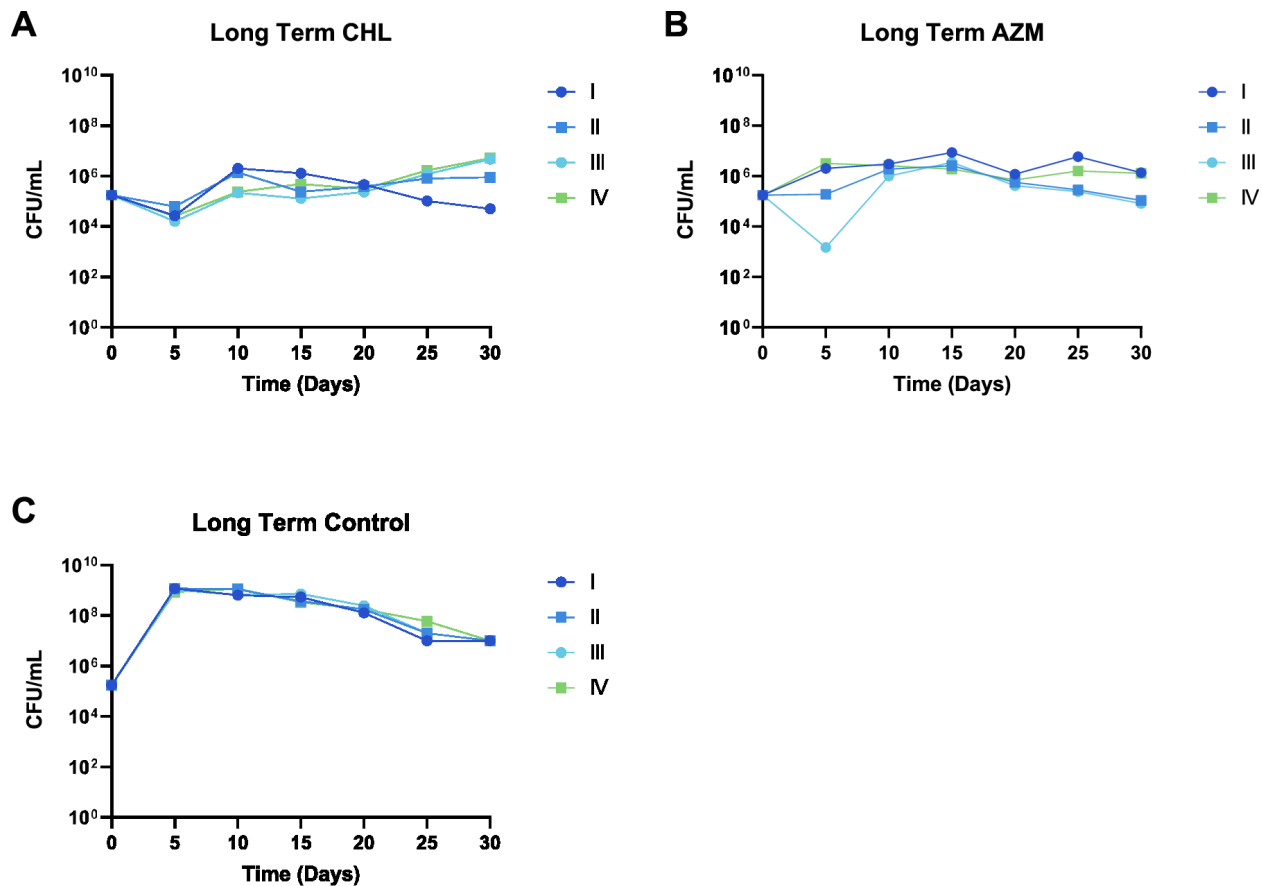


Fig 1. Long term exposure of *E. coli* to bacteriostatic drugs. Density in CFU/mL of *E. coli* MG1655 measured every 5 days for 30 days of 4 independent biological replicas (I-IV). **(A)** *E. coli* exposed to 4x MIC CHL (chloramphenicol); **(B)** *E. coli* exposed to 3x MIC AZM (azithromycin); **(C)** Drug-free control.

To determine how evolution is occurring in the apparent absence of net growth in the presence of the antibiotic, we performed a long term experiment using a conditionally non-replicative plasmid¹⁸ to identify if growth is occurring at the same rate as death (Figure 2). After 10 days the plasmid frequency decreased by 100-fold, and after 20 days the plasmid frequency was near the limit of detection. That means that the plasmid containing

cells are progressively diluted (as each cell division gives rise to a plasmid-free descendant) and indicates that the population is growing, replicating at least once a day and dying at the same rate. To explain how these results are consistent with the hypothesis that is occurring at the same rate as death, we constructed a mathematical and computer-simulation model of the plasmid being lost both with and without bacteriostatic drugs (Supplementary Text, Supplementary Equations 1-4, and Supplementary Figure 3).

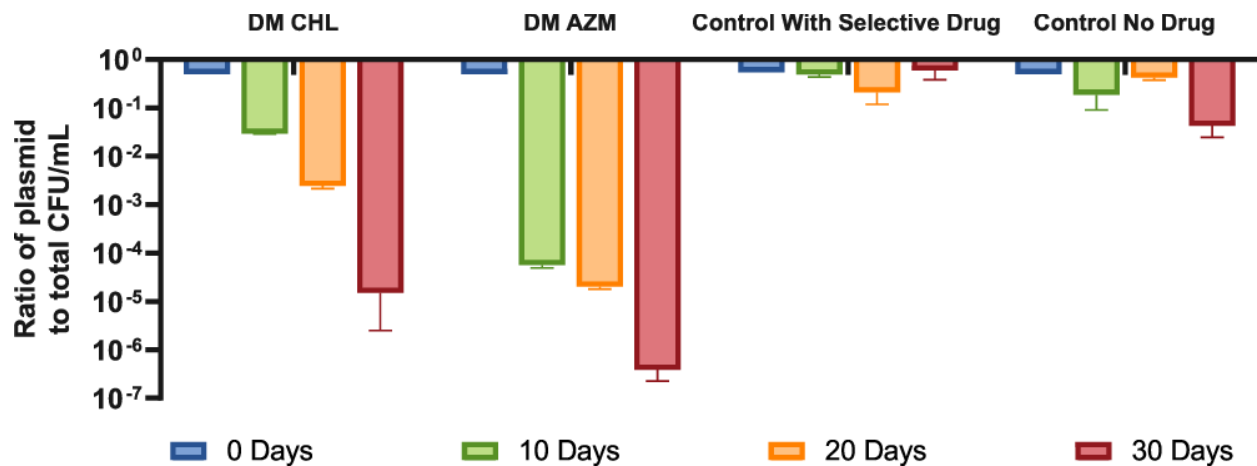


Fig 2. Long term experiment with a non-replicative plasmid. Ratio of the plasmid-containing cells to the total number of cells in CFU/mL of *E. coli* MG1655 with the non-replicative plasmid pAM34 which bears an ampicillin resistance cassette. The total cell density and density of cells bearing the plasmid were measured every 10 days for 30 days of 4 independent biological replicas for four conditions: i) minimal media with CHL (chloramphenicol), ii) minimal media with AZM (azithromycin), iii) minimal media with ampicillin– maximal plasmid retention, iv) minimal media with no antibiotic– maximal plasmid loss. In the absence of CHL or AZM the initial cultures can only grow two logs until arriving to a maximum stationary phase, explaining the maximum loss of two log in the absence of ampicillin.

Small Colony Variants Characterization

To determine what these SCVs are, we isolated 6 independently generated SCVs of MG1655 (CHL A, CHL B, CHL C, AZM A, AZM B, and AZM C) and characterized them phenotypically and genotypically. Firstly, to determine if the SCVs are a form of resistance that has emerged over the long-term experiment, their MIC to

the drugs they were previously exposed to (Figure 3). Each SCV showed at least an 8-fold change over the ancestral MG1655's MIC. On the other hand, normal-sized colonies from each culture were isolated and changes in MIC respecting the ancestral MG1655 were not observed in any of them. Each SCV has a distinct antibiotic susceptibility profile in terms of collateral susceptibilities and cross-resistances (Supplementary Figure 4).

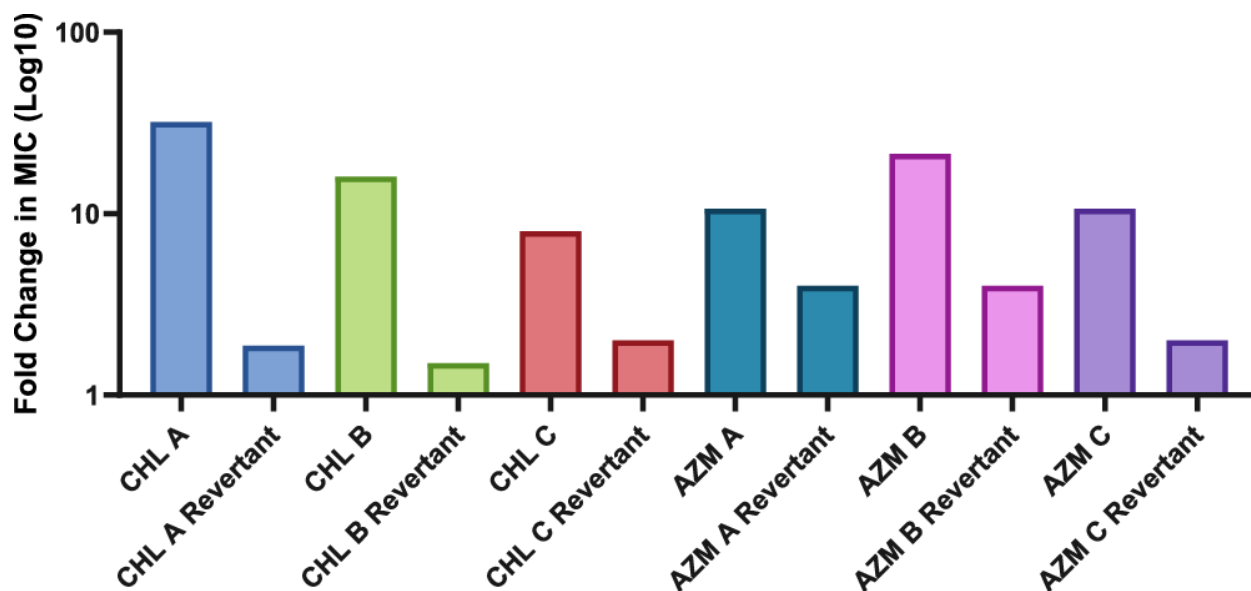


Fig 3. MIC of the SCVs to their respective drugs. Three SCVs were isolated from each condition from day 30 of the long term experiment, grown up in 1.5x *E. coli* MG1655's MIC for these respective drug, and then E-tested. Fold change respecting the MIC of the final evolved control populations, whose MIC was 6.25 $\mu\text{g}/\text{mL}$ as it was at the start of the long-term experiment.

Notably, although these SCVs are resistant to the bacteriostatic antibiotic to which they were exposed, there is very little net growth in the long term culture over the course of 30 days. To determine why a marked increase in density does not occur despite the evolution of resistance, we performed OD-based growth experiments of the SCVs with different concentrations of antibiotics. We found that even though these mutants are resistant, their growth rates and the maximum optical densities decreased proportionally to the drug concentration and

their lag time was substantially increased (Supplementary Figure 5). This result is consistent with previous observations¹³.

Antibiotic resistance in the small colonies obtained from both CHL and AZM cultures was unstable, that is, when streaked on LB plates without the drug the MIC of the SCVs decrease. After the genotypic characterization of these SCVs we do find genetic differences in most of them (Supplementary Table 1), but we could not find a clear mechanism that would explain this resistance. While we could not identify causal genetic differences between the SCVs and their ancestor MG1655, since both CHL and AZM prevent translation, we sought to determine if there were differences in the rate or total level of translation. Testing the level of a constitutively expressed enzyme, beta-galactosidase, we found that the six SCVs had higher levels of translation than the background MG1655 (Figure 4). Moreover, we found that the rate of translation decreases in a concentration-dependent manner to both CHL and AZM (Supplementary Figure 6). This is consistent with recent observations indicating partially compromised translation as a result of exposure to tetracycline, a translational inhibitor, which potentially accounts for the collateral susceptibility to this drug observed in Supplementary Figure 4¹⁹. Therefore, at the drug concentrations used in the long-term experiments, these SCVs are readily selected for over the ancestor, not only for their level of antibiotic resistance but also for their level of translation, explaining their ability to increase in frequency when rare.

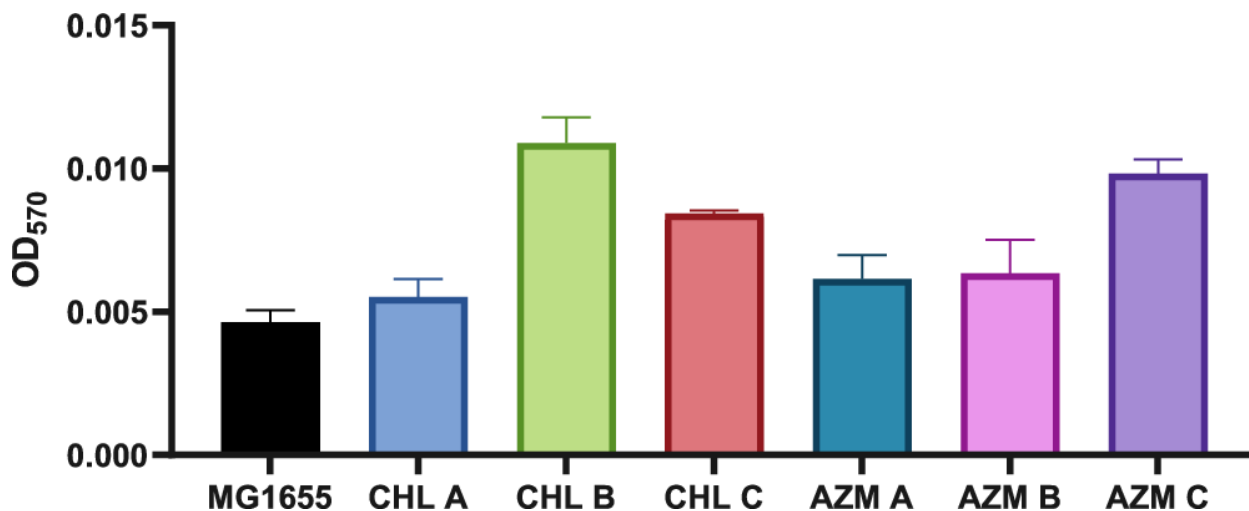


Figure 4. An assay of beta-galactosidase as a proxy for translation level. The beta-galactosidase levels as determined by absorbance for the ancestral *E. coli* MG1655 and the six SCVs. Shown are the means and standard deviations of three independent biological replicates.

Heteroresistance

Antibiotic heteroresistance (HR) is defined as, “a phenotype in which a bacterial isolate contains subpopulations of cells that show a substantial reduction in antibiotic susceptibility compared with the main population”, and is detected via a population analysis profile (PAP) test²⁰. The revertant populations obtained from these SCVs have a lower MIC than those of their small colony ancestor. These revertant populations are capable of rapidly regenerating the SCVs, which have a higher MIC – meeting the definition of antibiotic HR. The ancestral *E. coli* MG1655 is not capable of generating resistant subpopulations, as shown via PAP test (Supplementary Figure 7 Panels A and B). In Figure 5, we show PAP tests of CHL B (Panel A) and AZM C (Panel B). Both SCVs are shown to be heteroresistant based on the above criteria. Moreover, highly resistant colonies isolated from these PAP tests were found to be unstable and revert to the initial SCV state in 15 days, as shown by a decrease in the MIC (Fig. 3) as well as a decrease in the frequency of antibiotic-resistant subpopulations (Fig. 5). As shown in Supplementary Figure 7 Panels C and D, all SCVs obtained from the long term experiment meet the criteria for HR. Pursuing the genetic basis of this reversion we performed a genotypic characterization of these

revertants. We did find extra mutations in CHL B and AZM B (Supplementary Table 2), but once again we did not find mutations that can explain reversion.

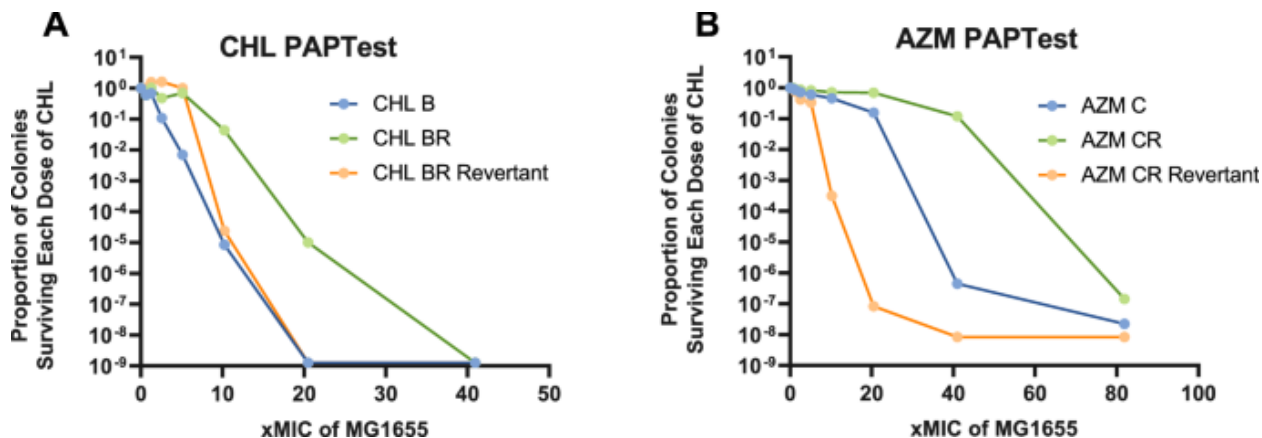


Fig 5. PAP tests of a CHL and an AZM SCV. (A) PAP tests of a chloramphenicol SCV (blue line), the most resistant isolate of this clone (green line), and the most resistant isolate after being grown without antibiotic pressure for 15 days (orange line). (B) PAP tests of an azithromycin SCV (blue line), the most resistant isolate of this clone (green line), and the most resistant isolate after being grown without antibiotic pressure for 15 days (orange line).

Mathematical Model and Computer Simulations

To explore the dynamics of the emergence of the SCVs and subsequently the evolution of HR described in the above experimental results, we constructed a mathematical and computer-simulation model. In particular, we are interested in explaining the timeframe and conditions in which the SCVs arise, why the SCVs fail to ascend to a nutrient-limited density, and why the evolution of HR is stable. In Figure 6 we depict the model graphically and in the Supplementary Text and Supplementary Equations 5-11 we describe the model and its equations.

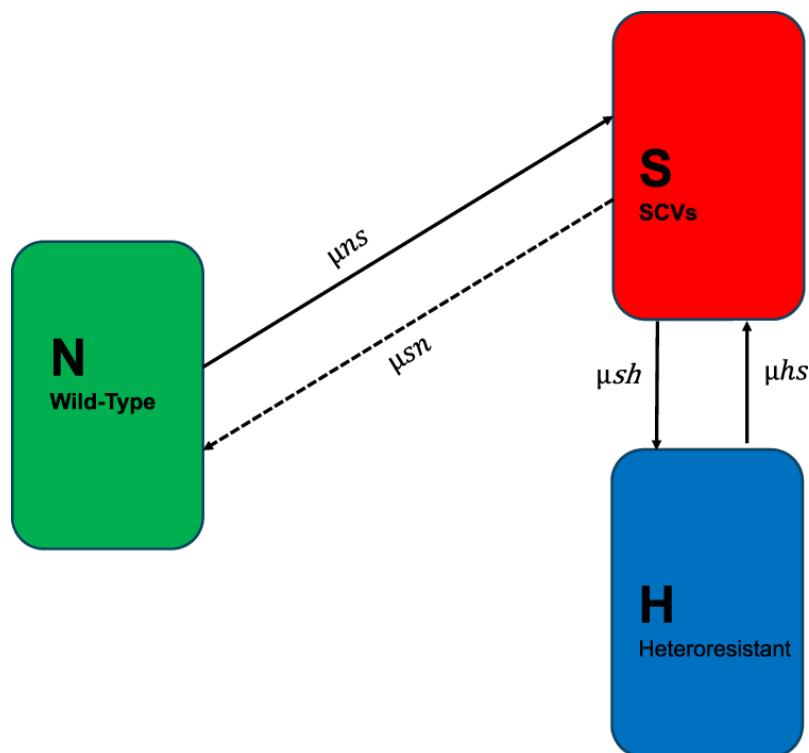


Fig 6. Diagram of a semi-stochastic model of the evolution of HR. The variables N, S, and H are, respectively, the wildtype *E. coli* MG1655, SCVs, and the heteroresistant bacteria in cells/mL. The parameters μ_{ns} , μ_{sn} , μ_{sh} and μ_{hs} are the transition rates, per cell per hour, between the different states.

In Figure 7A we illustrate how the presence of an antibiotic selects for the emergence and ascent of resistant SCVs and a heteroresistant population from an initially wild-type population. In Figure 7B, we show that an initial population of SCVs when grown without antibiotics will rapidly transition and give rise to a heteroresistant population which ascends and becomes limited by the resource. In Figure 7C, we show that exposing the heteroresistant population to the drug more rapidly selects for the emergence and dominance of resistant SCVs than when exposing the wild type population to the same concentration of the drug. In Figure 7D, we show the changes in average MIC for the three scenarios depicted in panels A, B, and C. In Supplementary Figure 8 we show the predicted dynamics of the above model with differing concentrations of the treating antibiotic. Notably, the emergence of the SCVs and HR is dependent on this concentration—critically, the drug concentration cannot exceed the MIC of the most resistant population. For a more detailed

consideration of this result and the impact that having multiple resistant states has on the emergence of HR, see ²¹. Additionally, in Supplementary Figure 9, we explore the sensitivity of our model to the governing parameters: the transition rates and relative fitness costs. Variations in the transition rates from the wild-type to the SCVs (Supplementary Figure 9A and B) simply alter the rate at which SCVs emerge and dominate, without changing the overall outcome. Similarly, adjusting the transition rates from SCVs to the heteroresistant population (Supplementary Figure 9C and D) only affects the frequency and timing of SCV dominance. Lastly, differing fitness costs of the SCVs (Supplementary Figure 9E and F) merely impact the time required for SCV dominance. Together, these mathematical simulations illustrate that our observations hold true across a wide range of biologically meaningful parameter values.

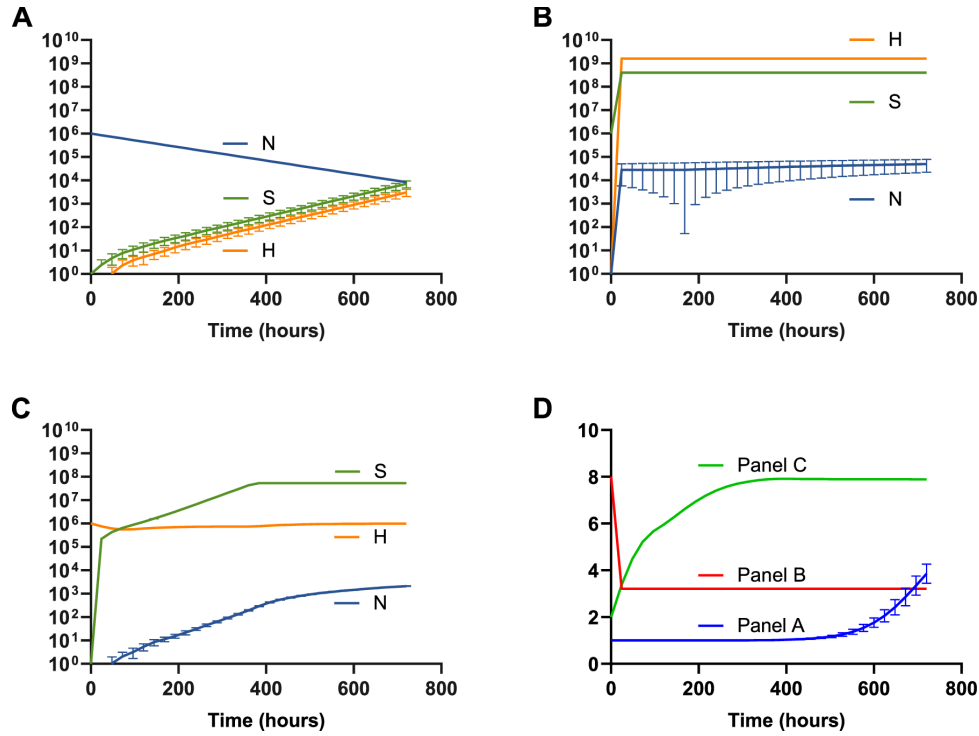


Figure 7. Computer simulations of the proposed model of evolved HR. Parameters used for these simulations are $e = 5 \times 10^{-7}$ $\mu\text{g}/\text{cell}$; $v_{\max N} = 1.0$, $v_{\max S} = 0.5$, $v_{\max H} = 1.0$ per cell per hour; $v_{\min} = -0.01$ per cell per hour; $K = 1$; $k = 1$; $\text{MIC}_N = 1.0$, $\text{MIC}_S = 8.0$, $\text{MIC}_H = 2.0$ $\mu\text{g}/\text{ml}$; $da = 0$ $\mu\text{g}/\text{hour}$; $\mu_{\text{ns}} = 1 \times 10^{-8}$, $\mu_{\text{sn}} = 1 \times 10^{-8}$, $\mu_{\text{sh}} = 1 \times 10^{-3}$, $\mu_{\text{hs}} = 1 \times 10^{-3}$ per cell per hour. The variables N, S, and H are, respectively, the wildtype *E. coli* MG1655, SCVs, and the heteroresistant bacteria in cells/mL. Note, points which do not appear to have error bars have standard deviations which are too small to be graphed. One hundred independent runs of the models were carried out in each condition. **(A)** H and S selection from an initial sensitive population. Parameters are $N = 1 \times 10^6$ cells/mL; $A = 3$ $\mu\text{g}/\text{mL}$. **(B)** H selection from an initial SCV population in the absence of the drug. Parameters are $S = 1 \times 10^6$ cells/mL; $A = 0$ $\mu\text{g}/\text{mL}$. **(C)** S selection from an initial H population in the presence of the drug. $H = 1 \times 10^6$ cells/mL; $A = 3$ $\mu\text{g}/\text{mL}$. **(D)** Changes in the average MIC of the system over the simulations shown (A, B, and C).

Discussion

The canonical distinction between bacteriostatic and bactericidal antibiotics has deeply influenced their clinical usage. Traditionally, bacteriostatic antibiotics were considered “weaker drugs”, but this traditional view is questionable. Drugs which are classified as bacteriostatic can and do kill bacteria in a concentration dependent manner²². Moreover, meta-analysis studies do not demonstrate differences in the clinical success of therapy with either types of drugs even in severe infections¹¹. Indeed, bactericidal agents could be reserved for life-threatening infections, particularly in immunocompromised patients or those suffering from chronic infections. A more extended use of bacteriostatic drugs could be beneficial to spare the use and overuse of bactericidal antibiotics which fosters resistance. A limitation to progress in the extended use of bacteriostatic drugs is the shortage of pharmacodynamic (PD) data with these drugs.

The distinction between bacteriostatic and bactericidal antibiotics is confounded by another factor: The primary cellular and molecular targets do not necessarily differ between these classes of drugs. Several bacteriostatic antibiotics have mechanisms of action that one would anticipate being bactericidal: mecillinam and cefsulodin inhibit cell wall synthesis²³; novobiocin inhibits DNA gyrase²⁴; and rifampin inhibits the DNA-dependent RNA polymerase which is bacteriostatic for *E. coli* and bactericidal for *Mycobacterium*^{25,26}. Most notably, drugs which target the ribosome and inhibit protein synthesis can be either bactericidal (such as gentamicin or tobramycin) or bacteriostatic (such as the macrolides, phenicols, tetracyclines, oxazolidinones, and spectinomycin)²⁷. Interestingly, the potential bactericidal effect of one of the ribosome-targeting drugs, chloramphenicol, is prevented by the production of (p)ppGpp in the exposed cells²⁸. This suggests that the difference between a bacteriostatic drug and a bactericidal one is a property of the treated cell rather than the antibiotic²⁹. All the above examples illustrate the need for a better understanding of the PD, population biology, and evolutionary biology of treatment with bacteriostatic antibiotics.

In this study, we present evidence that bacteriostatic drugs of two different classes (the phenicols and macrolides) inhibit the growth of *E. coli* for extended periods, i.e. 30 days, and moreover maintain the culture

in a kind of stationary phase where the density of viable bacterial cells is stable. Although, unlike stationary phase we found there to be an abundance of the limiting resource, implying that the cultures remain drug-limited even after a month. Most interestingly, despite the fact that the bacteria in the population appears to not be replicating due to the lack of net growth, evolution still occurred. A population of small colony variants (SCVs) emerged and ascended to become a significant population of bacteria. We attribute this evolution to the fact that even though the population at large was neither increasing nor decreasing in the cultures with bacteriostatic drugs, the population was replicating at a rate roughly equal to that at which it was dying. This finding is unanticipated and inconsistent with the common perception that bacteriostatic drugs simply arrest bacterial growth. This result questions the definition of bacteriostasis.

Our mathematical and computer-simulation model demonstrates that in the presence of an antibiotic, even when starting with an antibiotic susceptible population that generates resistant sub-populations at an extremely low rate, the resistant sub-population will ascend to dominate. When the selection pressure is removed this resistant sub-population will increase in susceptibility, however the population which then emerges to dominance is not the initial antibiotic susceptible population but is instead a population which readily generates resistant sub-populations. Stated another way, our model illustrates and our results confirm how HR can evolve in a population otherwise lacking this trait.

These SCVs were found to be highly resistant not only to the challenging agents, but even to some types of bactericidal agents, such as aminoglycosides and rifampin. Curiously, the resistance of the SCVs to chloramphenicol (CHL) and azithromycin (AZM) are not due to the canonical resistance mechanisms^{16,30}. SCVs have been implicated in treatment failure, primarily in *Staphylococcus aureus*, but there are limited reports of SCVs being associated with treatment failure in *E. coli*^{31,32}. Although SCVs of *E. coli* have been observed for a long time, they are under described both in their genetic basis and their role in bacterial communities. Two clinical isolates of *E. coli* SCVs have been studied, both of which have distinct metabolic disruptions by mutations in heme and thymidine biosynthesis pathways^{31,32}. Lab-generated SCVs have been described with

mutations in Q8, hemin, and lipoic acid biosynthesis³³⁻³⁵. However, none of these pathways appear to be disrupted in our SCVs.

We have yet to determine the genetic and molecular basis of the observed SCVs, but they appear to be distinct from the previously described mechanisms³³⁻³⁷. Certain mutations observed here (Supplementary Table 1) might account for changes in MICs in the SCVs. For instance, in the case of AZM-induced SCVs, missense variants of the *vitG* gene, encoding the 2-(5"-triphosphoribosyl)-3'-dephosphocoenzyme-A synthase, were consistently found. This mutation might alter members of the GntR family of transcriptional regulators which could influence the DNA-binding properties of the regulator resulting in repression or activation of transcription, or could directly impact ATP synthesis³⁸, leading to the generation of the SCVs. We did find extra mutations in CHL C, AZM A, and AZM C involving the AcrAB efflux pump, 50S ribosomal proteins L4 and L22, and the Lon protease, all of which can modify the antibiotic susceptibility. The mutations in AZM C found in *acrAB* could interfere with AZM membrane transport³⁹. The mutations found in CHL C and AZM A in the gene encoding the 50S ribosomal protein L4 (a known chloramphenicol binding site) and L22, respectively, are a known mechanism of macrolide resistance^{40,41}. The mutation in the Lon protease in AZM A is frequently associated with changes in susceptibility as well⁴². Taken together, these changes could account for the increase in the MIC to AZM and CHL but cannot account for the emergence of the SCVs. We found a mutation in a CHL-induced SCV in the gene encoding the Tyrosine-tRNA ligase. This mutation could account for the generation of SCVs, since inhibitors of this ligase strongly decrease bacterial growth, but this mutation was only found in one of the six SCVs⁴³. Most interestingly, we were unable to find any SNPs in one of the isolated CHL SCVs. However, all mutations found in the antibiotic-resistant SCVs were also found in the antibiotic-susceptible revertants (Supplementary Table 2), thus even if the mutations presented could account for the transition to resistance, they cannot account for the transition to susceptibility. This is also true of the transition to and from the SCV phenotype. We cannot exclude that the transition from normal cells to SCVs could be due to a kind of "structural epistasis" (not a genetic one) due to the altered interactions between intracellular machinery and molecules when the shape of the cell is altered by antibiotics⁴⁴.

Unexpectedly, the antibiotic resistance observed here is transient, as would be anticipated for heteroresistance (HR), suggesting a high fitness cost of the mutations detected. In support of this HR hypothesis we found that these SCVs meet all the criteria set forth for HR: there are subpopulations present at a frequency greater than 10^{-7} , with an MIC higher than 8x that of the main population, and reversion of the resistant subpopulation occurs in short order ²¹. To our knowledge, this is the first report of both the spontaneous evolution of HR as well as HR to bacteriostatic drugs.

Materials and Methods

Bacterial Strains. *E. coli* MG1655 was obtained from the Levin Lab bacterial collection ¹³. pAM34 with the origin of replication under control of an IPTG promoter and an ampicillin resistance cassette was obtained from Calin Guet from IST Austria ¹⁸.

Growth Media. LB (Lysogeny Broth) (244620) was obtained from BD. The DM (Davis Minimal) minimal base without dextrose (15758-500G-F) was obtained from Sigma Aldrich (7 g/L dipotassium phosphate, 2 g/L monopotassium phosphate, 0.5 g/L sodium citrate, 0.1 g/L magnesium sulfate, 1 g/L ammonium sulfate). MHI plates were made from MHI broth (212322) obtained from BD. Glucose (41095-5000) was obtained from Acros. LB agar (244510) for plates was obtained from BD.

Growth Conditions. Unless otherwise stated, all experiments were conducted at 37°C with shaking.

Sampling bacterial densities. The densities of bacteria were estimated by serial dilution in 0.85% saline and plating. The total density of bacteria was estimated on LB agar plates.

Antibiotics. Chloramphenicol (23660) was obtained from United States Pharmacopeia. Azithromycin (3771) was obtained from TOCRIS. Ampicillin (A9518-25G) was obtained from Sigma Aldrich. Isopropyl b-D-1-thiogalactopyranoside (IPTG; I56000-5.0) was obtained from Research Products International. All E-tests were obtained from bioMérieux.

Estimating Minimal Inhibitory Concentrations. Antibiotic MICs were estimated using E-tests on MHII plates or via broth microdilution ^{45,46}.

Long Term Experiments. Flasks containing 10 mL of DM with 1000 µg/mL of glucose and an initial density of 10⁵ CFU/mL cells were grown at 37°C with shaking for 30 days without transferring. For each biological replicate, initial inoculums were obtained from independent overnights of *E. coli* cultures. *E. coli* MG1655 was grown with either no drug, 4x MIC of CHL or 3x MIC of AZM. Samples were taken every 5 days and plated on LB agar plates. Twenty SCVs from each condition were isolated from the last time point and grown in the absence of antibiotic. Only those whose MIC was higher than the ancestral MG1655 after two overnight passages in the absence of the drug were selected.

Long Term Experiments with non-replicative plasmid. Flasks containing 10 mL of DM with 1000 µg/mL of glucose and an initial density of 10⁵ CFU/mL cells were grown at 37°C with shaking for 30 days. *E. coli* MG1655 pAM34 was grown with either 4x MIC of CHL, 3x MIC of AZM, ampicillin, or no selection. All experiments were performed in the absence of IPTG. pAM34 is a single copy number plasmid. Control Samples were taken every 5 days and plated on LB agar plates as well as 100 µg/mL Ampicillin and 0.5 mM IPTG LB agar plates.

Sequencing. Complete genomes were obtained with hybrid Illumina/Nanopore sequencing by SeqCenter. Samples were extracted from single colonies using Zymo Quick-DNA HMW MagBead Kit. Oxford Nanopore Sequencing library prep was performed with PCR-free ligation library prep using ONT's V14 chemistry. Long read sequencing was performed using R10.4.1 flowcells on a GridION with basecalling performed by Guppy in Super High Accuracy mode. Illumina libraries were prepared and sequenced per SeqCenter's standards. Quality control and adapter trimming was performed with bcl-convert and porechop for Illumina and ONT sequencing respectively. Hybrid assembly with Illumina and ONT reads was performed with Unicycler ⁴⁷. Assembly statistics were recorded with QUAST ⁴⁸. Assembly annotation was performed with Prokka ⁴⁹.

Beta-galactosidase assay. The BetaRed™ β-Galactosidase Assay Kit (Sigma Aldrich) was used to experimentally measure the translation level. Flasks containing 10 mL of DM with 1000 µg/mL of glucose and an initial density of 10⁵ CFU/mL cells were grown at 37 °C with shaking overnight in the absence or presence

of different concentrations of CHL or AZM. The manufacturer protocol was followed, and OD 570 nm was measured. The experiments were performed in triplicate.

Growth Rate Estimation. Exponential growth rates were estimated from changes in optical density (OD₆₀₀) in a Bioscreen C. For this, 24-hours stationary phase cultures were diluted in LB or glucose-limited liquid media to an initial density of approximately 10⁵ cells per mL. Five replicas were made for each estimate by adding 300 µl of the suspensions to the wells of the Bioscreen plates. The plates were incubated at 37°C and shaken continuously. Estimates of the OD (600nm) were made every five minutes for 24 hours in LB and 48 hours in glucose-limited medium. Normalization, replicate means and error, growth rate, lag and maximum OD were found using a novel R Bioscreen C analysis tool accessible at https://josheclf.shinyapps.io/bioscreen_app.

Residual Growth. After 30 days the cultures were centrifuged and filtered through a 0.22 µm filter. Strain resistant for CHL (Strain 1012 from the US Center for Disease Control's MuGSI Isolate Bank which is *cmlA5* positive), AZM (Strain 1007 from the US Center for Disease Control's MuGSI Isolate Bank which is *mph(A)* positive), or just MG1655 were added to the supernatants and allowed to grow for 24h.

Antibiotic stability. Initial (day 0) and final (day 30) cultures from the long term experiment in the presence of CHL or AZM were centrifuged and the supernatants filtrated. Twenty µL of these supernatants were spotted on 7 mm blank disk and MG1655 was used as the lawn. After 24h of incubation, the zone of inhibition was recorded.

Population Analysis Profile tests. Single colonies of the corresponding strain were inoculated into 10 mL of LB and grown overnight at 37 °C with shaking. Cultures were serially diluted in saline and all dilutions (10⁰ to 10⁻⁷) plated on LB agar plates containing 0, 1, 2, 4, 8, and 16 times the MIC of CHL or AZM. Plates were grown at 37 °C for 48 hours before the density of surviving colonies was estimated.

Numerical Solutions (Simulations): For our numerical analysis of the coupled, ordered differential equations presented (Supplementary Equations 1-12) we used Berkeley Madonna with the parameters presented in the captions of Figure 7 and Supplementary Figures 8 and 9. Copies of the Berkeley Madonna programs used for these simulations are available at www.eclf.net. Parameters were obtained from ^{21,50,51}. To calculate the average MIC in our simulations, we take a weighted average of the MIC of each population.

Acknowledgements

We would like to thank Danielle Steed for her discussion of the clinical implications and relevance of this work. We would also like to thank Jason Chen and LM Bradley for their unwavering assistance and support. We would also like to thank the other members of the Levin Lab. BRL would like to thank the US National Institute of General Medical Sciences for their funding support via R35 GM 136407 and the US National Institute of Allergy and Infectious Diseases for their funding support via U19 AI 158080-02.

Competing Interest Statement

The authors have no competing interests.

References

- 1 Bernatová, S. *et al.* Following the mechanisms of bacteriostatic versus bactericidal action using Raman spectroscopy. *Molecules* **18**, 13188-13199 (2013).
<https://doi.org/10.3390/molecules181113188>
- 2 Pankey, G. A. & Sabath, L. D. Clinical Relevance of Bacteriostatic versus Bactericidal Mechanisms of Action in the Treatment of Gram-Positive Bacterial Infections. *Clinical Infectious Diseases* **38**, 864-870 (2004). <https://doi.org/10.1086/381972>
- 3 Nemeth, J., Oesch, G. & Kuster, S. P. Bacteriostatic versus bactericidal antibiotics for patients with serious bacterial infections: systematic review and meta-analysis. *J Antimicrob Chemother* **70**, 382-395 (2015). <https://doi.org/10.1093/jac/dku379>
- 4 Regoes, R. R. *et al.* Pharmacodynamic functions: a multiparameter approach to the design of antibiotic treatment regimens. *Antimicrob Agents Chemother* **48**, 3670-3676 (2004).
<https://doi.org/10.1128/aac.48.10.3670-3676.2004>
- 5 William, A. Killing and regrowth of bacteria in vitro. *Scand. J. Infect. Dis. Suppl.* **74**, 63-70 (1991).
- 6 Bonapace, C. R., Friedrich, L. V., Bosso, J. A. & White, R. L. Determination of antibiotic effect in an in vitro pharmacodynamic model: comparison with an established animal model of infection. *Antimicrobial agents and chemotherapy* **46**, 3574-3579 (2002).
- 7 Craig, W. A. & Ebert, S. C. Killing and regrowth of bacteria in vitro: a review. *Scand J Infect Dis Suppl* **74**, 63-70 (1990).
- 8 Huemer, M., Mairpady Shambat, S., Brugger, S. D. & Zinkernagel, A. S. Antibiotic resistance and persistence—Implications for human health and treatment perspectives. *EMBO reports* **21**, e51034 (2020). <https://doi.org/https://doi.org/10.15252/embr.202051034>
- 9 Levin-Reisman, I., Brauner, A., Ronin, I. & Balaban, N. Q. Epistasis between antibiotic tolerance, persistence, and resistance mutations. *Proc Natl Acad Sci U S A* **116**, 14734-14739 (2019).
<https://doi.org/10.1073/pnas.1906169116>

- 10 Balaban, N. Q. *et al.* Publisher Correction: Definitions and guidelines for research on antibiotic persistence. *Nat Rev Microbiol* **17**, 460 (2019). <https://doi.org/10.1038/s41579-019-0207-4>
- 11 Wald-Dickler, N., Holtom, P. & Spellberg, B. Busting the Myth of "Static vs Cidal": A Systemic Literature Review. *Clin Infect Dis* **66**, 1470-1474 (2018). <https://doi.org/10.1093/cid/cix1127>
- 12 Rizk, M. L. *et al.* Considerations for Dose Selection and Clinical Pharmacokinetics/Pharmacodynamics for the Development of Antibacterial Agents. *Antimicrob Agents Chemother* **63** (2019). <https://doi.org/10.1128/aac.02309-18>
- 13 Berryhill, B. A. *et al.* What's the Matter with MICs: Bacterial Nutrition, Limiting Resources, and Antibiotic Pharmacodynamics. *Microbiology Spectrum* **11**, e04091-04022 (2023). <https://doi.org/doi:10.1128/spectrum.04091-22>
- 14 Lopatkin, A. J. *et al.* Clinically relevant mutations in core metabolic genes confer antibiotic resistance. *Science* **371** (2021). <https://doi.org/10.1126/science.aba0862>
- 15 Martela, K., Kuźniewicz, R., Pluskiewicz, W., Tabor, E. & Zagórski, P. Calcium supplementation from dairy products in the diet of women over the age of 55 from Zabrze (the Silesian Osteoactive Study - nutritional part). *Reumatologia* **56**, 382-387 (2018). <https://doi.org/10.5114/reum.2018.80716>
- 16 Fernández, M. *et al.* Mechanisms of resistance to chloramphenicol in *Pseudomonas putida* KT2440. *Antimicrob Agents Chemother* **56**, 1001-1009 (2012). <https://doi.org/10.1128/aac.05398-11>
- 17 Heidary, M. *et al.* Mechanism of action, resistance, synergism, and clinical implications of azithromycin. *J Clin Lab Anal* **36**, e24427 (2022). <https://doi.org/10.1002/jcla.24427>
- 18 Cronan, J. E. pBR322 vectors having tetracycline-dependent replication. *Plasmid* **84-85**, 20-26 (2016). <https://doi.org/10.1016/j.plasmid.2016.02.004>
- 19 Khusainov, I. *et al.* Bactericidal effect of tetracycline in *E. coli* strain ED1a may be associated with ribosome dysfunction. *Nat Commun* **15**, 4783 (2024). <https://doi.org/10.1038/s41467-024-49084-5>

- 20 Andersson, D. I., Nicoloff, H. & Hjort, K. Mechanisms and clinical relevance of bacterial heteroresistance. *Nature Reviews Microbiology* **17**, 479-496 (2019). <https://doi.org/10.1038/s41579-019-0218-1>
- 21 Levin, B. R. *et al.* Theoretical considerations and empirical predictions of the pharmaco- and population dynamics of heteroresistance. *Proc Natl Acad Sci U S A* **121**, e2318600121 (2024). <https://doi.org/10.1073/pnas.2318600121>
- 22 Baquero, F. & Levin, B. R. Proximate and ultimate causes of the bactericidal action of antibiotics. *Nature Reviews Microbiology* **19**, 123-132 (2021). <https://doi.org/10.1038/s41579-020-00443-1>
- 23 Satta, G. *et al.* Target for bacteriostatic and bactericidal activities of beta-lactam antibiotics against *Escherichia coli* resides in different penicillin-binding proteins. *Antimicrob Agents Chemother* **39**, 812-818 (1995). <https://doi.org/10.1128/aac.39.4.812>
- 24 Murphy, M. B., Mercer, S. L. & Dewese, J. E. in *Advances in Molecular Toxicology* Vol. 11 (eds James C. Fishbein & Jacqueline M. Heilman) 203-240 (Elsevier, 2017).
- 25 Kaur, P., Agarwal, S. & Datta, S. Delineating bacteriostatic and bactericidal targets in mycobacteria using IPTG inducible antisense expression. *PLoS One* **4**, e5923 (2009). <https://doi.org/10.1371/journal.pone.0005923>
- 26 Baudens, J. G. & Chabbert, Y. A. [Rifampicin: a bacteriostatic and bactericidal agent]. *Pathol Biol (Paris)* **17**, 392-397 (1969).
- 27 Levin, B. R. *et al.* A Numbers Game: Ribosome Densities, Bacterial Growth, and Antibiotic-Mediated Stasis and Death. *mBio* **8** (2017). <https://doi.org/10.1128/mBio.02253-16>
- 28 Yang, J., Barra, J. T., Fung, D. K. & Wang, J. D. *Bacillus subtilis* produces (p)ppGpp in response to the bacteriostatic antibiotic chloramphenicol to prevent its potential bactericidal effect. *mLife* **1**, 101-113 (2022). <https://doi.org/https://doi.org/10.1002/mlf2.12031>
- 29 Baquero, F., Rodríguez-Beltrán, J. & Levin, B.R. Bacteriostatic cells instead of bacteriostatic antibiotics? *Ecoevorxiv* (2023). <https://doi.org/https://doi.org/10.32942/X2R01T>

- 30 Gomes, C., Ruiz-Roldán, L., Mateu, J., Ochoa, T. J. & Ruiz, J. Azithromycin resistance levels and mechanisms in *Escherichia coli*. *Scientific Reports* **9**, 6089 (2019). <https://doi.org/10.1038/s41598-019-42423-3>
- 31 Roggenkamp, A. *et al.* Chronic prosthetic hip infection caused by a small-colony variant of *Escherichia coli*. *J Clin Microbiol* **36**, 2530-2534 (1998). <https://doi.org/10.1128/jcm.36.9.2530-2534.1998>
- 32 Negishi, T. *et al.* Characterization of clinically isolated thymidine-dependent small-colony variants of *Escherichia coli* producing extended-spectrum β -lactamase. *J Med Microbiol* **67**, 33-39 (2018). <https://doi.org/10.1099/jmm.0.000634>
- 33 Xia, H. *et al.* A *yigP* mutant strain is a small colony variant of *E. coli* and shows pleiotropic antibiotic resistance. *Canadian Journal of Microbiology* **63**, 961-969 (2017). <https://doi.org/10.1139/cjm-2017-0347>
- 34 Roggenkamp, A., Hoffmann, H. & Hornef, M. W. Growth control of small-colony variants by genetic regulation of the hemin uptake system. *Infect Immun* **72**, 2254-2262 (2004). <https://doi.org/10.1128/iai.72.4.2254-2262.2004>
- 35 Santos, V. & Hirshfield, I. The Physiological and Molecular Characterization of a Small Colony Variant of *Escherichia coli* and Its Phenotypic Rescue. *PLOS ONE* **11**, e0157578 (2016). <https://doi.org/10.1371/journal.pone.0157578>
- 36 Tashiro, Y., Eida, H., Ishii, S., Futamata, H. & Okabe, S. Generation of Small Colony Variants in Biofilms by *Escherichia coli* Harboring a Conjugative F Plasmid. *Microbes Environ* **32**, 40-46 (2017). <https://doi.org/10.1264/jsme2.ME16121>
- 37 Hirsch, H. M. Small colony variants of *Escherichia coli*. Mode of action of copper in variant recovery and population dynamics of cultures containing variants. *J Bacteriol* **81**, 448-458 (1961). <https://doi.org/10.1128/jb.81.3.448-458.1961>
- 38 Dworkin, J. Understanding the Stringent Response: Experimental Context Matters. *mBio* **14**, e0340422 (2023). <https://doi.org/10.1128/mbio.03404-22>

- 39 Trampari, E. *et al.* Functionally distinct mutations within AcrB underpin antibiotic resistance in different lifestyles. *npj Antimicrobials and Resistance* **1**, 2 (2023). <https://doi.org/10.1038/s44259-023-00001-8>
- 40 Moore, S. D. & Sauer, R. T. Revisiting the mechanism of macrolide-antibiotic resistance mediated by ribosomal protein L22. *Proc Natl Acad Sci U S A* **105**, 18261-18266 (2008). <https://doi.org/10.1073/pnas.0810357105>
- 41 Suryanarayana, T. Identification by affinity chromatography of Escherichia coli ribosomal proteins that bind erythromycin and chloramphenicol. *Biochem Int* **7**, 719-725 (1983).
- 42 Matange, N. Highly Contingent Phenotypes of Lon Protease Deficiency in Escherichia coli upon Antibiotic Challenge. *J Bacteriol* **202** (2020). <https://doi.org/10.1128/jb.00561-19>
- 43 Hughes, C. A., Gorabi, V., Escamilla, Y., Dean, F. B. & Bullard, J. M. Two Forms of Tyrosyl-tRNA Synthetase from Pseudomonas aeruginosa: Characterization and Discovery of Inhibitory Compounds. *SLAS Discov* **25**, 1072-1086 (2020). <https://doi.org/10.1177/2472555220934793>
- 44 Baquero, F. *et al.* Bacterial Subcellular Architecture, Structural Epistasis, and Antibiotic Resistance. *Biology (Basel)* **12** (2023). <https://doi.org/10.3390/biology12050640>
- 45 MA, W. Methods for dilution antimicrobial susceptibility tests for bacteria that grow aerobically: approved standard. *Clsi (Nccls)* **26**, M7-A7 (2006).
- 46 Brown, D. F. & Brown, L. Evaluation of the E test, a novel method of quantifying antimicrobial activity. *Journal of Antimicrobial Chemotherapy* **27**, 185-190 (1991).
- 47 Wick, R. R., Judd, L. M., Gorrie, C. L. & Holt, K. E. Unicycler: Resolving bacterial genome assemblies from short and long sequencing reads. *PLoS Comput Biol* **13**, e1005595 (2017). <https://doi.org/10.1371/journal.pcbi.1005595>
- 48 Gurevich, A., Saveliev, V., Vyahhi, N. & Tesler, G. QUAST: quality assessment tool for genome assemblies. *Bioinformatics* **29**, 1072-1075 (2013). <https://doi.org/10.1093/bioinformatics/btt086>

- 49 Seemann, T. Prokka: rapid prokaryotic genome annotation. *Bioinformatics* **30**, 2068-2069 (2014).
<https://doi.org/10.1093/bioinformatics/btu153>
- 50 Berryhill, B. A. *et al.* The book of Lambda does not tell us that naturally occurring lysogens of
Escherichia coli are likely to be resistant as well as immune. *Proc Natl Acad Sci U S A* **120**,
e2212121120 (2023). <https://doi.org/10.1073/pnas.2212121120>
- 51 Chaudhry, W. N. *et al.* Leaky resistance and the conditions for the existence of lytic bacteriophage.
PLoS Biol **16**, e2005971 (2018). <https://doi.org/10.1371/journal.pbio.2005971>

Supporting Information

SUPPLEMENTARY TEXT

Models for Non-replicating Plasmid

To explain how the results with the non-replicating plasmid in Figure 2 are consistent with our hypothesis that bacteria confronted with bacteriostatic antibiotics are replicating despite the absence of net growth, we present two models below. The first model parallels the long term exposure to bacteriostatic drugs while the second model parallels the control experiment in the absence of any drug.

Plasmid in the presence of a bacteriostatic drug

In this model we assume the net growth rate of the population at large is zero. We also assume that the plasmid bearing cells are not capable of increasing in absolute number, but instead decrease in frequency by transitioning to cells not bearing the plasmid at half of the growth rate. For this model, the replicating plasmid- free cells are labeled N in cells per mL which grow at some rate v , per cell per hour. The cells containing the plasmid, P cells per mL, also grow at the same rate v , per cell per hour. Since half of the divisions of the P population result in loss of the plasmid due to segregation loss, the transition between states P and N is effectively half the growth rate. Equations 1 and 2 detail this relationship.

$$\frac{dN}{dt} = 0.5 \cdot v \cdot P \quad \text{Eq. 1}$$

$$\frac{dP}{dt} = -0.5 \cdot v \cdot P \quad \text{Eq. 2}$$

Plasmid in the absence of a bacteriostatic drug

In this model we assume that all cells can grow, but since half the cells per division of P lose the plasmid and become N, the absolutely number of P remains constant while the frequency of P decreases. We also assume that there is an absolute carrying capacity such that when the total density of cells reaches that capacity all transitions and growth stops. All other assumptions for this model are as above. This relationship is giving by Equations 3 and 4.

$$\frac{dN}{dt} = (N \cdot v + 0.5 \cdot v \cdot P) \quad \text{Eq. 3}$$

$$\frac{dP}{dt} = 0 \quad \text{Eq. 4}$$

Model predictions

In Supplemental Figure 3 we illustrate with numerical solutions to the predicted results from the above equations. Shown in both panels in black are plasmid-free cells, and shown in blue is the frequency of plasmid-bearing to total cells as given by $(P/P+N)$.

Evolution of Heteroresistance Model

In the absence of antibiotics, the maximum growth rates of these populations are, respectively, v_{maxN} , v_{maxS} , and v_{maxH} (>0 per cell per hour). In the presence of antibiotics, the minimum growth rate (maximum death rates) of these populations are v_{minN} , v_{minS} , and v_{minH} (<0 per cell per hour), and the respective MICs of these populations are MIC_N , MIC_S , and MIC_H $\mu\text{g/mL}$. The net rates of growth of these three populations are proportional to the concentration of the resource, r $\mu\text{g/mL}$ and the concentration of the antibiotic, A $\mu\text{g/mL}$ ^{1,2}. The equations below are given in the general form where X is either N, S, or H.

$$\Pi_X(A, r) = v_{maxX} - \left[\frac{(v_{maxX} - v_{minX}) \cdot \left(\frac{A}{MIC_X}\right)^{K_X}}{\left(\frac{A}{MIC_X}\right)^{K_X} - \left(\frac{v_{minX}}{v_{maxX}}\right)} \right] \cdot \psi_X(r) \quad \text{Eq.5}$$

$$\psi = \frac{r}{(r+k_x)} \quad \text{Eq.6}$$

K_x , the Hill coefficient ¹, is a shape parameter where the greater the value of K_x the more acute the function. The parameter k_x , the Monod constant, is the concentration of the resource when the growth rate is half its maximum value ³.

With the above definitions and assumptions, the rates of change in the densities of the populations of bacteria and the change in resource and antibiotic concentrations are given by the below set of coupled differential equations (Eq. 7-11).

$$\frac{dN}{dt} = \Pi_N(A, r) \cdot (N + N \cdot (\mu_{sn} - \mu_{ns})) \quad \text{Eq. 7}$$

$$\frac{dS}{dt} = \Pi_S(A, r) \cdot (S + S \cdot (\mu_{ns} - \mu_{sn} + \mu_{hs} - \mu_{sh})) \quad \text{Eq. 8}$$

$$\frac{dH}{dt} = \Pi_H(A, r) \cdot (H + H \cdot (\mu_{sh} - \mu_{hs})) \quad \text{Eq. 9}$$

$$\frac{dr}{dt} = -e \cdot (N \cdot v_{maxN} + S \cdot v_{maxS} + H \cdot v_{maxH}) \quad \text{Eq. 10}$$

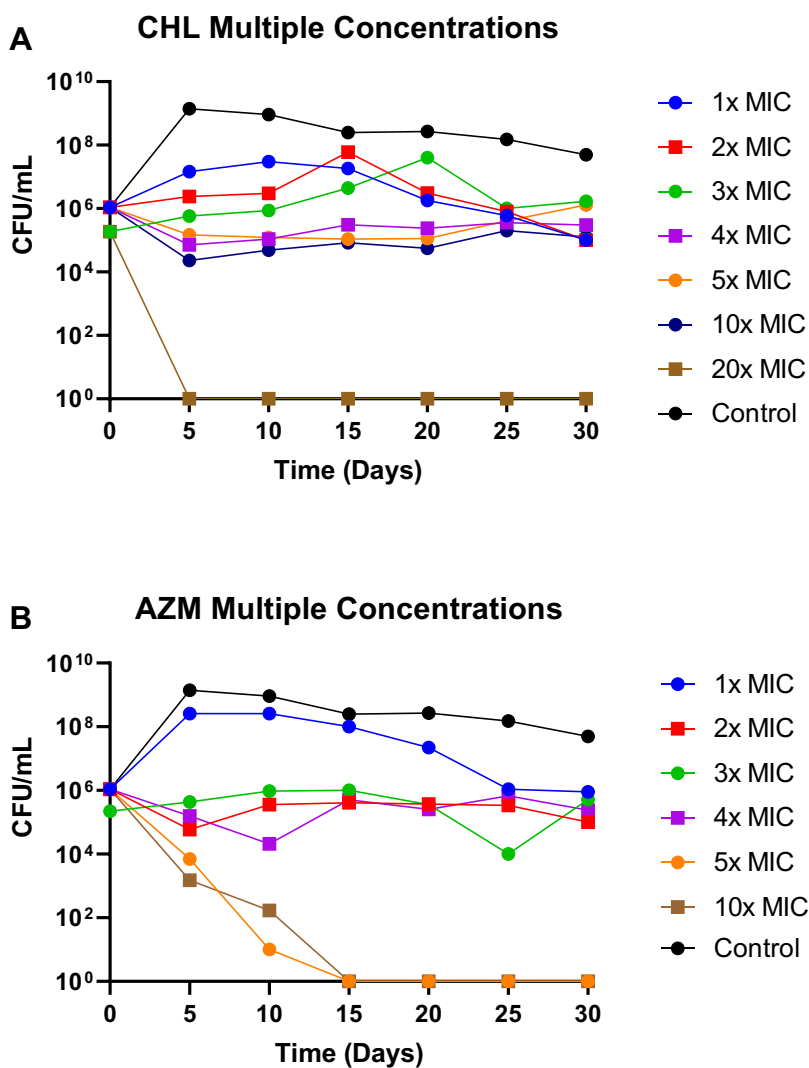
$$\frac{dA}{dt} = -da \cdot A \quad \text{Eq. 11}$$

The conversion efficiency, e μg^4 , is the amount of the limiting resource needed to produce a new cell (Eq. 10) and the parameter da is the hourly rate of decline in the concentration of the antibiotic in $\mu\text{g}/\text{hour}$ (Eq. 11).

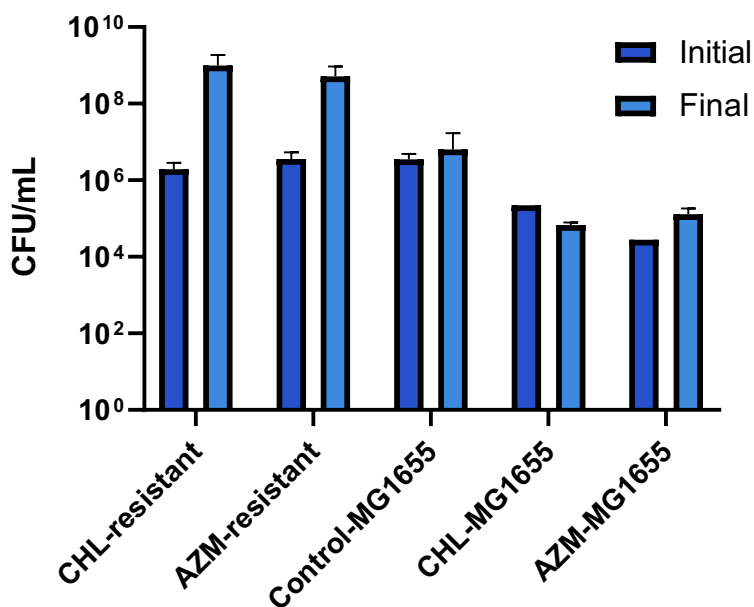
We use Berkeley Madonna and the Euler method to generate numerical solutions to these differential equations. In these simulations the changes in the densities of these populations and concentrations of the limiting resource are deterministic. The generation of mutants, however, is stochastic and simulated by a Monte Carlo process ⁵. At each time interval, t to $t + dt$ (where dt is the step size), a random number ($0 \leq z \leq 1$) from a rectangular distribution is generated. If the random number is less than the probability in Equation 12, we add $1/dt$ to the

X population. For Equation 12, Vol is the volume of the vessel which we simulate as 10 mL and X is the density of the respective population.

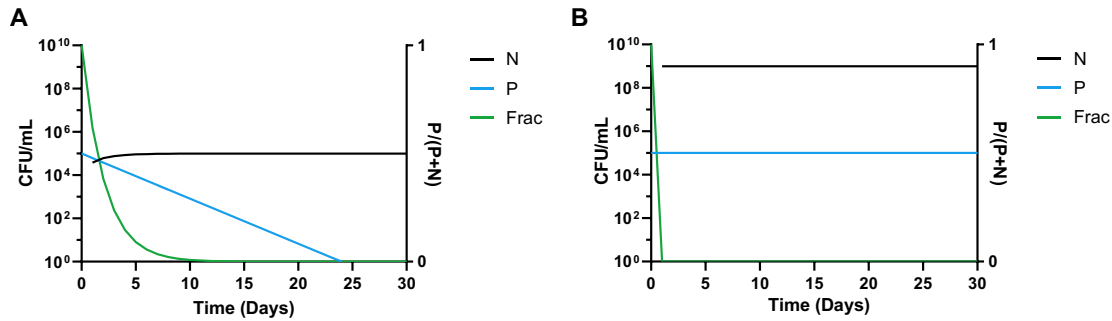
$$P(\mu) = \mu_X \cdot X \cdot dt \cdot \text{Vol} \quad \text{Eq. 12}$$



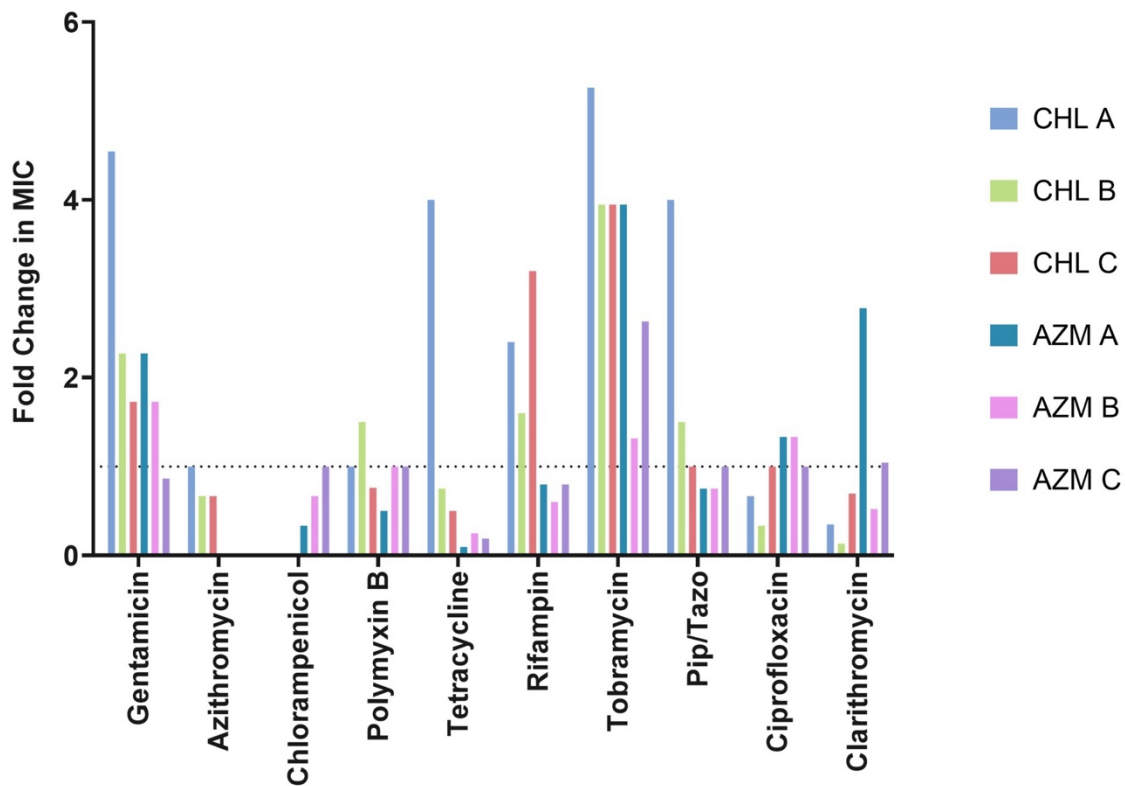
Supplementary Figure 1. Selection of bacteriostatic concentrations of CHL and AZM. CFU/mL of *E. coli* MG1655 in cultures with varying concentrations of **(A)** CHL or **(B)** AZM for 30 days. Blue line- 1x MIC, Red line- 2x MIC, Green line- 3x MIC, Purple line- 4x MIC, Orange line- 5x MIC, Brown line- 10x MIC, Black line- Drug-free control.



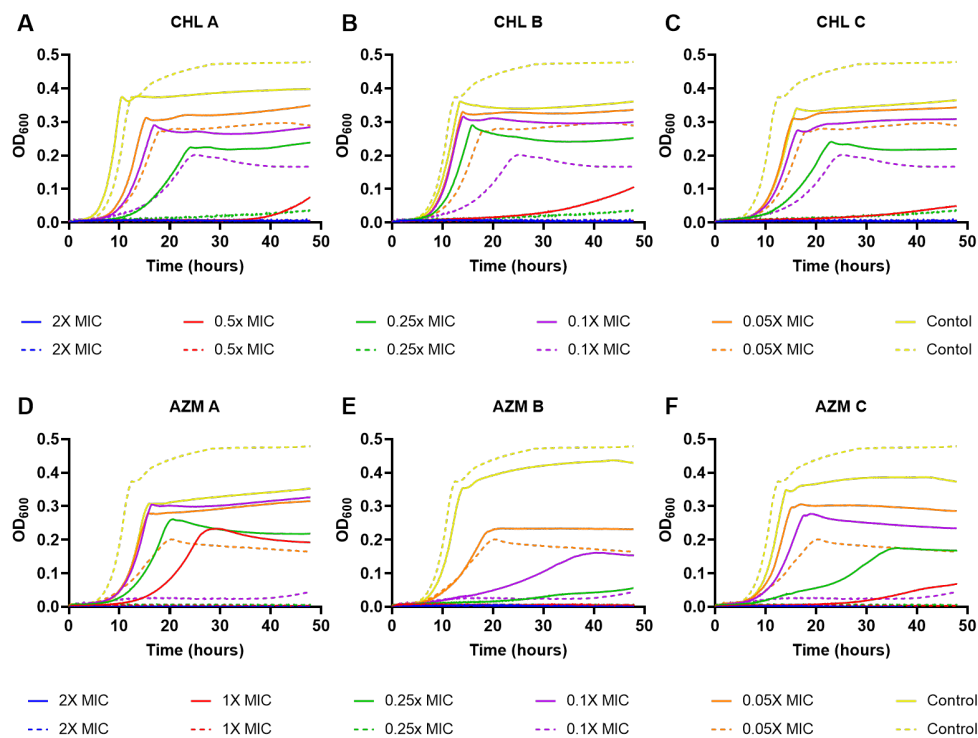
Supplementary Figure 2. Growth of *E. coli* strains in supernatants from day 30 of the long term experiments. 5×10^6 CFU/mL of AZM-resistant, CHL-resistant, or *E. coli* MG1655 strains when inoculated in the cell-free supernatants of the 30-day time point. The cell-free supernatants were plated on LB agar plates and no colonies were found. *E. coli* MG1655 was inoculated on cell-free supernatants from the control and both antibiotics and AZM-resistant or CHL-resistant strain on cell-free supernatants in which the corresponding antibiotic was present. Error bars represent the standard deviation of 4 biological replicates. Dark blue- Initial (Time= 0 hours), Light blue- Final (Time= 24 hours).



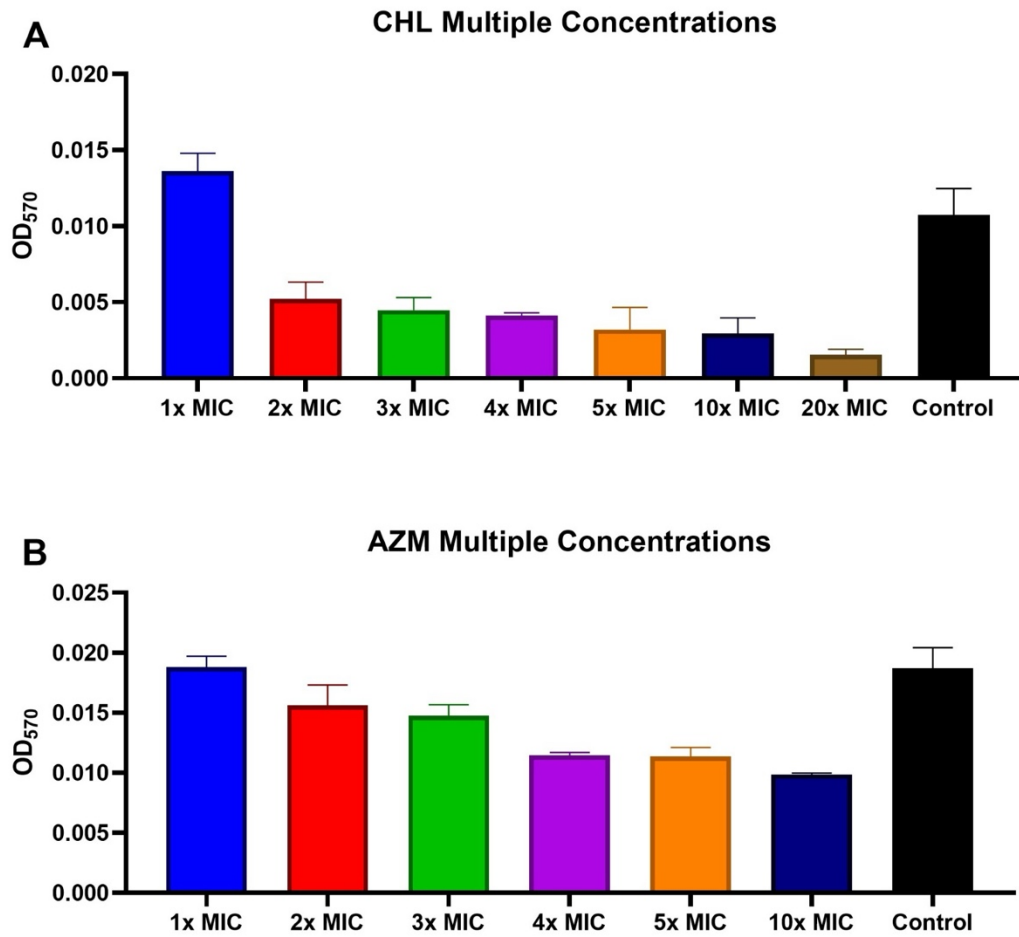
Supplementary Figure 3. Numerical Solutions for Simulations of The Non-replicating Plasmid. In both panels, Initial $N=0$ cells per mL, Initial $P=10^5$ cells per mL, $v=0.04$ per cell per hour (or one division per cell per day as calculated from Figure 2), and we assume a maximum density of 10^9 cells per mL. Shown on the left axis is CFU/mL and on the right axis “Frac” which is $P/(P+N)$. **A** Simulations in the presence of bacteriostatic drug. **B** Simulations in the absence of bacteriostatic drug.



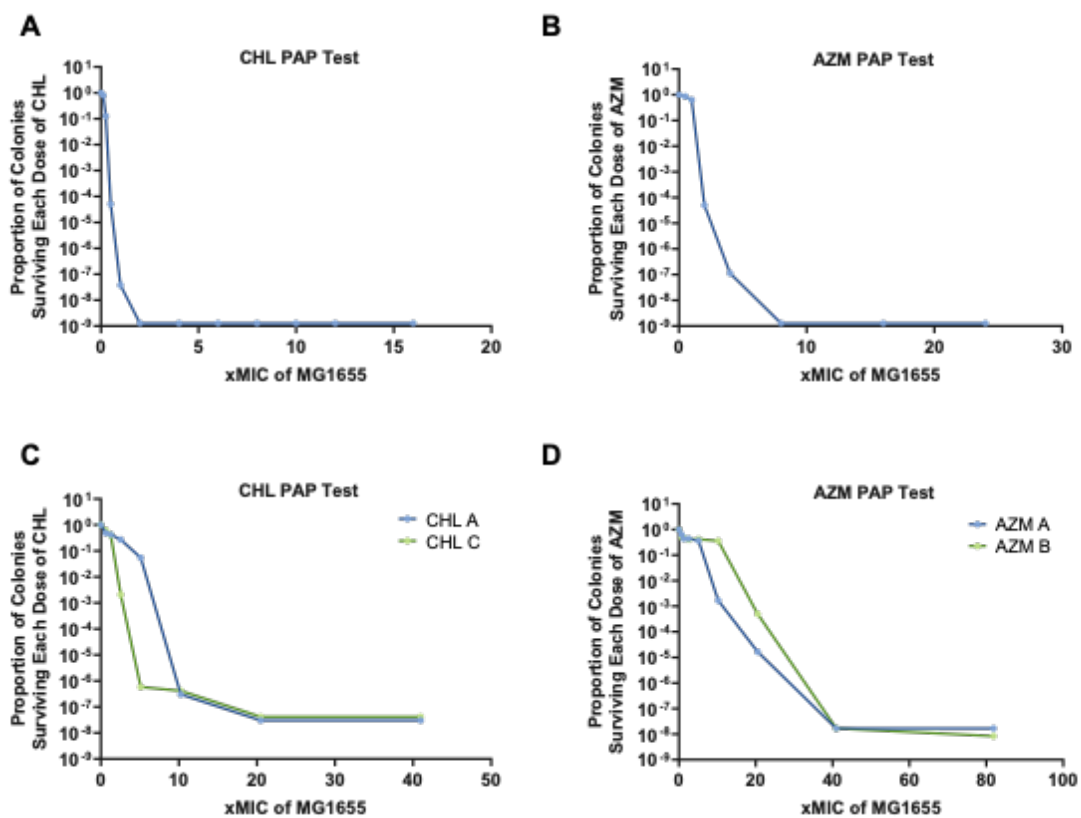
Supplementary Figure 4. SCV collateral susceptibilities and cross-resistances. Ratio of the MICs of the 6 SCVs compared to the ancestral *E. coli* MG1655 strain measured by E-test. Pip/Tazo stands for piperacillin/tazobactam.



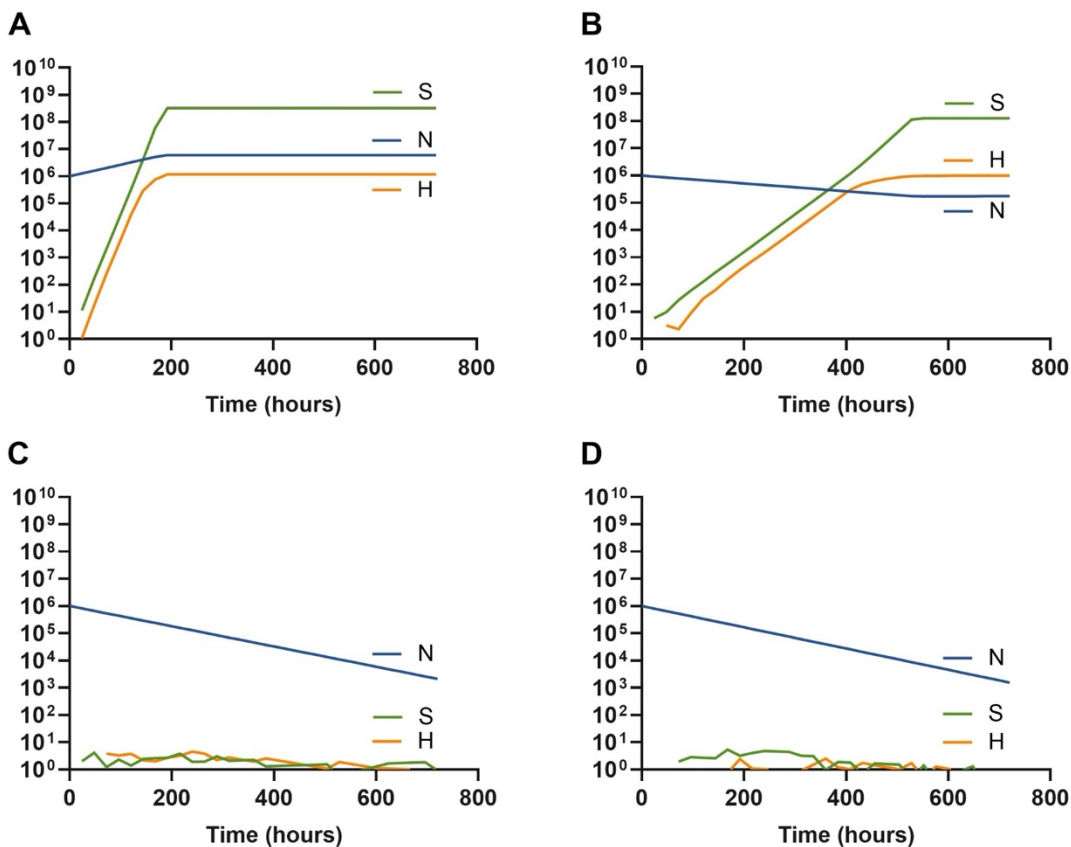
Supplementary Figure 5. Growth dynamics of CHL SCVs (solid lines A-C), AZM SCVs (solid lines D-F) and *E. coli* MG1655 (dashed lines A-F). Changes in optical density (600nm) of *E. coli* MG1655 exposed to five different concentrations of both drugs for 48 hours in minimal media. Lines are representative of the average of five technical replicas and normalized to the time zero optical density. Each concentration is shown as a fraction of the MIC of the SCV for the noted drug.



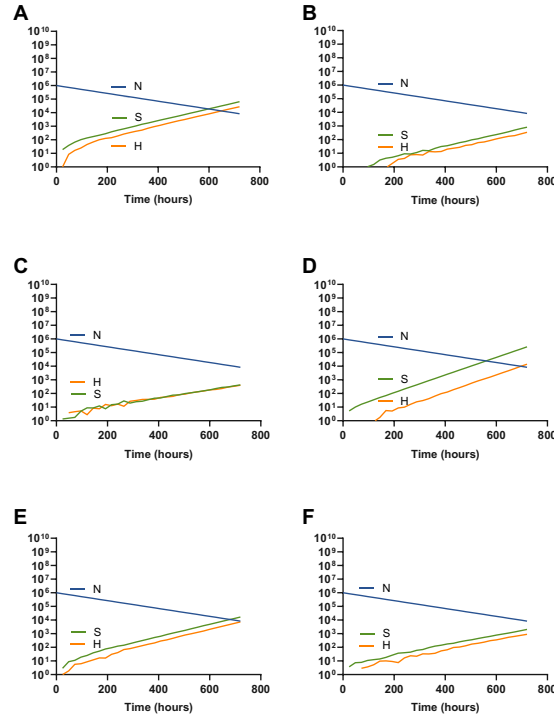
Supplementary Figure 6. An assay of beta-galactosidase as a proxy for translation level during antibiotic exposure. The beta-galactosidase levels as determined by absorbance for the ancestral *E. coli* MG1655 at different concentrations of (A) CHL and (B) AZM. Shown are means and standard deviations of three independent, biological replicates.



Supplementary Figure 7. PAP tests. (A) PAP test of *E. coli* MG1655 with CHL. (B) PAP test of *E. coli* MG1655 with AZM. (C) PAP test of CHL SCVs. (D) PAP test of AZM SCVs.



Supplementary Figure 8. Computer simulations of the proposed model of evolved HR with differing antibiotic concentrations. Parameters used for these simulations are $e = 5 \times 10^{-7} \mu\text{g}/\text{cell}$; $v_{\max N} = 1.0$, $v_{\max S} = 0.5$, $v_{\max H} = 1.0$ per cell per hour; $v_{\min} = -0.01$ per cell per hour; $K=1$; $k=1$; $\text{MIC}_N=1.0$, $\text{MIC}_S=8.0$, $\text{MIC}_H=2.0 \mu\text{g}/\text{mL}$; $da = 0 \mu\text{g}/\text{hour}$; $\mu_{ns}=1 \times 10^{-8}$, $\mu_{sn}=1 \times 10^{-8}$, $\mu_{sh}=1 \times 10^{-3}$, $\mu_{hs}=1 \times 10^{-3}$ per cell per hour. **(A)** $A = 0.5 \mu\text{g}/\text{mL}$. **(B)** $A = 1.5 \mu\text{g}/\text{mL}$. **(C)** $A = 7 \mu\text{g}/\text{mL}$, note the S population ascends at 1400 hours. **(D)** $A = 10 \mu\text{g}/\text{mL}$, note the S population fails to ascend even at 1400 hours.



Supplementary Figure 9. Computer simulations of the proposed model of evolved HR with differing transitions rates and fitness costs. H and S selection from an initial sensitive population. Common parameters used for these simulations are $e = 5 \times 10^{-7}$ $\mu\text{g}/\text{cell}$; $v_{\max N} = 1.0$, $v_{\max H} = 1.0$ per cell per hour; $v_{\min} = -0.01$ per cell per hour; $K=1$; $k=1$; $\text{MIC}_N=1.0$, $\text{MIC}_S=8.0$, $\text{MIC}_H=2.0$ $\mu\text{g}/\text{ml}$; $da = 0$ $\mu\text{g}/\text{hour}$; **(A)** Parameters used for these simulations are $v_{\max S} = 0.5$ per cell per hour; $\mu_{\text{ns}}=1 \times 10^{-7}$, $\mu_{\text{sn}}=1 \times 10^{-7}$, $\mu_{\text{sh}}=1 \times 10^{-3}$, $\mu_{\text{hs}} = 1 \times 10^{-3}$ per cell per hour. **(B)** Parameters used for these simulations are $v_{\max S} = 0.5$ per cell per hour; $\mu_{\text{ns}}=1 \times 10^{-9}$, $\mu_{\text{sn}}=1 \times 10^{-9}$, $\mu_{\text{sh}}=1 \times 10^{-3}$, $\mu_{\text{hs}} = 1 \times 10^{-3}$ per cell per hour. **(C)** Parameters used for these simulations are $v_{\max S} = 0.5$ per cell per hour; $\mu_{\text{ns}}=1 \times 10^{-8}$, $\mu_{\text{sn}}=1 \times 10^{-8}$, $\mu_{\text{sh}}=1 \times 10^{-2}$, $\mu_{\text{hs}} = 1 \times 10^{-2}$ per cell per hour. **(D)** Parameters used for these simulations are $v_{\max S} = 0.5$ per cell per hour; $\mu_{\text{ns}}=1 \times 10^{-8}$, $\mu_{\text{sn}}=1 \times 10^{-8}$, $\mu_{\text{sh}}=1 \times 10^{-4}$, $\mu_{\text{hs}} = 1 \times 10^{-4}$ per cell per hour. **(E)** Parameters used for these simulations are $v_{\max S} = 1$ per cell per hour; $\mu_{\text{ns}}=1 \times 10^{-8}$, $\mu_{\text{sn}}=1 \times 10^{-8}$, $\mu_{\text{sh}}=1 \times 10^{-3}$, $\mu_{\text{hs}} = 1 \times 10^{-3}$ per cell per hour. **(F)** Parameters used for these simulations are $v_{\max S} = 0.1$ per cell per hour; $\mu_{\text{ns}}=1 \times 10^{-8}$, $\mu_{\text{sn}}=1 \times 10^{-8}$, $\mu_{\text{sh}}=1 \times 10^{-3}$, $\mu_{\text{hs}} = 1 \times 10^{-3}$ per cell per hour.

Supplementary Table 1. SCV Genomic Changes

SCV	GENE	POSITION	TYPE	NUCLEOTIDE CHANGE	EFFECT	PRODUCT
CHL B	<i>tyrS</i>	2166796	Ins	T → TTAACGG	Conservative in-frame insertion Asn387→Gly388dup	Tyrosine-tRNA ligase
CHL C	<i>rplD</i>	431632	SNP	A → G	Missense variant Lys63Arg	50S ribosomal protein L4
		3178132	SNP	C → A		Unannotated region
AZM A	<i>rplV</i>	433741	Del	ATGAAGC GCATTATG CCGCGTGC AAAAGGTC GTGCAGAT CGCATCC → A	Disruptive in-frame deletion Ile85Arg99del	50S ribosomal protein L22
	<i>lon_1</i>	2864809	SNP	C → A	Stop gained Ser422	Lon protease
AZM B	<i>citG</i>	3235035	SNP	A → G	Missense variant Glu234Gly	2-(5"-triphosphoribosyl)-3'-dephosphocoenzyme-A synthase
	<i>citG</i>	3235041	SNP	G → T	Missense variant Gly236Val	2-(5"-triphosphoribosyl)-3'-dephosphocoenzyme-A synthase
AZM C	<i>citG</i>	3235035	SNP	A → G	Missense variant Glu234Gly	2-(5"-triphosphoribosyl)-3'-dephosphocoenzyme-A synthase
	<i>citG</i>	3235041	SNP	G → T	Missense variant Gly236Val	2-(5"-triphosphoribosyl)-3'-dephosphocoenzyme-A synthase
	<i>acrB_2</i>	3399923	SNP	G → T	Missense variant Gly236Val	Multidrug efflux pump subunit AcrB

Ins: insertion; SNP: Single Nucleotide Polymorphism; Del: deletion

Supplementary Table 2. Genomic Changes of Revertants

SCV	GENE	POSITION	TYPE	NUCLEOTIDE CHANGE	EFFECT	PRODUCT
CHL B	<i>tyrS</i>	2166796	Ins	T → TTAACGG	Conservative in-frame insertion Asn387→Gly388 dup	Tyrosine-tRNA ligase
	<i>rpoC</i>	4335806	SNP	C → A	Missense variant Asp410Tyr	DNA-directed RNA polymerase subunit beta
CHL C	<i>rplD</i>	431632	SNP	A → G	Missense variant Lys63Arg	50S ribosomal protein L4
		3178132	SNP	C → A		Unannotated region
AZM A	<i>rplV</i>	433741	Del	ATGAAGC GCATTAT GCCGCGT GCAAAAG GTCGTGC AGATCGC ATCC → A	Disruptive in-frame deletion Ile85Arg99del	50S ribosomal protein L22
	<i>lon_1</i>	2864809	SNP	C → A	Stop gained Ser422	Lon protease
AZM B	<i>rpoA</i>	443272	SNP	C → A	Missense variant Arg191Ser	DNA-directed RNA polymerase subunit alpha
	<i>citG</i>	3235035	SNP	A → G	Missense variant Glu234Gly	2-(5"-triphosphoribosyl)-3'-dephosphocoenzyme-A synthase
	<i>citG</i>	3235041	SNP	G → T	Missense variant Gly236Val	2-(5"-triphosphoribosyl)-3'-dephosphocoenzyme-A synthase
	<i>acrB_2</i>	3399923	SNP	T → C	Missense variant Leu828Ser	Multidrug efflux pump subunit AcrB
AZM C	<i>citG</i>	3235035	SNP	A → G	Missense variant Glu234Gly	2-(5"-triphosphoribosyl)-3'-dephosphocoenzyme-A synthase
	<i>citG</i>	3235041	SNP	G → T	Missense variant Gly236Val	2-(5"-triphosphoribosyl)-3'-dephosphocoenzyme-A synthase
	<i>acrB_2</i>	3399923	SNP	T → C	Missense variant Leu828Ser	Multidrug efflux pump subunit AcrB

Supplementary References

- 1 Regoes, R. R. *et al.* Pharmacodynamic functions: a multiparameter approach to the design of antibiotic treatment regimens. *Antimicrob Agents Chemother* **48**, 3670-3676, doi:10.1128/aac.48.10.3670-3676.2004 (2004).
- 2 Berryhill, B. A. *et al.* What's the Matter with MICs: Bacterial Nutrition, Limiting Resources, and Antibiotic Pharmacodynamics. *Microbiology Spectrum* **11**, e04091-04022, doi:doi:10.1128/spectrum.04091-22 (2023).
- 3 Monod, J. THE GROWTH OF BACTERIAL CULTURES. *Annual Review of Microbiology* **3**, 371-394, doi:10.1146/annurev.mi.03.100149.002103 (1949).
- 4 Stewart, F. M. & Levin, B. R. Partitioning of Resources and the Outcome of Interspecific Competition: A Model and Some General Considerations. *The American Naturalist* **107**, 171-198, doi:10.1086/282825 (1973).
- 5 Metropolis, N. & Ulam, S. The Monte Carlo Method. *Journal of the American Statistical Association* **44**, 335-341, doi:10.1080/01621459.1949.10483310 (1949).

Chapter 5

Chapter 5

Antibiotic killing of drug-induced bacteriostatic cells

Reprinted from: Berryhill BA, Gil-Gil T. 2025. Antibiotic killing of drug-induced bacteriostatic cells.

Antimicrobial Agents and Chemotherapy. <https://doi.org/10.1128/aac.00156-25>.

Abstract

Background: There is a long-standing belief that bacteriostatic drugs are inherently antagonistic to the action of bactericidal antibiotics. This belief is primarily due to the fact that the action of most bactericidal antibiotics requires the target bacteria to be growing. Since bacteriostatic drugs stop the growth of treated bacteria, these drugs would necessarily work against one another. We have recently shown that bacteria treated with high concentrations of bacteriostatic drugs retain some metabolic activity, dividing on average once per day.

Objectives: We seek to determine if this low level of growth is sufficient to allow for bactericidal antibiotics of different classes to still kill after bacteria are treated with bacteriostatic drugs.

Methods: We first treated *Escherichia coli* and *Staphylococcus aureus* with two different bacteriostatic drugs, followed by one of three bactericidal drugs of three different classes. The density of these bacteria was tracked over six days to determine the amount of killing that occurred.

Results: Our results question this long-standing belief by demonstrating conditions where sequential treatment with a bacteriostatic then bactericidal antibiotic is as or more effective than treatment with a bactericidal drug alone.

Conclusions: These results raise the need to investigate the pharmacodynamics of the joint action of bacteriostatic and bactericidal antibiotics *in vitro* and *in vivo*.

Introduction

The clinical outcomes of antibiotic treatments involving the administration of bacteriostatic (which inhibit bacterial growth) or bactericidal (which kill bacteria) antibiotics are complex and context-dependent ^{1,2}. While antibiotic co-administration strategies can be beneficial in specific contexts, they require careful consideration regarding the interaction of the drugs, individualized patient factors, infection types, and resistance patterns ³. Therefore, it is necessary to evaluate specific drug combinations rather than relying solely on their classification as bacteriostatic or bactericidal. Historically, the co-administration of bacteriostatic and bactericidal antibiotics has been discouraged due to the notion that bactericidal drugs require actively dividing, metabolically active bacteria to exert their effects—an action that is directly opposed by bacteriostatic drugs ⁴. Despite this anticipated antagonism, many multi-drug treatment regimens employed for difficult-to-treat infections use combinations of both of these drugs, often to some degree of success ⁵. International guidelines often recommend combining bacteriostatic drugs, such as third-generation tetracyclines (e.g., tigecycline) or oxazolidinones (e.g., linezolid), with bactericidal agents as a last-resort treatment option ^{6,7}. Thus, these antibiotics cannot be purely antagonistic as commonly believed. Recent work by Gil-Gil et al. has shown that, even under high concentrations of bacteriostatic drugs, cell division occurs albeit at a rate nearly 100 times slower than in untreated cultures ⁸. Taken together, these previously reported results provide potential evidence and a mechanism that runs counter to the maxim that bacteriostatic and bactericidal antibiotics should not be used together.

Here, we use a laboratory strain of *Escherichia coli* ⁹ and a clinical isolate of *Staphylococcus aureus* ¹⁰ with combinations of bacteriostatic and bactericidal drugs to determine how pre-exposure to bacteriostatic drugs changes the dynamics of subsequent treatment with bactericidal agents. Surprisingly, we did not observe any conditions that resulted in complete antagonism between bacteriostatic and bactericidal drugs. Instead, our findings revealed a spectrum of outcomes, including delayed culture clearance, accelerated culture clearance, and even prevention of resistance emergence. These results question the maxim that bacteriostatic and

bactericidal antibiotics should not be used together and raise the need to further investigate the pharmacodynamics of the use of both of these drug types together.

Results

Determining the concentration of bacteriostatic antibiotics

To open our exploration of the dynamics of joint treatment with bacteriostatic and bactericidal antibiotics, we first determined the Minimum Inhibitory Concentration (MIC) of each drug to the two bacteria used for this study, *E. coli* MG1655 and *S. aureus* MN8. The MIC values for *E. coli* were 6.25 µg/mL for chloramphenicol, 25 µg/mL for azithromycin, 0.03 µg/mL for ciprofloxacin, 12 µg/mL for gentamicin, and 25 µg/mL for ampicillin. For *S. aureus*, the MIC values were 8 µg/mL for chloramphenicol, 0.15 µg/mL for tetracycline, 0.15 µg/mL for ciprofloxacin, 1 µg/mL for gentamicin, and 256 µg/mL for ampicillin. We then determined the concentration of the bacteriostatic antibiotic that prevents net growth over the course of the 6-day experiment while not causing a substantial amount of death in these cultures (Figure 1). Based on these results, all further experiments were conducted using 4x MIC concentrations of chloramphenicol and azithromycin for *E. coli* and 4x MIC for chloramphenicol and 10x MIC for tetracycline when using *S. aureus*.

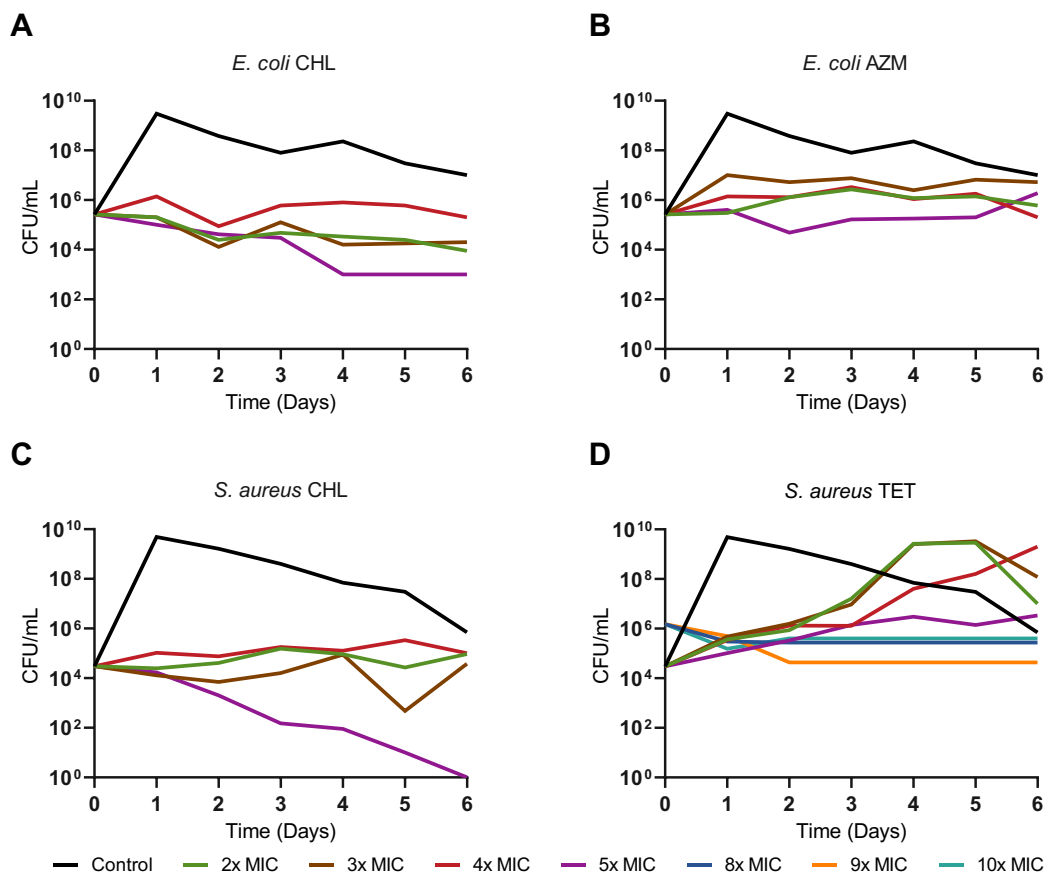


Figure 1. Exposure to varying concentrations of bacteriostatic drugs for six days without transferring.

Density in CFU/mL of *E. coli* MG1655 (A and B) and *S. aureus* MN8 (C and D) measured every day for six days at several concentrations of either chloramphenicol (CHL) (A and C), azithromycin (AZM) (B), or tetracycline (TET) (D). Shown in black for each panel is a control culture without antibiotics.

Treatment with a bacteriostatic then a bactericidal antibiotic

We initiated our joint action experiments by treating *E. coli* MG1655 with either chloramphenicol or azithromycin at a super-MIC concentration for one day. Following pre-treatment, we introduced one of several bactericidal drugs with differing mechanisms of action (Figure 2A, B, and C). Cultures were sampled each daily over a 6-day period. In every scenario where both drugs were used sequentially, the bacterial density at day 6 was consistently lower than in cultures containing just the bacteriostatic drug, indicating that bactericidal activity occurred. Notably, when gentamicin was administered after the bacteriostatic pre-treatment, bacterial clearance occurred faster than when gentamicin was used alone. This accelerated clearance is likely because, without the bacteriostatic pre-treatment, small colony variants resistant to gentamicin emerge; the pre-treatment effectively prevented the appearance of these resistant variants – thereby, enhancing the overall efficacy of gentamicin. However, the dynamics of treatment with ciprofloxacin and ampicillin following the bacteriostatic drug were slower than those when either ciprofloxacin or ampicillin were used alone.

When a clinical isolate of *S. aureus* was treated first with either chloramphenicol or tetracycline followed by a bactericidal drug, the results obtained are qualitatively like those obtained with *E. coli* (Figure 2C, D, and E). Interestingly, the combination of bacteriostatic drugs followed by ampicillin led to significantly greater culture clearance than ampicillin alone. While both bacteriostatic drugs combined with gentamicin or ciprofloxacin resulted in high levels of bacterial killing, these combinations slowed down the dynamics of both bactericidal drugs.

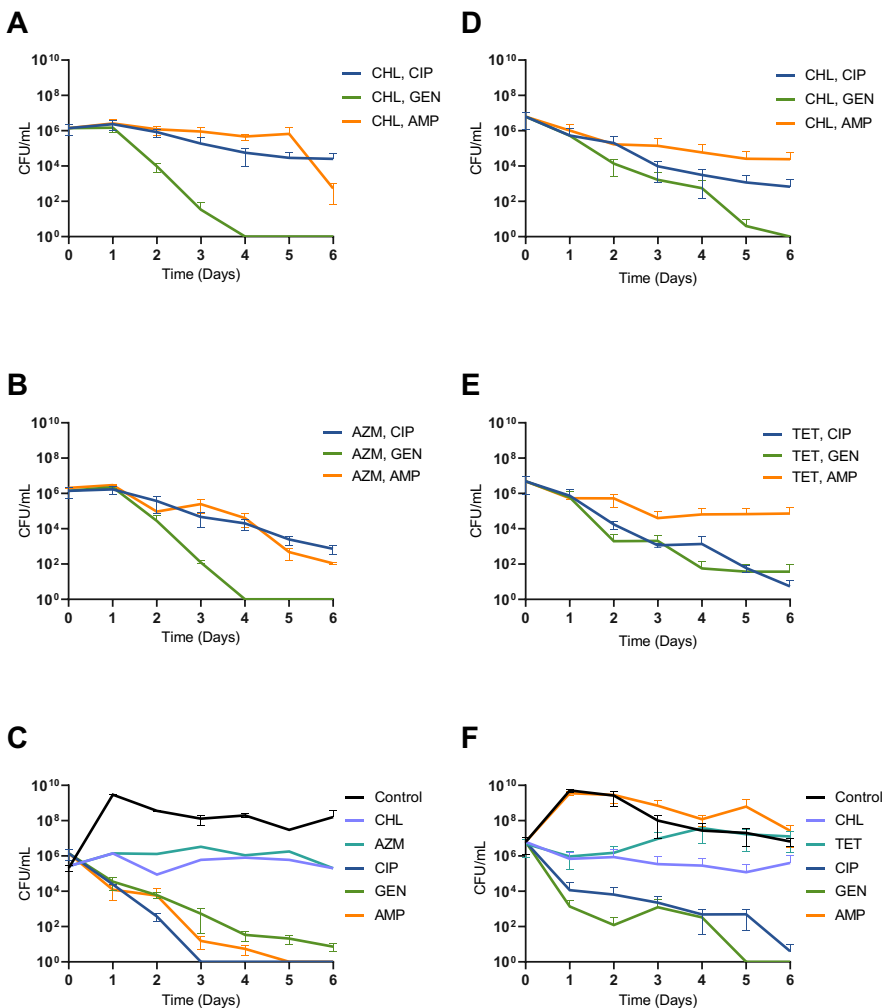


Figure 2. The treatment of *E. coli* and *S. aureus* with bacteriostatic followed by bactericidal antibiotics.

Shown are bacterial densities in CFU/mL, each point represents the mean and standard deviation of three biological replicates. Cultures are sampled every day for six days and are not transferred. A, B, and C correspond to *E. coli* experiments and D, E, and F to *S. aureus* experiments. Chloramphenicol is at 4x MIC, azithromycin at 4x MIC, tetracycline is at 10x MIC, and the bactericidal drugs are all at 4x MIC for *E. coli* and 12x MIC for *S. aureus*. For panels A, B, D, and E cultures were treated with either chloramphenicol, azithromycin, or tetracycline for one day before the subsequent addition of a bactericidal antibiotic. Figure C and F are a control where cultures were treated with only a bactericidal or bacteriostatic drug.

Discussion

Contrary to the maxim that bacteriostatic drugs are completely antagonistic to bactericidal agents ⁴, our findings indicate that bactericidal action does occur after bacteriostatic pre-treatment. In neither *E. coli* nor *S. aureus*, pre-treatment with bacteriostatic antibiotics was completely antagonistic to the subsequent action of bactericidal drugs. Quite to the contrary, pre-treatment with bacteriostatic drugs in several cases allowed for a higher degree of killing than treatment with just the bactericidal agents alone. Two key observations emerged from our study. First, bacteriostatic pre-treatment effectively suppressed the emergence of gentamicin-resistant small colony variants in *E. coli* that ascend with the treatment of gentamicin alone, increasing the rate of bacterial clearance ¹¹. Second, in the case of *S. aureus* MN8, an inducible beta-lactamase producer, pre-treatment with bacteriostatic drugs facilitated better control of bacterial density by ampicillin, although a significant population of what are likely persister cells remained. These results are consistent with the concept of cellular hysteresis and open the door to looking at collateral susceptibility with pairings of bacteriostatic and bactericidal antibiotics ^{12,13}.

As with all *in vitro* studies of antibiotics, the role of the host's immune system was not considered in our experiments, a critical factor in the success of antibiotic therapy ¹⁴. One hypothesis regarding why antibiotic therapy is successful *in vivo* is that the drugs slow down growth or reduce the density of bacteria, providing an opportunity for the host's innate immune response to control and potentially eliminate the infecting bacteria ¹⁵. While our study did not achieve complete bacterial clearance in all scenarios, whether through single-drug therapy or combined bacteriostatic and bactericidal treatments, we suggest that stopping the net growth of bacteria and achieving a higher degree of clearance over time would be sufficient for the host's immune system to control the residual bacterial population effectively. Subsequently, it is essential to further explore the pharmacodynamics of combined bacteriostatic and bactericidal treatments, both *in vitro* and *in vivo*, to better design antibiotic treatment protocols.

Materials and Methods

Growth media– LB broth (244620) was obtained from BD. Muller Hinton II (MHII) Broth (90922-500G) obtained from Millipore. LB agar (244510) for plates was obtained from BD.

Growth conditions– All experiments were conducted at 37°C and shaken continuously.

Bacterial strains– *E. coli* MG1655 was obtained from the Levin Lab Bacterial collection. *Staphylococcus aureus* MN8 was obtained from Tim Read of Emory University.

Antibiotics– Ciprofloxacin (A4556) was obtained from AppliChem Panreac, Chloramphenicol (23660) was obtained from USB, Ampicillin (A9518-25G) was obtained from Sigma Aldrich, Azithromycin (3771) was obtained from TOCRIS, Gentamicin (BP918-1) was obtained from Fisher BioReagents, and Tetracycline (T17999) was obtained from Research Products International.

Sampling bacterial densities– The densities of bacteria were estimated by serial dilution in 0.85% saline and plating. The total density of bacteria was estimated on Lysogeny Broth (LB) plates with 1.6% agar.

Minimum inhibitory concentrations– Antibiotic MICs were estimated using a 2-fold microdilution procedure as described in ¹⁶.

Antibiotic killing assays– For these experiments, overnight cultures of *E. coli* MG1655 or *S. aureus* MN8 were added to LB broth or MHII at an initial density of approximately 10⁶ cells per mL, followed by a 24 h incubation with a bacteriostatic drug at the concentrations indicated in the figure captions. After the 24 h incubation, a bactericidal antibiotic was added at the concentrations indicated in the figure captions. The cultures containing both drugs were incubated for five days without transferring. Bacterial densities were estimated before the addition of the bacteriostatic drugs (t=0), before the addition of the bactericidal drug (t=1), and on each subsequent day.

Acknowledgements

The authors would like to thank their principal investigator Bruce R. Levin for his kibitzing on this project. We would also like to thank Andrew P. Smith and Fernando Baquero for their comments and suggestions on this manuscript.

Funding

This project was funded by two awards to Bruce R. Levin, one from the US National Institute of General Medical Sciences via R35 GM 136407 and the other from the US National Institute of Allergy and Infectious Diseases via U19 AI 158080-02.

Transparency Declarations

The authors have no competing interests to declare.

References

1. Nemeth J, Oesch G, Kuster SP. Bacteriostatic versus bactericidal antibiotics for patients with serious bacterial infections: systematic review and meta-analysis. *J Antimicrob Chemother* 2015; **70**(2): 382-95.
2. Wald-Dickler N, Holtom P, Spellberg B. Busting the Myth of "Static vs Cidal": A Systemic Literature Review. *Clin Infect Dis* 2018; **66**(9): 1470-4.
3. Liu J, Shu Y, Zhu F, et al. Comparative efficacy and safety of combination therapy with high-dose sulbactam or colistin with additional antibacterial agents for multiple drug-resistant and extensively drug-resistant *Acinetobacter baumannii* infections: A systematic review and network meta-analysis. *J Glob Antimicrob Resist* 2021; **24**: 136-47.
4. Ocampo PS, Lázár V, Papp B, et al. Antagonism between bacteriostatic and bactericidal antibiotics is prevalent. *Antimicrob Agents Chemother* 2014; **58**(8): 4573-82.
5. Morales-Durán N, León-Buitimea A, Morones-Ramírez JR. Unraveling resistance mechanisms in combination therapy: A comprehensive review of recent advances and future directions. *Heliyon* 2024; **10**(6): e27984.
6. Lawandi A, Yek C, Kadri SS. IDSA guidance and ESCMID guidelines: complementary approaches toward a care standard for MDR Gram-negative infections. *Clin Microbiol Infect* 2022; **28**(4): 465-9.
7. Averbuch D, Cordonnier C, Livermore DM, et al. Targeted therapy against multi-resistant bacteria in leukemic and hematopoietic stem cell transplant recipients: guidelines of the 4th European Conference on Infections in Leukemia (ECIL-4, 2011). *Haematologica* 2013; **98**(12): 1836-47.
8. Gil-Gil T, Berryhill BA, Manuel JA, et al. The Evolution of Heteroresistance via Small Colony Variants in *Escherichia coli* Following Long Term Exposure to Bacteriostatic Antibiotics. *bioRxiv* 2024.
9. Berryhill BA, Gil-Gil T, Manuel JA, et al. What's the Matter with MICs: Bacterial Nutrition, Limiting Resources, and Antibiotic Pharmacodynamics. *Microbiol Spectr* 2023; **11**(3): e0409122.
10. Su M, Lyles JT, Petit Iii RA, et al. Genomic analysis of variability in Delta-toxin levels between *Staphylococcus aureus* strains. *PeerJ* 2020; **8**: e8717.

11. Noaman KA, Alharbi NS, Khaled JM, et al. The transmutation of *Escherichia coli* ATCC 25922 to small colony variants (SCVs) *E. coli* strain as a result of exposure to gentamicin. *J Infect Public Health* 2023; **16**(11): 1821-9.
12. Roemhild R, Gokhale CS, Dirksen P, et al. Cellular hysteresis as a principle to maximize the efficacy of antibiotic therapy. *Proc Natl Acad Sci U S A* 2018; **115**(39): 9767-72.
13. Roemhild R, Andersson DI. Mechanisms and therapeutic potential of collateral sensitivity to antibiotics. *PLoS Pathog* 2021; **17**(1): e1009172.
14. Berti A, Rose W, Nizet V, Sakoulas G. Antibiotics and Innate Immunity: A Cooperative Effort Toward the Successful Treatment of Infections. *Open Forum Infect Dis* 2020; **7**(8): ofaa302.
15. Ankomah P, Levin BR. Exploring the collaboration between antibiotics and the immune response in the treatment of acute, self-limiting infections. *Proc Natl Acad Sci U S A* 2014; **111**(23): 8331-8.
16. Jorgensen JH, Ferraro MJ. Antimicrobial susceptibility testing: a review of general principles and contemporary practices. *Clin Infect Dis* 2009; **49**(11): 1749-55.

Chapter 6

Chapter 6

The Future of Phage Therapy in the United States

Reprinted from: Berryhill BA, Gil-Gil T, Smith AP, Levin BR. 2025. The Future of Phage Therapy in the United States. Trends in Molecular Medicine. Accepted.

Abstract

Fueled by the increasing abundance of antibiotic-resistant pathogens, there has been a resurrection in the use of bacteriophage (phage) for therapeutic applications. Phage therapy was used in the early 20th century to limited success, which we attribute to its haphazard employment. To avoid repeating the mistakes of the past, this opinion first evaluates the historical reasons for the failure of phage therapy, analyzes the current state of the field, and ultimately makes recommendations for how to proceed with contemporary phage therapy. Despite many advances in the biology of bacteriophage, critical gaps in our knowledge persist. Our recommendations require physicians, scientists, and public-policy leaders to cooperate to bridge the outstanding gaps around phage therapy to develop phage into a useful therapeutic tool.

Phage therapy: where we were and where we are

Fueled by increasing frequencies of antibiotic-resistant pathogens, in recent years there has been a resurrection of research on and the application of bacteriophage (phage) to treat and prevent bacterial infections in humans, animals, and plants [1-3]. The original use of these viruses for treating bacterial infection, phage therapy, dates back more than a century to the work of Felix d'Herelle and his collaborators [4]. Although phage therapy remains an active enterprise in limited parts of the world [5], in the USA and most other western countries phages are not commonly used to treat bacterial infections [6,7].

Why did research and the application of phage therapy wane in Western science and medicine? Part of the answer to this question is that it was eclipsed by the development and application of antibiotics. However, the decline in phage therapy in Western medicine started before the widespread use of antibiotics in a time where there were no effective treatments for most bacterial infections. We postulate that much of the decline in phage therapy in the USA and Western medicine at large before its eclipse by antibiotics can be attributed to a two-part widely read perspective published in the Journal of the American Medical Association in 1934 by Eaton and Bayne-Jones [8].

Upon reading these two articles in a modern context, we see them not as a criticism of phage therapy as a clinical procedure but instead as a critique of the science behind it. In particular, these articles discuss: i) the lack of proper, clinically relevant controls; ii) the lack of a basic science understanding of how phage are effective and even what phage are; iii) the failure to consider established infections in experimentation; and iv) the inability to distinguish the direct action of the phage versus some other mechanism such as vaccination.

However, these articles on the clinical application of phage from the early 1900s are not entirely negative as these early reports provide support that phage were potentially viable in treating infections in some conditions such as bladder infections, abscesses, and infections with Staphylococcus, Streptococcus, Salmonella, and several species which were Bacillus at the time including *B. anthracis*, *Escherichia coli*, *B. subtilis*, and *Shigella spp.* This notwithstanding, these modest successes were not able to overcome the overall negative criticism in these

articles. We postulate due to the well-read nature of JAMA by microbiologists and clinicians at the time, faith in phage therapy was eroded and, consequently, it never developed into a broadly accepted clinical practice. Just one year after publication of these articles, sulfonamides were developed and used for treating bacterial infections and thus the era of antibiotics began and phage therapy was ultimately eclipsed [9].

As a consequence of antibiotic resistance, the revival of phage therapy has begun to emerge once again. We seek to continue the discussion that Eaton and Bayne-Jones began almost one century ago such that we can avoid repeating the mistakes that led to the decline of phage therapy previously. Here, we provide a brief summary of the state of phage therapy focusing on Western medicine and particularly in the USA, a critical analysis of the phage therapy enterprise as of 2025 and offer recommendations for how to best employ phage in these times to avoid repeating the mistakes of the past.

Phage therapy since 1934

Basic science advances in phage biology

While phage therapy may have all but ceased in the Western world after 1934, there were several advances addressing the knowledge gaps raised by Eaton and Bayne-Jones. In 1943, Renee Dubois presented compelling evidence that phage replicate *in vivo* using *Shigella dysenteriae* in mice [10]. Moreover, Dubois provided direct evidence that the phage were responsible for a decrease in mortality with otherwise fatal infections. A further line of evidence that phage replicate *in vivo* and can be an effective treatment of otherwise fatal *Escherichia coli* infections was provided in 1982 by Smith and Huggins [11]. Interestingly, Smith and Huggins found in mice that the phage were more effective than antibiotics in preventing mortality and that, in this particular case, the phage were exerting a selection pressure for reduced virulence by selecting for phage-resistant mutants. To address the concerns of phage resistance, research began into employing cocktails of multiple phages. Smith and Huggins showed in 1983 that with a cocktail of two phages, resistance only arose to one phage and that double-resistant mutants did not occur [11]. Similar results have been obtained by others since then [12,13]. While the above studies have focused on how phage interact with bacteria in animal models, progress has also been made to elucidate the role of the host response against phage [14,15], i.e., their pharmacokinetics. Work by Merrill *et al.* has shown that phage are antigenic and elicit a neutralizing antibody response and that phage are readily cleared from the bloodstream [16,17]. These and other works have emphasized and confirmed the need for using toxin-free bacteriophage lysates in treating animal models [18]. Numerous experiments have also illustrated the utility of phage to disperse biofilms [19,20]. Critically, during this time, studies were conducted on a variety of bacterial species showing phage efficacy for treating infections in experimental animals with a plethora of pathogens [21]. Taken together, the above-described animal model experiments begin to resolve the basic knowledge gaps presented by Eaton and Bayne-Jones.

The resurrection of phage therapy

Phage as personalized medicine

2017 marked the beginning of a new era for phage therapy to treat infections in humans in the USA. As detailed in the seminal work, *A Perfect Predator*, two cocktails of *A. baumannii* phages were employed to treat a long-term case of necrotizing pancreatitis after numerous courses of antibiotics had failed [22]. The administration of these phages was associated with the subsequent clearance of the infection and ultimately with saving the patient's life [23]. This treatment was performed as compassionate therapy using the FDA's Emergency Investigational New Drug (eIND) mechanism [24]. Under this mechanism a physician requests to the FDA to use an unapproved drug in an emergency for a small number of patients. Since then, there have been numerous cases of phage application under this eIND process [25]. These cases include but are not limited to: prosthetic joint infections (predominately those with *Staphylococcus* and *Pseudomonas*), left ventricular assist device infections with a variety of biofilm-forming bacteria, bacterial infections of cystic fibrosis patients, *Mycobacterium* infections (for both nontuberculosis and tuberculosis), and bacteremia with both Gram-positive and Gram-negative bacteria [26]. There have been reported successes for each of the bacteria and conditions listed but not every individual reported patient has had a successful treatment outcome. However, for a patient to qualify for eIND phage application they must have exhausted all appropriate antibiotic treatment options [25], meaning that this population is composed of the sickest patients that often have the most virulent infections. There are very narrow circumstances where phage therapy would fall under the traditional IND protocol rather than eIND. In these cases, local institutional review board approval would be sought before applying to the FDA, thus the timeline for administering phage under this mechanism is substantially longer. The reason this mechanism is uncommon for phage therapy is that the infection must have failed all previous treatment options, but with little immediate risk of mortality for the patient. Such examples include chronic infections such as infections of cystic fibrosis patients, acne, and chronic sinusitis infections as well as infections with guaranteed surgical remedy such as prosthetic joint infection and bone infections.

Clinical trials with phage

While phage application under the eIND mechanism focuses on the treatment of one individual, there is a need to generate a robust understanding of the efficacy and safety of using phage to treat infections more broadly. To achieve this end, there have been 84 documented clinical trials with phage as of October 2024 registered on ClinicalTrials.gov: 34 of these are ongoing and 50 are completed, terminated, or withdrawn. These clinical trials are being performed by academic institutions, government agencies, and biotechnology companies. At this juncture, there have been several high-profile successes. Included among these successes are: [27-29]. Alongside these successes, there have been several reported failures such as [30-32] and those described in [33]. In these cases, several reasons for failure have been identified including insufficient phage coverage, low titer of phage lysate, and the low density of target bacteria. Curiously, there are no listed failures of phage therapy that can be attributed to the emergence of phage-resistant bacteria. However, it is not clear whether these generally under-resourced clinical trials actually systematically looked for this, nor is it clear if the emergence of phage resistance would have any effect on clinical outcome despite all of the concerns around phage resistant bacteria [5].

Non-clinical applications of phage therapy

While much of the focus of phage therapy is on clinical intervention, particularly those for humans, there have also been limited applications of phage for other purposes. There are currently nine FDA-approved and three European Food Safety Authority (EFSA)-approved phage preparations commercially available for the treatment of infections in companion animals, including cocktails for canine otitis caused by *P. aeruginosa* and pyoderma caused by *Staphylococcus intermedius* [34]. The FDA has also approved *ex vivo* applications of phage for food preparation applications such as those used to decontaminate raw meat, vegetables, and frozen foods of *Salmonella*, *E. coli*, *Listeria monocytogenes*, and *Shigella* [35]. There are also several applications of phage in the field of agriculture. These uses include the treatment of farmed fish with phages for *Flavobacterium* [36]. Phage have also been approved for treating crops such as tomatoes for a variety of bacteria [37], kiwifruit for *Pseudomonas syringea* [38], and grapes, citrus, peaches, olives, and coffee against several pathogens [39].

Outside of the FDA's purview, phages have seen a litany of uses in food supplements and cosmetic products. Several products have been developed for the treatment of *Cutibacterium acnes* [40]. Phages have also seen extensive use in the probiotic realm for the over-the-counter treatment of enteric dysbiosis [41]. As these products do not fall under regulatory purview any governmental agency, there is very little quality control and almost no high-quality evidence of their efficacy [42].

Critical analysis of the current state of the research on, and the application of, phage therapy

While the above-described advances in bacteriophage biology and phage therapy are important, there is still much work to be done. We see major gaps in our understanding of the basic science of phage therapy, the particular means by which phage are being applied for therapy in humans, and the regulatory framework and oversight provided by the US government. For a summary of the major open questions in phage therapy, see the Outstanding questions.

Gaps in basic science

There are many open questions about how phage interact with the host's innate and adaptive immune systems [43-45]. Infections in humans are treated not merely when patients are infected, but when patients are sick. As such, by the time a patient has symptoms and begins treatment, the infection is established, and the structure and physiology of the infecting bacterial populations are very different than those constructed in a laboratory setting both *in vitro* and *in vivo* in experimental animals. Furthermore, by the time a patient is seen in a clinical setting, the innate immune system has already either controlled, or failed to control, the infection and the adaptive immune system has likely begun to respond to the infection [46]. In many cases, the bacteria are located in sites not amenable to immune response or access to antibiotics and phage such as abscesses, biofilms, and poorly vascularized tissues [47]. Yet, experimental analogues for these conditions are highly lacking and thus the contribution of these factors to the course of phage therapy remains unknown or poorly understood.

Much of the research performed with phage focuses on mechanisms of and conditions for the emergence of phage resistance *in vitro* [48]. Consequently, the criteria for selecting phages for clinical applications are based on *in vitro* parameters such as the ability to control bacteria in broth and the lack of emergence of resistance [49]. However, little is known about how resistance and virulence estimated *in vitro* correlates with the successes obtained in clinical applications. Critically, there are no guidelines available for the standardization of phage susceptibility. For antibiotics, the techniques for screening which antibiotics to employ only determine the amount of drug needed to prevent the replication of a bacteria; it is only when this amount is compared to a

standard provided by a group such as the Clinical and Laboratory Standards Institute (CLSI) or the European Committee on Antimicrobial Susceptibility Testing (EUCAST) that an isolate can be deemed as susceptible or resistant to a given drug [50,51]. There are no parallel groups for bacteriophage nor is there enough data for these groups to generate guidelines that can direct treatment. Thus, there is an outstanding need for improvement and standardization of phage susceptibility testing backed up by data of *in vitro* and *in vivo* correlates of success.

With eIND applications of phage, antibiotics are virtually always administered both prior to and concurrent with phage. Since these patients had to have failed multiple lines of antibiotics, they are often concurrently on multiple antibiotics of different classes and with different mechanisms of actions at the initiation of phage therapy. Yet, we know relatively little about how these antibiotics impact the course of infection and the bacteria's physiological state, and we know even less about how adding phage into this treatment milieu will impact its course.

Gaps in human applications

The primary application of phage to humans is “as you find them”—which is to say, these patients have already failed or are failing standard clinical interventions, are highly compromised, and generally are the most complicated cases. These complicated cases are not well understood to begin with and are the worst way of evaluating the efficacy of any therapeutic intervention, including phage. For example, we know a lot about the course of infection for uncomplicated bacterial pneumonia, yet these cases would never qualify for phage therapy, therefore we have no true way to measure the potential efficacy of phage in these more common infections. Yet, phage therapy is currently used against a wide variety of pathogens, several of which have been shown to not be amenable to phage therapy such as *Burkholderia* [37,52]. Perhaps most crucially, while we report successes readily there are relatively few reports of failures, and thus, we do not know the true denominator of the frequency of success.

We see very little interplay between basic and clinical science in the field of phage therapy, and arguably this is most common with phage therapy companies where there is primarily a profit motivation. To advance the field, there is a clear need to understand not only when and how phage therapy succeeds, but also when and how it fails. This is particularly important, because the failures of the large-scale clinical trials with phage are highly visible, yet the science investigating these failures lacks thoroughness and dissemination in the popular press. As illustrated in the Eaton and Bayne-Jones article [8], treating physicians are keenly aware of these failures and this could, and likely will, influence the application of phages to treat infections.

Gaps in regulation

The regulatory guidelines for the application of phage for the treatment of bacterial infections in humans is, at the same time, not adequately rigorous and too prohibitive. The standards for eIND application of phage are relatively low, which enables physicians to treat the sickest patients, but in the process provides virtually no incentive to explore the reasons for success and failure or even the generality of results obtained. However, under the clinical trial guidelines, where more generalizable results are obtained, phage are treated as a small-molecule drug [53]; thus, the restrictions are nearly insurmountable. These restrictions can only be overcome with considerable capital, greatly restricting who can do these trials and reducing what infections are examined to those that promise the most profit, rather than the infections best suited for resolution via phage. Moreover, the approval via the clinical trial process for specific phages is likely to be of marginal value as there are no guarantees that the phage approved for one infection will be of use to any other infections. However, we are not advocating for blanket approval of phages, as this could lead to the shelves being filled with phages that are useless for most infections.

Recommendations

We see the above gaps as dispositive for the future of phage therapy. The cornerstone of phage therapy and its future lies in increasing our understanding of the basic science underlying phage therapy. Towards this end, we make several suggestions that will facilitate more robust and clinically relevant experimentation. To avoid a repeat of the past described nearly a century ago by Eaton and Bayne-Jones, we make the below suggestions with some urgency. For a physician-centric view of the recommendations, see the Clinician's corner.

Clinical phage and bacteria repository

Critical to increasing our understanding of the conditions behind and the reasons for the successes and failures of phage therapy, in humans and domestic animals, is the ability to recapitulate the course of treatment. We are unable to do this currently due to the lack of preservation and access to both the infecting bacterial strains and the phages employed for treating those infections. To this end, we recommend the development of a common, global repository of these bacteria and phages. The idea of storing and cataloguing bacterial pathogens and phages, generally, is not novel [54,55]. For some time, there have been banks of phages and pathogenic bacteria, but none to our knowledge store both phages and bacteria, and they certainly do not store them in a way that allows determination of which phages were employed for treating which particular pathogen. We believe that samples of the infecting bacteria before, during, and after the course of treatment with a phage are essential, enabling monitoring of things such as the emergence of phage resistance. The ability to determine and have access to the phages which were used to treat a particular bacteria and access to that bacterium is paramount to understanding the mechanisms and dynamics underlying the course of infections and their treatment. We do realize that this endeavor requires a large amount of personnel, data, and resources. Such biobanks are best managed by sizeable national and international consortia and agencies [56].

Creation of these repositories enables a different, albeit more meaningful, clinical trial design for phage therapy. Currently, clinical trial enrollment criteria are primarily based on disease indication, e.g. people with Staphylococcal diabetic foot osteomyelitis [57]. However, the creation of these large phage repositories would

enable a clinical trial with a new criterion: having a specific disease indication for which there are multiple phages with lytic activity against the identified pathogen. Adding in this extra criterion will enable the comparison of treatment outcomes across similar infections. We would not evaluate the efficacy of a given antibiotic to treat infections with bacteria which are resistant to that drug; however, with the current clinical trial designs for phage, this is precisely what we do.

A more comprehensive clinical dataset

One of the fundamental failings on the clinical side of phage therapy is not knowing the true frequency of success, stemming from not knowing the total number of cases. This is driven by the absence of incentive and means to publish negative results. Few biotechnology companies, academic researchers, and scientific journals are motivated to do so; however, when, why, and how phage therapy fails cannot be elucidated from only successes. To address this issue, we recommend the preregistration in publicly accessible databases or journals of all cases which intend to employ phage therapeutically. We believe this is currently viable given the relative rarity of phage therapy in humans. As part of this preregistration, we suggest publishing the following: i) the target bacteria; ii) information about the site, nature, and course of the infection; iii) the patient's treatment history; iv) the treatment plan to include the proposed phage and its density, the administration method, the administration frequency and dosing, the co-administered antibiotics and their dosing; and v) what data will be generated and reported over the course of treatment. It should be noted, these five points are markedly similar to that already required to be provided to the FDA for phage therapy approvals [53]. This preregistration creates solvency for the above issues and enables the determination of the true number of phage therapy attempts. These preregistrations should act as a commitment to the database or journal that data about the outcome of the treatment attempt will be provided regardless of treatment outcome.

Apart from preregistration, we need to improve the quality as well as the quantity and consistency of the data generated from phage treatment. We believe several points of data are crucial to our understanding of the dynamics of the application of phage to treat bacterial infections and reporting these data should be standard

within these reports. The data should include bacterial and phages densities upon the initiation and throughout the course of therapy. In the course of estimating these densities, frequent samples from the patient can be obtained and stored. Having these frequent samples enables retrospective investigation into longitudinal changes both in antibiotic and phage susceptibility of the target bacteria and the host's innate and adaptive immune response.

As with the development of new datasets, there are many ways to achieve the same end. While we do not prefer one particular method, we do suggest the following as a feasible approach. For this, a phage library of cocktails would be generated that can cover a large swath of the strains of pathogens commonly seen in clinic which are amenable to phage therapy such as *S. aureus*, *E. coli*, *Klebsiella spp.*, and *Pseudomonas aeruginosa* [58]. These cocktails would then be made available under eIND or IND at low to no cost to the treating physician should the physician agree to collect the critical data described above. The infecting bacteria would then also be submitted to the repository for storage and characterization.

Development of new model systems

A variety of model systems are needed to bridge the gap between basic *in vitro* research and the clinical application of phage. Currently, the default *in vivo* model for understanding and treating bacterial infection is laboratory mice [59]. However, the results demonstrated in laboratory mice have been shown to have poor correlation with treatment outcomes in humans, raising concerns about the clinical translation of these results [60]. Having model systems with physiological conditions that mimic the biology at play in human infections is crucial to the development of effective phage therapy. The development of these models should prioritize specific hypothesis-based questions with conditions relevant to the clinical context in which phage would be employed in humans. Just as ferrets have been shown to be an optimal system for addressing questions related to the biology of influenza in the context of human infections [61], so too should we considerate alternative model systems for addressing questions of how best to employ phage for treating differing infections in humans. In Table 1 we provide a list of model systems and the types of questions they may be useful in addressing.

Table 1. Model systems for phage therapy

System	Utility	Refs
Pigs	Studying gut microbiota and systemic infections	[62-64]
Rats	Studying the immune response, tissue penetration (abscesses and blood–brain barrier), and biodistribution	[65-67]
Guinea pigs	Studying the immune response and tissue penetration	[68,69]
Non-human primates	Direct clinical/translational research	[70]
Rabbits	Studying abscesses and soft tissue infections	[71-73]
Mice	Studying gut decontamination	[74,75]

Using these animals as models for phage therapy not only increases our understanding of the application of phage for treatment in humans, but we also gain an understanding of how phage can be employed to minimize antibiotic use in livestock and thereby minimize the pressure for antibiotic resistance [76]. This knowledge also opens the door to using phage to treat infections in these domestic animals.

Changing the regulatory landscape

We recommend two modifications to the current regulatory landscape. First, the application of phage as a clinical product should have their own, unique regulatory guidelines and not be licensed as small-molecule drugs. Second, the approval process of phage needs to be refined, both for eIND and clinical trials. At present, specific single phage or cocktails of multiple, specified phages are approved for administration. This is untenable. While we do not have specific solvency for this issue, we believe that the FDA needs to engage in

discourse with academics, biotechnology companies, and physicians to determine reasonable guidelines for the approval of phages. One method for the approval of phages for clinical use could be approval of methods rather than the phages themselves, e.g. phage isolation, characterization, propagation, and preparation pipelines could be targets for regulatory approval. While we are making the above suggestions to facilitate phage therapy, they should not be read as loosening the requires for the type of data needed to proceed to clinical trials, but rather to have specific criteria for phages. The type of data one would expect from similar small molecule trials such as pharmacodynamic and pharmacokinetic data supporting the proposed trial are paramount and should not be compromised.

Concluding remarks

The previous critical analysis of phage therapy performed by Eaton and Bayne-Jones in 1934 abated the interest in and research on phage and facilitated antibiotics eclipsing phage therapy; that is certainly not the intent of this opinion article. Rather, we hope we accomplish the opposite, in that we intend this article to motivate both the research on and application of phage for therapy in conjunction with antibiotics. Unfortunately, we believe today's phage therapy is walking in the shadow of its predecessor, and our desire is that our analysis and suggestions above prevent phage therapy from once again being relegated to research exclusively performed by academics for non-clinical purposes. While there are many changes that need to occur to the field of phage therapy, those we discuss above and summarize in Figure 1, are the primary issues that need to be addressed.

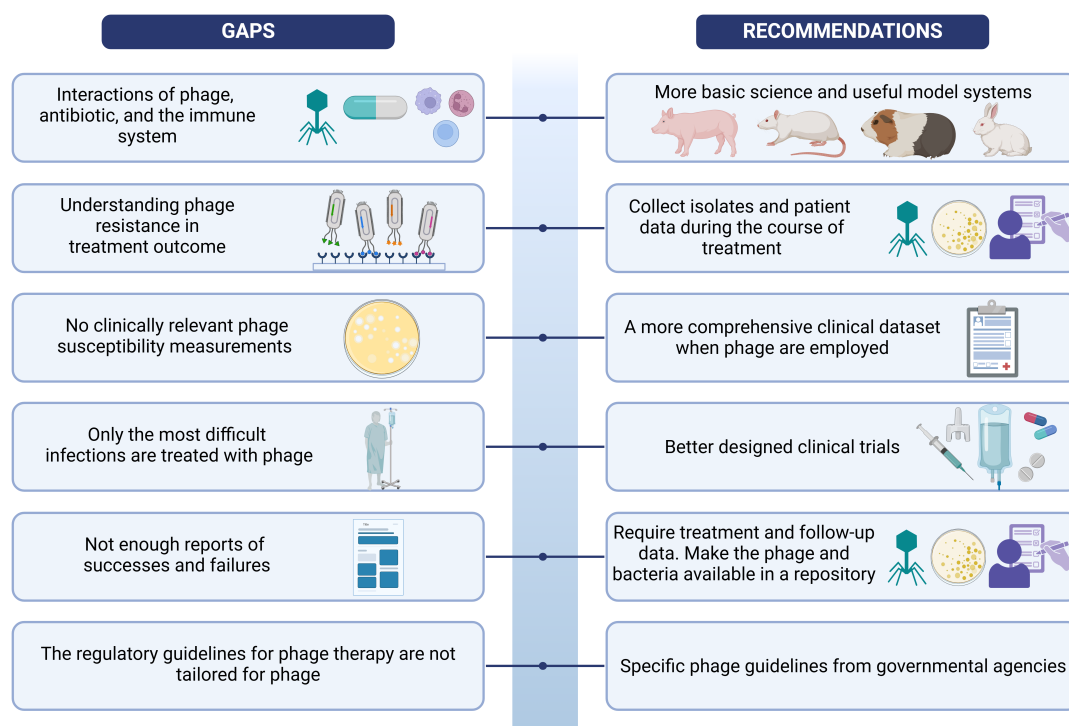


Figure 1. Gaps and recommendations for phage therapy. Shown on the left are the gaps we have identified in the field of phage therapy; shown on the right are our suggested recommendations for addressing these gaps.

Clinician's corner

- The use of bacteriophage to treat bacterial infections has the potential to help overcome the antibiotic-resistance crisis.
- Little is known about how and why phage therapy succeeds in or fails in treating bacterial infections. Elements of this include the lack of understanding about the interactions of phage, antibiotics, and the host's biology. Relevant features of the host's biology which we do not know include how the innate and adaptive immune responses interact with phage, how variation in the source and site of infection changes the course of treatment, and the pharmacokinetics of phage in human hosts.
- There is a need for the voice of clinicians in discussions with both patients and governmental regulatory agencies in advancing phage therapy as a clinical practice.

Highlights

- Following a high-profile success in 2016, the field of phage therapy has been reinvigorated. Numerous biotechnology companies, academic groups, and hospitals are now developing and using bacteriophage to treat bacterial infections.
- Recently, several clinical trials along with many of the personalized, medical applications of phage have failed.
- Due to a lack of basic science, the reasons behind when and why phage therapy fails, and indeed when and why it succeeds, to treat infections is not understood.
- The regulatory framework governing the application of phage for the treatment of infections is not amenable to the development and expansion of phage therapy.

Outstanding questions

- What models or model systems can be best used to study bacteriophage and how they interact with antibiotics, the host's immune systems, and the physiology of humans to more accurately mimic what occurs during the clinical application of phage during the treatment of bacterial infections?
- How can we establish research frameworks which enable and encourage basic scientists to follow-up on the results of phage therapy obtained in the clinic?
- How we can we make the regulations promulgated by governmental agencies more amenable to the development and application of phage for therapy while at the same time staying as rigorous as those applied to other drugs?

Acknowledgements

We would like to thank Alysha Ismail and the rest of the Levin Lab as well as Dr. Jason Chen for their discussion of this manuscript. The authors are very grateful to Professor James J Bull for his insightful discussion and comments on this manuscript throughout the entire writing process. BRL would like to thank the US National Institute of General Medical Sciences for their funding support via R35GM136407.

Declaration of interests

The authors have no competing interests to declare.

References

1. Hatfull, G.F. *et al.* (2022) Phage Therapy for Antibiotic-Resistant Bacterial Infections. *Annu Rev Med* 73, 197-211
2. Vila, M. *et al.* (2024) Phage Delivery Strategies for Biocontrolling Human, Animal, and Plant Bacterial Infections: State of the Art. *Pharmaceutics* 16, 374
3. Cahan, E. (2023) As Superbugs Flourish, Bacteriophage Therapy Recaptures Researchers' Interest. *Jama* 329, 781-784
4. Summers, W.C. (2016) Félix Hubert d'Herelle (1873-1949): History of a scientific mind. *Bacteriophage* 6, e1270090
5. Pirnay, J.P. *et al.* (2024) Personalized bacteriophage therapy outcomes for 100 consecutive cases: a multicentre, multinational, retrospective observational study. *Nat Microbiol* 9, 1434-1453
6. Parfitt, T. (2005) Georgia: an unlikely stronghold for bacteriophage therapy. *Lancet* 365, 2166-2167
7. Aswani, V.H. and Shukla, S.K. (2021) An Early History of Phage Therapy in the United States: Is it Time to Reconsider? *Clin Med Res* 19, 82-89.
8. EATON, M.D. and BAYNE-JONES, S. (1934) BACTERIOPHAGE THERAPY: REVIEW OF THE PRINCIPLES AND RESULTS OF THE USE OF BACTERIOPHAGE IN THE TREATMENT OF INFECTIONS. *Journal of the American Medical Association* 103, 1769-1776.
9. Hutchings, M.I. *et al.* (2019) Antibiotics: past, present and future. *Curr Opin Microbiol* 51, 72-80
10. Dubois, R.J. *et al.* (1943) The multiplication of bacteriophage *in vivo* and its protective effect against an experimental infection with *Shigella dysenteriae*. *J Exp Med* 78, 161-168

11. Smith, H.W. and Huggins, M.B. (1982) Successful treatment of experimental *Escherichia coli* infections in mice using phage: its general superiority over antibiotics. *J Gen Microbiol* 128, 307-318
12. Antoine, C. *et al.* (2021) In Vitro Characterization and In Vivo Efficacy Assessment in *Galleria mellonella* Larvae of Newly Isolated Bacteriophages against *Escherichia coli* K1. *Viruses* 13, 2005-2024
13. Henry, M. *et al.* (2013) Predicting in vivo efficacy of therapeutic bacteriophages used to treat pulmonary infections. *Antimicrob Agents Chemother* 57, 5961-5968.
14. Nang, S.C. *et al.* (2023) Pharmacokinetics/pharmacodynamics of phage therapy: a major hurdle to clinical translation. *Clin Microbiol Infect* 29, 702-709.
15. Dąbrowska, K. (2019) Phage therapy: What factors shape phage pharmacokinetics and bioavailability? Systematic and critical review. *Med Res Rev* 39, 2000-2025
16. Merrill, C.R. *et al.* (1996) Long-circulating bacteriophage as antibacterial agents. *Proc Natl Acad Sci U S A* 93, 3188-3192
17. Geier, M.R. *et al.* (1973) Fate of bacteriophage lambda in non-immune germ-free mice. *Nature* 246, 221-223
18. Hietala, V. *et al.* (2019) The Removal of Endo- and Enterotoxins From Bacteriophage Preparations. *Front Microbiol* 10, 1674
19. Liu, S. *et al.* (2022) Phages against Pathogenic Bacterial Biofilms and Biofilm-Based Infections: A Review. *Pharmaceutics* 14, 427
20. Kovacs, C.J. *et al.* (2024) Disruption of Biofilm by Bacteriophages in Clinically Relevant Settings. *Mil Med* 189, e1294-e1302

21. Sulakvelidze, A. *et al.* (2001) Bacteriophage therapy. *Antimicrob Agents Chemother* 45, 649-659
22. Steffanie Strathdee, T.B., and Thomas Patterson (2019) *The perfect predator : a scientist's race to save her husband from a deadly superbug : a memoir* Hachette Books, New York, NY, 2020
23. Schooley, R.T. *et al.* (2017) Development and Use of Personalized Bacteriophage-Based Therapeutic Cocktails To Treat a Patient with a Disseminated Resistant *Acinetobacter baumannii* Infection. *Antimicrob Agents Chemother* 61, 1-14
24. Van Norman, G.A. (2016) Drugs, Devices, and the FDA: Part 1: An Overview of Approval Processes for Drugs. *JACC Basic Transl Sci* 1, 170-179.
25. McCallin, S. *et al.* (2019) Current State of Compassionate Phage Therapy. *Viruses* 11, 343
26. Hitchcock, N.M. *et al.* (2023) Current Clinical Landscape and Global Potential of Bacteriophage Therapy. *Viruses* 15, 1020
27. Tamma, P.D. *et al.* (2022) Safety and microbiological activity of phage therapy in persons with cystic fibrosis colonized with *Pseudomonas aeruginosa*: study protocol for a phase 1b/2, multicenter, randomized, double-blind, placebo-controlled trial. *Trials* 23, 1057
28. Wright, A. *et al.* (2009) A controlled clinical trial of a therapeutic bacteriophage preparation in chronic otitis due to antibiotic-resistant *Pseudomonas aeruginosa*; a preliminary report of efficacy. *Clin Otolaryngol* 34, 349-357
29. Ooi, M.L. *et al.* (2019) Safety and Tolerability of Bacteriophage Therapy for Chronic Rhinosinusitis Due to *Staphylococcus aureus*. *JAMA Otolaryngol Head Neck Surg* 145, 723-729

30. Jault, P. *et al.* (2019) Efficacy and tolerability of a cocktail of bacteriophages to treat burn wounds infected by *Pseudomonas aeruginosa* (PhagoBurn): a randomised, controlled, double-blind phase 1/2 trial. *Lancet Infect Dis* 19, 35-45.
31. Leitner, L. *et al.* (2021) Intravesical bacteriophages for treating urinary tract infections in patients undergoing transurethral resection of the prostate: a randomised, placebo-controlled, double-blind clinical trial. *Lancet Infect Dis* 21, 427-436
32. Sarker, S.A. *et al.* (2016) Oral Phage Therapy of Acute Bacterial Diarrhea With Two Coliphage Preparations: A Randomized Trial in Children From Bangladesh. *EBioMedicine* 4, 124-137
33. Górski, A. *et al.* (2020) Phage Therapy: Towards a Successful Clinical Trial. *Antibiotics (Basel)* 9, 827
34. Strathdee, S.A. *et al.* (2023) Phage therapy: From biological mechanisms to future directions. *Cell* 186, 17-31
35. Moye, Z.D. *et al.* (2018) Bacteriophage Applications for Food Production and Processing. *Viruses* 10, 205
36. Sundell, K. *et al.* (2020) Bacteriophages as Biocontrol Agents for *Flavobacterium psychrophilum* Biofilms and Rainbow Trout Infections. *Phage (New Rochelle)* 1, 198-204
37. Villalpando-Aguilar, J.L. *et al.* (2022) Phage Therapy for Crops: Concepts, Experimental and Bioinformatics Approaches to Direct Its Application. *Int J Mol Sci* 24, 325
38. Frampton, R.A. *et al.* (2014) Identification of bacteriophages for biocontrol of the kiwifruit canker phytopathogen *Pseudomonas syringae* pv. *actinidiae*. *Appl Environ Microbiol* 80, 2216-2228
39. Hopkins, D.L. and Purcell, A.H. (2002) *Xylella fastidiosa*: Cause of Pierce's Disease of Grapevine and Other Emergent Diseases. *Plant Dis* 86, 1056-1066.

40. Golembo, M. *et al.* (2022) Development of a topical bacteriophage gel targeting *Cutibacterium acnes* for acne prone skin and results of a phase 1 cosmetic randomized clinical trial. *Skin Health Dis* 2, e93
41. Kiani, A.K. *et al.* (2020) Bacteriophages in food supplements obtained from natural sources. *Acta Biomed* 91, e2020025
42. Verbeken, G. *et al.* (2007) European regulatory conundrum of phage therapy. *Future Microbiol* 2, 485-491
43. Van Belleghem, J.D. *et al.* (2018) Interactions between Bacteriophage, Bacteria, and the Mammalian Immune System. *Viruses* 11, 10
44. Berkson, J.D. *et al.* (2024) Phage-specific immunity impairs efficacy of bacteriophage targeting Vancomycin Resistant Enterococcus in a murine model. *Nat Commun* 15, 2993
45. Stellfox, M.E. *et al.* (2024) Bacteriophage and antibiotic combination therapy for recurrent Enterococcus faecium bacteremia. *mBio* 15, e0339623.
46. López-Nevado, M. *et al.* (2021) Primary Immune Regulatory Disorders With an Autoimmune Lymphoproliferative Syndrome-Like Phenotype: Immunologic Evaluation, Early Diagnosis and Management. *Front Immunol* 12, 671755.
47. Gondil, V.S. and Subhadra, B. (2023) Biofilms and their role on diseases. *BMC Microbiol* 23, 203
48. Labrie, S.J. *et al.* (2010) Bacteriophage resistance mechanisms. *Nat Rev Microbiol* 8, 317-327
49. Hyman, P. (2019) Phages for Phage Therapy: Isolation, Characterization, and Host Range Breadth. *Pharmaceuticals (Basel)* 12, 35

50. Giske, C.G. *et al.* (2022) Update from the European Committee on Antimicrobial Susceptibility Testing (EUCAST). *Journal of Clinical Microbiology* 60, e00276-00221
51. Weinstein, M.P. and Lewis, J.S., 2nd (2020) The Clinical and Laboratory Standards Institute Subcommittee on Antimicrobial Susceptibility Testing: Background, Organization, Functions, and Processes. *J Clin Microbiol* 58, 1-9
52. Lim, Y.M. *et al.* (2022) Effective Therapeutic Options for Melioidosis: Antibiotics versus Phage Therapy. *Pathogens* 12, 11
53. National Institute of Allergy and Infectious Diseases, & Center for Biologics Evaluation and Research. (2021). Science and Regulation of Bacteriophage Therapy. In *Science and Regulation of Bacteriophage Therapy Workshop*. FDA (Food and Drug Administration), 1-225.
54. De Paoli, P. (2005) Bio-banking in microbiology: from sample collection to epidemiology, diagnosis and research. *FEMS Microbiol Rev* 29, 897-910.
55. Nagel, T. *et al.* (2022) Phage banks as potential tools to rapidly and cost-effectively manage antimicrobial resistance in the developing world. *Curr Opin Virol* 53, 101208
56. Lin, R.C. *et al.* (2021) Phage Biobank: Present Challenges and Future Perspectives. *Curr Opin Biotechnol* 68, 221-230
57. Sawa, T. *et al.* (2024) Current status of bacteriophage therapy for severe bacterial infections. *J Intensive Care* 12, 44
58. El Haddad, L. *et al.* (2018) A Systematic and Critical Review of Bacteriophage Therapy Against Multidrug-resistant ESKAPE Organisms in Humans. *Clinical Infectious Diseases* 69, 167-178

59. Sarkar, S. and Heise, M.T. (2019) Mouse Models as Resources for Studying Infectious Diseases. *Clin Ther* 41, 1912-1922
60. Burkhardt, A.M. and Zlotnik, A. (2013) Translating translational research: mouse models of human disease. *Cell Mol Immunol* 10, 373-374
61. Belser, J.A. *et al.* (2020) A Guide for the Use of the Ferret Model for Influenza Virus Infection. *Am J Pathol* 190, 11-24
62. Fairbairn, L. *et al.* (2011) The mononuclear phagocyte system of the pig as a model for understanding human innate immunity and disease. *J Leukoc Biol* 89, 855-871.
63. Meurens, F. *et al.* (2012) The pig: a model for human infectious diseases. *Trends Microbiol* 20, 50-57
64. Zhang, Q. *et al.* (2013) A pig model of the human gastrointestinal tract. *Gut Microbes* 4, 193-200
65. McDannold, N. *et al.* (2020) Blood-brain barrier disruption and delivery of irinotecan in a rat model using a clinical transcranial MRI-guided focused ultrasound system. *Scientific Reports* 10, 8766
66. Matsumoto, K. *et al.* (2015) Pharmacokinetics and skin-tissue penetration of daptomycin in rats. *Clin Pharmacol* 7, 79-82
67. Lin, Y.W. *et al.* (2020) Pharmacokinetics/pharmacodynamics of antipseudomonal bacteriophage therapy in rats: a proof-of-concept study. *Clin Microbiol Infect* 26, 1229-1235
68. Padilla-Carlin, D.J. *et al.* (2008) The guinea pig as a model of infectious diseases. *Comp Med* 58, 324-340
69. Barbero, A.M. and Frasch, H.F. (2009) Pig and guinea pig skin as surrogates for human in vitro penetration studies: a quantitative review. *Toxicol In Vitro* 23, 1-13.

70. Chen, L. *et al.* (2019) Nonhuman primate species as models of human bacterial sepsis. *Lab Animal* 48, 57-65
71. Malachowa, N. *et al.* (2022) Toward Optimization of a Rabbit Model of Staphylococcus aureus (USA300) Skin and Soft Tissue Infection. *Microbiology Spectrum* 10, e02716-02721
72. Wills, Q.F. *et al.* (2005) Experimental bacteriophage protection against Staphylococcus aureus abscesses in a rabbit model. *Antimicrob Agents Chemother* 49, 1220-1221
73. Feldenzer, J.A. *et al.* (1987) Experimental spinal epidural abscess: a pathophysiological model in the rabbit. *Neurosurgery* 20, 859-867
74. Reyes, A. *et al.* (2013) Gnotobiotic mouse model of phage-bacterial host dynamics in the human gut. *Proc Natl Acad Sci U S A* 110, 20236-20241.
75. Amorim, N. *et al.* (2022) Refining a Protocol for Faecal Microbiota Engraftment in Animal Models After Successful Antibiotic-Induced Gut Decontamination. *Front Med (Lausanne)* 9, 770017
76. Ghimpețeanu, O.M. *et al.* (2022) Antibiotic Use in Livestock and Residues in Food-A Public Health Threat: A Review. *Foods* 11, 1430

Chapter 7

Chapter 7

The book of Lambda doesn't tell us that naturally occurring lysogens of *Escherichia coli* are likely to be resistant and not only immune to phage coded by their prophage

Reprinted from: Berryhill BA, Garcia R, McCall IC, Manuel JA, Chaudhry W, Petit MA, Levin BR. 2023. The book of Lambda does not tell us that naturally occurring lysogens of *Escherichia coli* are likely to be resistant as well as immune. Proceedings of the National Academy of Sciences of the United States of America. <https://doi.org/10.1073/pnas.2303941120>.

Abstract

The most significant difference between bacteriophages functionally and ecologically is whether they are purely lytic (virulent) or temperate. Virulent phages can only be transmitted horizontally by infection, most commonly with the death of their hosts. Temperate phages can also be transmitted horizontally, but upon infection of susceptible bacteria, their genomes can be incorporated into that of their host's as a prophage and be transmitted vertically in the course of cell division by their lysogenic hosts. From what we know from studies with the temperate phage Lambda and other temperate phages, in laboratory culture, lysogenic bacteria are protected from killing by the phage coded for by their prophage by immunity; where upon infecting lysogens, the free temperate phage coded by their prophage are lost. Why are lysogens not also resistant as well as immune to the phage coded by their prophage since immunity does not confer protection against virulent phages? To address this question, we used a mathematical model and performed experiments with temperate and virulent mutants of the phage Lambda in laboratory culture. Our models predict and experiments confirm that selection would favor the evolution of resistant as well as immune lysogens, particularly if the environment includes virulent phage that share the same receptors as the temperate. To explore the validity and generality of this prediction, we examined ten lysogenic *Escherichia coli* from natural

populations. All ten were capable of forming immune lysogens but their original hosts were resistant to the phage coded by their prophage.

Significance Statement

The temperate bacteriophages that abound in natural populations of bacteria play a prominent role in the horizontal transmission of genes between clones of bacteria. These phages often code for toxins and other characters responsible for the virulence of pathogenic bacteria. While a great deal is known about these viruses' genetics and molecular biology, we know relatively little about their population and evolutionary biology in natural communities of bacteria. The results of this jointly theoretical and experimental study predict and present evidence contrary to what is anticipated from laboratory studies of temperate phages and lysogeny, as we found that naturally occurring lysogens are likely to be resistant (refractory) and not only immune to the phage coded for by their prophage.

Introduction

Functionally and ecologically, the single most significant difference among bacteriophages is whether they are virulent (“purely lytic”) or temperate. Virulent phages, a major source of bacterial mortality (1), can only be transmitted horizontally, commonly with the death of the infected bacterium and subsequent release of phage particles (2). Temperate phages can also be transmitted horizontally in this way, but with a low probability, their genomes can become incorporated into that of the infected bacterium as prophage (3), forming lysogens. The infected lysogens survive and the phage genome, borne by these lysogenic bacteria, is transmitted vertically during cell division (3, 4).

Be the phage virulent or temperate, selection will favor bacteria that can survive when confronted by these viruses. Bacteria have several mechanisms that facilitate their survival in the presence of phage. We divide these mechanisms into two functionally distinct classes based on whether or not the phage genome enters the cell. We refer to the mechanisms where the phage genome enters the cells, but the infecting phage are prevented from replicating and are lost, as immunity. Included amongst these immunity mechanisms are CRISPR-Cas (5), restriction-modification (6), abortive infection (7), and super infection exclusion (8). The latter mechanism obtains when lysogens are infected by the phage coded by their prophage. The most prominent mechanism by which phage genomes are prevented from entering cells is receptor site modification, which we define as resistance. Though, other mechanisms for resistance based survival exist such as O-antigen display in which the bacteriophage are sterically inhibited from adsorbing to the bacteria (9). Critical to this definition of resistance is the fact that the phage virion does not attach to the cell and thus the bacteria is refractory to the phage.

Though immunity is the primary mechanism by which lysogens are protected from super infection by the phage coded by their prophage, the vast majority of infections of a naïve host by a temperate phage result in a lytic cycle. Moreover, virulent mutants of temperate phages, ex-temperate phages (10), can be generated by mutation and there may well be virulent phages that share the same receptor as temperate phages. Why then does selection not also lead to the evolution of resistant lysogens? To address this question,

we use a mathematical model of the population and evolutionary dynamics of temperate phages in bacteria capable of generating resistant mutants in sensitive cells and lysogens. The results of our numerical analysis of the properties of our model with parameters in the range estimated for *Escherichia coli* and its phages, predict that when populations of sensitive bacteria are confronted by temperate phages, immune lysogens, resistant non-lysogens, and resistant lysogens will emerge and ascend. The ascent of resistant lysogen is particularly prevalent, if the community includes virulent, ex-temperate phages, or other phages that share the same receptors as the temperate. Our tests of this prediction with *E. coli* and temperate and virulent mutants of the phage lambda respectively, Lambda and Lambda^{VIR} are consistent with it.

To explore the real-world generality of this prediction, we examined the susceptibility of ten naturally occurring lysogenic *E. coli* to the phage coded for by their prophage. All ten temperate phages generated by induction of these wild lysogens were capable of infecting and forming immune lysogens in a laboratory strain of *E. coli*. Most critically, as predicted by our models and experiments with the phage Lambda, all ten of the naturally occurring *E. coli* lysogens studied were resistant (refractory) to the phage coded for by their prophage. We discuss the implications of these results to our understanding of the evolution and ecology of lysogenic bacteria and temperate phages.

Results

The mathematical model: In Figure 1, we present a diagram of our mathematical model of the population and evolutionary dynamics of virulent and temperate bacteriophages and their bacterial hosts. This model includes populations of non-lysogens (N) and lysogens (L), and free temperate phages (P), as cells and particles per mL, respectively. It also allows for a virulent phage population (V) that shares the same receptor as the temperate phage, and resistant mutants of the lysogens (L_R), as well as resistant non-lysogens, (N_R).

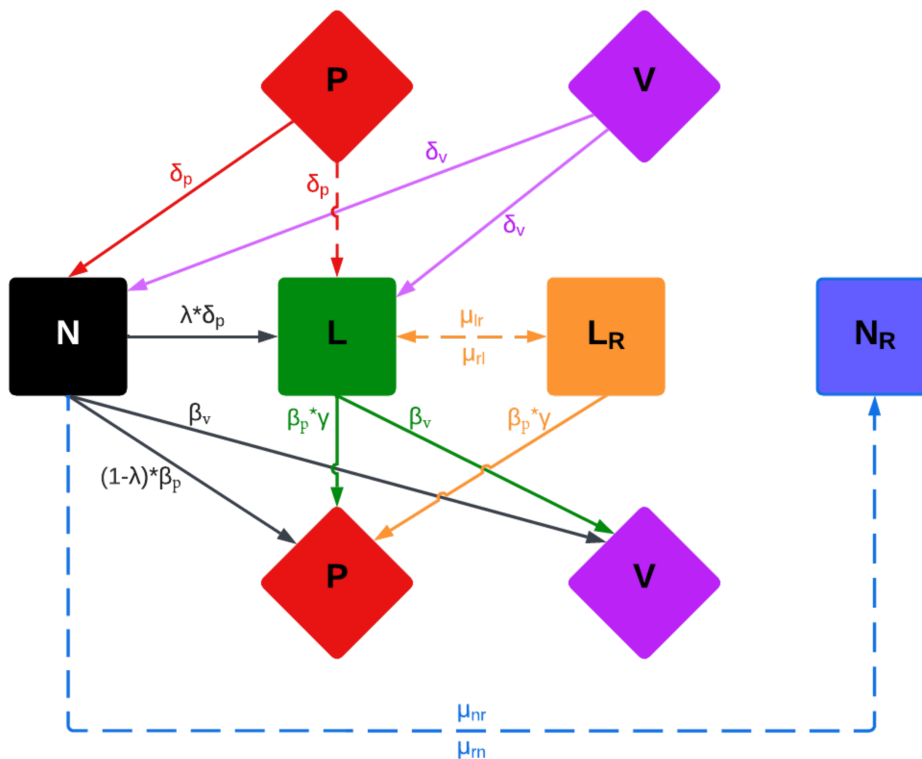


Figure 1. Model of the population and evolutionary dynamics of temperate and lytic phages. There is a population of temperate phage, P; a population of virulent phage, that shares the same receptor with the temperate phage, V; a phage-sensitive non-lysogenic bacterial population, N; a refractory non-lysogenic bacterial population, N_R ; a phage-sensitive lysogenic, L; and a refractory lysogenic bacterial population, L_R . See the text for a description of the model and Supplemental Table 1 for the definitions, dimensions, of the parameters and the values used in our numerical solutions to the equations, simulations.

Phage infection is a mass action process where the viruses adsorb to the bacteria at rates proportional to the product of the bacterial densities and rate constants δ_p and δ_v , ml attacks per phage particle per cell per hour, for the temperate and virulent phages, respectively (11). With a probability λ Lambda ($0 \leq \lambda \leq 1$), infections of sensitive bacteria with temperate phage form lysogens. The remaining fraction $(1-\lambda)$ of infections by the temperate phages enter a lytic cycle, and each infected bacterium bursts to yield β_p phage particles. Infections of sensitive non-lysogenic and lysogenic bacteria with the virulent phages produces β_v phage particles.

The rate of growth of the bacteria is equal to the product of their maximum rates v_n, v_{nr}, v_l, v_{lr} (per hour) and a hyperbolic function, $\psi(R)$, of the concentration of a limiting resource (R , $\mu\text{g/ml}$) $\psi(R) = \frac{R}{(R+k)}$, where k is the concentration of the limiting resource where the net growth rate is half its maximum value (12). The limiting resource is consumed at a rate equal to the product of $\psi(R)$, the sum of the products of the densities and maximum growth rate of the bacterial populations, and a conversion efficiency parameter, e , $\mu\text{g/cell}$ (13). The rates of mutations $L \rightarrow L_R, L_R \rightarrow L, N \rightarrow N_R, \text{ and } N_R \rightarrow N$ are, respectively $\mu_{lr}, \mu_{rl}, \mu_{nr}$ and μ_{rn} per cell per hour (14). To account for the decline in the physiological state as the bacteria approach stationary phase ($R = 0$), we assume that the rates of phage infection and mutation decline at rates proportional to $\psi(R)$.

With these definitions and assumption, neglecting the lag phase of the bacteria and the latent periods for the phages, and assuming that the likelihood of lysogeny is independent of the multiplicity of infection (15, 16), the rates of change in the concentration of the resource, densities of the different populations of bacteria and the phage are given by the set of coupled differential equations described in supplemental equations sEQ1-sEQ8.

The definitions, dimensions and values of parameters used for our numerical solutions to these equations (simulations) are presented in Supplemental Table 1. Although our primary focus in this study is temperate phages and lysogeny, this is a general model of the population and evolutionary dynamics of bacteria and their virulent and temperate phages. The generality of this model can be seen in Supplemental

Figure S1 where we present the predictions of the model and in Figure S2 where we present a set of parallel experiments with *E. coli* and the phages Lambda and Lambda^{Vir} confirming the predictions of the model. For the limitations of this model, see the supplemental text.

Model-based predictions and experimental results: We open this consideration with a comparison between the predicted population dynamics generated by numerical solutions to differential equations of this model, simulations, and the corresponding dynamics observed for *E. coli* and the phages Lambda and Lambda^{Vir} in serial transfer culture.

In Figure 2A, we follow the simulated changes in the densities of bacteria and phage in serial transfer population initiated with 10^6 sensitive bacteria, N , 10^4 resistant non-lysogens, N_R , and 10^5 temperate phage, P . Within short order, lysogens, L , are produced and ascend in density, as do resistant non-lysogens, N_R . With these parameters and starting conditions, lysogens and resistant non-lysogens become the dominant bacterial populations. A population of resistant lysogens, L_R also emerged and increased in frequency, but remained a minority population. As a consequence of induction, free temperate phage are continually produced by the lysogens and resistant lysogens and maintain their population.

The parallel serial transfer experiments were initiated with a low density of free Lambda temperate phages, a population of Lambda-sensitive *E. coli*, and a population of Lambda-resistant *E. coli* (Fig. 2B). As predicted by our model, the resistant non-lysogens increased in frequency, as did a novel population that was both resistant (refractory) to phage Lambda and lysogenic for Lambda, resistant lysogens.

To more extensively explore the conditions under which populations of resistant lysogens ascend and are maintained, we initiated our simulated serial transfer populations with sensitive bacteria, temperate phage, and a virulent phage that shares the same receptor as the temperate. Under these conditions, selection for resistance should be more intense. This can be seen in Figure 2C, where resistant lysogens (L_R), as well as resistant non-lysogens (N_R), became the dominant bacterial populations. To explore the validity of this prediction experimentally, we initiated serial transfer populations with sensitive *E. coli* and both temperate and virulent Lambda (Fig. 2D). The results of this experiment (and its replicas in Figure S3) are qualitatively

consistent with the predictions of the simulations. Resistant non-lysogens, with *malT* mutations similar to what has been reported in other *E. coli* resistant to Lambda-phage ((17, 18); Fig. S4), ascend and become the dominant bacterial population followed by lysogens and resistant lysogens (see Fig. S5 for the evidence that the resistant lysogens appear refractory).

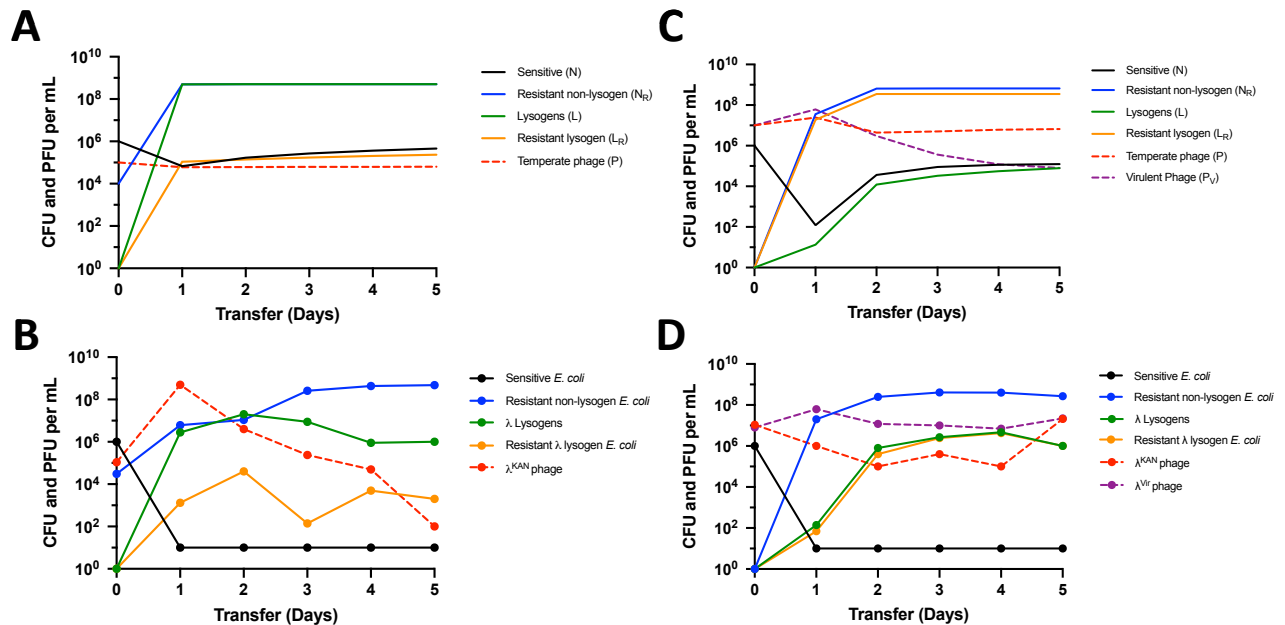


Figure 2. Population dynamics for lysogeny in mixed populations with and without the presence of a virulent phage. (Top section) Simulation results with parameter values in the range estimated for *Escherichia coli* and lambda (Lambda) phage (Table S1). (Lower section) Experiments with sensitive and Lambda-resistant *E. coli*, Lambda^{KAN}, and Lambda^{vir}. Changes in bacteria (colony-forming units per mL) and phage (plaque-forming units per mL) densities in a 24 h serial transfer populations with a 1/100 dilution factor are shown for: (A) Simulation initiated with 10^6 sensitive bacteria, and 10^4 resistant non-lysogens with 10^5 temperate phage per mL; (B) experimental culture initiated with $\sim 10^6$ Lambda-sensitive *E. coli* and $\sim 10^4$ Lambda-resistant *E. coli* marked with a streptomycin resistance marker, and $\sim 10^5$ temperate phage with a kanamycin resistance marker, Lambda^{KAN}; (C) simulation initiated with 10^6 phage-sensitive bacteria, 10^7 temperate phages, and 10^7 virulent phages that share the same receptor as the temperate phage; (D) experimental culture

initiated with $\sim 10^6$ Lambda-sensitive bacteria, $\sim 10^7$ temperate phage with kanamycin resistance, Lambda^{KAN}, and $\sim 10^7$ virulent mutants of Lambda, Lambda^{VIR}.

Our model and experiments make two predictions: (i) When a population of sensitive bacteria are infected by temperate phages, in addition to the generation and ascent of lysogens, resistant lysogens will be generated and increase in density; (ii) If the community includes virulent phages that share the same receptor as the temperate phage, the resistant lysogens will ascend and become the dominant population of lysogenic bacteria. To explore the validity and generality of these predictions, we used a set of naturally occurring (wild) lysogenic *E. coli* with different prophages from sewage and the gut microbiomes of infants (19) (Table S2). We induced these wild lysogens to produce free temperate phages which we then used to infect the lysogens from whence they came.

Consistent with the prediction of our model and experiments with Lambda, all ten naturally occurring lysogens were refractory to the free phages generated by induction of their host lysogens (Figure 3A). To determine whether this resistance is property of the host bacteria rather than the prophage, Lambda-sensitive *E. coli* C, Lambda lysogens, and Lambda^{VIR}-resistant bacteria were infected with a temperate Lambda-phage coding for kanamycin resistance, Lambda^{KAN}. As anticipated, the phages replicated on the sensitive non-lysogens but not the Lambda^{VIR}-resistant *E. coli*. However, not anticipated was the marked increase in the density of free phages in a control experiment with Lambda lysogens infected by temperate Lambda-phage (Figs. 3A and 3B, shaded areas).

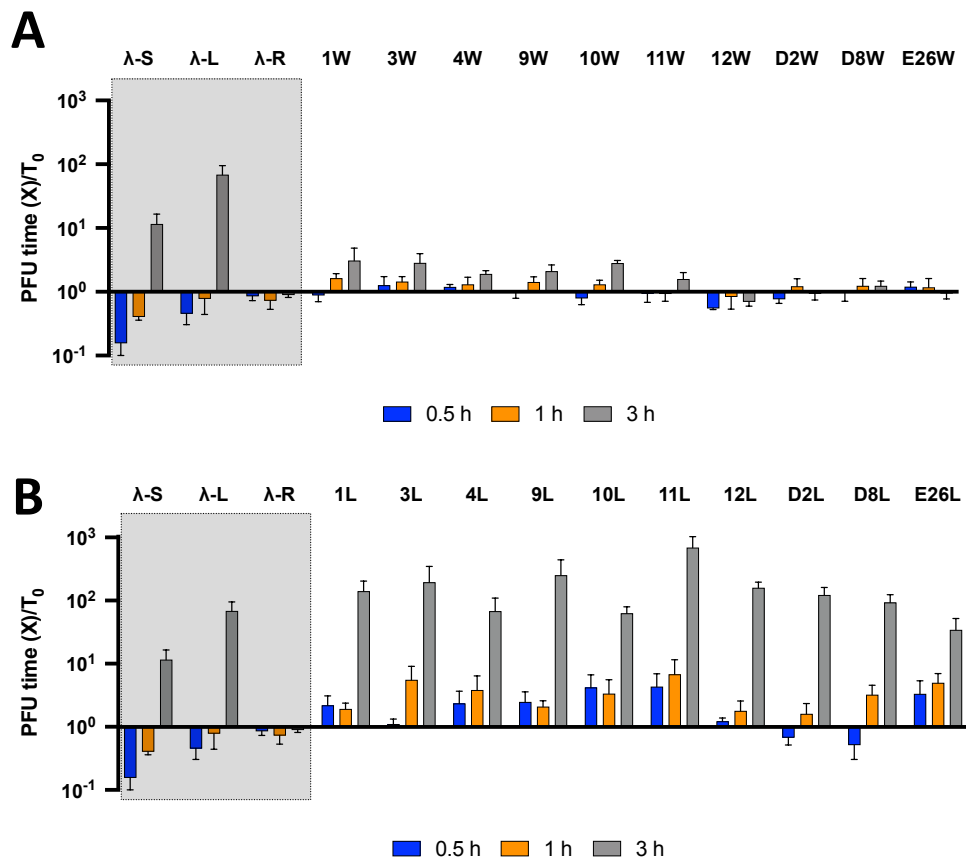


Figure 3. Susceptibility and resistance of naturally occurring and *E. coli* C constructed

lysogens. Ratios of free phage density after 0.5, 1, and 3 h relative to that at 0 h (T_0). Means and standard deviations of the ratios of three replicas of this experiment. Shaded regions infections with phage lambda (Lambda) in three distinct bacterial states: Lambda-sensitive (Lambda-S), Lambda-lysogen (Lambda-L), and Lambda-resistant (Lambda-R). All statistics were computed by comparing each of the control groups to the unbinned experimental data with $\alpha=0.05$ **(A)** Naturally occurring lysogens (W) infected with a low multiplicity of infection of the induced free phages for which they are lysogenic. Kruskal-Wallis Chi-squared= 16.07, df= 3, $p= 0.001$. Dunn's Test wild lysogens to Lambda-S $p= 0.012^*$, wild lysogens to Lambda-L $p= 0.005^*$, wild lysogens to Lambda-R $p= 0.119$ **(B)** *E. coli* C lysogens constructed (L) from the prophage induced from the corresponding wild lysogen (W) infected with a low multiplicity of induced wild phages for which they are lysogenic. Kruskal-Wallis Chi-squared= 14.34, df= 3, $p= 0.0000$. Dunn's Test constructed

lysogens to Lambda-S $p= 0.021^*$, constructed lysogens to Lambda-L $p= 0.301$, constructed lysogens to Lambda-R $p= 0.006^*$. See Table S2 for designations and sources of the naturally occurring lysogenic *E. coli*.

Previous works (20) have shown there to be an abundance of prophage encoded mechanisms which confer a resistance phenotype to their host, an idea consistent with the dynamics of Figure 3A. To test the hypothesis that the resistance of our naturally occurring lysogens to the phages coded by their prophages is a property of the bacteria rather than that of the prophage, we infected *E. coli C* with the temperate phages induced from the naturally occurring lysogens. None of the ten wild prophage bearing lysogens of *E. coli C*, were resistant (refractory) to the free phages coded by their prophage (Fig. 3B). They behaved like Lambda lysogens infected with Lambda (Fig. 3B, shaded area). Most intriguingly, similar to the Lambda lysogens in the control experiment (shaded areas of Fig. 3), when the *E. coli C* wild phage lysogens were infected with a low density of free temperate phages, high densities of free phages were produced.

The observation that when infected with free phages both the Lambda lysogens, and the *E. coli C* lysogens bearing the wild temperate phage produce high densities of free phages (Fig. 3B) was unexpected. It suggested that lysogens were induced when infected with the temperate phages coded by their prophage. We postulate that infections with temperate phages induce lysogens by mounting an SOS response, as would be the case when lysogens are exposed to ultraviolet light or other SOS-inducing insults (21-23). To test this hypothesis, a $\Delta recA$ *E. coli* construct obtained from the KEIO collection was lysogenized with Lambda and reinfected with free Lambda phage (24). Contrary to that observed with the $recA^+$ lysogen (Fig. 3B), infections of the $\Delta recA$ Lambda lysogen with free Lambda-phage did not generate a high density of free phage (Fig. S6A). To further test the hypothesis that infections with free Lambda induce Lambda lysogens by generating an SOS response, we transformed the $\Delta recA$ *E. coli* Lambda lysogens with plasmids either lacking or bearing *recA* (Fig. S7). With the cells bearing a functional *recA* in *trans*, the lysogens were induced at a high rate (Fig. S6B). This did not occur with the plasmid without *recA* (Fig. S6C).

Discussion

Bacteria are protected from being killed by infecting phage via two distinct mechanisms: immunity and resistance. In the case of immunity, the phage injects its genetic material, but phage replication does not occur, and the infecting phage are lost. This is the case for defense systems such as CRISPR-Cas (5), restriction modification (6), abortive infection (7), and lysogeny (8). In the case of resistance, the phage virion fails to bind to the host bacterium, for example due to modification of the receptor site in the bacteria or the display of the O-antigen (9). For resistance, the bacteria are refractory to the bacteriophage and the phage are not lost.

When sensitive populations of bacteria are confronted with virulent phages, selection favors the evolution of mutants that are resistant to those phages or immune. In accord with what is known about lysogeny, what “the book of Lambda” tells is, when populations of sensitive bacteria are confronted with temperate phage, a fraction of the infected bacteria acquire and maintain the genome of the phage, as a prophage, and the resulting lysogens are immune to super-infection with the phage coded for by their prophage; the phage infecting lysogens are lost. What “the book of Lambda” does not say is that when populations of sensitive bacteria are exposed to temperate phages, resistant bacteria will also emerge and ascend, as presented in this theoretical and experimental study with *E. coli* and Lambda phage. Moreover, if the community contains virulent phages that share the same receptors as the temperate phages coded by the prophage of lysogens, resistant lysogens will emerge and rise to become the dominant population of lysogens.

To explore the generality of this prediction in the real world, by induction we isolated temperate phage from ten naturally occurring lysogens. All ten of these “wild” temperate phages were capable of forming immune lysogens with a laboratory strain of *E. coli*. And, as predicted by our models and experiments with *E. coli* and Lambda, all ten of these naturally occurring lysogens were resistant (refractory) to the phage coded for by their prophage. This resistance was found to be coded for by a genomic element and not by an element on the resident phages (20). Based on these theoretical and experimental results, we predict that

naturally occurring lysogenic bacteria will be resistant as well as immune to the phage coded for by their prophage.

The results of this study provide another observation not anticipated from the “book of Lambda”. It is known that the rate of induction of prophage is augmented when lysogens are infected with phages other than those coded by their prophage (25, 26). The results of our assay indicated that the rate of induction of lysogens is also increased due to phage infection with the temperate phages coded by their prophage. Our analysis indicates that by promoting an SOS response, infections of lysogens by free phage increase the rate of induction and the production of free phage by populations of lysogens.

The subtitle of a not-quite-ancient theoretical study of the population dynamics of lysogeny raised the question of “why be temperate?” (13). In retrospect, it would seem the interesting question that should have been raised is “why be virulent”? From an ecological and evolutionary perspective, a temperate mode of replication and transmission would be better than a virulent one for a phage. Unless their rates of adsorption and burst sizes are markedly less than that of virulent phage, when invading a population of sensitive bacteria temperate phage will be spread nearly as fast as virulent. By forming lysogens and thereby being transmitted vertically, temperate phages can be maintained in the community when the density of their host population is too low for them to persist as virulent phage (11, 27). Moreover, the phage genome can also increase in frequency when the prophage encodes a phenotype that augments the fitness of its host bacterium (28). Resistance to the phages coded for by their prophage, would be an additional asset to temperate phages. The prophage genome will be transmitted vertically in the course of cell division and the free temperate phages will be continually produced by induction. These free temperate phages will then be capable of infecting sensitive non-lysogens, thereby expanding the range of bacteria bearing that prophage. These lysogens, and thereby the temperate phages they encode, will not be subject to extinction by virulent phages capable of adsorbing to the same receptors as those of the temperate phages.

The molecular biologist Jacques Monod quipped that “What is true for *E. coli* is true for elephants, only more so” (29). While we appreciate this form of inductive inference, we understand that all of the

experiments reported here were conducted only with *E. coli*. We postulate that naturally occurring lysogenic bacteria of any species that can produce resistant mutants will be resistant to the phages coded by their prophage.

Materials and Methods

Numerical solutions (simulations). For our numerical analysis of the properties the model of population and evolutionary dynamics of temperate and virulent phage (Figure 1 and equations 1-7), were solved with Berkeley Madonna, using parameters in the ranges estimated experimentally with *E. coli* and virulent and temperate Lambda phages (Table 1). In these numerical solutions (simulations), the changes in states, $N \rightarrow N_R$, $N_R \rightarrow N$, $L \rightarrow L_R$ and $L_R \rightarrow L$ are stochastic processes modeled with a Monte Carlo protocol. All other changes are deterministic. Copies of the Berkeley Madonna program used for these simulations are available at www.eclf.net.

Growth media— LB broth (244620) was obtained from BD. The DM (Davis Minimal) minimal base without dextrose (15758-500G-F) was obtained from Sigma Aldrich. LB agar (244510) for plates was obtained from BD. Phage plates are prepared with 1g/L Yeast Extract (BD- 241750), 10 g/L Bacto-Tryptone (Fischer-BP1421), 8 g/L NaCl (Fischer-S271), 10 g/L Agar (BD-214010), 1g/L Glucose (Sigma-G5767) and 2 mM CaCl₂ (Sigma-C5080). Double-layer soft agar was prepared with 1 g/L Yeast Extract, 10 g/L Bacto-Tryptone, 8 g/L NaCl, 7 g/L Agar, 1g/L Glucose and 2 mM CaCl₂.

Bacterial strains—*E. coli* MG1655 was obtained from the Levin Lab Bacterial collection. The wild strains and *E. coli* C were obtained from Marie-Agnès Petit. All lysogens were made in the Levin Lab and saved at -80°C. *E. coli* Δ RecA was obtained from the Keio collection.

Phages— Temperate Lambda, Lambda^{KAN}, and Lambda^{VIR} were obtained from Maroš Pleška at The Rockefeller University.

Plasmids– All inserts were synthesized and cloned into the plasmids by GenScript (NJ, USA).

Primers– All primers were ordered from Integrated DNA Technologies (Iowa, USA) as custom oligos with standard desalting.

Antibiotics– Ampicillin (A9518), Kanamycin (127K0058) and Streptomycin (081K1275) were obtained from Sigma Aldrich (USA).

Sampling bacterial and phage densities– The densities of bacteria and phage were estimated by serial dilution in 0.85% saline and plating. The total density of bacteria was estimated on Lysogeny Broth (LB) IN hard (1.6%) agar plates. In competition experiments with multiple bacterial populations, diluted samples were plated on LB hard (1.6%) agar plates supplemented with kanamycin (2.5 ug/mL) or streptomycin (4 ug/mL) to distinguish between sensitive, resistant, and lysogenic bacteria. To estimate the densities of free phage, chloroform was added to suspensions before serial dilution. These suspensions were plated at various dilutions on lawns with 0.1 mL of overnight Davis Minimal (DM) Glucose-grown cultures (about 5×10^8) of *E. coli* MG1655 or *E. coli* MG1655 lysogenized with lambda (to distinguish Lambda^{Vir} from temperate Lambda) and 4mL of LB soft (0.7%) agar on top of hard (1.6%) LB agar plates.

Testing for Resistance– Bacteria were tested for resistance to Lambda^{VIR} by streaking colonies across a line made with 200 μ L of a Lambda^{Vir} lysate ($>10^8$ pfu/mL) on LB hard (1.6%) agar plates. Continuous lines were interpreted as evidence for resistance and broken lines sensitivity.

Testing for whether the bacteria are refractory or immune to the phage– High densities of bacteria were exposed to phage at a low multiplicity of infection (0.01-0.1) in 10ml of DM-Glucose media. The density of phage in these cultures were estimate at the time of first exposures, T=0, and T= 0.5, 1.0 and 3.0 hours later. The bacteria were considered refractory to the phage if there was little or no net change in their density. The bacteria were considered immune, if the density of phage declined or increased in later samples.

Growth rate estimation– Exponential growth rates were estimated from changes in optical density (OD_{600}) in a Bioscreen C. For this, 48-hour stationary phase cultures were diluted in DM glucose liquid media to an initial density of approximately 10^5 cells per mL. Ten replicas were made for each estimate by adding 300 μ l of the suspensions to the wells of the Bioscreen plates. The plates were incubated at 37°C and shaken continuously. Estimates of the OD (600nm) were made every five minutes.

Burst size estimation– The burst sizes for Lambda and Lambda^{Vir}, β_p and β_v , were estimated with a one-step growth protocol similar to that first presented in 1939 (Ellis and Delbrück, 1939) and employed in (Stewart et al. 1977). Exponentially growing cultures of *E. coli* MG1655 in DM minimal glucose were used as the host bacteria for these estimates.

Statistical Methods– Statistical analysis of significance was carried out by a Kruskal-Wallis rank sum test (30) followed by a Dunn's post hoc test with a Benjamini-Hochberg p-value correction. Calculations were performed using RStudio (31) version 2022.07.1+554.pro3.

Serial transfer experiments– All serial transfer experiments were carried out in 50 ml Erlenmyer flasks with 10 mL DM minimal glucose media at 37 °C with vigorous shaking. Unless otherwise noted, these serial transfer cultures were initiated by a 1:100 dilution from 10-mL overnight cultures grown from single colonies. Phages were added to these cultures at the initial densities shown in the figures. At the end of each transfer, 0.1 mL of the cultures were transferred into flasks with fresh medium (1:100 dilution). Subsequently, 0.1 mL samples were taken to estimate the densities of bacteria and phage.

Sequencing and analyses– Phage DNA was extracted using Invitrogen's (California, USA) PureLink Viral RNA/DNA extraction kit (Cat# 12280-050) using the manufacturer's protocol and bacterial DNA was extracted using Promega's (Wisconsin, USA) Wizard Genomics DNA Purification Kit (Cat# A1120) using the manufacturer's protocol. The extracted DNA was quantified on ThermoFisher's NanoDrop One^C microvolume spectrophotometer (Cat# ND-ONE-W). Samples were sent to the Microbial Genome Sequencing Center in Pittsburgh, Pennsylvania, USA, for whole genome sequencing on the Illumina NextSeq

2000 platform. Analysis of FASTAq files received from the Microbial Genome Sequencing Center were analyzed using Geneious Prime version 2022.0.1.

Primer design and PCR– Primers were designed using PrimerBLAST (NCBI). PCR was carried out using Thermo Scientific's (Lithuania) Phusion Blood Direct PCR Master Mix (Cat# F-175L). Products were visualized on a 1% agarose/TAE gel with Biotium's (California, USA) 10,000X GelRed Nucleic Acid Stain.

RecA-expressing plasmid construction– A pMAL-c4X-RecA plasmid was synthesized by GenScript (NJ, USA) using as a backbone the plasmid pMAL-c4X (Addgene #75288) and cloning between the NdeI and BamHI restriction sites in the plasmid a *recA*-tt construct (1,196 bp) designed with the *recA* CDS (1,059 bp, Genbank: EU896799.1), a TAGTAGAG linker sequence (BioBrick standard RFC[10]) added to the 3'-terminal end of the *recA* CDS stop codon followed by a downstream double-terminator sequence (BioBrick Part:BBa_B0015). This puts the *recA* CDS under the control of the lactose-inducible TAC promoter, therefore RecA can be complemented in *trans* with induction by IPTG.

RecA complementation assay– Plasmids pMAL-c4X-RecA and pMAL-c4X were electroporated with 1 pulse of 2.5 kV using a MicroPulse electroporator (Bio-rad, USA) into electrocompetent Lambda-lysogenized *E. coli* $\Delta recA$ cells prepared from an overnight growth in LB media, followed by three cycles of centrifugation at 13,000g and a wash with ice-cold 10% glycerol solution. Transformants were selected on LB plates supplemented with 12 ug/mL Ampicillin and incubated at 37°C overnight, colonies were then streaked two times for isolation.

To confirm the presence of the plasmid, Colony-PCR (described previously) was performed using the M13/pUC_Reverse (5'-AGCGGATAACAATTTCACACAGG-3') and M13/pUC_Forward (5'-CCCAGTCACGACGTTGTAAAACG-3') primers. The IPTG-induction of the *recA* gene in the complemented Lambda-lysogenized strain *E. coli* $\Delta recA$ / pMAL-c4X-RecA was performed in a culture of 100 mL LB broth supplemented with 15 ug/mL Ampicillin inoculated with a 5% volume from an overnight culture, the cells were grown aerobically at 37°C until an OD₆₀₀ of 0.3 and growth was maintained for 3 hours after the addition of 10 mM Isopropyl β -D-1-thiogalactopyranoside (IPTG). The refractory phenotype (described

previously) was confirmed directly from IPTG-induced Lambda-lysogenized cultures, using as plasmid-free and insert-free controls the strains *E. coli* $\Delta recA$, and *E. coli* $\Delta recA$ / pMal-c4X, respectively.

Resistance genotype analysis– The 2,706 bp region of the *malT* gene of the sensitive non-lysogens (MalT WT) and resistant non-lysogens (MalT R) were amplified via two-overlapping PCRs with primers shared by Marie-Agnès Petit. The first product using the primers malT up (5'-GTGACACAGTGCAAATTCAG-3') and malTint down (5'-CTAGCAGGGTGTAACTTC-3') amplifies a 1,297 bp 5'-end region of the *malT* gene with a 138 bp upstream non-coding segment, the second product used the primers Int-up malt (5'-TCCGCAGTTGGTGTATTG-3') and malTdown2 (5'-GGTGCGGTTTAGTTTGATAG-3') to amplify an 1,483 bp 3'-end region of the *malT* gene and a 97 bp downstream segment. These products were purified by running on a 1% agarose gel and gel extracted using the GenElute™ Gel Extraction kit (Sigma-Aldrich, USA). The extracted bands were Sanger sequenced by Eurofins (USA) and the resulting sequences analyzed, and a full *malT* gene sequence is obtained with the pairwise alignment of both products. The *malT* sequences were *in silico* translated with an *E. coli* translation table to obtain the amino acid sequences of the MalT receptors, alignments were generated using Clustal Omega 1.2.3 using default parameters and a graphical representation of the alignment was obtained using Geneious 2022.0.1

Acknowledgements

The authors thank Melony Ivey, Esther Lee, Adithi Govindan, Nicole Vega, Ross Greenberg, Joanna Goldberg, David Goldberg, Thomas O'Rourke, Teresa Gil-Gil, Eduardo Rodriguez-Roman, and Andrew Smith for their comments on the manuscript, feedback on experiments, and support in the laboratory.

Funding

US National Institutes of General Medical Sciences grant R35 GM 136407 (BRL)

References

1. F. Rohwer *et al.*, *Life in Our Phage World: A Centennial Field Guide to the Earth's Most Diverse Inhabitants* (Wholon, 2014).
2. M. Adams, *Bacteriophages* (Interscience, New York, 1959).
3. A. Lwoff, Lysogeny. *Bacteriological Reviews* **17**, 269 (1953).
4. M. Ptashne, *The Genetic Switch* (Cold Spring Harbor Press, New York, 2004), vol. 3rd.
5. E. R. Westra, S. van Houte, S. Gandon, R. Whitaker, The ecology and evolution of microbial CRISPR-Cas adaptive immune systems. *Philosophical Transactions of the Royal Society B: Biological Sciences* **374**, 20190101 (2019).
6. R. Korona, B. R. Levin, Phage-Mediated Selection and the Evolution and Maintenance of Restriction-Modification. *Evolution* **47**, 556-575 (1993).
7. A. B. Isaev, O. S. Musharova, K. V. Severinov, Microbial Arsenal of Antiviral Defenses. Part II. *Biochemistry (Moscow)* **86**, 449-470 (2021).
8. S. T. Abedon, Bacterial 'immunity' against bacteriophages. *Bacteriophage* **2**, 50-54 (2012).
9. A. V. Letarov, E. E. Kulikov, Adsorption of Bacteriophages on Bacterial Cells. *Biochemistry (Mosc)* **82**, 1632-1658 (2017).
10. J. K. Cornuault *et al.*, The enemy from within: a prophage of *Roseburia intestinalis* systematically turns lytic in the mouse gut, driving bacterial adaptation by CRISPR spacer acquisition. *The ISME Journal* **14**, 771-787 (2020).
11. F. M. Stewart, B. R. Levin, The population biology of bacterial viruses: Why be temperate. *Theoretical Population Biology* **26**, 93-117 (1984).
12. J. Monod, The growth of bacterial cultures. *Annual Review of Microbiology* **3**, 371-394 (1949).
13. F. M. Stewart, B. R. Levin, Partitioning of Resources and the Outcome of Interspecific Competition: A Model and Some General Considerations. *The American Naturalist* **107**, 171-198 (1973).
14. W. N. Chaudhry *et al.*, Leaky resistance and the conditions for the existence of lytic bacteriophage. *PLoS Biol* **16**, e2005971 (2018).

15. P. Kourilsky, A. Knapp, Lysogenization by bacteriophage lambda: III. - Multiplicity dependent phenomena occurring upon infection by lambda. *Biochimie* **56**, 1517-1523 (1975).
16. G. Li, M. H. Cortez, J. Dushoff, J. S. Weitz, When to be temperate: on the fitness benefits of lysis vs. lysogeny. *Virus Evolution* **6** (2020).
17. M. De Paepe *et al.*, Carriage of λ Latent Virus Is Costly for Its Bacterial Host due to Frequent Reactivation in Monoxenic Mouse Intestine. *PLoS Genetics* **12**, e1005861 (2016).
18. M. De Paepe *et al.*, Trade-Off between Bile Resistance and Nutritional Competence Drives *Escherichia coli* Diversification in the Mouse Gut. *PLoS Genetics* **7**, e1002107 (2011).
19. A. Mathieu *et al.*, Virulent coliphages in 1-year-old children fecal samples are fewer, but more infectious than temperate coliphages. *Nature Communications* **11**, 378 (2020).
20. J. Bondy-Denomy *et al.*, Prophages mediate defense against phage infection through diverse mechanisms. *ISME J* **10**, 2854-2866 (2016).
21. N. Otsuji, M. Sekiguchi, T. Iijima, Y. Takagi, Induction of Phage Formation in the Lysogenic *Escherichia coli* K-12 by Mitomycin C. *Nature* **184**, 1079-1080 (1959).
22. A. Matsushiro, K. Sato, H. Miyamoto, T. Yamamura, T. Honda, Induction of prophages of enterohemorrhagic *Escherichia coli* O157:H7 with norfloxacin. *Journal of bacteriology* **181**, 2257-2260 (1999).
23. B. J. Barnhart, S. H. Cox, J. H. Jett, Prophage induction and inactivation by UV light. *Journal of virology* **18**, 950-955 (1976).
24. T. Baba *et al.*, Construction of *Escherichia coli* K-12 in-frame, single-gene knockout mutants: the Keio collection. *Molecular systems biology* **2**, 2006.0008-2006.0008 (2006).
25. S. Campoy *et al.*, Induction of the SOS response by bacteriophage lytic development in *Salmonella enterica*. *Virology* **351**, 360-367 (2006).
26. I. Lamont, A. M. Brumby, J. B. Egan, UV Induction of Coliphage 186: Prophage Induction as an SOS Function. *Proceedings of the National Academy of Sciences of the United States of America* **86**, 5492-5496 (1989).

27. L. Chao, B. R. Levin, F. M. Stewart, A Complex Community in a Simple Habitat: An Experimental Study with Bacteria and Phage. *Ecology* **58**, 369-378 (1977).
28. C. C. Wendling, D. Refardt, A. R. Hall, Fitness benefits to bacteria of carrying prophages and prophage-encoded antibiotic-resistance genes peak in different environments. *Evolution* **75**, 515-528 (2021).
29. C. Zimmer, Microcosm: E. coli and the New Science of Life. 256 (2008).
30. M. Hollander, D. A. Wolfe, E. Chicken, *Nonparametric statistical methods* (John Wiley & Sons, 2013).
31. J. Allaire, RStudio: integrated development environment for R. *Boston, MA* **770**, 165-171 (2012).

Supporting Information

Supplemental Text

Deviations from the theory. The utility of mathematical models and theory come in their ability to make predictions about the qualitative dynamics of the system, as opposed to making quantitative predictions. It is not at all surprising that there are quantitative deviations between the predictions of the model and what is observed in our experiments. Part of these deviations are due to the parametric inaccuracy that is inherent in generating these types of models. One such example is that the level of maintenance of free temperate bacteriophage, which is determined by the rate of induction, which is likely not to be a fixed value, but rather a distribution of rates which is not incorporated into our model. Another reason contributing to these deviations is the constraints imposed by the experimental system. For example, in Figure 2A, the theory predicts a large pool of sensitive non-lysogens, but experimentally we have no way of screening for sensitive non-lysogens when they are a minority population, as such Figure 2B makes the assumption that this population is down at the limit of detection. A similar limitation leads to discrepancies in the densities of the resistant lysogen and the sensitive lysogen populations; experimentally, we are only able to estimate both of these populations as a fraction of the total lysogen population.

Supplemental Equations

$$\Psi(R) = \frac{R}{K+R} \quad \text{sEQ. 1}$$

$$\frac{dR}{dt} = -\Psi(R) \cdot e \cdot (v \cdot N + v_{nr} \cdot N_R + v_l \cdot L + v_{lr} \cdot L_R) \quad \text{sEQ. 2}$$

$$\frac{dN}{dt} = \Psi(R) \cdot (v \cdot N - \delta_v \cdot N \cdot V - \delta_p \cdot N \cdot P - \mu_{nr} \cdot N + \mu_{rn} \cdot N_R) \quad \text{sEQ. 3}$$

$$\frac{dN_R}{dt} = \Psi(R) \cdot (v_{nr} \cdot N_R + \mu_{nr} \cdot N - \mu_{rn} \cdot N_R) \quad \text{sEQ. 4}$$

$$\frac{dL}{dt} = \Psi(R) \cdot (v_l \cdot L + \lambda \cdot \delta_p \cdot N \cdot P - \delta_v \cdot V \cdot L - \gamma \cdot L - \mu_{lr} \cdot L + \mu_{rl} \cdot L_R) \quad \text{sEQ. 5}$$

$$\frac{dL_R}{dt} = \Psi(R) \cdot (v_{lr} \cdot L_R - \gamma \cdot L_R - \mu_{rl} \cdot L_R + \mu_{lr} \cdot L) \quad \text{sEQ. 6}$$

$$\frac{dP}{dt} = \Psi(R) \cdot (\delta_p \cdot N \cdot (1 - \lambda) \cdot P \cdot (\beta_p - 1) - \delta_p \cdot L \cdot P + \gamma \cdot (L + L_R) \cdot \beta_p) \quad \text{sEQ. 7}$$

$$\frac{dV}{dt} = \Psi(R) \cdot \delta_v \cdot (N + L) \cdot (\beta_v - 1) \cdot V \quad \text{sEQ. 8}$$

Supplemental Figures

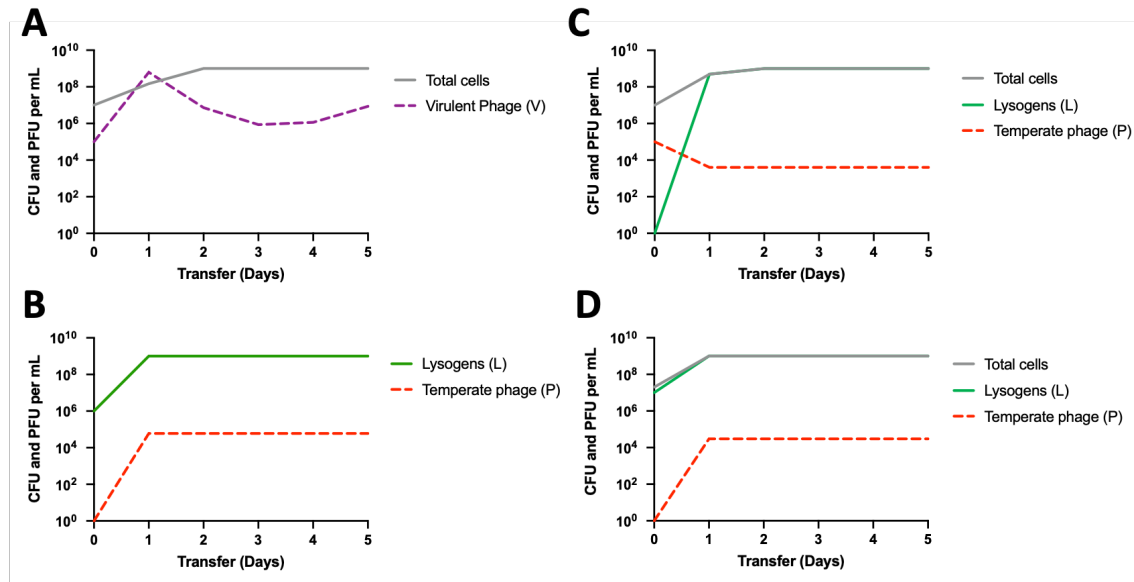


Fig. S1. Simulation results for basic phage-bacteria interactions. Shown are the simulated changes in the densities of phage (PFU/mL) and bacteria (CFU/mL) in serial transfer culture. Save for time zero, the densities are presented as the output at each 24-hour interval. (A) A simulation of 10^7 sensitive cells being confronted with 10^5 virulent phages (dashed purple). Shown are the density of phages and the total density (grey) of cells ($N + N_r$). (B) A simulation initiated with 10^6 lysogenic bacteria (green) with free temperate phages (dashed red) being produced by spontaneous induction. (C) A simulated population initiated with 10^7 sensitive cells being confronted by 10^5 temperate phages. Shown are the densities of lysogenic bacteria (green), temperate phage (dashed red), and total cells ($N + L + N_r$, in grey). (D) A simulation started with equal densities (10^7) of sensitive cells and lysogens. Shown are the lysogens (green) and temperate phage (dashed red) populations as well as total cells ($N + L$, in grey).

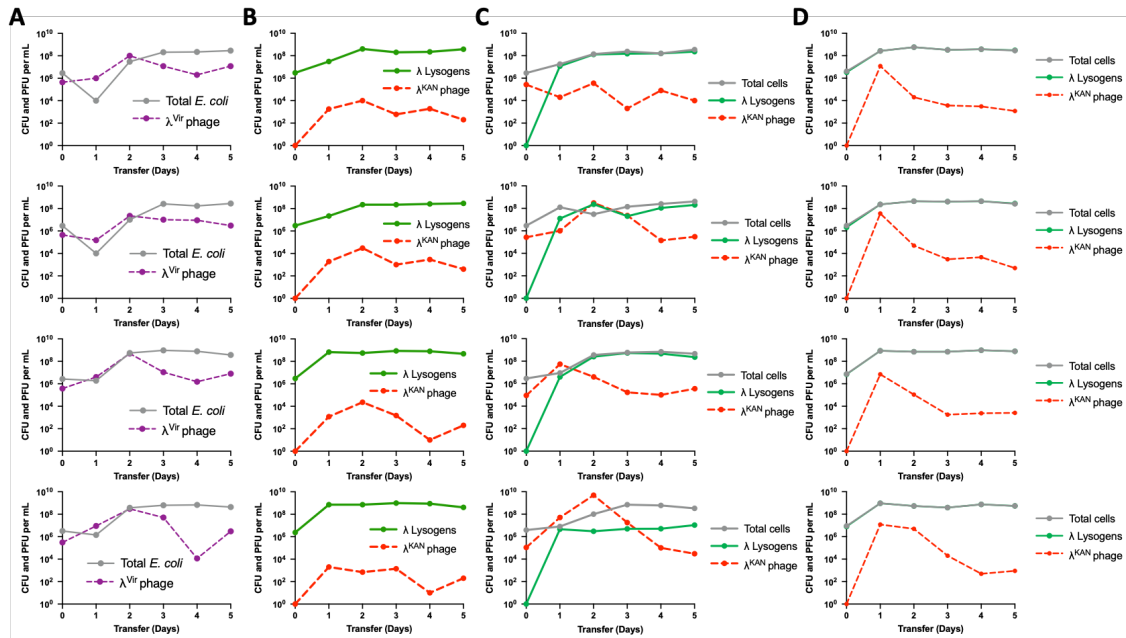


Fig. S2. Experimental exploration of the predictions of the model. Presented are four biological cells replicas of four experiments in parallel to the modelling results in Figure 2. Shown are the changes in the densities of phage (PFU/mL) and bacteria (CFU/mL) in serial transfer culture sampled at 24-hour intervals. (A) Cultures of $\sim 10^7$ sensitive *E. coli* confronted with $\sim 10^5$ virulent phages. Shown are the densities of virulent phage (dashed purple) and the total cell population (grey). (B) A population of $\sim 10^6$ sensitive λ lysogens (green) growing in the absence of phage and generating free temperate λ^{KAN} phages (dashed red) via spontaneous induction. (C) A population of $\sim 10^7$ sensitive *E. coli* confronted with 10^5 λ^{KAN} phages. Shown are the densities of total cells (grey), *E. coli* lysogenic for λ^{KAN} (green), and the density of free λ^{KAN} phage (dashed red). (D) Experimental cultures started with equal densities (10^7) of sensitive non-lysogenic *E. coli* and sensitive λ^{KAN} lysogens. Shown are the lysogens (green) and temperate phage (dashed red) populations as well as total cells (grey). Total cells are superimposed on top of lysogenic *E. coli*.

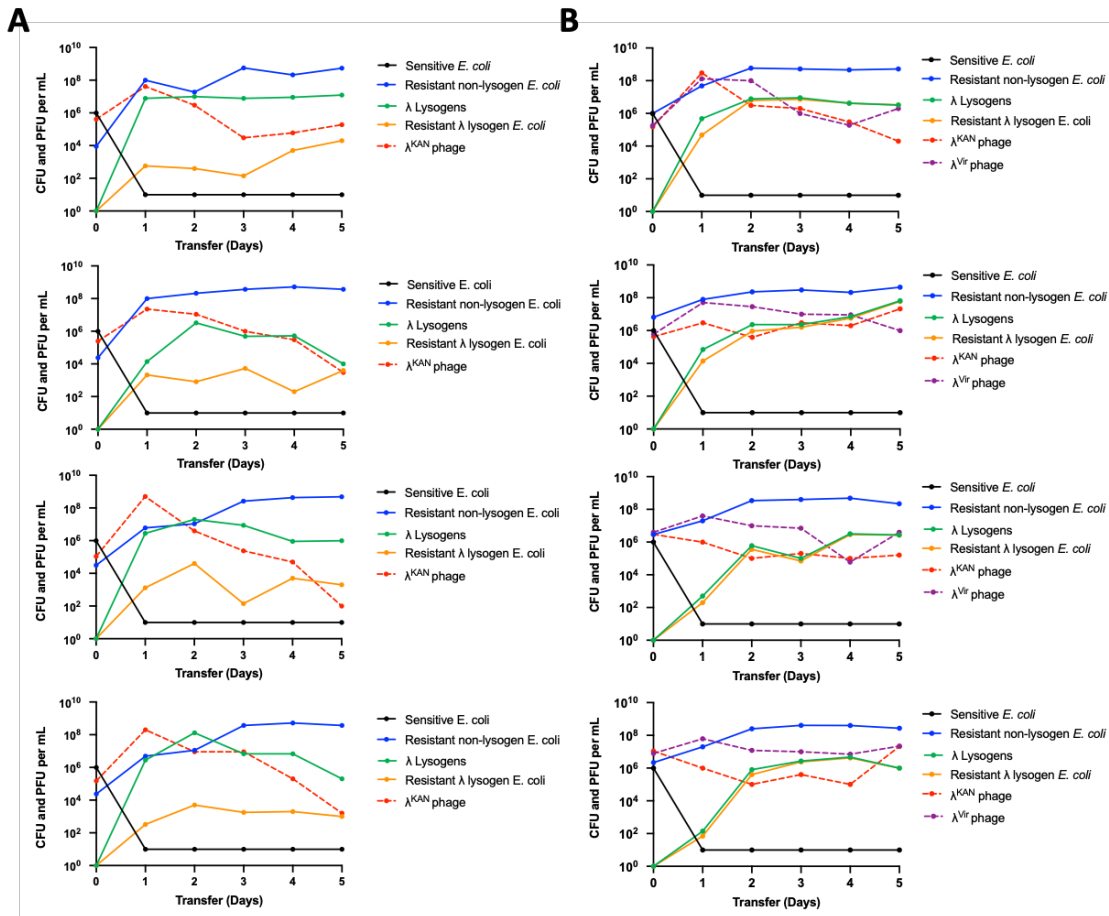


Fig. S3. Replicas of Figures 2B and 2D. Four biological replicates of experiments initiated with sensitive (black) and resistant non-lysogenic *E. coli* (blue), λ^{KAN} (dashed red), and λ^{Vir} (dashed purple), notable is the emergence of the resistant λ lysogenic *E. coli* (orange). Changes in the densities of bacteria (CFU per mL) and phage (PFU per mL) in 24-hour serial transfer populations with a 1/100 dilution factor are shown for: (A) Experimental cultures initiated with $\sim 10^6$ λ -sensitive *E. coli*, and $\sim 10^4$ lambda-resistant STR^R *E. coli*, and $\sim 10^5$ temperate phage coding for kanamycin resistance, λ^{KAN} . (B) Experimental culture initiated with $\sim 10^6$ λ -sensitive bacteria, $\sim 10^7$ temperate phage coding for kanamycin resistance temperate phage, λ^{KAN} and $\sim 10^7$ virulent mutants of lambda, λ^{Vir} .

```

          10          20          30          40          50          60
Consensus MLIPSKLSRP VRLDHTVVRE RLLAKLSGAN NFRALALITSP AGYGKTTLIS QWAAGKNDIG
MaLT WT    MLIPSKLSRP VRLDHTVVRE RLLAKLSGAN NFRALALITSP AGYGKTTLIS QWAAGKNDIG
MaLT R     MLIPSKLSRP VRLDHTVVRE RLLAKLSGAN NFRALALITSP AGYGKTTLIS QWAAGKNDIG

          70          80          90          100         110         120
Consensus WYSLDEGDNQ QERFASYLIA AVQQATNGHC AICETMAQKR QYASLTSLFA QLFIELAEWH
MaLT WT    WYSLDEGDNQ QERFASYLIA AVQQATNGHC AICETMAQKR QYASLTSLFA QLFIELAEWH
MaLT R     WYSLDEGDNQ QERFASYLIA AVQQATNGHC AICETMAQKR QYASLTSLFA QLFIELAEWH

          130         140         150         160         170         180
Consensus SPLYLVIDDY HLITNPVIHE SMRFFIRHQP ENLTLVVLSR NLPQLGIANL RVRDQLEIG
MaLT WT    SPLYLVIDDY HLITNPVIHE SMRFFIRHQP ENLTLVVLSR NLPQLGIANL RVRDQLEIG
MaLT R     SPLYLVIDDY HLITNPVIHE SMRFFIRHQP ENLTLVVLSR NLPQLGIANL RVRDQLEIG

          190         200         210         220         230         240
Consensus SQQLAFTHQE AKQFFDCRLS SPIEAAESSR ICDDVSGWAT ALQLIALSAR QNTHSAHKSA
MaLT WT    SQQLAFTHQE AKQFFDCRLS SPIEAAESSR ICDDVSGWAT ALQLIALSAR QNTHSAHKSA
MaLT R     SQQLAFTHQE AKQFFDCRLS SPIEAAESSR ICDDVSGWAT ALQLIALSAR QNTHSAHKSA

          250         260         270         280         290         300
Consensus RRLAGINASH LSDYLVDEVL DNVDLATTRH LLKSAILRSM NDALITRVTG EENGQMRLEE
MaLT WT    RRLAGINASH LSDYLVDEVL DNVDLATTRH LLKSAILRSM NDALITRVTG EENGQMRLEE
MaLT R     RRLAGINASH LSDYLVDEVL DNVDLATTRH LLKSAILRSM NDALITRVTG EENGQMRLEE

          310         320         330         340         350         360
Consensus IERQGLFLQR MDDTGEWFCY HPLFGNFLRQ RCQWELAAEL PXXXXXXXXX XXXXXXXXXXXX
MaLT WT    IERQGLFLQR MDDTGEWFCY HPLFGNFLRQ RCQWELAAEL PEIHRAAAS WMA---QGFP
MaLT R     IERQGLFLQR MDDTGEWFCY HPLFGNFLRQ RCQWELAAEL PVGTGGGAAG NPPCRRRKLD

          370         380         390         400         410         420
Consensus XXXIXXXXXX XXAGXXXXXX XXXXXXXXXSX XNHSELSLLE ESLKALPWDS LLENPQLVLL
MaLT WT    SEAIH---HA LAAGDALMLR DILLNHAWSL FNHSELSLLE ESLKALPWDS LLENPQLVLL
MaLT R     GPGISQRSNS SCAGGRRCAD A----ARYSA *-----

```

430 440 450 460 470 480
 Consensus QAWLMQSQHR YGEVNTLLAR AEHEIKDIRE DTMHAEFNAL RAQVAINDGN PDEAERLAKL

Malt WT QAWLMQSQHR YGEVNTLLAR AEHEIKDIRE DTMHAEFNAL RAQVAINDGN PDEAERLAKL

Malt R -----

490 500 510 520 530 540
 Consensus ALEELPPGWF YSRIVATSVL GEVLHCKGEL TRSLALMQQT EQMARQHDVW HYALWSLIQQ

Malt WT ALEELPPGWF YSRIVATSVL GEVLHCKGEL TRSLALMQQT EQMARQHDVW HYALWSLIQQ

Malt R -----

550 560 570 580 590 600
 Consensus SEILFAQGFL QTAWETQEKA FQLINEQHLE QLPMHEFLVR IRAQLLWAWA RLDEAEASAR

Malt WT SEILFAQGFL QTAWETQEKA FQLINEQHLE QLPMHEFLVR IRAQLLWAWA RLDEAEASAR

Malt R -----

610 620 630 640 650 660
 Consensus SGIEVLSSYQ PQQQLQCLAM LIQCSSLARGD LDNARSQLNR LENLLGNGKY HSDWISNANK

Malt WT SGIEVLSSYQ PQQQLQCLAM LIQCSSLARGD LDNARSQLNR LENLLGNGKY HSDWISNANK

Malt R -----

670 680 690 700 710 720
 Consensus VRVIYWQMTG DKAAAANWLR HTAKPEFANN HFLQGQWRNI ARAQILLGEF EPAEIVLEEL

Malt WT VRVIYWQMTG DKAAAANWLR HTAKPEFANN HFLQGQWRNI ARAQILLGEF EPAEIVLEEL

Malt R -----

730 740 750 760 770 780
 Consensus NENARSLRLM SDLNRNLLLL NQLYWQAGRK SDAQRVLLDA LKLANRTGFI SHFVIEGEAM

Malt WT NENARSLRLM SDLNRNLLLL NQLYWQAGRK SDAQRVLLDA LKLANRTGFI SHFVIEGEAM

Malt R -----

```

              790          800          810          820          830          840
Consensus  AQLRQLIQL NTLPELEQHR AQRILREINQ HHRHKFAHFD ENFVERLLNH PEVPELIRTS
MaLT WT    AQLRQLIQL NTLPELEQHR AQRILREINQ HHRHKFAHFD ENFVERLLNH PEVPELIRTS
MaLT R     -----
              850          860          870          880          890          900
Consensus  PLTQREWQVL GLIYSGYSNE QIAGELEVAA TTIKTHIRNL YQKLGVAHRQ DAVQHAQQLL
MaLT WT    PLTQREWQVL GLIYSGYSNE QIAGELEVAA TTIKTHIRNL YQKLGVAHRQ DAVQHAQQLL
MaLT R     -----

Consensus  KMMGYGV
MaLT WT    KMMGYGV
MaLT R     -----

```

Fig S4. Analysis of the amino acid sequence of the MalT receptor of phage λ in wild type and resistant isolates. Shown is a Clustal Omega 1.2.3 analysis of the amino acid sequences of the consensus (top), wild type- sensitive (middle), and resistant (bottom) *E. coli* isolates. Presented in green are the identical sequence in both isolates, in blue is the insertion sequence that leads to a frameshift in the resistant isolate, and presented in red is the site of an early stop codon in the resistant isolate.

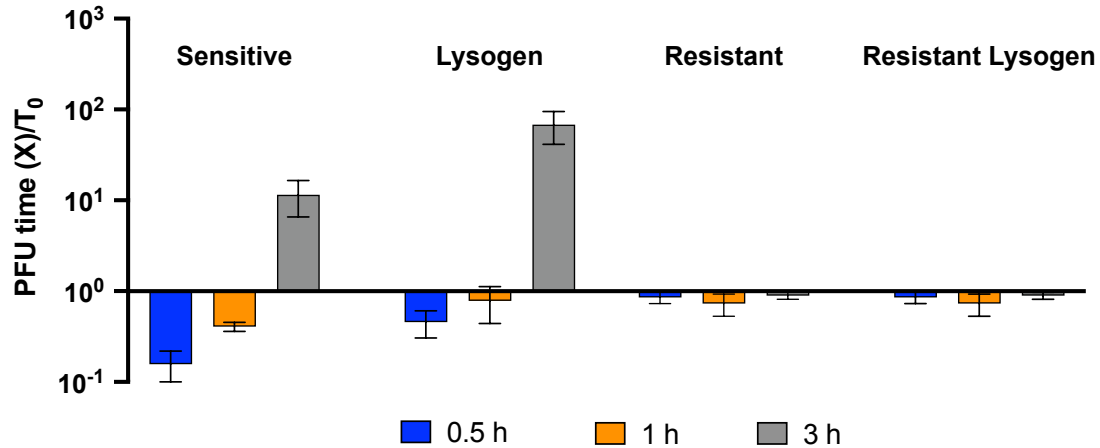


Fig. S5. Evidence that the resistant lysogen population in Figure 2 are refractory to λ . Ratios of the free phage density at times 0.5 (blue), 1 (orange), and 3 (grey) hours relative to that at time 0 (T_0). Presented are means and standard deviations of the ratios of three replicas. Infections with a low multiplicity of infection of phage λ to three known bacterial states (λ sensitive, λ lysogens, and resistant non-lysogens) as well as the presumptive resistant lysogens. Shown for the sensitive population are phage densities consistent with our estimates of phage λ 's adsorption rate (blue) and latent period (orange).

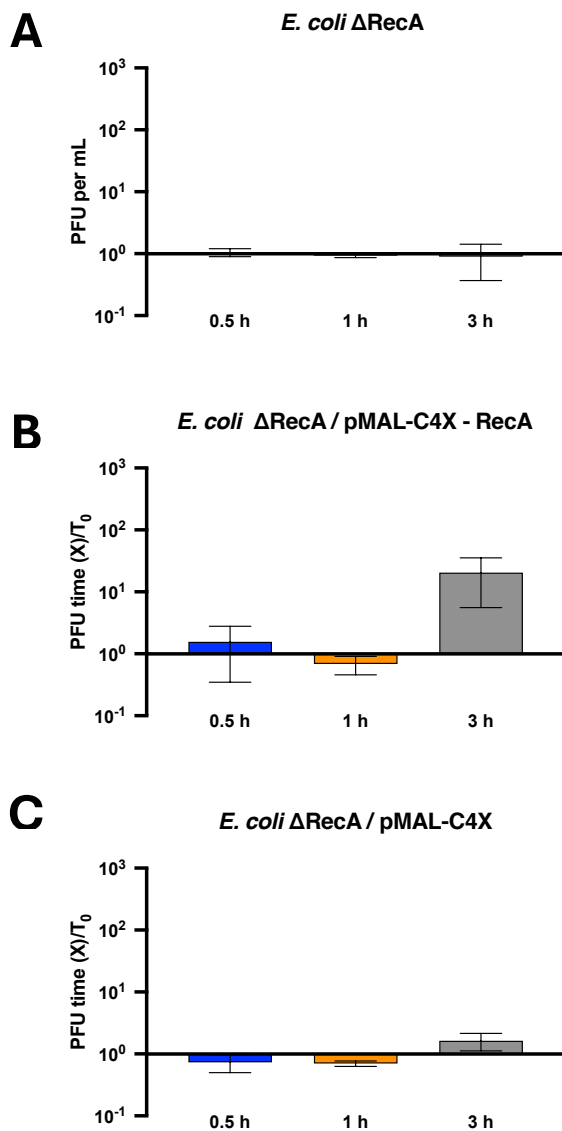


Fig. S6. *recA* knockout and complementation assay. Ratios of the free phage density at times 0.5 (blue), 1 (orange), and 3 (grey) hours relative to that at time 0 (T_0). Presented are means and standard deviations of the ratios of three replicas. Infections with a low multiplicity of infection of phage λ . **(A)** Infections of a Δ *recA* *E. coli* lysogenized with phage λ . **(B)** Infections of a Δ *recA* *E. coli* lysogenized with phage λ and transformed with plasmid pMal-c4X-RecA that codes the *recA* gene in *trans*. **(C)** Infections of a Δ *recA* *E. coli* lysogenized with phage λ and transformed with the empty plasmid pMal-c4X.

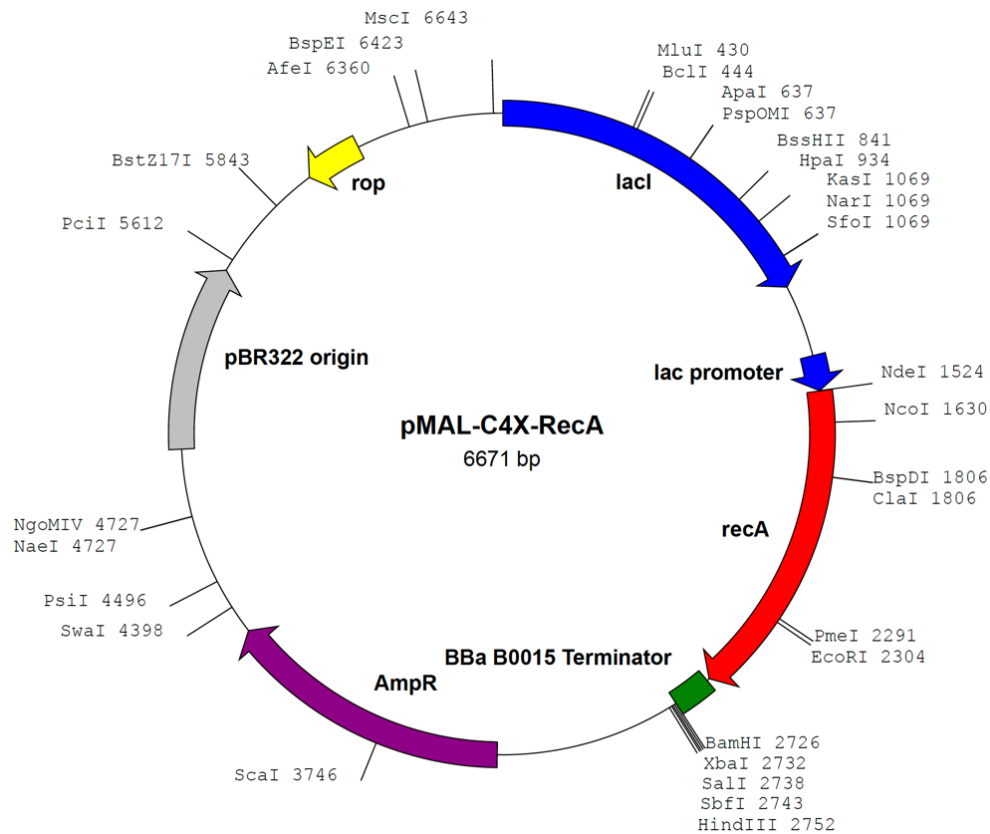


Fig. S7. Plasmid pMal-c4X – RecA map. Annotated diagram of the plasmid used for figure S5 to complement *recA* in *trans*.

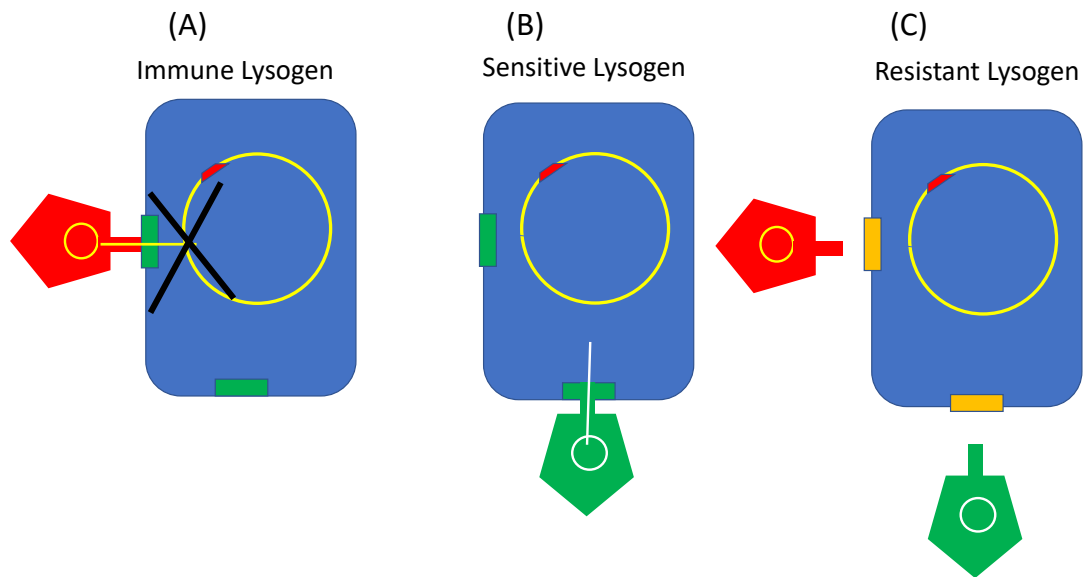


Fig. S8. Graphical representation of bacterial states. (A) Lysogens, the Blue boxes, are immune to the temperate phage, Red, coded for by their prophage, Red insert on the Yellow chromosome. The temperate phage coded-for by the prophage adsorb to specific sites, the Green rectangles, and inject their DNA. The DNA inserted by the infecting temperate phage is denatured, and the infecting temperate phage is lost. (B) Lysogens are sensitive to lytic phages some of which can adsorb to the same sites as the temperate phage coded for by their prophage. (C) Selection favors mutants with receptor sites, Orange, that are resistant (refractory) to the temperate as well as lytic phage. These phages do not adsorb.

Supplemental Table S1. The definitions and values of the parameters used in the model

Parameter	Values (dimensions)	Description	Source
v, v_{nr}, v_l, v_{lr}	$0.7(h^{-1})$	Maximum growth rates	This paper
μ_{nr}, μ_{rn}	$5e^{-5}, 5e^{-5}(h^{-1})$	Transitions $N \rightarrow N_R, N_R \rightarrow N$	Chaudhry <i>et al.</i> (2018)
μ_{lr}, μ_{rl}	$1e^{-5}, 1e^{-5}(h^{-1})$	Transitions $L \rightarrow L_R, L_R \rightarrow L$	This paper*
δ_p, δ_v	$1e^{-7}, 2e^{-7}(h^{-1} \cdot mL^{-1})$	Adsorption rate constants	Chaudhry <i>et al.</i> (2018)
β_p, β_v	$60 (PFU \cdot CFU^{-1})$	Burst sizes	This paper
K	$1 (\mu g)$	Monod constant	Stewart and Levin (1973)
γ	$1e^{-4}(h^{-1})$	Induction rate	This paper*
λ	$1e^{-2}$	Probability of lysogeny	This paper*
e	$5e^{-7}(\mu g \cdot CFU^{-1})$	Substrate conversion efficiency	Stewart and Levin (1973)

* Estimated via numerical analysis of the results and predictions illustrated in Figure S1 and Figure S2.

Supplemental Table S2. Wild phage genomes, their sources, and primers used to detect them

Wild Lysogen	Prophage(s)	Isolated Lysogen	Phage genome*	C Lysogen	Primers (5' – 3')
4C10 ¹	Lambda_4C10	1W	OM475428 LR595861	1L	Fw: CGCACGAAGAGCAGCATTAC Rv: GCGTGTTATACGCCCGTTTC
4A7 ¹	Lambda_4A7 P2_4A7	3W	OM475430 ³ LR595864	3L	Fw: ATGGTTGGCAGTAGGCTTCC Rv: CACAATGAGTGCGGCAACAA
4C7 ¹	Lambda	4W	OM475432	4L	Fw: GACGGCTGGTATCAGGTACG Rv: CTGTTCAGCAGCAGCTTTTT
E26 ²	Lambda	E26W	OM475435	E26L	Fw: AGCCTGTAGCTCCCTGATGA Rv: GCTTATGCTTGCCGAGATGG
D2 ²	Lambda-like	D2W	OM475427	D2L	Fw: CCCTTCACTGGTGACCATCC Rv: GTAATGCTGCTCTTCGTGCG
2H4 ¹	P2_2H4	9W	OM475431 LR595869	9L	Fw: ACCCTAGCCTTACCCCGATT Rv: CAACGGTGACCGGTTTTGAC
4C9a ¹	P2_4C9	10W	OM475433 LR595883	10L	Fw: CGATGCGTTTCTGGCTGATG Rv: CAATATTGTGCCGGTCAGCG
4C9b ¹	P2-like	11W	OM475429	11L	Fw: CAATATTGTGCCGGTCAGCG Rv: CGATGCGTTTCTGGCTGATG
4D9 ¹	P2_4E6b	12W	OM475434 LR595885	12L	Fw: TTGTACAGGACAGACTCGC Rv: CTGCAAAAACAGCGACGTGA
D8 ²	P2_4E6b	D8W	OM475426	D8L	Fw: CACACAGGGACGCACTTTTG Rv: TTCAGCTTTGTTGCTGTGCG

¹ Obtained from human microbiomes.

² Obtained from sewage water.

³ Only the lambda prophage was used for the C lysogen construction.

* Previous reported genomes and the generated in this study are presented in some cases.

SI References

1. W. N. Chaudhry *et al.*, Leaky resistance and the conditions for the existence of lytic bacteriophage. *PLoS Biol* **16**, e2005971 (2018).
2. F. M. Stewart, B. R. Levin, Partitioning of Resources and the Outcome of Interspecific Competition: A Model and Some General Considerations. *The American Naturalist* **107**, 171-198 (1973).

Chapter 8

Chapter 8

Enteric Populations of *Escherichia coli* are Likely to be Resistant to Phages Due to O Antigen Expression

Reprinted from: Brandon A. Berryhill, Kylie B. Burke, Jake Fontaine, Catherine E. Brink, Mason G. Harvill, David A. Goldberg, Konstantinos T. Konstantinidis, Bruce R. Levin, Michael H. Woodworth. 2023. Enteric Populations of *Escherichia coli* are Likely to be Resistant to Phages Due to O Antigen Expression. bioRxiv. <https://doi.org/10.1101/2023.11.08.566299>

Abstract

Metagenomic data provide evidence that bacteriophage (phage) abound in the enteric microbiomes of humans. However, the contribution of these viruses in shaping the bacterial composition of the gut microbiome and how these phages are maintained remain unclear. We performed experiments with 751 combinations of 54 *Escherichia coli* and 14 phage isolates from four fecal microbiota transplantation (FMT) doses as samples of non-dysbiotic human enteric microbiota. We also developed a mathematical model of the population and evolutionary dynamics of bacteria and phage. Our experiments predict that as a consequence of the production of the O antigen, most of the *E. coli* in the human enteric microbiome will be resistant to infections with the array of co-occurring phages. Our modeling suggests that phages are maintained in these enteric communities due to the high rates of transition between the O antigen resistant and sensitive states. Based on our observations and predictions from this theory, we postulate that the phage found in the human gut are likely to play little role shaping the strain composition of *E. coli* of healthy individuals. Although we only investigated *E. coli*, the mechanism of resistance described here is shared among most of the Gram-negative bacteria.

Introduction

The human microbiome is composed of trillions of microbes, including bacteria, viruses, fungi, protozoa, and archaea (1). The composition of the enteric microbiome has been tightly linked to human health and well-being (2-4) as well as many prevalent diseases such as cardiovascular disease, malignancy, malnutrition, and antimicrobial resistance (5-11). Interventions to modify the enteric microbiome may provide new tools to address many of these threats. However, optimal microbiome treatment strategies remain undefined. The answer to these questions requires an understanding of the factors that determine both the composition and diversity of microbes in this habitat. For the enteric microbiome, bioinformatic data has identified not only genetically diverse arrays of *E. coli*, but also genetic diversity amongst the viruses that prey on these bacteria, i.e., their bacteriophages (phages) (12). However, the contribution of these predatory viruses in determining the densities and distribution of species and strains of the bacteria in the human enteric microbiome is largely unknown.

For these phages to play a role in determining the densities and diversity of *E. coli* in the gut microbiome, the dominant populations of *E. coli* in this habitat must be susceptible rather than immune or resistant to the co-existing phage. There are many mechanisms by which bacteria can become immune to phage. In phage immunity, phage adsorb and inject their genetic material into the bacteria but do not replicate; this is distinct from phage resistance. In phage resistance, the bacteria prevents the phage from adsorbing in the first place. There are also several ways bacteria can become resistant to phage. The best studied of these mechanisms is envelope resistance, where because of modification of the receptor sites to which the phage adsorb, the bacteria are resistant to infections with these phage (13). Similar to this mechanism – and most relevant for this study – the O antigen component of the lipopolysaccharides (LPS) of Gram-negative bacteria can mask

the receptor sites of a number of phages, making the bacteria at least partially resistant to phages (other than those that use the O antigen as a receptor) (14-17).

The results of our experiments and analysis of the properties of a mathematical model make two predictions. Firstly, as a consequence of O antigens, the dominant populations of *E. coli* in the human fecal microbiome are resistant to the dominant population of co-existing phages in this habitat. Secondly, the observed O antigen-mediated resistance is leaky, meaning there is a high rate of transition from the resistant to sensitive states, thereby generating phage-sensitive minority populations of *E. coli* that can maintain the phage in this habitat.

Results

A method to isolate phages from fecal samples and test for the sensitivity of co-existing *E. coli* to these phages.

To ascertain the susceptibility of bacteria from gut microbiomes of humans to the co-existing phages, we used Fecal Microbiota Transplantation (FMT) doses as sources of enteric *E. coli* from non-dysbiotic hosts. FMT doses are simple suspensions of human donor stool in sterile normal saline, homogenized with a benchtop stomacher device and filtered to exclude large particulate matter. We attempt to isolate phages from these samples in three ways: first, by directly assaying for the presence of phage in these samples by spotting bacteria-free filtrates of these FMT doses onto agar lawns of a broadly phage-sensitive laboratory strain of *E. coli* and searching for zones of inhibition; second, by incubating FMT doses with Lysogeny Broth (LB) to allow the phage in the FMT doses to replicate on the *E. coli* already present in these samples and then spotting the incubated suspensions onto lawns of a broadly phage-sensitive laboratory strain of *E. coli*; third, by adding both the broadly phage-sensitive laboratory strain of *E. coli* and LB to the FMTs and plating on a laboratory strain of *E. coli*. If *E. coli*-specific phage are present in the sample spotted on the lawns, either clear or turbid zones of inhibition are generated. To obtain cells from minority populations of *E. coli* from these fecal samples, we isolated the bacteria from cultures on *E. coli*-specific (minimal lactose) agar containing different antibiotics. The methods employed to isolate phages and *E. coli* are illustrated in Figure 1, and described in more detail in the materials and methods. *E. coli* and phage isolates in these fecal samples

underwent whole genome sequencing and the diversity and relationships of these bacteria and phage to each other were analyzed with comparative genomic analyses.

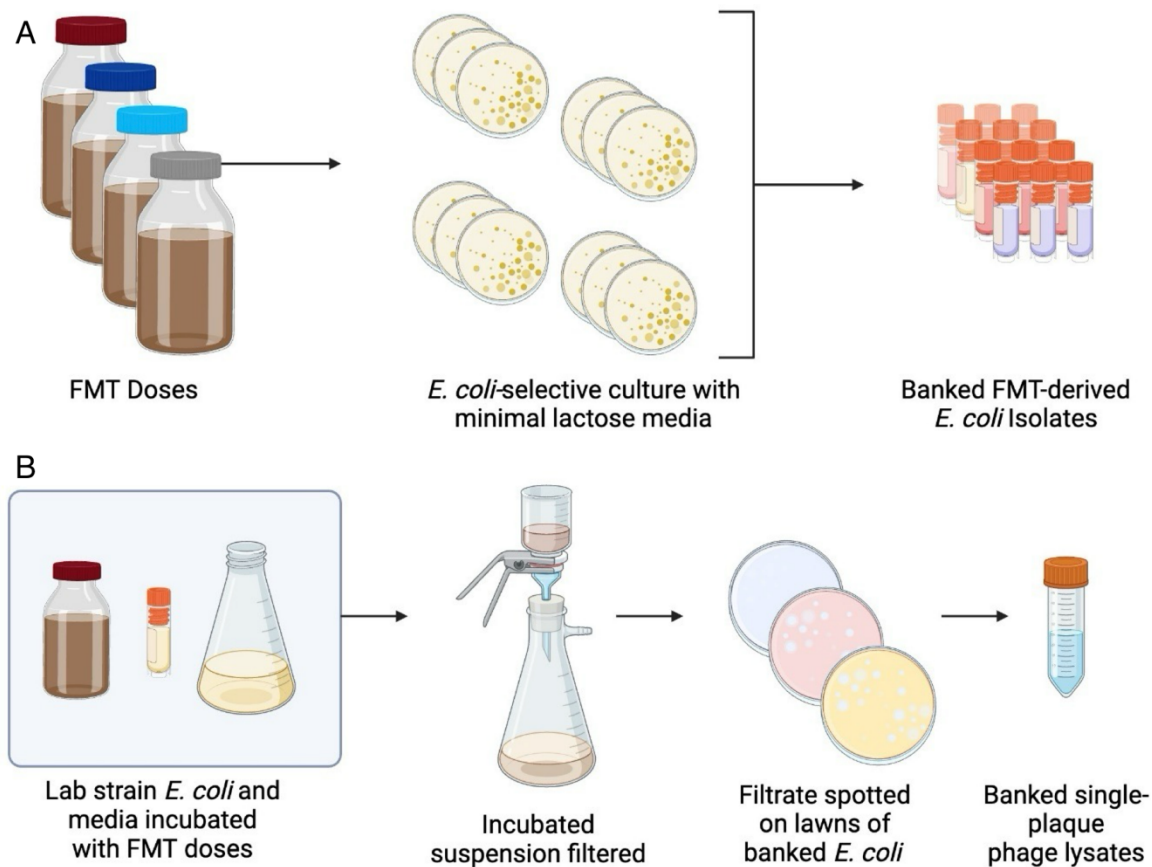


Figure 1. Diagram of bacteria and phage isolation protocol. (A) The method employed for isolating the dominant as well as minority populations of *E. coli* from the FMT samples. **(B)** The method employed for isolating bacteriophage from the FMT samples.

E. coli and phage isolated from the FMT doses

We were not able to recover any phage by direct plating of FMT filtrates on lawns of either the laboratory strains or fecal-derived *E. coli*, indicating that the phages in these FMT samples are likely to be of low density, absent, or unable to infect and replicate on the tested *E. coli* strains. We were also not able to isolate phage after

incubating the FMT doses with LB, indicating that the *E. coli* in these samples were not able to support the growth of the co-existing phages. We were able to obtain phages from three out of four of the FMTs studied by adding both the broadly phage-sensitive *E. coli* strain and LB in combination, indicating that there are low densities of phages in these fecal samples that can replicate on the lab strain of *E. coli*. The phages obtained in this way were not able to replicate on the *E. coli* isolated from these different FMTs, including almost all those from the minority of populations of *E. coli* isolated on the antibiotic plates.

Why were we able to isolate phage by adding both broth and a lab strain of *E. coli*, but not by simply adding broth? One explanation that could explain this observation is that *E. coli* in these fecal samples are already phage-resistant. We hypothesized that these FMT-derived *E. coli* are resistant to the co-existing phage and the laboratory strain is not due to the expression of the O antigen masking the phage receptor site of these bacteria. Two lines of evidence support this hypothesis. First, these *E. coli* isolated from FMTs bear genes coding for the O antigen. Second, serological tests of these *E. coli* confirm the expression of O antigens (Table 1). Neither the sequence data nor the serological tests demonstrated the existence of the O antigen in the laboratory strains of *E. coli*.

Table 1. O antigen type and production of FMT-derived *E. coli* isolates.

Strain	Predicted O antigen Type	Serological Confirmation
EC1A16	132	Positive
EC1B11	1	Negative
EC1B13	8	Positive
EC1B14	1	Positive
EC1B22	167	Positive
EC1B24	1	Positive
EC1C2	17/44	Positive
EC1C7	17/77	Positive
EC1C11	17/77/44	Positive
EC1C12	17/77	Positive
EC1C14	17/44	Positive
EC1C15	16	Positive
EC1C19	17/44	Positive
EC1C20	17/44	Positive
EC1C21	17/44	Positive
EC1C22	17/44	Positive
EC1C16	17/44	Positive
EC1C18	17/44	Positive
EC1D1	17/77	Positive
EC1D2	17/77/44	Positive
EC1D4	17/77/44	Positive
EC1D6	74	Positive
EC1D7	74	Positive
EC1D8	17/77	Positive
EC1D9	17/77	Positive
EC1D12	74	Positive
EC1D13	74	Positive
EC1D14	74	Positive
EC1D15	17/44	Positive
EC1D17	17/44	Positive
EC1D18	17/77/44	Positive
EC1D19	17/77	Positive
EC1D10	17/77	Positive
EC1D11	74	Positive

The expression of the O antigen makes *E. coli* resistant to phage.

To test the hypothesis that O antigen production by *E. coli* mediates resistance, we performed spot assays with MG1655 (an O antigen-negative lab strain), MG1655L5 (an isogenic mutant of MG1655 producing a medium level of the O antigen), and MG1655L9 (an isogenic mutant of MG1655 strongly producing the O antigen), and the phage T7. For further details on the bacterial strains and their sources see the Materials and Methods. We have restricted the assays with our constructed O antigen strains to phage T7 for two reasons: i) this phage is known to have its receptor masked via steric inhibition due to the production and display of the O antigen, and ii) bacteria require two genomic mutations to generate classical receptor site resistance to this phage, making the evolution of resistance unlikely in our assays (18). When phage are spotted onto lawns of MG1655L9, no plaques are observed. This observation is parallel to the corresponding experiments with the *E. coli* strains isolated from FMT doses. Lawns of MG1655L5 do support the production of plaques, but those plaques are turbid rather than clear as they are on MG1655. We interpret the turbidity of the plaques found with the highly lytic phage T7 and MG1655L5 as support for the proposition of intermediate phage susceptibility.

Accounting for the presence of phage in the apparently resistant populations of *E. coli*.

If the dominant populations of *E. coli* in these fecal samples are resistant to the co-existing phage, how are the phage isolated from these samples maintained in the host enteric microbiota? Our lytic phage model (described in Supplemental Figure 1 and within the Supplemental Text section entitled “*Model of the population dynamics of resistant O antigen bearing bacteria and lytic phage*”) illustrates that if the rate of transition from the O antigen-resistant state to the sensitive state are sufficiently high (10^{-4} per cell per hour or higher), the phage will be maintained by growing on the minority sensitive population, the predictions of which are described in Figure 2.

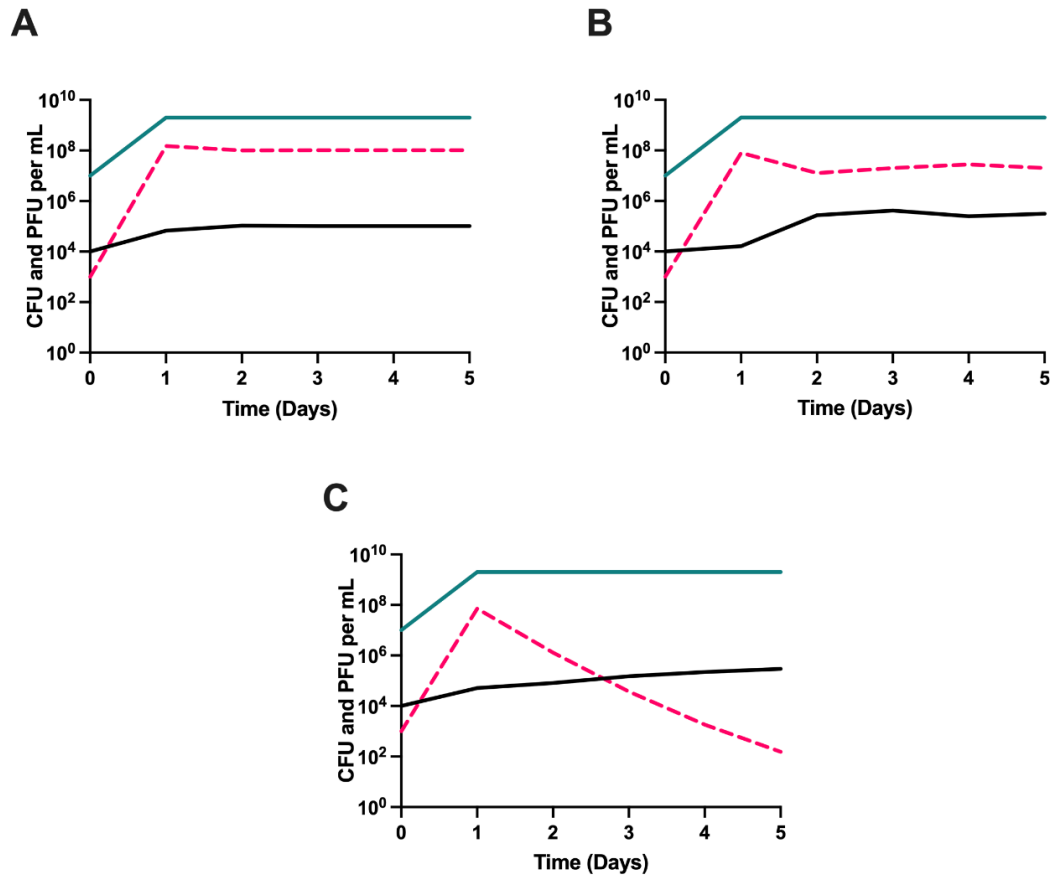


Figure 2. Predicted serial transfer dynamics of O antigen-mediated resistance and a lytic phage.

Simulation results showing the densities of bacteria and phage in serial transfer culture with three different transition rates between the resistant and sensitive states. At each simulated transfer, media containing 1,000 $\mu\text{g}/\text{mL}$ of the limiting resource is added along with 0.01 mL of the culture at 24 hours after the previous transfer. We assume no fitness cost to resistance, and the transition rate in both directions is the same. **(A)** Transition rates from sensitive to resistant and from resistant to sensitive at 10^{-3} per cell per hour. **(B)** Transition rates from sensitive to resistant and from resistant to sensitive at 10^{-4} per cell per hour. **(C)** Transition rates from sensitive to resistant and from resistant to sensitive at 10^{-5} per cell per hour. O antigen-expressing cells shown in green, sensitive cells shown in black, and phage shown in pink broken lines.

The model described above assumes no fitness cost for resistance, and assumes that the transition rate is the same whether bacteria are transitioning to sensitive or resistant. In Supplemental Figure 2, we consider the effects of varying fitness costs and unequal transition rates between sensitive and resistant, and find their impact to be negligible. We further explore in Supplemental Figure 3 the effects of using a temperate phage, with the model described in the Supplemental Text section entitled “*Model of the population dynamics of resistant O antigen bearing bacteria and temperate phage*”. While the dynamics do differ slightly, the maintenance of free phage can still be explained by leaky resistance.

To empirically test this leaky resistance hypothesis, we performed serial transfer experiments with the phage T7, MG1655 (O antigen non-producer), MG1655L5 (medium O antigen producer), and MG1655L9 (strong O antigen producer). The results of these experiments are presented in Figure 3. In serial transfer culture, the O antigen negative strain of *E. coli* maintained a high density of phage T7. Lower densities of these phage were maintained for the *E. coli* constructs that produce low and higher frequencies of cells bearing the O antigen, respectively, MG1655L5 and MG1655L9. The predictions of our model, along with these experimental results, explain how phage can be maintained in populations of bacteria resistant to these viruses. This accounts for how we were only able to recover phages after adding an O antigen-negative strain of *E. coli* and LB.

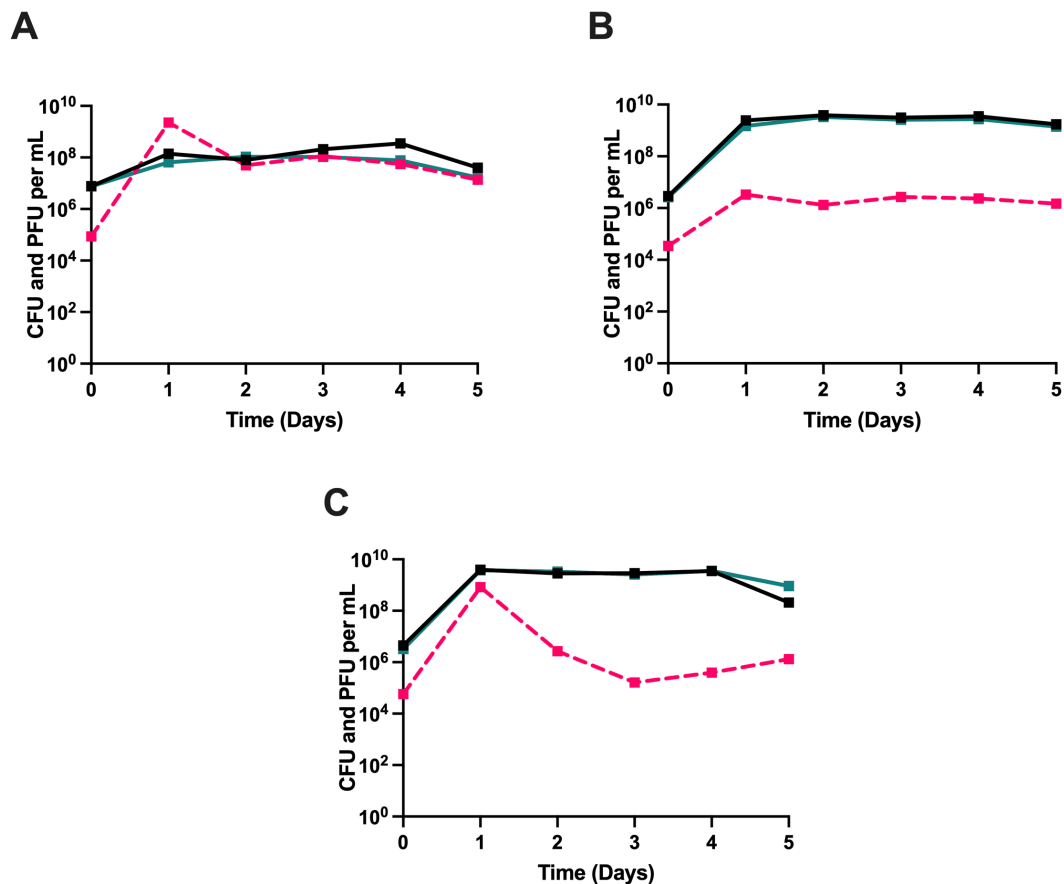


Figure 3. Serial transfer with phage T7 and strains of *E. coli* MG1655 lacking and expressing different levels of the O antigen. Three variants of *E. coli* MG1655 serially transferred for five days in LB broth with the phage T7. Shown in solid lines are bacterial densities with the black line representing a phage-free control. The broken pink lines represent phage densities. Shown is one of three biological replicates. **(A)** Wild-type MG1655 that does not produce the O antigen. **(B)** MG1655L5, which produces a medium amount of the O antigen. **(C)** MG1655L9, which produces a high amount of the O antigen. Two other, qualitatively similar, replicates are presented in Supplemental Figure 4. These results show lower but consistently measurable phage densities in *E. coli* populations expressing O antigen.

Genomic diversity of *E. coli* and its phages in FMT doses

We identified an apparent dominant and several minority *E. coli* strains in each FMT dose. These results demonstrate successful isolation of distinct populations of *E. coli* in the fecal microbiomes of several healthy donors. For each FMT donor, we assessed the diversity of recovered *E. coli* strains via alignment of predicted gene clusters, average nucleotide identity (ANI), *in silico* multi-locus sequence type (MLST), and *in silico* H and O serotype prediction; we display these results in Figure 4A. We chose to predict the H and O serotype *in silico* as the diverse expression of these antigens were traditionally a measure of *E. coli* diversity (19). When applying an ANI-based genomovar definition of $\geq 99.5\%$ ANI, we identified a median of 2.5 (range 2-3) culturable *E. coli* strains per donor (20). In general, classification by MLSA was consistent with the ANI-based clustering. However, strains with similar ANI and of the same MLST displayed a greater diversity in predicted O antigen type. These findings mirror previous studies (21) which found that healthy individuals carry diverse *E. coli* strains, confirming that our methods are readily capable of capturing the diversity in the fecal microbiome.

Of the four FMT donors, phages were recovered from three donors (Donors B, C, and D). Three unique phages were recovered from each of these three donors; thus, we recovered a total of nine distinct phages. Of note, we were not able to recover any phages from Donor A with any of the above-described isolation methods. A phylogenetic analysis of the phage genomes was conducted by generating an average amino acid identity (AAI) heatmap (Supplemental Figure 5) and consensus maximum likelihood phylogenetic trees based on the core phage genomes (Figure 4B). The reference *Peduvovirus* genomes, genomes isolated in this study, and the IMG/VR genomes shared AAI values of 90%, which reflects the high similarity in gene content between these phage. The consensus tree of these gene trees, estimated using Astral (22), is shown in Figure 4B. The phylogeny demonstrates that the genomes of Donor D are only distantly related to those of B and C. The phages from Donors B and C also appear to cluster separately, with the exception of a single phage, which is closely related to the phage genomes of Donor B despite being isolated from Donor C. This suggests that each FMT donor has multiple distinct culturable phage populations and that the populations within each donor are largely distinct from the other donors.

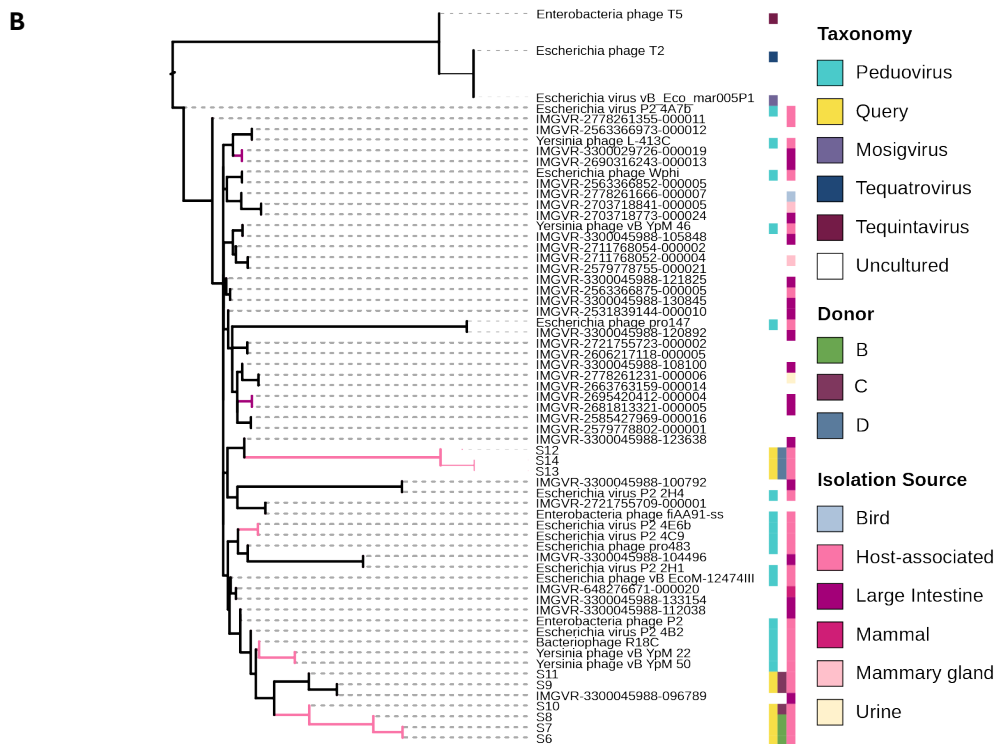
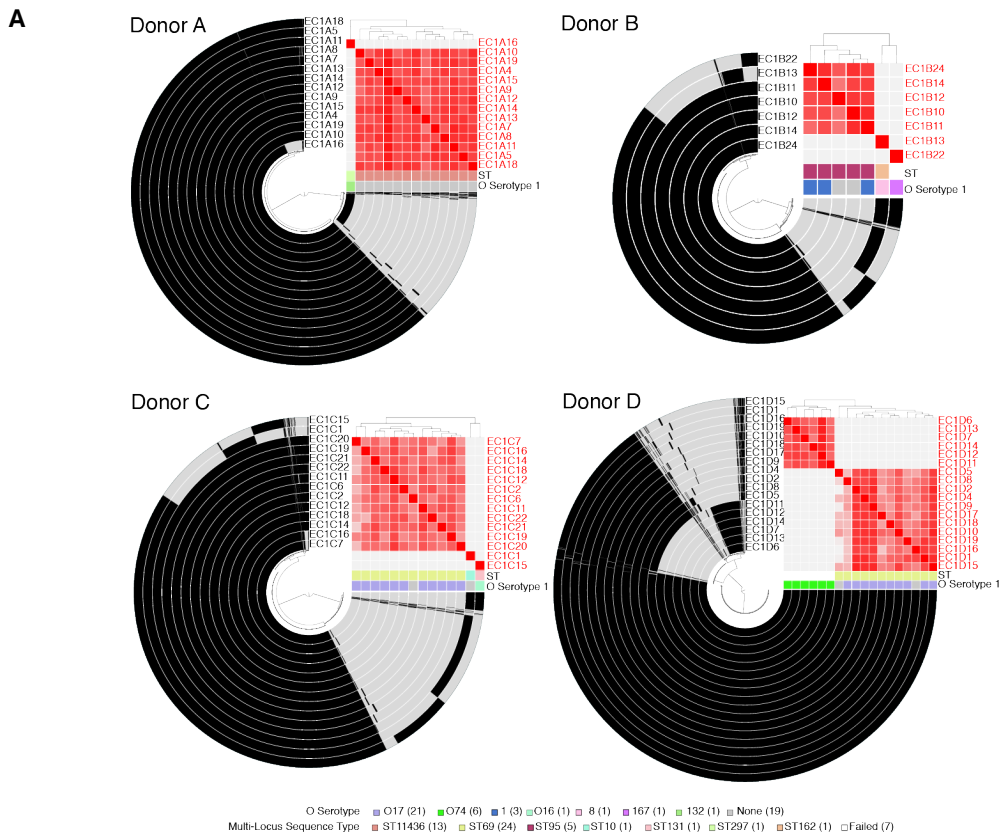


Figure 4. Diversity of isolated *E. coli* and phages. **(A)** Circular clustered gene alignments of *E. coli* isolated from four healthy donors show maintenance of minority populations that differ by ANI (shown as red heat map scaled from 0.995 to 1.0), gene content (with singleton gene clusters ranging from 0 to 722), *in silico* MLST classification, and *in silico* predicted O antigens. **(B)** Bacteriophage consensus maximum likelihood phylogenetic tree based on core genes of the phage genomes in this study and close relatives from public databases. Thirty-two genes were shared in more than 55/60 of the genomes in the major AAI cluster of Supplemental Figure 5 and were used to build individual trees as described in the Methods Section.

Susceptibility of *E. coli* isolates to phage

Our results indicate that while a high level of expression of the O antigen is sufficient to allow phage resistance, phage are still able to be maintained by that resistant population. Furthermore, the diverse *E. coli* isolated from the FMTs were found to display a variety of O antigen types. These observations, taken together, suggest that *E. coli* isolated from healthy human enteric microbiota are likely to be resistant to a diversity of *E. coli* phages, including those from the same community.

To get a better idea of the phage susceptibility/resistance of the *E. coli* in the FMTs we spot tested three classes of phage on lawns of each of the genetically distinct bacteria isolated from the FMTs: i) five well-characterized laboratory phages not isolated from feces; ii) the co-existing phages isolated from the same donor; and iii) phages isolated from the other donors. In total, we tested 751 combinations of 54 bacterial isolates and 14 phage isolates.

Lawns of the laboratory strain *E. coli* C lab displayed clear plaques in spot tests with the 14 tested lab and FMT-derived phages tested (Figure 5). This is not the case for lawns with the FMT-derived *E. coli* isolates, which give either no plaques (217/265, 81.9%) or turbid plaques (42/265, 15.8%). There is one exception: The phage T3 spotted on EC1D8 generated a clear plaque (0.3%). On lawns of the FMT-derived *E. coli* isolates, 392/477 (82.2%) produced no plaques and 85/477 (17.8%) produced turbid plaques.

For phages in the FMT doses to shape the composition of a recipient's enteric microbiota, the recipient's *E. coli* must be sensitive to FMT-derived phage. However, when comparing combinations of FMT-derived phage and *E. coli* isolated from the same or different donors, we do not find sensitivity. We found a significantly higher proportion of turbid plaques with autologous (bacteria and phage from the same donor) phage-*E. coli* combinations compared to allogeneic (bacteria and phage from different donors) phage-*E. coli* combinations (29/117, 24.5% vs 56/360, 15.6%; chi-square p-value 0.033). Further analysis of these and the above pairs of bacteria and phage are described in Supplemental Table 1. These results, taken together, indicate that FMT-derived *E. coli* are less sensitive to phages than laboratory *E. coli* strains—not just FMT-derived phages, but phages in general.

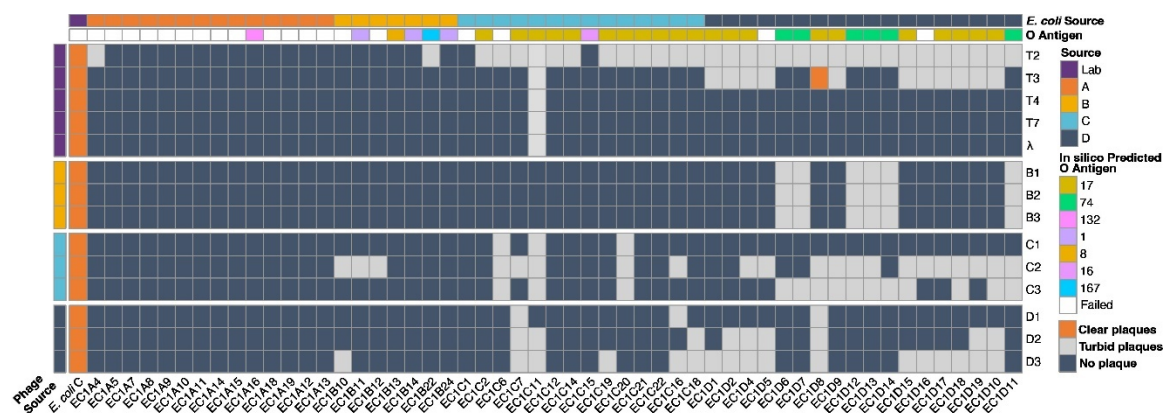


Figure 5. FMT-isolated *E. coli* do not give clear plaques when spotted with laboratory or FMT-derived bacteriophages. Well-characterized laboratory and FMT-derived *E. coli* strains (indicated by Source as Lab or Donor A through D) were spotted with well-characterized laboratory phages (T2, T3, T4, T7, and a virulent mutant of phage λ) and FMT-derived bacteriophages (isolated from FMT Donors B through D). Dark blue denotes no plaque formation, light grey denotes turbid plaque formation, and orange denotes clear plaque formation. Clear plaques were almost exclusively produced by the tested phages on lawns of a laboratory strain of *E. coli* C indicating broad resistance or immunity of FMT-derived *E. coli* to phages from all sources.

Interestingly, the expression of the O antigen in the population is not merely coincidental. We find that the O antigen is selected for in the presence of phage, as shown in Supplemental Figure 6. Could phage be one of the many selective pressures responsible for the ubiquity of the O antigen in natural populations of *Enterobacteriaceae*?

Discussion

We set out to elucidate the role of bacteriophages in shaping the composition of *E. coli* in the enteric microbiome of healthy humans. Our interpretation of these results is that bacteriophages likely play little role in determining the strain composition of co-occurring *E. coli* due to the high prevalence of phage resistance in the enteric microbiome of healthy individuals. In the case of *E. coli*, the expression of the O antigen is sufficient to confer phage resistance while allowing for the maintenance of phage due to the random transition between a phage-resistant and -sensitive state, which we call leaky resistance. Several diverse mechanisms can convey bacteriophage resistance (such as receptor site mutation and the carriage of phage resistance genes on prophage (23, 24)) but we demonstrate that expression of the O antigen alone is sufficient to account for the resistance of *E. coli* to a broad swath of phages, including those to which they have never been exposed. Our models and experiments support the hypothesis that despite this resistance, phage will be maintained in communities of these O antigen-expressing bacteria. Moreover, we expect that this same resistance could be observed in many natural populations of *Enterobacteriaceae*, as this family broadly expresses the O antigen. Stated another way, we postulate that resistance to co-occurring phages will be the dominant characteristic of bacteria in stable natural communities (25). This prediction is consistent with experimental studies of lytic and temperate bacteriophages *in vitro* (18, 26).

Resistant mutants almost always emerge and ascend to become the dominant population of bacteria in *in vitro* experiments with laboratory strains of bacteria and lytic phages. Nevertheless, phages are commonly maintained in these cultured populations that are dominated by resistant bacteria (26, 27). There are a variety of mechanisms by which the phage can be maintained, but their maintenance appears to play little role in regulating the densities of these bacterial cultures, and these bacterial populations are more likely shaped by other factors such as resource availability. We postulate this could also be the case in the gut microbiome. While there are many other mechanisms by which phages can be maintained, such as physical refugia as a consequence of the structure of the gut or spontaneous temperate phage induction (Supplemental Figure 3),

we have demonstrated that leaky resistance is sufficient to independently account for the results observed here. There is, however, a caveat to our purported mechanism for phage maintenance in that one prediction of our model is that the density of bacteria would exceed that of phage in natural populations. How common that is in natural communities is unclear as in marine settings it is thought that the density of phage far exceeds that of the bacteria (28, 29), though recent studies have questioned how high this ratio actually is (30). There is another caveat in that we have restricted our study to human samples because of the clinical relevance. Other studies by colleagues have examined the phage and *E. coli* interactions in the microbiome of other animals such as horses (31). Despite these caveats, we believe the mechanism proposed here happens not only in the gut but more broadly in nature. We cannot say definitively how pervasive these observations are, but this question of generality could be answered by other investigators with culture-independent approaches.

We expect that the approach developed in this study also has broader utility for translational phage investigation. If phages are to be developed as therapeutics or as components of therapeutic consortia, we expect that this will require complementary culture-based and culture-independent techniques that include experimental isolation, characterization, and strain-resolved analysis in the context of complex communities.

The increasing incidence of antibiotic-resistant infections in recent years has resurrected interest in using phage to treat bacterial infections. When it comes to utilizing bacteriophages therapeutically, one would expect a tradeoff between this generalized resistance mechanism and bacterial virulence. This phenomenon was illustrated in a classical study by Smith and Huggins, where they utilized a phage targeting the K antigen of pathogenic *E. coli* (32). Interestingly, the mechanism of resistance explored here, the O antigen, is known to be the target of some bacteriophages (33). If the results presented here for *E. coli* are supported in other *Enterobacteriaceae*, we would expect difficulties in isolating phage capable of lysing specific bacterial isolates. This anticipated result is echoed by investigators working on isolating phage for therapy where the rates of

finding phage for an isolate are less than 50% for some pathogens (34-36). Here we provide one explanation for why this could be the case: that is, resistance associated with production of the O antigen.

Materials and Methods

Fecal Microbiota Transplant Doses. Healthy human participants were recruited and provided informed consent to participate in a stool donor protocol approved by the Emory University Institutional Review Board (Protocol 00112302, PI Woodworth). Donors completed health and behavior questionnaires, blood, urine, and stool laboratory testing to screen for potential pathogens as described in the PREMIX trial (37). Each stool specimen from a single donor was divided by weight with 50-100g of stool in a Seward filter bag and suspended in 250mL USP sterile saline using a Seward benchtop stomacher at 200 rpm for 30 seconds twice. After removing the filter bag, the remaining suspension of stool in saline was transferred back to the 250mL saline bottle and delivered fresh without freezing for *E. coli* and phage isolation as described below. Additional aliquots with and without 10% glycerol by starting volume were prepared and stored at -80 °C.

Bacterial Strains. *E. coli* C was obtained from Marie-Agnès Petit at INRAE in Joy-en-Josas, France. MG1655 L9 and L5 were obtained from Douglas Browning at Aston University in Birmingham, UK (38). Briefly, these constructs were made by cloning either the *rfb* cluster or *nmbl* into isogenic MG1655. Wild *E. coli* were isolated from fecal microbiota transplantation doses as described below.

Bacteriophages. Phages Lambda^{VIR}, T2, T3, T4, and T7 were acquired from the Levin Lab's phage collection. Wild phages were isolated from fecal microbiota transplantation doses as described below.

Growth Media and Conditions. Unless otherwise noted, all bacteria were cultured in Lysogeny Broth (LB) at 37 °C. Lysogeny broth (LB) prepared according to manufacturer instructions (Difco, 244620). LB soft agar made with 0.7% w/v agarose, and LB plates made with 1.6% agarose, LB phage plates prepared as LB plates supplemented with 20 mM CaCl₂.

Isolating Bacteria from the FMTs. Serial dilutions of FMT in 0.85% NaCl solution was followed by plating on Davis Minimal (DM) plates (Sigma-Aldrich, 15758) supplemented with 0.4% w/v lactose (Sigma-Aldrich,

L3750). Individual colonies were randomly chosen and picked with a sterile stick and simultaneously streaked onto an EMB plate and a DM plate. Both were incubated at 37 °C overnight. Isolates colored green on the EMB plate were picked from their respective minimal plate and serially streaked from the DM lactose plate onto another DM lactose plate and incubated at 37 °C overnight. Each isolate was labeled, stored, and frozen.

Isolating Phage from the FMTs. 0.1 mL of FMT suspension was inoculated into 10mL LB broth with $\sim 1e^7$ CFU/mL *E. coli* C. These flasks were grown with shaking at 37 °C overnight. The next day, samples were centrifuged and filtered through a 0.22-micron filter (Basix, 13-1001-06). These rough lysates were then plated for single plaques. Individual plaques were picked with a sterile stick and resuspended as described above to obtain clonal phage lysates.

AAI heatmap. We identified the closest relatives to the genomes of this study (query genomes) using whole-genome searches against public genome databases. The final set of genomes used in subsequent analyses consisted of 98 genomes – including the 9 query genomes, 34 genomes from the IMG/VR v4 database (39), and 55 genomes that are publicly available on NCBI. Prodigal v2.6.3 (40) was used for gene prediction with default settings, and pairwise all versus all Average Amino acid Identity (AAI) was calculated using the *aai.rb* script from the Enveomics collection (41) using default settings except for decreasing the number of minimum hits to 20. The final heatmap was constructed using the *pheatmap* package in R. Accession numbers of the public genomes are labelled in the figure.

Core gene tree. The subset of genomes that make up the major cluster in the AAI heatmap were used for gene clustering at 30% identity with *MMseqs2* v 13.4511 (42). The resulting clusters were used to identify the core genome – the genes that are found in 55/60 (~90%) of the genomes. The 32 core genes were extracted using *seqtk*-1.4 and individual gene alignments were generated using *MUSCLE* v3.8.31 (43) with default settings. Each alignment was used to generate a maximum likelihood gene tree in *MEGA11* (43) with default parameters. These gene trees were concatenated and passed into *Astral* 5.7.8 (22) to generate the final consensus tree as *Astral* has a built-in algorithm to deal with any missing data in the input gene trees. The final tree was visualized and annotated in *iTol* (44) and is shown in Figure 4B. The tree was rooted using

Escherichia virus vB_eco_mar005P1. The additional two genomes used as outgroups to root this tree were added manually.

Phage Susceptibility Testing. $\sim 1e^6$ of each phage lysate was spotted onto lawns of the bacteria using the double-layer soft agar technique as described in (45). Phage lysates were diluted 1:100 prior to spotting to minimize lysis from without.

Sampling Bacterial and Phage Densities. Bacteria and phage densities were estimated by serial dilutions in 0.85% NaCl solution followed by plating. The total density of bacteria was estimated on LB (1.6%) agar plates. To estimate the densities of free phage, chloroform was added to suspensions before serial dilutions and double-layer soft agar enumeration.

Serial Transfer Experiments. All serial transfer experiments were carried out in 10 mL LB broth cultures grown at 37 °C with vigorous shaking. The cultures were initiated by 1:100 dilution from 10 mL overnight cultures grown from single colonies. Phage was added to these cultures to reach the initial density of $\sim 10^7$ PFU/mL. At the end of each transfer, 0.1 mL of each culture was transferred into flasks with fresh medium (1:100 dilution). Simultaneously, 0.1 mL samples were taken for estimating the densities of CFUs and PFUs as described above.

Antibiotics and Their Sources. Streptomycin (S6501) was obtained from Sigma-Aldrich; Tetracycline (T1700) from Research Products International; Gentamicin (BP918-1) from Fisher BioReagents; Chloramphenicol (C5793) from Sigma-Aldrich; Ciprofloxacin (A4556) from AppliChem; Ceftriaxone (C5793) from Sigma-Aldrich; Meropenem (QH-8889) from Combi-Blocks; Azithromycin (3771) from Tocris; Fosfomycin (P5396) from Sigma-Aldrich; and Colistin (C4461) from Sigma-Aldrich. All antibiotic Sensi-Discs were obtained from Becton Dickinson.

O Antigen Antisera Assay. *E. coli* O antigen-specific antisera was obtained from SSI Diagnostica and used as detailed in their protocol for the slide agglutination assay. A known O antigen negative lab strain (MG1655) and its construct bearing the O antigen (MG1655L9) were used as negative and positive controls respectively.

Whole-Genome Sequencing. Samples were sent to MIGS (Pittsburgh, USA) as bacterial colonies grown on an agar plate or as sterile phage lysates for extraction and Illumina sequencing. Individual colonies and lysates

were extracted per the manufacturer's protocol using the Zymo DNA miniprep bead beating lysis kit. Sample libraries were prepared for Illumina sequencing using Illumina's DNA Prep kit and IDT 10bp unique dual indices and sequenced on an Illumina NovaSeq 6000, producing paired end 151bp reads. Demultiplexing, quality control, and adapter trimming was performed with bcl-convert (v4.1.5). Illumina reads were quality filtered using Trimmomatic (46). *E. coli* C host sequences were depleted from phage lysate sequencing data by mapping to a closed *E. coli* C genome with bowtie2 (47). After trimming and host decontamination (for phage lysates), remaining reads were and assembled *de novo* using SPAdes v3.13 (48). Pairwise comparisons of average nucleotide identity on the assembled genomes were performed with the Mashmap method using fastANI v1.32 as in (49). Gene sequences were predicted with Prodigal v2.6.3 (40) and annotated with Prokka v1.14.6 (50). O and H antigens were predicted *in silico* with ECtyper (51). Bacterial pangenome figures were created with anvio v.7.1 (52).

Numerical Solutions (Simulations). For our numerical analysis of the coupled, ordered differential equations presented in the Supplemental Text, we used Berkeley Madonna with the parameters presented in Supplemental Table 2. Copies of the Berkeley Madonna programs used for these simulations are available at www.eclf.net.

Statistical Analysis. Statistical tests of difference in proportions of phage plaquing results tabulated as a contingency table were performed with the chisq.test function in stats package version 4.3.0 in R version 4.3.0 using the R studio interface version 2023.06.0. Resulting p-values <0.05 were considered statistically significant.

Acknowledgements

We thank Dalia Gulick, Amanda Strudwick, Amalia Cruz, and Candace Miller for their help obtaining and processing the FMTs. We also thank the other members of the Levin Lab for their collaboration and discussion, in particular Andrew Smith, Josh Manuel, Teresa Gil-Gil, Thomas O'Rourke, Ingrid McCall, and Eduardo Roman. We would like to thank BioRender for their software which was used to create the schematic figure. We are particularly grateful to Andrey Letarov for his comments on the BioRxiv version of this manuscript and discussion, which improved this report.

Funding Sources

National Institute of Allergy and Infectious Diseases grant K23AI144036 (MHW)

Southern Society for Clinical Investigation Research Scholar Award (MHW)

National Institute of General Medical Sciences grant R35GM136407 (BRL)

The content is solely the responsibility of the authors and does not necessarily represent the official views of the National Institutes of Health or the Southern Society for Clinical Investigation.

Data Availability

The Berkeley Madonna program used for the simulations are available at www.eclf.net. All raw sequence data for the *E. coli* and phage genomes shown have been deposited in the sequence read archive (SRA, NCBI, Bethesda, MD, USA) and can be found with bioproject accession PRJNA1028583.

References

1. Matijašić M, Meštrović T, Paljetak H, Perić M, Barešić A, Verbanac D. Gut Microbiota beyond Bacteria-Mycobiome, Virome, Archaeome, and Eukaryotic Parasites in IBD. *Int J Mol Sci.* 2020;21(8).
2. Ogunrinola GA, Oyewale JO, Oshamika OO, Olasehinde GI. The Human Microbiome and Its Impacts on Health. *Int J Microbiol.* 2020;2020:8045646.
3. Hou K, Wu Z-X, Chen X-Y, Wang J-Q, Zhang D, Xiao C, et al. Microbiota in health and diseases. *Signal Transduction and Targeted Therapy.* 2022;7(1):135.
4. Wilmanski T, Diener C, Rappaport N, Patwardhan S, Wiedrick J, Lapidus J, et al. Gut microbiome pattern reflects healthy ageing and predicts survival in humans. *Nature Metabolism.* 2021;3(2):274-86.
5. Davar D, Dzutsev AK, McCulloch JA, Rodrigues RR, Chauvin J-M, Morrison RM, et al. Fecal microbiota transplant overcomes resistance to anti-PD-1 therapy in melanoma patients. *Science.* 2021;371(6529):595-602.
6. Zhu W, Gregory JC, Org E, Buffa JA, Gupta N, Wang Z, et al. Gut Microbial Metabolite TMAO Enhances Platelet Hyperreactivity and Thrombosis Risk. *Cell.* 2016;165(1):111-24.
7. Liu KH, Owens JA, Saeedi B, Cohen CE, Bellissimo MP, Naudin C, et al. Microbial metabolite delta-valerobetaine is a diet-dependent obesogen. *Nat Metab.* 2021;3(12):1694-705.
8. Woodworth MH, Hayden MK, Young VB, Kwon JH. The Role of Fecal Microbiota Transplantation in Reducing Intestinal Colonization With Antibiotic-Resistant Organisms: The Current Landscape and Future Directions. *Open Forum Infect Dis.* 2019;6(7).
9. Tomkovich S, Dejea CM, Winglee K, Drewes JL, Chung L, Housseau F, et al. Human colon mucosal biofilms from healthy or colon cancer hosts are carcinogenic. *J Clin Invest.* 2019;129(4):1699-712.
10. DeStefano Shields CE, Van Meerbeke SW, Housseau F, Wang H, Huso DL, Casero RA, Jr., et al. Reduction of Murine Colon Tumorigenesis Driven by Enterotoxigenic *Bacteroides fragilis* Using Cefoxitin Treatment. *J Infect Dis.* 2016;214(1):122-9.
11. Smith MI, Yatsunenکو T, Manary MJ, Trehan I, Mkakosya R, Cheng J, et al. Gut microbiomes of Malawian twin pairs discordant for kwashiorkor. *Science.* 2013;339(6119):548-54.

12. Camarillo-Guerrero LF, Almeida A, Rangel-Pineros G, Finn RD, Lawley TD. Massive expansion of human gut bacteriophage diversity. *Cell*. 2021;184(4):1098-109.e9.
13. Egido JE, Costa AR, Aparicio-Maldonado C, Haas PJ, Brouns SJJ. Mechanisms and clinical importance of bacteriophage resistance. *FEMS Microbiol Rev*. 2022;46(1).
14. Burmeister AR, Fortier A, Roush C, Lessing AJ, Bender RG, Barahman R, et al. Pleiotropy complicates a trade-off between phage resistance and antibiotic resistance. *Proceedings of the National Academy of Sciences*. 2020;117(21):11207-16.
15. Golomidova AK, Efimov AD, Kulikov EE, Kuznetsov AS, Belalov IS, Letarov AV. O antigen restricts lysogenization of non-O157 *Escherichia coli* strains by Stx-converting bacteriophage phi24B. *Scientific Reports*. 2021;11(1):3035.
16. Letarov AV. Bacterial Virus Forcing of Bacterial O-Antigen Shields: Lessons from Coliphages. *International Journal of Molecular Sciences*. 2023;24(24):17390.
17. Kulikov EE, Golomidova AK, Prokhorov NS, Ivanov PA, Letarov AV. High-throughput LPS profiling as a tool for revealing of bacteriophage infection strategies. *Scientific Reports*. 2019;9(1):2958.
18. Chao L, Levin BR, Stewart FM. A Complex Community in a Simple Habitat: An Experimental Study with Bacteria and Phage. *Ecology*. 1977;58(2):369-78.
19. Ørskov F, Ørskov I. 2 Serotyping of *Escherichia coli***The terminology used to describe the different classes of bacterial antigens is explained in the Preface. However, the authors would like to mention that a different convention is used in some laboratories, for example O:l, K:l, H:7 is equivalent to O1:K1:H7. In: Bergan T, editor. *Methods in Microbiology*. 14: Academic Press; 1984. p. 43-112.
20. Rodriguez-R LM, Conrad RE, Feistel DJ, Viver T, Rosselló-Móra R, Konstantinidis KT. A natural definition for a bacterial strain and clonal complex. *bioRxiv*. 2022:2022.06.27.497766.
21. Hu D, Fuller NR, Caterson ID, Holmes AJ, Reeves PR. Single-gene long-read sequencing illuminates *Escherichia coli* strain dynamics in the human intestinal microbiome. *Cell Reports*. 2022;38(2):110239.
22. Mirarab S, Reaz R, Bayzid MS, Zimmermann T, Swenson MS, Warnow T. ASTRAL: genome-scale coalescent-based species tree estimation. *Bioinformatics*. 2014;30(17):i541-i8.

23. Egido JE, Costa AR, Aparicio-Maldonado C, Haas P-J, Brouns SJJ. Mechanisms and clinical importance of bacteriophage resistance. *FEMS Microbiology Reviews*. 2021;46(1).
24. Labrie SJ, Samson JE, Moineau S. Bacteriophage resistance mechanisms. *Nature Reviews Microbiology*. 2010;8(5):317-27.
25. Shkoporov AN, Hill C. Bacteriophages of the Human Gut: The “Known Unknown” of the Microbiome. *Cell Host & Microbe*. 2019;25(2):195-209.
26. Berryhill BA, Garcia R, McCall IC, Manuel JA, Chaudhry W, Petit M-A, et al. The book of Lambda does not tell us that naturally occurring lysogens of *Escherichia coli* are likely to be resistant as well as immune. *Proceedings of the National Academy of Sciences*. 2023;120(11):e2212121120.
27. Stewart FM, Levin BR. The population biology of bacterial viruses: Why be temperate. *Theoretical Population Biology*. 1984;26(1):93-117.
28. Paul JH, Sullivan MB, Segall AM, Rohwer F. Marine phage genomics. *Comparative Biochemistry and Physiology Part B: Biochemistry and Molecular Biology*. 2002;133(4):463-76.
29. Chibani-Chennoufi S, Bruttin A, Dillmann ML, Brüssow H. Phage-host interaction: an ecological perspective. *J Bacteriol*. 2004;186(12):3677-86.
30. Roux S, Brum JR. Counting dots or counting reads? Complementary approaches to estimate virus-to-microbe ratios. *The ISME Journal*. 2023;17(10):1521-2.
31. Golomidova A, Kulikov E, Isaeva A, Manykin A, Letarov A. The diversity of coliphages and coliforms in horse feces reveals a complex pattern of ecological interactions. *Appl Environ Microbiol*. 2007;73(19):5975-81.
32. Smith HW, Huggins MB. Successful treatment of experimental *Escherichia coli* infections in mice using phage: its general superiority over antibiotics. *J Gen Microbiol*. 1982;128(2):307-18.
33. Efimov AD, Golomidova AK, Kulikov EE, Belarov IS, Ivanov PA, Letarov AV. RB49-like Bacteriophages Recognize O Antigens as One of the Alternative Primary Receptors. *Int J Mol Sci*. 2022;23(19).

34. Mattila S, Ruotsalainen P, Jalasvuori M. On-Demand Isolation of Bacteriophages Against Drug-Resistant Bacteria for Personalized Phage Therapy. *Front Microbiol.* 2015;6:1271.
35. Aslam S, Lampley E, Wooten D, Karris M, Benson C, Strathdee S, et al. Lessons Learned From the First 10 Consecutive Cases of Intravenous Bacteriophage Therapy to Treat Multidrug-Resistant Bacterial Infections at a Single Center in the United States. *Open Forum Infectious Diseases.* 2020;7(9).
36. Benler S, Yutin N, Antipov D, Rayko M, Shmakov S, Gussow AB, et al. Thousands of previously unknown phages discovered in whole-community human gut metagenomes. *Microbiome.* 2021;9(1):78.
37. Woodworth MH, Conrad RE, Haldopoulos M, Pouch SM, Babiker A, Mehta AK, et al. Fecal microbiota transplantation promotes reduction of antimicrobial resistance by strain replacement. *Sci Transl Med.* 2023;15(720):eabo2750.
38. Browning DF, Wells TJ, França FLS, Morris FC, Sevastyanovich YR, Bryant JA, et al. Laboratory adapted *Escherichia coli* K-12 becomes a pathogen of *Caenorhabditis elegans* upon restoration of O antigen biosynthesis. *Molecular Microbiology.* 2013;87(5):939-50.
39. Camargo AP, Nayfach S, Chen I-MA, Palaniappan K, Ratner A, Chu K, et al. IMG/VR v4: an expanded database of uncultivated virus genomes within a framework of extensive functional, taxonomic, and ecological metadata. *Nucleic Acids Research.* 2022;51(D1):D733-D43.
40. Hyatt D, Chen G-L, LoCascio PF, Land ML, Larimer FW, Hauser LJ. Prodigal: prokaryotic gene recognition and translation initiation site identification. *BMC Bioinformatics.* 2010;11(1):119.
41. Rodriguez-R LM, Konstantinidis KT. The enveomics collection: a toolbox for specialized analyses of microbial genomes and metagenomes. *PeerJ Preprints.* 2016;4:e1900v1.
42. Steinegger M, Söding J. MMseqs2 enables sensitive protein sequence searching for the analysis of massive data sets. *Nature Biotechnology.* 2017;35(11):1026-8.
43. Tamura K, Stecher G, Kumar S. MEGA11: Molecular Evolutionary Genetics Analysis Version 11. *Molecular Biology and Evolution.* 2021;38(7):3022-7.
44. Letunic I, Bork P. Interactive Tree Of Life (iTOL) v5: an online tool for phylogenetic tree display and annotation. *Nucleic Acids Research.* 2021;49(W1):W293-W6.

45. Kropinski AM, Mazzocco A, Waddell TE, Lingohr E, Johnson RP. Enumeration of bacteriophages by double agar overlay plaque assay. *Methods Mol Biol.* 2009;501:69-76.
46. Bolger AM, Lohse M, Usadel B. Trimmomatic: a flexible trimmer for Illumina sequence data. *Bioinformatics.* 2014;30(15):2114-20.
47. Langmead B, Salzberg SL. Fast gapped-read alignment with Bowtie 2. *Nat Methods.* 2012;9(4):357-9.
48. Prjibelski A, Antipov D, Meleshko D, Lapidus A, Korobeynikov A. Using SPAdes De Novo Assembler. *Curr Protoc Bioinformatics.* 2020;70(1):e102.
49. Jain C, Rodriguez-R LM, Phillippy AM, Konstantinidis KT, Aluru S. High throughput ANI analysis of 90K prokaryotic genomes reveals clear species boundaries. *Nature Communications.* 2018;9(1):5114.
50. Seemann T. Prokka: rapid prokaryotic genome annotation. *Bioinformatics.* 2014;30(14):2068-9.
51. Bessonov K, Laing C, Robertson J, Yong I, Ziebell K, Gannon VPJ, et al. ECTyper: in silico *Escherichia coli* serotype and species prediction from raw and assembled whole-genome sequence data. *Microb Genom.* 2021;7(12).
52. Eren AM, Kiefl E, Shaiber A, Veseli I, Miller SE, Schechter MS, et al. Community-led, integrated, reproducible multi-omics with anvi'o. *Nat Microbiol.* 2021;6(1):3-6.

Supporting Information

Supplemental Text

In the following, we use a mathematical-computer simulation model to illustrate how populations dominated by phage-resistant, O antigen-bearing bacteria will maintain populations of lytic and temperate phages.

Model of the population dynamics of resistant O antigen bearing bacteria and lytic phage

There are two populations of bacteria, one bears an O antigen, O, that masks the phage receptor, and the other is a variant of the O antigen-bearing bacteria, S, for which the receptor is available for the phage to adsorb. There is a single population of lytic phage, P. The variables O, S, and P are the designations of these populations and their densities, cells and particles per ml for the bacteria and phage, respectively.

The bacteria replicate at a rate proportional to their maximum growth rates, respectively v_O and v_S , and a

hyperbolic function of the concentration of a limiting resource, r $\mu\text{g/ml}$. $\psi(r) = \frac{r}{(k+r)}$ where k is the

resource concentration when the growth rate is half its maximum value, the Monod constant (1). For our analysis of the properties of this model, we use the same value of k for both O and S. The limiting resource is taken up at a rate proportional to the sum of the product of the densities of the populations, their maximum growth rates, the Monod function, $\psi(r)$ and a conversion efficiency parameter, e μg per cell. The phage infects the bacteria at a rate equal to the product of the densities of bacteria and phage and rate parameter, δ_O and δ_S per ml, ml attacks per phage particle per cell per hour with, $\delta_O \ll \delta_S$. Each infected bacterium produces β phage particles. The O population transitions to S, and the S transition to O at a rate of μ_{OS} and μ_{SO} per cell per hour, respectively. To account for the decline in the physiological state of the bacteria as the resource decline, we assume the rates of phage infection and transition between states are proportional to $\psi(r)$ (2, 3).

With these definitions and assumptions, the rates of change in the concentration of the limiting resource and densities of the bacteria and phage are given by,

$$\begin{aligned}\frac{dr}{dt} &= -\psi(r) \cdot e \cdot (v_o \cdot O + v_s \cdot S) \\ \frac{dO}{dt} &= v_o \cdot O \cdot \psi(r) - \delta_o \cdot O \cdot P \cdot \psi(r) + (\mu_{so} \cdot S - \mu_{os} \cdot O) \cdot \psi(r) \\ \frac{dS}{dt} &= v_s \cdot S \cdot \psi(r) - \delta_s \cdot S \cdot P \cdot \psi(r) + (\mu_{os} \cdot S - \mu_{so} \cdot O) \cdot \psi(r) \\ \frac{dP}{dt} &= \delta_o \cdot O \cdot P \cdot \psi(r) \cdot \beta + \delta_s \cdot S \cdot P \cdot \psi(r) \cdot \beta\end{aligned}$$

To solve these equations and those that follow for the temperate phage, we use Berkeley Madonna. In these numerical solutions, simulations, we assume the populations are maintained in serial transfer culture. Every 24 hours, the populations of bacteria are diluted by a factor of 1/100, and 1000µg/ml of fresh resource is added.

In Figure 4, we present the results of simulations with three rates of transition between O and S, μ_{os} and μ_{so} per cell per hour.

If the rate of transition between the sensitive, S, and resistant O antigen-bearing state is great enough, the phage is maintained in a population dominated by resistant O antigen-bearing bacteria. In the above simulations, we are assuming sensitive and resistant, S and O, bacteria have the same growth rate. The conditions for the maintenance of the phage would be greater if the O antigen mediated resistance had a fitness cost, $v_o < v_s$.

Model of the population dynamics of resistant O antigen bearing bacteria and temperate phage

There are two populations of lysogenic bacteria, one bearing the O antigen and one without the O antigen, with designations and densities OL and L, respectively. There is a single population of free temperate phage of density PT particles per ml. The phage can adsorb to L, with a rate constant δ , but cannot adsorb to the OL. Temperate phages that adsorb to lysogens are lost. With rates of ind_{OL} and ind_L , the OL and L lysogens are induced and produce β_{OL} and β_L phage particles, respectively, with the induced OL and L dying. As with

the lytic phage model, we assume that all rates are proportional to the concentration of the limiting resource by a Monod function, $\psi(r) = \frac{r}{(r+k)}$, and the limiting resource is taken up at a rate proportional $\psi(r)$, their growth rates and densities, and a conversion efficiency parameter, e $\mu\text{g}/\text{per cell}$. We neglect the loss of the prophage by the OL and L lysogens.

With these definitions and assumptions, the rates of change in the densities of bacteria are given by,

$$\frac{dr}{dt} = -\psi(r) \cdot e \cdot (v_{OL} \cdot OL + v_L \cdot L)$$

$$\frac{dOL}{dt} = v_O \cdot OL \cdot \psi(r) - ind_{OL} \cdot OL \cdot \psi(r) + (\mu_{LOL} \cdot L - \mu_{OLL} \cdot OL) \cdot \psi(r)$$

$$\frac{dL}{dt} = v_L \cdot L \cdot \psi(r) - ind_L \cdot L \cdot \psi(r) + (\mu_{OLL} \cdot OL - \mu_{LOL} \cdot L) \cdot \psi(r)$$

$$\frac{dPT}{dt} = ind_{OL} \cdot OL \cdot \beta_{OL} \cdot \psi(r) + ind_L \cdot L \cdot \beta_L \cdot \psi(r) - \delta \cdot PT \cdot L \cdot \psi(r)$$

In Supplemental Figure 3, we present the results of simulations of the population dynamics of temperate phage and lysogens that mask the receptor and do not adsorb the phage, OL, and lysogens with the receptor open to adsorption by PT, L.

In all cases bacterial populations are dominated by “resistant”, O antigen bearing lysogens, substantial densities of free temperate phage are maintained.

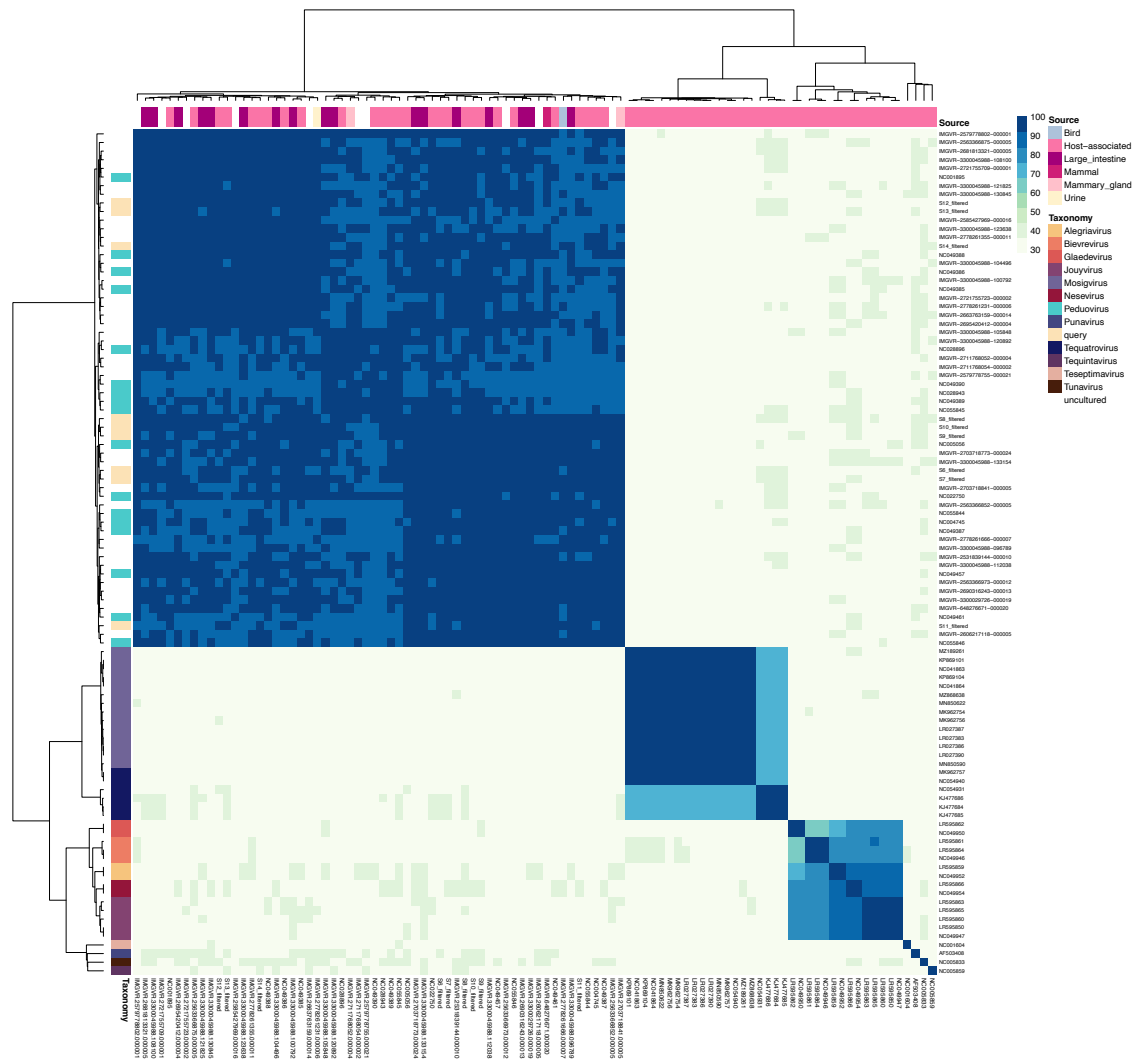


Figure S1. Heatmap of average amino acid identities (AAIs) among genomes of this study and selected reference genomes from public databases. AAI was estimated based on BLAST+ whole-genome comparisons using a minimum alignment identity of 20% and at least 20 genes shared between two genomes. Genomes of this study were clearly placed in the major AAI cluster that included all *Peduovirus* genomes from IMG/VR and several close relatives from NCBI.

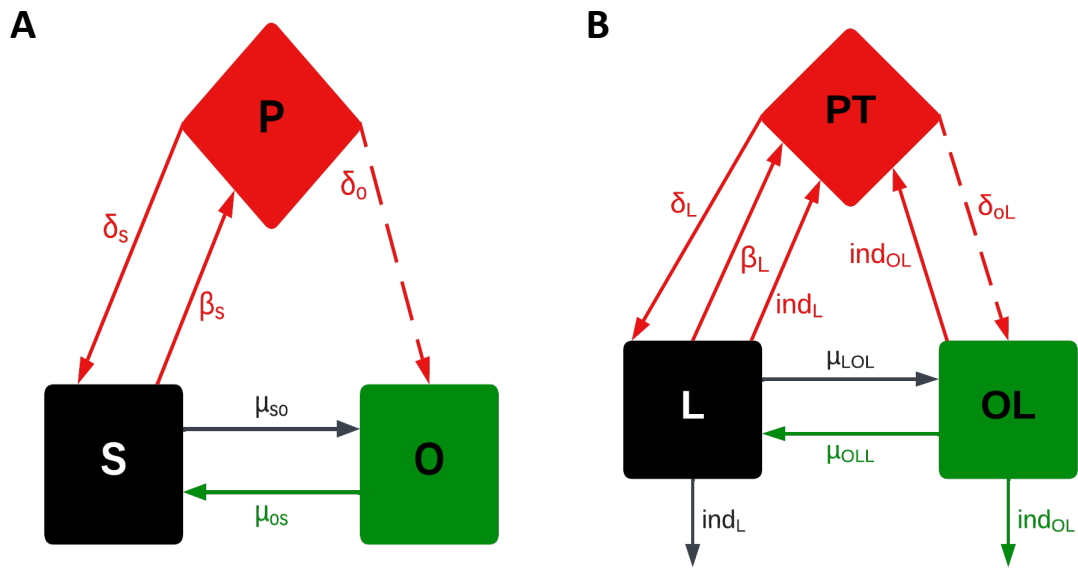


Figure S2. Models of the population and evolutionary dynamics of O antigen mediated phage resistance. See the supplemental text for a description of the model and Supplemental Table 1 for the definitions and dimensions of the parameters and the values used in our numerical solutions to the equations and simulations. **A)** There is a population of lytic phage, P; a population of phage-sensitive bacteria, S; and a population of phage-resistant, O antigen producing cells, O. **B)** There is a population of temperate phage, PT; a population of immune lysogens, L; and a population of phage-resistant, O antigen producing lysogens, OL.

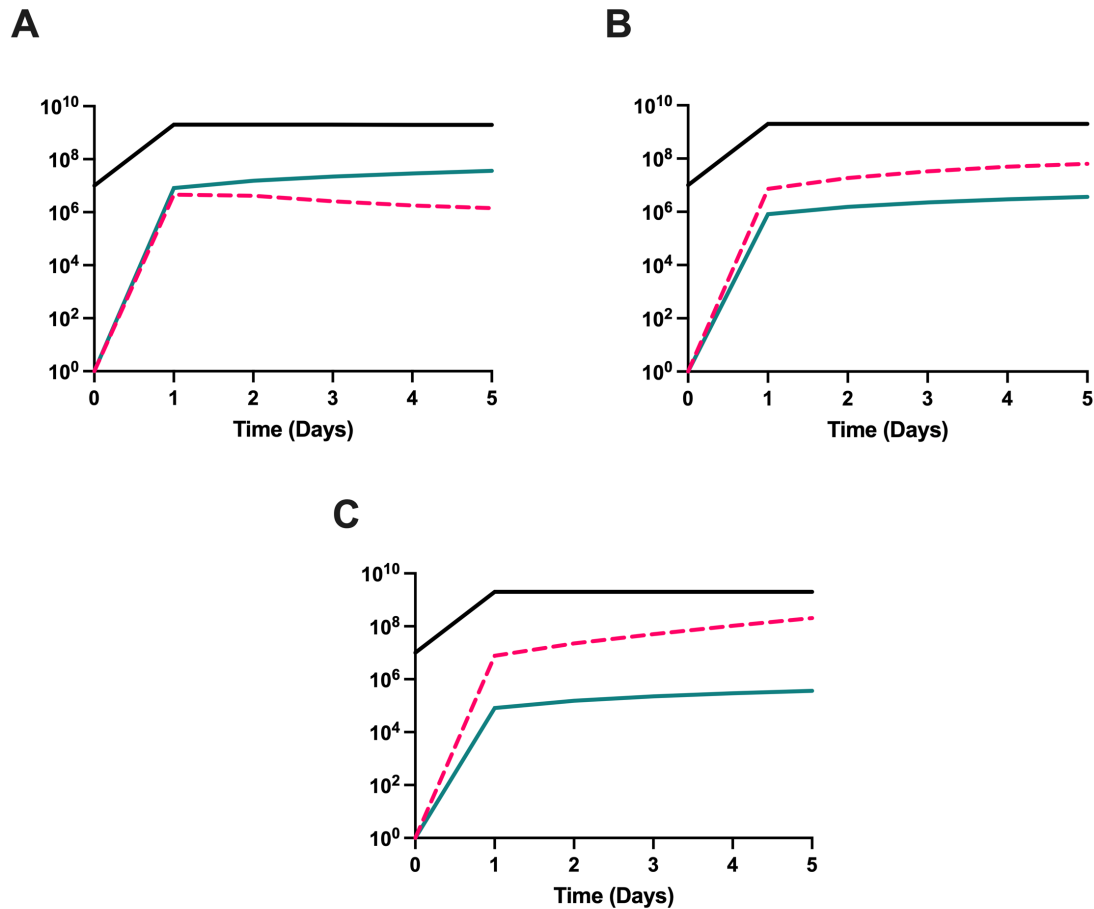


Figure S3. Predicted serial transfer dynamics of O antigen mediated resistance and a temperate phage. Simulation results, changes in the initial and end of transfer densities of bacteria and phage in serial transfer culture. 1000 $\mu\text{g}/\text{ml}$ of the limiting resource is added at each transfer. Standard parameters, $v_O = v_S = 2.0$ per cell per hour, $e = 5 \times 10^{-7}$ $\mu\text{g}/\text{cell}$, $k=1.0$, $\beta=50$, $\delta_O=0$, $\delta_S = 2 \times 10^{-7}$ per phage per cell per hour. **A-** $\mu_{OS}=\mu_{SO}=10^{-5}$ per cell per hour. **B-** $\mu_{OS}=\mu_{SO}=10^{-4}$ per cell per hour, and **C-** $\mu_{OS}=\mu_{SO}=10^{-3}$ per hour. O antigen expressing lysogenic cells- turquoise, Lysogenic cells-black, Phage – pink.

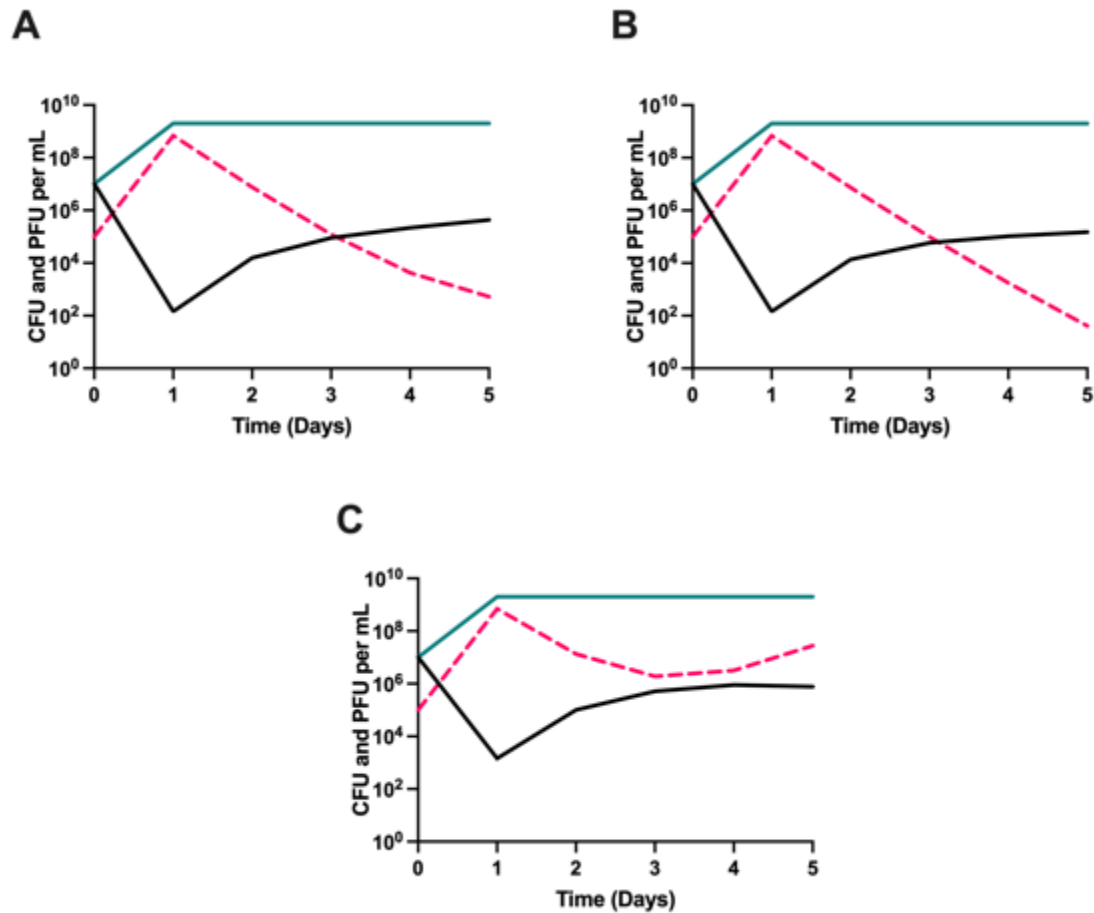


Figure S4. The effect of fitness cost and unequal transition rates on phage maintenance. Simulation results, changes in the initial and end of transfer densities of bacteria and phage in serial transfer culture. 1000 μ g/ml of the limiting resource is added at each transfer. Standard parameters unless otherwise stated, $v_O = v_S = 2.0$ per cell per hour, $e = 5 \times 10^{-7}$ μ g/cell, $k=1.0$, $\beta=50$, $\delta_O=0$, $\delta_S = 2 \times 10^{-7}$ per phage per cell per hour, $\mu_{OS}=\mu_{SO}=10^{-5}$ per cell per hour. **A-** $v_O = 1.8$ per cell per hour, $v_S = 2.0$ per cell per hour. **B-** $\mu_{OS} = 10^{-5}$ per cell per hour, $\mu_{SO}=10^{-4}$ per cell per hour. **C-** $\mu_{OS} = 10^{-4}$ per cell per hour, $\mu_{SO}=10^{-5}$ per cell per hour. O antigen expressing cells- turquoise, Cells not expressing the O antigen-black, and Phage – pink.

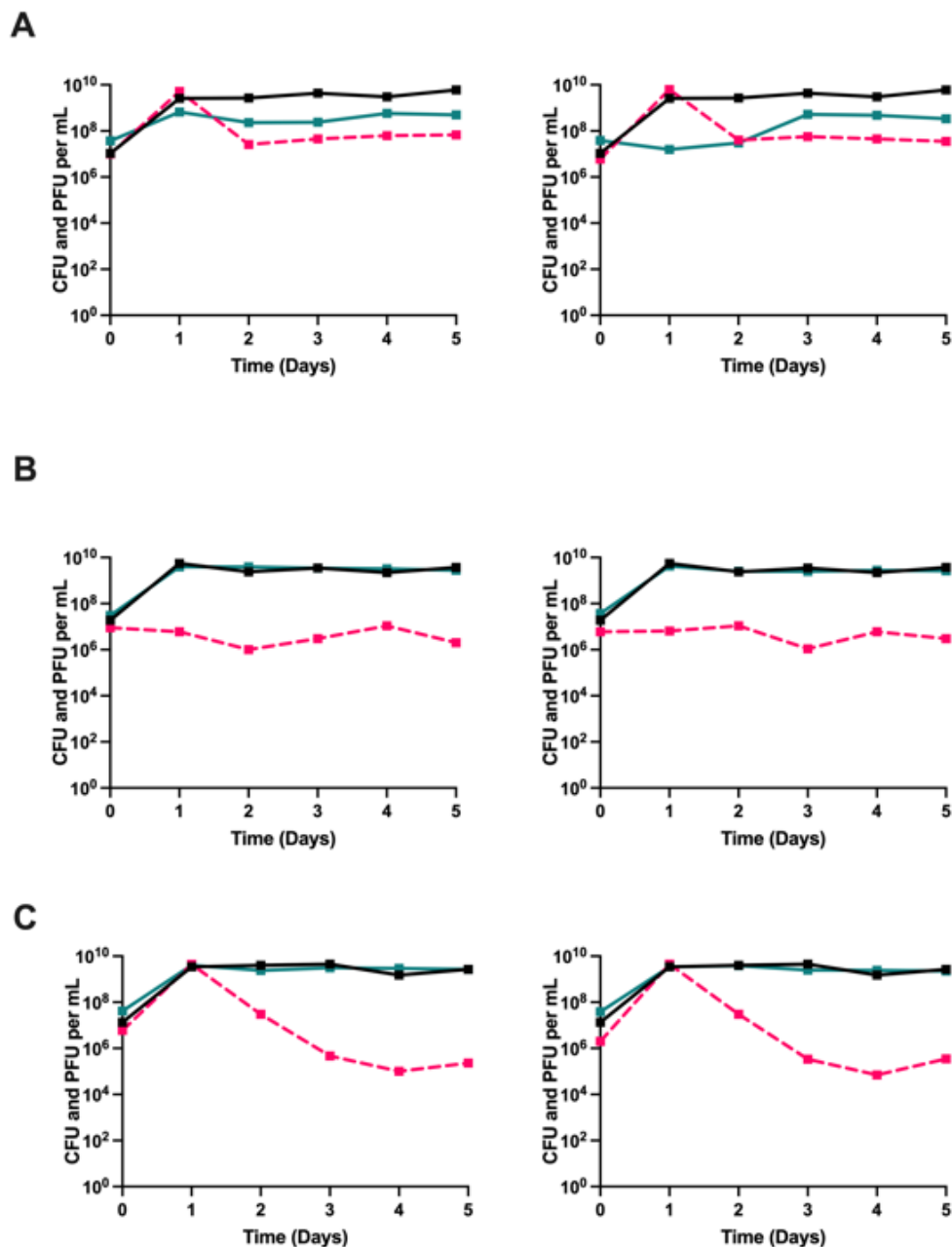


Figure S5. Serial transfer replicates of T7 with MG1655 lacking and expressing the O antigen. Three variants of *E. coli* MG1655 serially transferred for five days in LB broth with the phage T7. Shown in solid lines are bacterial densities with the black line representing a phage free control. The broken lines present phage densities. Shown side by side two of three biological replicates. **(A)** Wild type MG1655 not expressing the O antigen. **(B)** MG1655L5 expressing a medium amount of the O antigen. **(C)** MG1655L9 expressing a high amount of the O antigen

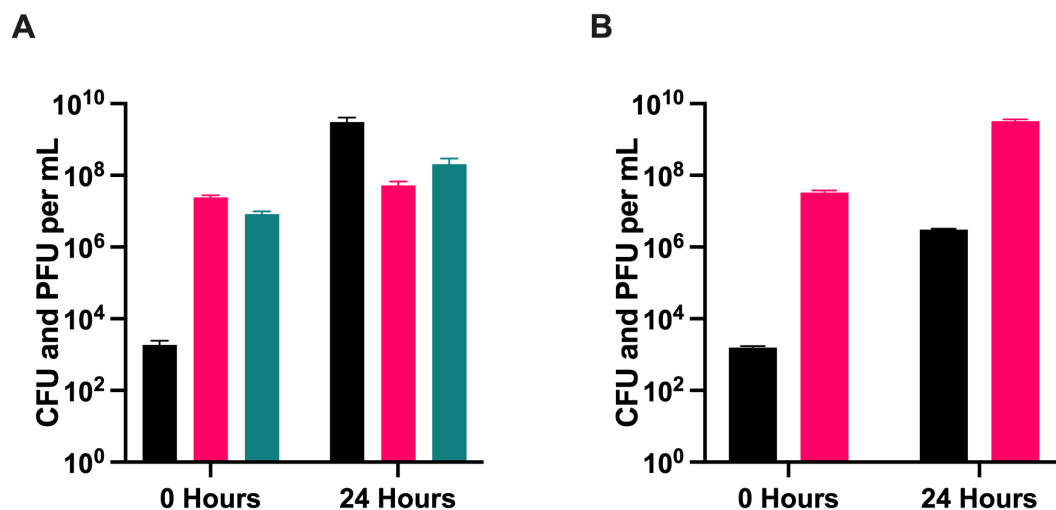


Figure S6. Invasion when rare experiment of O antigen expressing cells into a population of O antigen deficient cells. Shown are the results of an experiment initiated with (A) 10^3 O-antigen expressing cells, 10^7 O-antigen deficient cells, and 10^7 lytic phage or (B) 10^3 O-antigen expressing cells, 10^7 O-antigen deficient cells, and no phage. Shown are mean and standard deviations of three biological replicates. O antigen expressing cells are in black, O antigen deficient cells in fuchsia, and a lytic phage in turquoise.

Table S1: Summary of lysate spotting experimental results.

	None (N=392)	Turbid (N=85)	P-value
FMT_cross			
Allogeneic	304 (77.6%)	56 (65.9%)	0.0334
Autologous	88 (22.4%)	29 (34.1%)	
O1			
17	143 (36.5%)	46 (54.1%)	<0.001
74	27 (6.9%)	27 (31.8%)	
132	9 (2.3%)	0 (0%)	
1	26 (6.6%)	1 (1.2%)	
8	9 (2.3%)	0 (0%)	
16	9 (2.3%)	0 (0%)	
167	9 (2.3%)	0 (0%)	
None predicted	160 (40.8%)	11 (12.9%)	
O2			
1	9 (2.3%)	0 (0%)	<0.001
16	9 (2.3%)	0 (0%)	
44	76 (19.4%)	14 (16.5%)	
74	14 (3.6%)	13 (15.3%)	
77	67 (17.1%)	32 (37.6%)	
132	9 (2.3%)	0 (0%)	
None predicted	208 (53.1%)	26 (30.6%)	
O3			
17	64 (16.3%)	17 (20.0%)	0.754

	None (N=392)	Turbid (N=85)	P-value
44	13 (3.3%)	5 (5.9%)	
None predicted	315 (80.4%)	63 (74.1%)	
O4			
44	10 (2.6%)	8 (9.4%)	0.0146
77	54 (13.8%)	9 (10.6%)	
None predicted	328 (83.7%)	68 (80.0%)	
Distinct O Antigen			
Mean (SD)	1.15 (1.16)	1.67 (1.00)	<0.001
Median [Min, Max]	1.00 [0, 3.00]	2.00 [0, 3.00]	
H			
4	9 (2.3%)	0 (0%)	<0.001
5	9 (2.3%)	0 (0%)	
7	41 (10.5%)	4 (4.7%)	
8	9 (2.3%)	0 (0%)	
9	9 (2.3%)	0 (0%)	
18	162 (41.3%)	54 (63.5%)	
19	9 (2.3%)	0 (0%)	
39	27 (6.9%)	27 (31.8%)	
45	117 (29.8%)	0 (0%)	

Table S2. Parameter definitions, units, and values used in generating the mathematical models and computer simulations.

Parameter	Value (dimensions)	Description	Source
v_o, v_s	2.0 (h^{-1})	Maximum growth rates	This paper
μ_{OS}, μ_{SO}	$1e^{-5}, 1e^{-5}, \text{ or } 1e^{-4}$ (h^{-1})	Transitions $O \rightarrow S, S \rightarrow O$	Chaudhry 2018 (4)
δ_o, δ_s	$2e^{-7}$ ($h^{-1} \cdot mL^{-1}$)	Adsorption rate constants	Chaudhry 2018 (4)
β	60 (PFU \cdot CFU $^{-1}$)	Burst size	Berryhill 2023 (5)
λ	$1e^{-2}$	Probability of lysogeny	Berryhill 2023 (5)
ind	$1e^{-4}$ (h^{-1})	Induction rate	Berryhill 2023 (5)
k	1 (μg)	Monod constant	Stewart and Levin 1973 (3)
e	$5e^{-7}$ ($\mu g \cdot CFU^{-1}$)	Conversion efficiency	Stewart and Levin 1973 (3)

SI References

1. Monod J. THE GROWTH OF BACTERIAL CULTURES. Annual Review of Microbiology. 1949;3(1):371-94.
2. Levin BR, Stewart FM, Chao L. Resource-Limited Growth, Competition, and Predation: A Model and Experimental Studies with Bacteria and Bacteriophage. The American Naturalist. 1977;111(977):3-24.
3. Stewart FM, Levin BR. Partitioning of Resources and the Outcome of Interspecific Competition: A Model and Some General Considerations. The American Naturalist. 1973;107:171 - 98.
4. Chaudhry WN, Pleška M, Shah NN, Weiss H, McCall IC, Meyer JR, et al. Leaky resistance and the conditions for the existence of lytic bacteriophage. PLoS Biol. 2018;16(8):e2005971.
5. Berryhill BA, Garcia R, McCall IC, Manuel JA, Chaudhry W, Petit M-A, et al. The book of Lambda does not tell us that naturally occurring lysogens of *Escherichia coli* are likely to be resistant as well as immune. Proceedings of the National Academy of Sciences. 2023;120(11):e2212121120.

Chapter 9

Chapter 9

The ecological consequences and evolution of retron-mediated suicide as a way to protect

Escherichia coli from being killed by phage

Reprinted from: Berryhill BA, Gil-Gil T, Manuel JA, Garcia R, Levin BR. 2023. The ecological consequences and evolution of retron-mediated suicide as a way to protect *Escherichia coli* from being killed by phage.

PLOS One. <https://doi.org/10.1371/journal.pone.0285274>

Abstract

Retrons were described in 1984 as DNA sequences that code for a reverse transcriptase and a unique single-stranded DNA/RNA hybrid called multicopy single-stranded DNA (msDNA). It would not be until 2020 that a function was shown for retons, when compelling evidence was presented that retons activate an abortive infection pathway in response to bacteriophage (phage) infection. When infected with the virulent mutant of the phage lambda, λ^{VIR} , and to a lesser extent, other phages, a retron designated Ec48 is activated, the *Escherichia coli* bearing this retron element dies, and the infecting phage is lost. With the aid of a mathematical model, we explore the *a priori* conditions under which retons will protect bacterial populations from predation by phage and the conditions under which retron-bearing bacteria will evolve in populations without this element. Using isogenic *E. coli* with and without Ec48 and λ^{VIR} , we estimated the parameters of our model and tested the hypotheses generated from our analysis of its properties. Our models and experiments demonstrate that cells expressing a retron-mediated abortive infection system can protect bacterial populations. Our results demonstrate that retron bearing bacteria only have a competitive advantage under a limited set of conditions.

Introduction

Retrons, DNA sequences that code for a reverse transcriptase and a unique single-stranded DNA/RNA hybrid called multicopy single-stranded DNA (msDNA), were discovered in 1984 (1) and were the first example of a reverse transcriptase coded for by bacteria (2, 3). These elements were initially found in *Mycococcus xanthus*, but subsequently have been observed in a number of bacterial species, including *Escherichia coli* (4, 5). Like CRISPR-Cas, retons are being employed for genome engineering (5, 6, 7), and are capable of doing editing tasks that cannot be done by CRISPR-Cas (8). Also like CRISPR-Cas, the function of retons was not determined for decades after their discovery and molecular characterization (9). For retons, the identification of a function came in 2020 when Millman and collaborators presented compelling evidence that retons mediate an abortive infection (abi) response (10).

With this abi mechanism, the infected cell dies along with the infecting phage (11). From an evolutionary perspective, abi raises interesting questions. Phage-defense systems like envelope resistance, restriction-modification, and CRISPR-Cas are to the advantage of the individual bacteria expressing them. This is not the case for abi; where the defense against phage is through suicide and thereby not to the advantage of the individual bacteria expressing this defense mechanism. To account for the evolution of abortive infection mechanisms, it has been postulated that abi is an altruistic trait which provides an advantage to the collective, clonal population (12, 13). Individual cells that commit suicide due to phage infection prevent these viruses from infecting and killing other, genetically identical, members of their population.

Using agent-based models and experiments with *E. coli* and its phages, Fukuyo and colleagues and Berngruber and colleagues (12, 13), provide a theoretical basis and experimental support for this altruistic suicide hypothesis for the ecological role and evolution of abi. They show that in physically structured habitats, abi can successfully protect populations against invasion by phage, and phage-mediated selection can lead to the evolution of abortive infection.

Here we investigate the conditions under which, by abortive infection, retrons can protect bacterial populations from invasion by lytic phages and the extent to which *abi* will be selected for in otherwise isogenic bacterial populations lacking this trait. Using a mathematical model of the population and evolutionary dynamics of bacteria and phages in mass culture, we explore the *a priori* conditions under which retron-mediated *abi* can protect populations of bacteria from invasion by lytic phages, and that phage-mediated selection will enable retrons to become established and maintained in bacterial populations. Using *E. coli* MG1655 bearing the retron Ec48 described by Millman and colleagues (10) and a virulent mutant of the phage lambda, λ^{vir} , for which Millman et al. showed the Ec48 mechanism functions reduces plaquing efficiency the most, we estimate the parameters of this model and test the validity of the predictions generated from our numerical analysis of its properties for both the protection and evolution hypotheses in liquid and two forms of physically structured habitats- one where the colonies are growing in a 2D structure as colonies and another where the colonies are expanding in 3D within a soft agar matrix.

The results of our experiments support the proposition that, in liquid and the two physically structured habitats studied, retrons can protect populations of bacteria from infection by phages. Our models and experiments also indicate that the conditions for retrons playing this ecological role are restrictive; the abortive infection mechanism has to be nearly perfect, and there cannot be phage-susceptible retron⁻ bacteria that can support the growth of the phages. As anticipated by our models and the theory and experiments reported in (12, 13), in liquid culture in the presence of phage, retrons will not become established in populations of bacteria susceptible to these viruses. Contrary to these earlier studies, in the physically structured habitat of soft agar, abortive infection alone cannot account for the evolution of the retron in populations lacking this element. However, when growing in the structured habitat of colonies on the surface of agar in the presence of phages, a retron⁺ population increases in frequency within a retron⁻ population. Moreover, in all three habitats, in the presence of λ^{vir} , envelope resistant mutants which do not allow for phage adsorption emerge in both retron⁺

(bacteria with the Ec48 retron) and retron⁻ (bacteria lacking Ec48) *E. coli* populations and ascend to become the dominant population of bacteria.

Results

A model of retron-mediated abortive infection

To build the theoretical background to generate hypotheses, design experiments, and interpret their results, we employ a mathematical model. This model is based on the interactions of the populations illustrated in Figure 1, along with the definitions and parameters defined in Supplemental Table 1. In accord with this model, the rates of change in the densities of bacteria and phage and the concentration of the limiting resource are given by the system of time-dependent, coupled differential equations listed in Supplemental Equations (1) – (6).

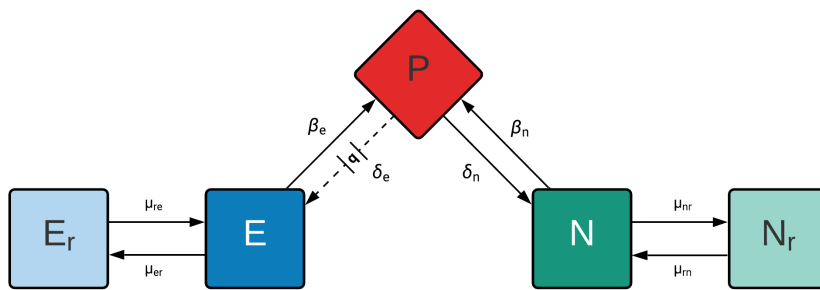


Figure 1. Diagram of a model of the population and evolutionary dynamics of lytic phage and bacteria with and without a retron-mediated abortive infection mechanism. There is a single population of lytic phage, P; a phage-sensitive retron-encoding (retron⁺) population, E; an envelope resistant retron⁺ population, E_r; a phage-sensitive (retron⁻) population, N; and an envelope resistant retron⁻ population, N_r. The phage adsorbs to the N and E bacteria with rate constants, δ_n and δ_e (ml·cells/hour), respectively. The phage replicates on the N population with each infection producing β_n phage particles, the burst size. A fraction q ($0 \leq q \leq 1$) of the phages that adsorb to E population are lost and thus do not replicate. The remaining $(1 - q)$ of infections of E produce β_e phage particles. At rates μ_{nr} and μ_{er} per cell per hour, the bacteria transition from their respective phage sensitive to phage resistant states, and at rates μ_{rn} and μ_{re} they transition from the resistant to their respective phage sensitive states.

Protection against lytic phages mediated by retrons

We open with an exploration of the population and evolutionary dynamics of retron-mediated abortive infection with an analysis of the ability of retrons to protect from predation by lytic phages. For this theoretical and experimental considerations of retron-mediated abi, we present the predicted and observed densities of bacteria and phage when their populations first encounter each other, time 0, and at 24 hours (Figure 2). We performed a theoretical analysis using the parameters and values estimated for this system (Table S1) to determine the minimum efficacy of retron-mediated abi needed to protect populations from phage infection. We tested a range of values of abi effectiveness, q , from 0.95 to 1.0 with steps of 0.001. We found that at least 98% of the infection events have to be aborted by the retron to protect the population from phages (Figure S1). In other words, q must be at least 0.98 for retron-mediated abi to be protective. With these results in mind, we selected q values of 1.00 and 0.95 to illustrate abortive infection success and failure, respectively, Figures 2A and 2B.

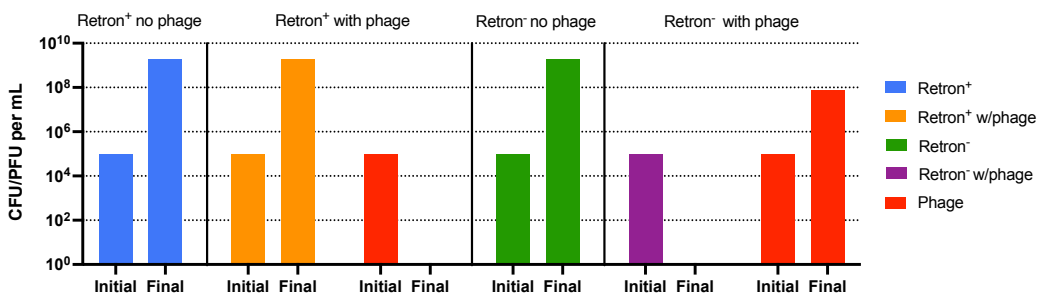
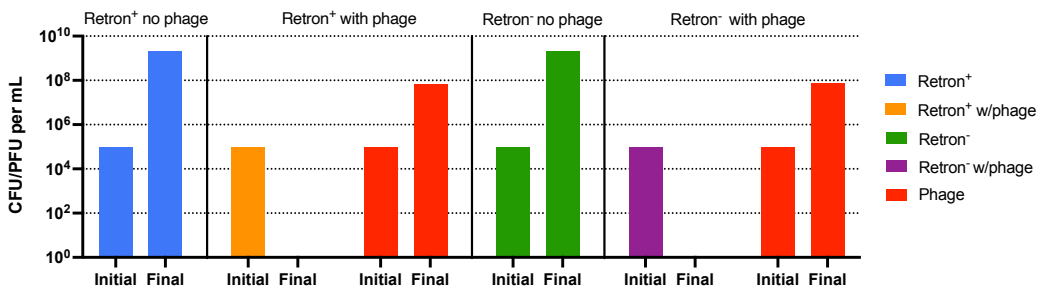
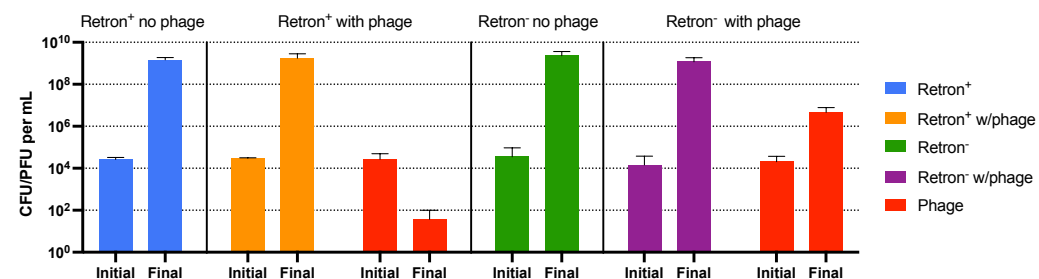
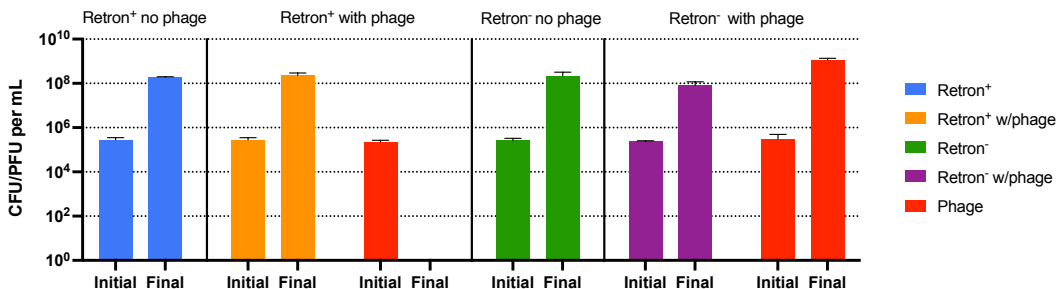
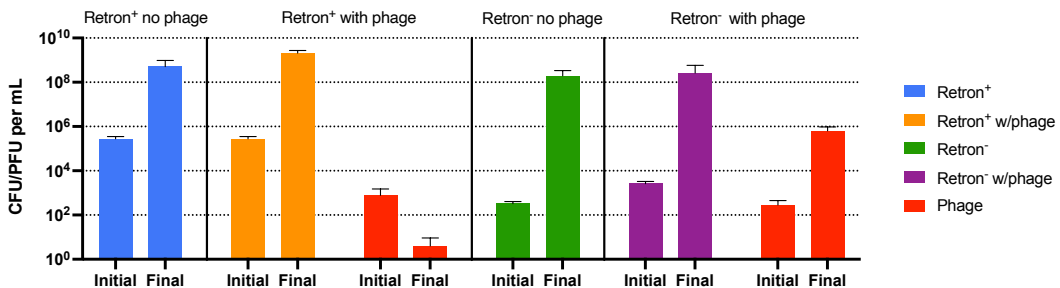
A**B****C****D****E**

Figure 2. Conditions under which retrons protect monoclonal bacterial populations from phage infection. Computer simulation results without envelope resistance and experimental results. The computer simulation model dynamics in the liquid environment. Shown are the densities of a retron⁺ bacterial population in the absence (blue) and presence (orange) of phage (red) and a retron⁻ bacterial population in the absence (green) and presence (purple) of phage at 0 (Initial) and 24 hours (Final). The parameters used for the simulations were: $k=1$, $e=5 \times 10^{-7}$ ug/cell, $v_e = v_n = 2.0 \text{ h}^{-1}$, $\delta_e = \delta_n = 2 \times 10^{-7} \text{ h}^{-1} \text{ cell}^{-1}$, $\beta_e = \beta_n = 60$ phages/cell, $\mu_{nr} = \mu_{rn} = \mu_{er} = \mu_{re} = 0$. **A, B-** Computer simulation results with a completely effective (**A**, $q=1.00$) and incompletely effective (**B**, $q=0.95$) abortive infection system. **C, D, E-** Protection experiments in liquid (**C**), soft agar (**D**), and with colonies growing on a surface (**E**). Plotted are means and standard deviation of three biological replicas.

As can be seen in Figure 2A, a completely effective retron-mediated abi defense system ($q=1.00$) is able to protect a population of retron⁺ bacteria from predation by phages. By 24 hours, the phage population is gone and the retron⁺ population is at its maximum resource-limited density. When the retron⁻ populations are confronted with phage, by 24 hours, the bacteria are eliminated and there is a substantial density of free phages. The ability of the retron to prevent the ascent of the phage and protect the bacterial population is critically dependent on the efficacy (q) of retron-mediated abortive infection (Figure 2A, 2B, and S1).

In Figures 2C, 2D, and 2E we present the results of our experimental tests of the retron protection hypothesis presented in Figures 2A and 2B using the retron⁺ *E. coli* Ec48 (10) and a lytic mutant of the phage lambda, λ^{VIR} . As a retron⁻ control, we use a λ^{VIR} -sensitive *E. coli* MG1655, otherwise isogenic to Ec48. As anticipated from the model (Figures 2A and 2B), when confronting the retron⁺ bacteria the λ^{VIR} population is gone or nearly so by 24 hours and the bacterial density is at the level of a phage-free control (Figure 2C, blue bar). The results of the experiment with the λ^{VIR} and the retron⁻ sensitive strain are inconsistent with the prediction of the model. As anticipated by the model, the phage density increased over 24 hours, but contrary to what is expected from

the model, the bacteria were not lost, but rather increased to a density similar to that in the absence of phage (Figure 2C). These consistencies and inconsistencies between the experiments and the model occur regardless of the habitat in which the experiments. In both soft agar (Figure 2D) and when growing as colonies (Figure 2E) the bacteria were able to survive phage predation regardless of the presence or absence of the retron system, but in populations bearing the retron, the phages were lost.

One possible reason for the survival of the bacteria lacking the retron system in the presence of phages is that the bacteria recovered at 24 hours from the retron⁻ population are resistant to λ^{VIR} . To test this hypothesis, we employed the cross-streak method on colonies isolated at 24 hours to determine their susceptibility to λ^{VIR} (Table S3). By this criterion, the vast majority of the initially sensitive retron⁻ bacteria recovered at 24 hours are resistant to λ^{VIR} . This is also the case for the retron⁺ bacteria recovered at 24 hours.

Invasion of retrons

Central to the hypothesis of adaptive evolution is the ability of a novel character to increase when initially rare as would be the case for a new mutant. In this interpretation, if retron mediated abortive infection evolved because it provides an advantage when phages are present, it should be able to increase in frequency when it is initially rare. In Figure 3 we explore the predicted and observed conditions under which a population bearing the retron will be able to increase in frequency from an initial 1:100 ratio in competition with a population of retron⁻ bacteria. Stated another way, we explore the conditions under which the retron⁺ population will be able to invade when rare.

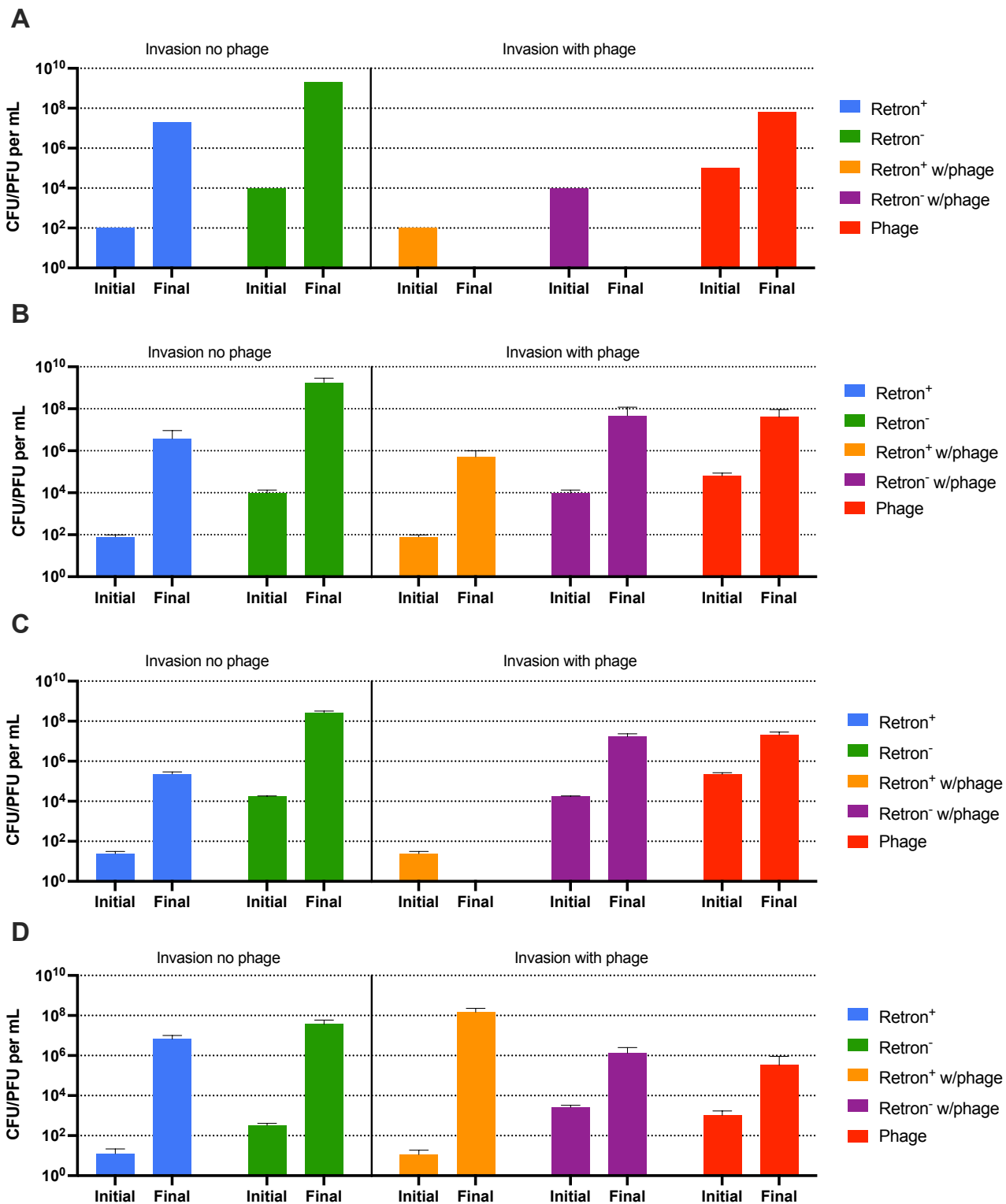


Figure 3. Conditions for the invasion of a retron⁺ population into a community dominated by a retron⁻ population. Computer simulations in the absence of envelope resistance, and experimental results. Bacteria and phage densities at time 0 (Initial) and 24 hours (Final). **Left side:** retron⁺ (blue) and a retron⁻ bacterial population (green) co-cultured in the absence of phage. **Right side:** retron⁺ (orange) and a retron⁻ bacterial population (purple) co-cultured in the presence of phage (red). The parameters used for the simulations were: $k=1$, $e=5 \times 10^{-7}$ ug/cell, $v_e = v_n = 2.0 \text{ h}^{-1}$, $\delta_e = \delta_n = 2 \times 10^{-7} \text{ h}^{-1} \text{ cell}^{-1}$, $\beta_e = \beta_n = 60 \text{ phages/cell}$, $\mu_{nr} = \mu_{rn} = \mu_{er} = \mu_{re} = 0$, $q=1.00$. **A-** Computer simulation results for an invasion condition with a completely effective abortive infection system. **B, C, D-** Invasion experiments in liquid (**B**), soft agar (**C**), and with colonies growing on a surface (**D**). Shown are means and standard deviation of three independent experiments with biological replicas.

As seen in the left side of Figure 3, in the absence of phage in all three habitats, as predicted by the model of mass culture (Figure 3A), the retron⁺ population does not increase in frequency relative to the retron⁻ population, it does not invade when rare. Shown in the right side, and as seen in Figure 2, there is a qualitative difference in the prediction of the model and the observed experiments in the presence of phage (Figure 3B). The model predicts that there will be no bacteria present after 24 hours, yet in all three habitats we find bacteria at the end of the experiment. Consistent with the model (Figure 3A), in liquid (Figure 3B) as well as in soft agar (Figure 3C), the retron⁺ population is not able to invade when rare. Nevertheless, the retron⁻ population at 24 hours reaches a final density similar to the phage-free invasion experiments. In contrast, when growing as colonies in the presence of phage (Figure 3D), the retron⁺ population invades when rare.

To account for the differences in the results of our experiments and those predicted by the model, we performed computer simulations with the model presented in Figure 1, but we now allowed for the generation of phage-resistant retron⁺ (E_r) and retron⁻ (N_r) bacterial populations. As noted in Chaudhry *et al.* (14), there is a high rate of generation of λ^{VIR} resistant *E. coli*, suggesting transition rates, μ_{er} , μ_{nr} , μ_{re} , and μ_{rn} of 10^{-5} per cell per hour. With these rates, both the phage and resistant bacteria ascend (Figure 4). The generation of resistance

is also consistent with the growth of the retron^+ and retron^- populations in the invasion experiments (Figure 3B). Stated another way, if we allow for phage resistant mutants to be generated in our model, the retron^+ population can increase in density (Figure 4B, hashed orange), but the dominant population will still be phage-resistant retron^- cells (Figure 4B, hashed purple).

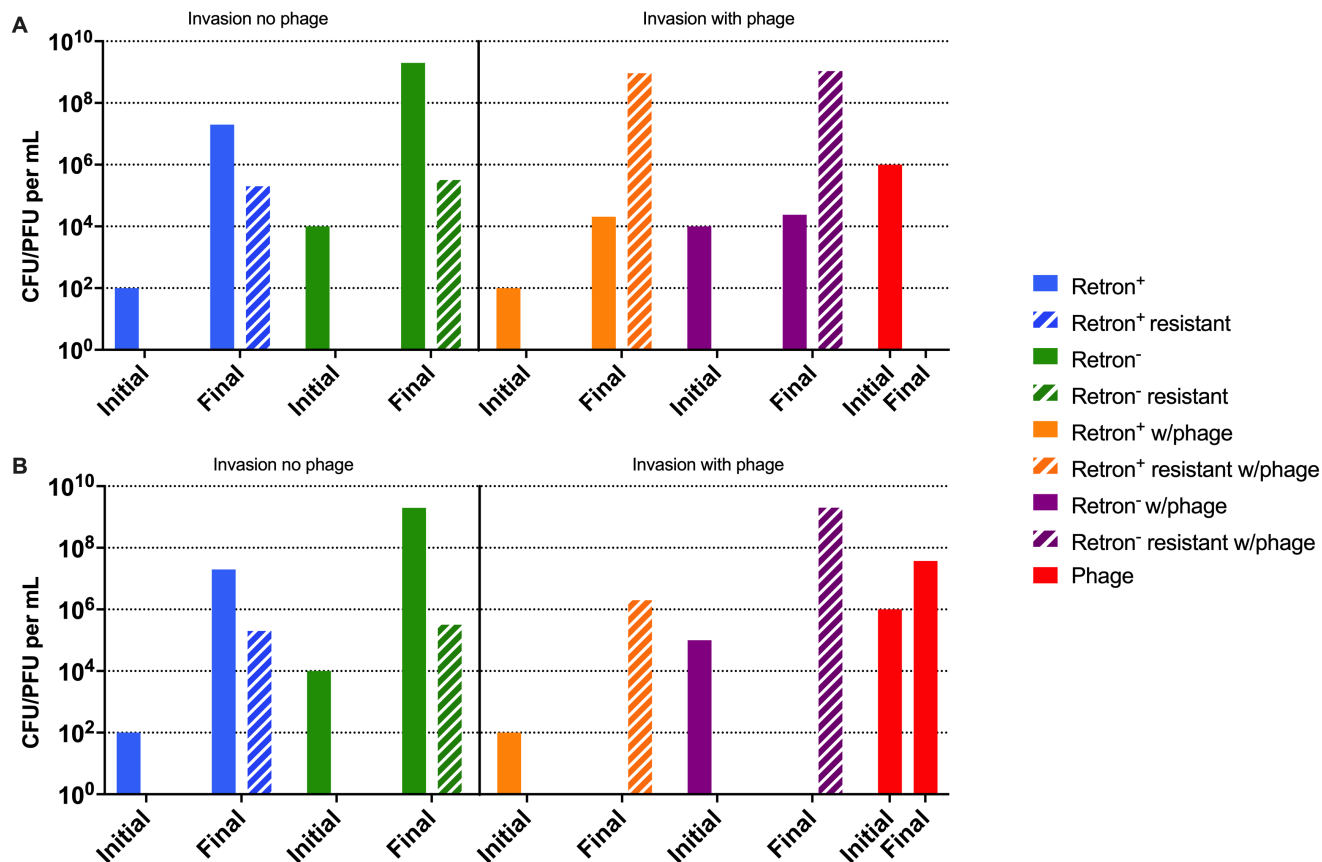


Figure 4. Computer simulations of retron population dynamics with envelope resistance. The simulation conditions are similar to those in Figure 3A but allow for the generation of resistance, $\mu_{er} = \mu_{re} = \mu_{nr} = \mu_{rn} = 10^{-5}$ per cell per hour. Densities of bacteria and phage at time 0 (Initial) and 24 hours (Final) for two invasion conditions. **Left side:** retron^+ (blue) and retron^- (green) bacteria in the absence of phage. **Right side:** retron^+ (orange) and retron^- bacteria (purple) in the presence of phage (red). The densities of phage-resistant mutant bacteria are noted by bars with white hashing next to the bar of the sensitive population. **A-** Simulations with

a completely effective abortive infection system ($q=1.00$). **B-** Simulations with a less-than completely effective abortive infection system ($q=0.95$).

Discussion

We began the study with two goals: First, to determine the conditions under which retrons will protect populations of bacteria from predation by virulent (lytic) bacteriophages. Second, to determine the conditions under which retron-encoding bacteria will evolve, that is increase in frequency when rare in populations of bacteria without this element. We found that retrons are able to protect populations of retron⁺ bacteria in the presence of phages in mass-liquid culture, structured soft agar, and when growing as colonies on surfaces. Our results also indicate that the conditions under which retron-encoding bacteria are able to invade when rare are narrow. In addressing both of these goals, in our experiments, we found that envelope resistant mutants emerge and become the dominant trait, suggesting that retrons are only one step in the mechanisms that bacteria employ as a defense against phage predation.

Our mass action models predict that retron-mediated abi can prevent the populations of bacteria coding for them from being preyed upon by lytic phages, but only if the retron-mediated abi is nearly completely effective, and when there are no other bacterial populations that can support the replication of the phages. The results of our experiments, like those of Millman and colleagues (10) with the retron-encoding abi system in *E. coli* Ec48, and the phage λ^{VIR} , are consistent with these predictions. In addition to this protection result occurring in mass, liquid culture, our experiments demonstrate that the protection against lytic phages happens in physically structured populations of bacteria maintained in soft agar or as colonies on surfaces. Our model also predicts if retron-mediated abortive infection is less than 98% effective, with more than 2% of infections being lytic and producing phages, or when there are retron⁻ populations that can support the replication of the phage, retrons will not be able to protect a population from predation by lytic phages. We were unable to test this < 98% efficacy hypothesis experimentally, because our experimental results show that the retron-mediated abortive infection is overshadowed by selection for mutants resistant to the phages. However, since our retron⁺ population was capable of eliminating the phage population when alone, we interpret this to suggest that the

efficacy of the Ec48 abortive infection system is over 98%. Even though this retron-mediated abortive infection system is highly effective, when the bacteria are capable of generating envelope resistant mutants, retron⁺ or retron⁻ resistant mutants ascend to dominate the bacterial populations.

There is a caveat to this study, only a single phage population was considered. Part of the reason for this is that the study by Milliman and colleagues found the phage λ^{VIR} to be the most efficient at activating the retron Ec48 (10). While they provided evidence that other phages are sensitive to the abortive infection mediated by this retron, the effects were small. Part of the reason for this variability is that to activate the retron, the phage has to inhibit RecBCD, which is unlikely to occur across different *E. coli* phage species. Be that as it may, the effectiveness of retron-mediated immunity against multiple phages is an interesting but open question.

Our model predicts that in liquid culture even if a retron-mediated abi defense system is 100% effective in preventing lytic phage replication, and there are an abundance of phages, the retron⁺ population will not be able to evolve by abortive infection alone. Stated another way, when initially rare, the retron⁺ bacteria will not be able to become established in a population of retron⁻ bacteria of similar fitness. Our experiments testing this hypothesis were consistent with this prediction in soft agar as well as liquid culture. As in both habitats, the retron-encoding populations were unable to become established in populations dominated by retron⁻ competitors. However, when growing as colonies in surfaces, we found that the retron-encoding bacteria were able to increase in frequency when initially rare. In all three tested habitats, the *E. coli* population surviving an encounter with λ^{VIR} , was dominated by λ^{VIR} resistant mutants.

It had been postulated that in the presences of phages, bacteria with other abortive infection mechanisms can evolve and become established when rare in populations without these mechanisms. Using agent-based models, Fukuyo and colleagues (12) and Berngruber and colleagues (13) predicted that in physically structured communities, where the bacteria are growing as colonies, there are conditions where bacteria with abi systems can invade. Using a constructed abi system, Fukuyo and colleagues (12) found that in the physically structured habitat of soft agar (12, 15), in the presence of phages, their abi-encoding bacteria has an advantage over bacteria without this abi system, but not in a habitat without structure. Similar results were obtained by Berngruber and

colleagues (13). In their experiments with *E. coli* growing as colonies in structured environments, depending on the number and size of the colonies, bacteria with their *abi* system were substantially more fit than the competing population of *abi*⁻ *E. coli*. In neither of these studies, was the abortive infection system able to evolve in liquid culture. Contrary to these two results, with the retron-mediated *abi* λ^{VIR} system used in this study, the retron-encoding population was unable to evolve in the physically structured habitat of soft agar, it was only when growing as colonies on a surface that we saw the invasion. At this juncture, we do not know why certain types of physically structured habitats are sufficient to allow for the invasion of the *abi* trait. Why should soft agar be different than colonies growing on a surface?

Materials and Methods

The Mathematical Model

In Figure 1, we illustrate our model of the population dynamics of lytic phage and bacteria with and without a retron-mediated abortive infection system and envelope resistance. There is a single population of phage, P , particles per ml and four bacterial populations of bacteria, E , E_r , N , and N_r cells per ml. The phage sensitive retron population, E , has a functional *abi* system. Though it also has a function *abi* system, the E_r population is refractory to the phage. The N and N_r populations are retron negative, retron-, that are, respectively sensitive and resistant to the phage. When a phage infects a bacterium of state E , there is a probability q ($0 \leq q \leq 1$), that the bacteria will die and the infecting phage will be lost. The N population and $1-q$ of the E population support the replication of the phage while E_r and N_r are refractory to the phage.

The bacteria grow at maximum rates, v_e , v_{er} , v_n , and v_{nr} , per cell per hour, for E , E_r , N and N_r , respectively with the net rate of growth being equal to the product of maximum growth rate, v_{max} and the concentration of a limiting resource, r $\mu\text{g/ml}$, $v_{max} \cdot \psi(R)$ (16), Supplemental Eq (7). The parameter k , the Monod constant, is the concentration of the resource, at which the net growth rate of the bacteria is half its maximum value. By mutation or other processes, the bacteria change states, $E \rightarrow E_r$ and $E_r \rightarrow E$, at rates μ_{er} and μ_{re} , per cell per hour, and $N \rightarrow N_r$ and $N_r \rightarrow N$ at rates μ_{nr} and μ_{rn} .

The limiting resource is consumed at a rate equal to the product of $\psi(R)$, a conversion efficiency parameter, e $\mu\text{g/cell}$ (17) and the sum of products of the maximum growth rates of the bacteria and their densities. We assume phage infection is a mass action process that occurs at a rate equal to the product of the density of bacteria and phage and a rate constants of phage infection, δ_e and δ_n ($\text{ml} \cdot \text{cells}/\text{hour}$) for infections of E and N , respectively (18). Infections of N by P produce β_n phage particles, and the $(1-q)$ of the infections of E by P that do not abort, produce β_e phage particles. To account for the decline in physiological state as the bacteria approach stationary phase, $R=0$, we assume phage infection and mutation rates decline at a rate proportional to Eq.1. The lag before the start of bacterial growth and latent period of phage infection are not considered in this model or the numerical solution employed to analyze its properties.

The changes in the densities of bacteria and phage in this model are expressed as the series of coupled differential equations presented in the supplemental material.

Numerical solutions – computer simulations.

To analyze the properties of this model we use Berkeley Madonna to solve the differential equations (Supplemental Equations (1) – (7)). The growth rate and phage infections parameters used for these simulations are those estimated for *E. coli* and λ^{VIR} . Copies of this program are available at www.eclf.net.

Growth media and strains

Bacterial cultures were grown at 37 °C in MMB broth (LB broth (244620, Difco) supplemented with 0.1 mM MnCl₂ and 5 mM MgCl₂). The *E. coli* strain of MG1655 containing the Ec48 retron plasmid was obtained from Rotem Sorek. The sensitive *E. coli* used for controls was *E. coli* MG1655 marked with streptomycin resistance, and the Ec48 was marked with ampicillin resistance to differentiate in the invasion experiments. The λ^{VIR} phage lysates were prepared from single plaques at 37 °C in LB medium alongside *E. coli* C. Chloroform was added to the lysates and the lysates were centrifuged to remove any remaining bacterial cells and debris. The λ^{VIR} strain used in these experiments was obtained from Sylvain Moineau.

Sampling bacterial and phage densities

Bacteria and phage densities were estimated by serial dilution in 0.85% saline followed by plating. The total density of bacteria was estimated on LB hard (1.6%) agar plates. In invasion experiments, diluted samples were placed on LB hard (1.6%) agar plates supplemented with ampicillin (2.5%) or streptomycin (4%) plates to distinguish retron⁺ and retron⁻ *E. coli*. To estimate the densities of free phage, chloroform was added to suspensions before serial dilution. These suspensions were plated at various dilutions on lawns made up of 0.1 mL of overnight LB-grown cultures of *E. coli* MG1655 (about 5×10⁸ cells per mL) and 4 mL of LB soft (0.65%) agar on top of hard (1.6%) LB agar plates.

The Liquid culture experiments

Bacterial overnight cultures grown at 37 °C in MMB Broth were serially diluted in 0.85% saline to approximate

initial density and 100 μL were added to flasks containing 10 mL MMB. λ^{VIR} lysate ($>10^8$ pfu/mL) was serially diluted to a multiplicity of infection (MOI) of ~ 1 and 100 μL was added to the appropriate flask (where bacteria and phage densities are equal). These flasks were sampled for both phage and bacterial initial densities ($t = 0$ h) and were then grown at 37°C with constant shaking. The flasks were, once again, sampled for phage and bacterial densities ($t = 24$ h).

Experiments in soft agar cultures

Bacterial cultures grown at 37°C in MMB and λ^{VIR} lysate were serially diluted in 0.85% saline to the initial densities shown in the figures. The final dilutions were sampled for phage and bacterial initial densities and 100 μL of diluted phage and bacteria were added to 4 mL of LB soft (0.65%) agar and poured into small petri dishes which were grown at 37°C . After 24 hours, the agar was placed into a tube containing 6 mL of saline, vortexed and sonicated in a water bath for 1 hour. These tubes were serially diluted and sampled for final phage and bacterial densities.

Experiments in SSS

The method employed in the experiments with colonies on surfaces is that developed and employed by Lone Simonsen for a study of the population dynamics of conjugative plasmid transfer in physically structured habitats (19). A volume 4mL of LB agar was pipetted onto a glass microscope slide and allowed to harden. 0.1mL of a phage lysate diluted to the initial densities shown in the figures was placed on one side of the slide and 0.1mL of a bacterial overnight diluted to the initial densities shown was placed on the other side. The liquids were mixed via spreading with a plastic spreader over the surface of the microscope slide and allowed to grow overnight at 37°C . After 24 hours, the agar was placed into a tube containing 6 mL of saline, vortexed, and sonicated in a water bath for 1 hour. These tubes were serially diluted and sampled for final phage and bacterial densities.

Resistance Testing with Cross Streaks

Bacteria were tested by streaking in straight lines ten colonies from 24-hour plates across 20 μL of a λ^{VIR} lysate ($>10^8$ plaque-forming units [pfu]/mL) on LB hard (1.6%) agar plates. Susceptibility to λ^{VIR} was noted as breaks

in the lines of growth. Continuous lines were interpreted as evidence for resistance. 100 colonies were selected from each culture with 10 colonies being streaked on each plate, data reported as ratio of resistant colonies per plate.

Growth Rate Estimations

Growth rates were estimated in a Bioscreen C. 48-hour overnights of each strain to be tested were diluted in MMB broth to an initial density of approximately 10^5 cells per ml. 10 technical replicas of each strain were loaded into 100-well plates and grown at 37c with shaking for 24 hours taking OD (600nm) measurements every five minutes.

Acknowledgements

We thank Rotem Sorek and his colleagues at the Weizmann Institute for providing us with the phage and bacteria used in this study. We thank Kylie Burke, Teresa Gil-Gil, Jake Fontaine, Thomas O'Rourke, Yixuan Peng, Ingrid McCall, Eduardo Rodriguez-Roman, and Andrew Smith for their comments and reviews of this manuscript. We are grateful to Ingrid McCall and David Goldberg, for advice and help with the experimental work.

Materials Availability Statement

All materials used in this study are available by contacting Blevin@emory.edu. The programs used to generate the simulations in the study are available on eclf.net. All data generated are available in this manuscript and its supplemental material.

Competing Interests

The authors have no competing interests to declare.

References

1. Yee T, Furuichi T, Inouye S, Inouye M. Multicopy single-stranded DNA isolated from a gram-negative bacterium, *Myxococcus xanthus*. *Cell*. 1984;38(1):203-9.
2. Inouye S, Hsu MY, Eagle S, Inouye M. Reverse transcriptase associated with the biosynthesis of the branched RNA-linked msDNA in *Myxococcus xanthus*. *Cell*. 1989;56(4):709-17.
3. Temin HM. Reverse transcriptases. Retrons in bacteria. *Nature*. 1989;339(6222):254-5.
4. Simon DM, Zimmerly S. A diversity of uncharacterized reverse transcriptases in bacteria. *Nucleic Acids Res*. 2008;36(22):7219-29.
5. Rice SA, Lampson BC. Phylogenetic comparison of retron elements among the myxobacteria: evidence for vertical inheritance. *J Bacteriol*. 1995;177(1):37-45.
6. Rice SA, Bieber J, Chun JY, Stacey G, Lampson BC. Diversity of retron elements in a population of rhizobia and other gram-negative bacteria. *J Bacteriol*. 1993;175(13):4250-4.
7. Simon AJ, Ellington AD, Finkelstein IJ. Retrons and their applications in genome engineering. *Nucleic Acids Res*. 2019;47(21):11007-19.
8. Move over CRISPR, the retons are coming [Internet]. 2021.
9. Ishino Y, Shinagawa H, Makino K, Amemura M, Nakata A. Nucleotide sequence of the *iap* gene, responsible for alkaline phosphatase isozyme conversion in *Escherichia coli*, and identification of the gene product. *J Bacteriol*. 1987;169(12):5429-33.
10. Millman A, Bernheim A, Stokar-Avihail A, Fedorenko T, Voichek M, Leavitt A, et al. Bacterial Retrons Function In Anti-Phage Defense. *Cell*. 2020;183(6):1551-61 e12.
11. Lopatina A, Tal N, Sorek R. Abortive Infection: Bacterial Suicide as an Antiviral Immune Strategy. *Annu Rev Virol*. 2020;7(1):371-84.

12. Fukuyo M, Sasaki A, Kobayashi I. Success of a suicidal defense strategy against infection in a structured habitat. *Sci Rep.* 2012;2:238.
13. Berngruber TW, Lion S, Gandon S. Evolution of suicide as a defence strategy against pathogens in a spatially structured environment. *Ecol Lett.* 2013;16(4):446-53.
14. Chaudhry WN, Pleska M, Shah NN, Weiss H, McCall IC, Meyer JR, et al. Leaky resistance and the conditions for the existence of lytic bacteriophage. *PLoS Biol.* 2018;16(8):e2005971.
15. Chao L, Levin BR. Structured habitats and the evolution of anticompertitor toxins in bacteria. *Proc Natl Acad Sci U S A.* 1981;78(10):6324-8.
16. Monod J. The growth of bacterial cultures. *Annual Review of Microbiology.* 1949;3:371-94.
17. Stewart FM, Levin BR. Resource partitioning and the outcome of interspecific competition: a model and some general considerations. *American Naturalist.* 1973;107:171-98.
18. Chao L, Levin BR, Stewart FM. A complex community in a simple habitat: an experimental study with bacteria and phage. *Ecology.* 1977;58:369-78.
19. Simonsen L. The Existence Conditions for Bacterial Plasmids: Theory and Reality. *Microbial Ecology.* 1991;22(2):187-205.

Supporting Information

Supplemental Equations

$$\frac{dR}{dt} = -\Psi(R) \cdot e \cdot (v_n \cdot N + v_{nr} \cdot N_r + v_e \cdot E + v_{er} \cdot E_r)$$

SEq. (1)

$$\frac{dN}{dt} = \Psi(R) \cdot (v_n \cdot N - \delta_n \cdot N \cdot P + (\mu_{rn} \cdot N_r - \mu_{nr} \cdot N))$$

SEq. (2)

$$\frac{dN_r}{dt} = \Psi(R) \cdot (v_{nr} \cdot N_r - (\mu_{rn} \cdot N_r - \mu_{nr} \cdot N))$$

SEq. (3)

$$\frac{dE}{dt} = \Psi(R) \cdot (v_e \cdot E + (\mu_{re} \cdot E_r - \mu_{er} \cdot E))$$

SEq. (4)

$$\frac{dE_r}{dt} = \Psi(R) \cdot (v_{er} \cdot E_r - (\mu_{re} \cdot E_r - \mu_{er} \cdot E))$$

SEq. (5)

$$\frac{dP}{dt} = \Psi(R) \cdot (\delta_n \cdot \beta_n \cdot P \cdot N - q \cdot \delta_e \cdot P \cdot E + (1 - q) \cdot \delta_e \cdot \beta_e \cdot P \cdot E)$$

SEq. (6)

$$\Psi(R) = \frac{R}{R+K}$$

SEq. (7)

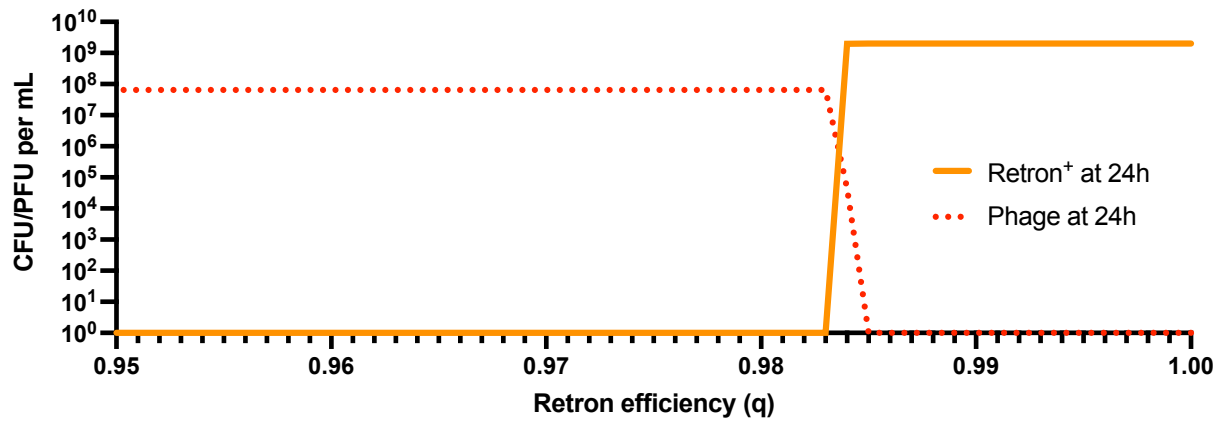


Figure S1. Computer simulation results for the effect of the retron efficiency as values of q . Changes in the densities of a retron⁺ bacterial population in the presence (orange) of phage (red) at 24 hours. Shown are 50 simulations with values of q ranging from 0.95 to 1 with a step size of 0.001. The parameters were the same as in Figure 2.

Table S1. Parameter values used in the simulations.

Parameter	Values (dimensions)	Description	Source (Reference)
v_e, v_{er}, v_n, v_{nr}	$2.00(h^{-1})$	Maximum growth rates	This paper (Table S2)
μ_{nr}, μ_{rn}	$1e^{-5}, 0 (h^{-1})$	Transitions $N \rightarrow N_r, N_r \rightarrow N$	(1)
μ_{er}, μ_{re}	$1e^{-5}, 0 (h^{-1})$	Transitions $E \rightarrow E_r, E_r \rightarrow E$	(1)
δ_e, δ_n	$2e^{-7}(h^{-1} \cdot mL^{-1})$	Adsorption rate constants	(1)
β_e, β_n	$60 (PFU \cdot CFU^{-1})$	Burst sizes	(1)
e	$5e^{-7}(\mu g \cdot CFU^{-1})$	Substrate Conversion Efficiency	(2)
K	$1 (\mu g)$	Monod constant	(2)
q	$0 \leq q \leq 1$	Effectiveness of Abi system	This paper*

*Estimated via numerical analysis of the predictions illustrated in Figure S1.

Table S2. Growth rate determination.

Strain (Population)	Symbol	Growth rate (h^{-1}) \pm SE
<i>Escherichia coli</i> Ec48 (E)	v_e	2.27 ± 0.06
<i>Escherichia coli</i> Ec48 (E _r)	v_{er}	2.17 ± 0.02
<i>Escherichia coli</i> MG1655 (N)	v_n	2.37 ± 0.04
<i>Escherichia coli</i> MG1655 resistant (N _r)	v_{nr}	2.27 ± 0.02

Table S3. Cross-streak results at 24 hours.

Strain	Plate number	Resistant ratio*
<i>Escherichia coli</i> Ec48	1	1
	2	1
	3	1
	4	1
	5	1
	6	1
	7	1
	8	1
	9	1
	10	1
<i>Escherichia coli</i> MG1655	1	1
	2	1
	3	1
	4	0.9
	5	1
	6	1
	7	1
	8	1
	9	1
	10	1

* Each colony with a minimum number of 7 from a 10^{-7} dilution plate were tested for phage resistance (λ^{vir}) and the ratio of resistant/total was calculated.

Supplemental Information References

1. Chaudhry, W. N., et al. (2018). "Leaky resistance and the conditions for the existence of lytic bacteriophage." PLoS Biol **16**(8): e2005971.
2. Stewart, F. M. and B. R. Levin (1973). "Resource partitioning and the outcome of interspecific competition: a model and some general considerations." American Naturalist **107**: 171-198.

Chapter 10

Chapter 10

Evaluating the potential efficacy and limitations of a phage for joint antibiotic and phage therapy of *Staphylococcus aureus* infections

Reprinted from: Berryhill BA, Huseby DL, McCall IC, Hughes D, Levin BR. 2021. Evaluating the potential efficacy and limitations of a phage for joint antibiotic and phage therapy of *Staphylococcus aureus* infections.

Proceedings of the National Academy of Sciences of the United States of America.

<https://doi.org/10.1073/pnas.2008007118>

Abstract

In response to increasing frequencies of antibiotic-resistant pathogens, there has been a resurrection of interest in the use of bacteriophage to treat bacterial infections: phage therapy. Here we explore the potential of a seemingly ideal phage, PYO^{Sa}, for combination phage and antibiotic treatment of *Staphylococcus aureus* infections. This K-like phage has a broad host range; all 83 tested clinical isolates of *S. aureus* tested were susceptible to PYO^{Sa}. Because of the mode of action of PYO^{Sa}, *S. aureus* is unlikely to generate classical receptor-site mutants resistant to PYO^{Sa}; none were observed in the 13 clinical isolates tested. PYO^{Sa} kills *S. aureus* at high rates. On the downside, the results of our experiments and tests of the joint action of PYO^{Sa} and antibiotics raise issues that must be addressed before PYO^{Sa} is employed clinically. Despite the maintenance of the phage, PYO^{Sa} does not clear populations of *S. aureus*. Due to the ascent of a phenotypically diverse array of small-colony variants following an initial demise, the bacterial populations return to densities similar to that of phage-free controls. Using a combination of mathematical modeling and in vitro experiments, we postulate and present evidence for a mechanism to account for the demise–resurrection dynamics of PYO^{Sa} and *S. aureus*. Critically for phage therapy, our experimental results suggest that treatment with PYO^{Sa} followed by bactericidal antibiotics can clear populations of *S. aureus* more effectively than the antibiotics alone.

Significance

This study explores the potential of a phage, PYO^{Sa}, for treating *Staphylococcus aureus* infections in combination with antibiotics. Population dynamic and genomic analysis identified a limitation and potential liability of using PYO^{Sa} for therapy. Due to the production of potentially pathogenic atypical small colony variants, PYO^{Sa} alone cannot eliminate *S. aureus* populations. However, we demonstrate that by following the administration of PYO^{Sa} with bactericidal antibiotics, this limitation and potential liability can be addressed. The methods used in this investigation to explore the efficacy of combinations of PYO^{Sa} and antibiotics for treating *S. aureus* infections can be employed to evaluate the clinical potential and facilitate the design of treatment protocols for any bacteria and phage that can be cultured in vitro.

Introduction

Driven by well-warranted concerns about the increasing frequencies of infections with antibiotic-resistant pathogens, there has been a resurrection of interest in, research on, and clinical trials with a therapy that predates antibiotics by more than 15 years: bacteriophage (1-4). One direction phage therapy research has taken is to engineer lytic (virulent) phages with properties that are anticipated to maximize their efficacy for treating bacterial infections in mammals (5-7). Primary among these properties are (i) a broad host range for the target bacterial species, (ii) mechanisms that prevent the generation of envelope or other kinds of high-fitness resistance in the target bacteria (8), (iii) the capacity to thwart the innate and adaptive immune systems of bacteria, respectively restriction-modification and CRISPR-Cas (7, 9, 10), (iv) the ability to survive, kill, and replicate on pathogenic bacteria colonizing or infecting mammalian hosts (11, 12) and (v) little or no negative effects on the treated host (8).

To these five desired properties for therapeutic bacteriophage, we add a sixth: synergy with antibiotics. Phage-only treatment may be reasonable for compassionate therapy where the bacteria responsible for the infection are resistant to all available antibiotics (13-15). But from a practical perspective, for phage to become a widely employed mechanism for treating bacterial infections, they would have to be effective in combination with antibiotics. It would be unethical and unacceptable to clinicians and regulatory agencies to use phage independently for infections that can be effectively treated with existing antibiotics.

Although not specifically engineered for these properties, there is a *Staphylococcal* phage isolated from a therapeutic phage collection from the Eliava Institute in Tbilisi; we call PYO^{sa} that on first consideration appears to have all six of the properties required to be an effective agent for therapy. (i) PYO^{sa} is likely to have a broad host range for *S. aureus*. The receptor of this K-like Myoviridae is N-acetylglucosamine in the wall-teichoic acid backbone of *Staphylococcus aureus* and is shared among most (16), if not all *S. aureus*; thereby suggesting PYO^{sa} should be able to adsorb to and potentially replicate on and kill a vast number of clinical isolates of *S. aureus*. (ii) *S. aureus* does not generate classical, surface modification mutants resistant to PYO^{sa}.

Since the structure of the receptor of PYO^{Sa} is critical to the viability, replication, and virulence of these bacteria, the modifications in this receptor (17) may not be consistent with the viability or pathogenicity of *S. aureus* (18). (iii) The replication of PYO^{Sa} is unlikely to be prevented by restriction-modification (RM) or CRISPR-Cas. Despite a genome size of 127 KB, the PYO^{Sa} phage has no GATC restriction sites for the *S. aureus* restriction enzyme Sau3A1 and only one restriction site, GGNCC, for the Sau961 restriction endonuclease (19, 20). There is no evidence for a functional CRISPR-Cas system in *S. aureus* or, to our knowledge, other mechanisms by which *S. aureus* may prevent the replication of this phage (21). (iv) There is evidence that PYO^{Sa}-like phages can replicate in mammals. Early treatment with a phage with a different name but the same properties as PYO^{Sa}, Statuv, prevented mortality in otherwise lethal peritoneal infections of *S. aureus* in mice (22). A PYO^{Sa}-like phage has also been successfully used therapeutically in humans (23). (v) No deleterious effects of a PYO^{Sa}-like phage were observed in recent placebo-controlled trials with volunteers asymptotically colonized by *S. aureus* (19). (vi) Finally, there is evidence to suggest synergy with antibiotics. *In vitro*, PYO^{Sa} increased the efficacy of low concentrations of antibiotics for the treatment of biofilm populations of *S. aureus* (24).

With *in vitro* parameter estimation, population and evolutionary dynamic studies, and experiments with PYO^{Sa} and *S. aureus* Newman in combination with three different bacteriostatic and six different bactericidal antibiotics, we explore just how well PYO^{Sa} fits the above criteria for combination antibiotic and phage therapy. Our results suggest that PYO^{Sa} scores well on most of these tests but does not get an “A”. As a consequence of selection for potentially pathogenic small colony variants, by itself PYO^{Sa} does not clear *S. aureus* infections; after an initial demise when confronted with this phage, although the phage continue to be present, the densities of the bacteria return to levels similar to those observed in the absence of this virus. By employing antibiotics and phage against *S. aureus* we could demonstrate synergy in clearing the bacterial population. However, there were significant differences in effectiveness depending on whether the antibiotics and phage were used simultaneously or in succession, and on whether the antibiotics used were bacteriostatic or bacteriocidal. Our most important result from a therapeutic perspective is that treatment of *S. aureus* cultures with PYO^{Sa}, followed by the administration of bacteriocidal antibiotics, is more effective at clearing the bacterial population than treatment with these antibiotics alone.

Results

Bacteriophage PYO^{Sa} has a broad host range for *S. aureus*: We use two assays to determine the host range of PYO^{Sa}: (i) the production of zones of inhibition in soft agar lawns and (ii) changes in the optical density of exponentially growing liquid cultures of *S. aureus* mixed with this phage. By both criteria, *S. aureus* Newman and 12 clinical isolates of methicillin-sensitive *S. aureus* from the Network on Antimicrobial Resistance (NARSA) collection (25) were all sensitive to PYO^{Sa} and appeared to be unable to generate classically resistant mutants. Additional evidence for a broad host range of PYO^{Sa} comes from a survey of 71 clinical isolates of *S. aureus*, including 54 MRSA strains and phylogenetically similar species performed by LabCorp™ (*SI Appendix*, Table S1).

S. aureus appears to be unable to generate classical, surface modification, mutants resistant to PYO^{Sa}: Evidence for this comes from experiments with *S. aureus* Newman and 12 clinical isolates from the NARSA collection (25). Single colonies of each strain were grown in the presence of $\sim 10^6$ phage particles per ml, and after 24 hours of exposure to the phage in liquid culture, the optical densities of exponentially growing *S. aureus* were no greater than that of the media without the bacteria, and by plating, we were unable to detect colonies from these cultures.

Bacterial population heterogeneity and the maintenance of phage: With the bacterial growth and phage infection parameters estimated for *S. aureus* Newman and PYO^{Sa}, a complete clearance of the bacteria in these experiments after less than 24 hours of exposure to PYO^{Sa} is anticipated from a simple mass action model of the population dynamics of bacteria and phage (26). To determine whether this is the case empirically, we divided a culture with $\sim 10^4$ *S. aureus* Newman into 28 tubes. We let these cultures replicate for 2 hours, for an average density of 3×10^7 and then added $\sim 6 \times 10^8$ PYO^{Sa}. At 24 hours, all 28 cultures were clear, and no bacterial colonies were found on the LB plate samplings of these cultures. However, by day seven, 26 of these 28 independent cultures were turbid or somewhat turbid. These turbid cultures all had phage at densities in excess of 5×10^6 . Upon plating these 7-day cultures, colonies were detected with two distinct phenotypes:

colonies similar in size to the ancestral wild-type *S. aureus* Newman and much smaller colonies, small colony variants (Fig. 1A).

To elucidate why PYO^{Sa} does not kill all of the *S. aureus* Newman in these liquid cultures, we prepared three independent 10 ml cultures with $\sim 10^8$ *S. aureus* Newman and $\sim 10^7$ PYO^{Sa} and serially passaged these cultures for five days, transferring 1/100 of these cultures to fresh media each day. The results of these serial transfer experiments are presented in Fig. 1B. As anticipated from the experiment with the 28 tube cultures, at 24 hours, all the flasks were clear. The densities of bacteria remaining in these cultures estimated by plating, $\sim 10^3$ per ml, is probably an underestimate of the real density due to killing by phage on the plates. Additional support for the hypothesis that the densities of *S. aureus* in these liquid cultures is substantially greater than the CFU estimate is that the density of the PYO^{Sa} phage did not decline at each transfer, and therefore, the phage must have been replicating. This hypothesis was evaluated with a simple model (26) using the phage infection parameters estimated for PYO^{Sa} and *S. aureus* Newman. To maintain a population in a culture diluted by 100-fold the phage density must increase by at least 100-fold at each transfer and for this to occur, the product of the adsorption rate constant, δ , the burst size β , and the density of sensitive bacteria, N , has to exceed 100. With the estimated values, $\delta=4.8 \times 10^{-7}$ and $\beta=80$, the density of bacteria in these cultures would have to be at least 2.6×10^6 for the phage not to be diluted out.

Most intriguingly, in all three independent serial transfer populations with the PYO^{Sa} phage present, the CFU estimates of the density of *S. aureus* started to increase after the 2nd transfer. By the 4th and 5th transfer, the density of cells in these cultures was similar to that of the phage-free controls, and the phage continued to be maintained, presumably because of the continued presence of phage-susceptible populations. To test this we spread bacterial aliquots onto agar and observed heterogeneity in colony growth with both fast-growing and small colony variants. Using a spot test we showed that cultures grown from fast-growing colonies, henceforth called the evolved bacteria, were susceptible to the original PYO^{Sa} as well as to the co-existing PYO^{Sa}. In

contrast, the spot test showed that cultures grown from small colony variants isolated from these late transfer cultures were resistant to lysis by PYO^{Sa}.

To further evaluate the different bacterial phenotypes present in the late transfer cultures we serially passaged two small colony cultures in the presence of PYO^{Sa} (Fig. 1C). We observed that cultures generated from small colony variants were unable to support the phage. These data, and the spot test data suggest an explanation for the maintenance of bacteria and phage throughout the original transfer experiment (Fig. 1B). Our hypothesis is that the bacterial population is polymorphic and includes sensitive cells capable of supporting phage growth as well as a non-sensitive population. We tested this hypothesis by mixing wild-type *S. aureus* Newman in equal frequency with small colony variants, and observed, consistent with the hypothesis, that the phage were maintained throughout the serial transfers and that the total bacterial population density remained similar to that in phage-free controls (Fig. 1D). As a separate test of the polymorphic population hypothesis, we made serial transfer experiments initiated with mixtures of PYO^{Sa} phage and evolved bacteria isolated from the 5th transfer cultures (Fig. 1E). The results of these experiments are consistent with this reduced susceptibility hypothesis. Moreover, within a single transfer, the bacterial density returned to that of the phage-free controls and the phage declined, albeit at a rate less than that anticipated if they were not replicating at all, in two of the three cultures. In the two cultures where the phage declined significantly, the dominant bacterial population were small colony variants; while, the replicate with the co-existing phage was dominated by bacteria that generated wild-type colony morphologies. See *SI Appendix*, Section II for a consideration of the between experiment variation in the population dynamics observed in Fig. 1B and 1E.

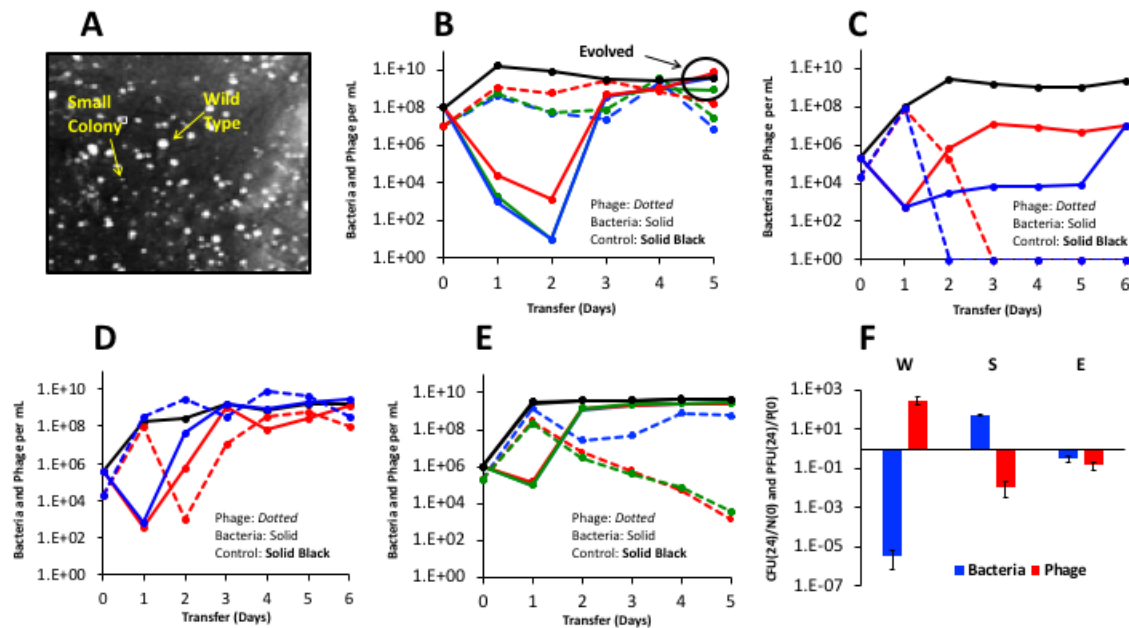


Fig. 1. Small colony variants and the population dynamics of PYO^{Sa} and *S. aureus* Newman in serial transfer culture. **A.** Wild type *S. aureus* and small colony variants visualized. **B.** Changes in densities of *S. aureus* Newman and PYO^{Sa} in three independent (red, green, blue) serial transfer experiments diluted 1/100 in fresh media daily. **C.** Changes in densities of *S. aureus* Newman and PYO^{Sa} in serial transfer cultures initiated with two small colony variants isolated from the 5th transfer of the cultures with PYO^{Sa} and *S. aureus* Newman in panel B. **D.** Changes in densities of *S. aureus* Newman and PYO^{Sa} in serial transfer cultures initiated with PYO^{Sa} and equal densities of cultures derived from small colonies and the ancestral *S. aureus* Newman. **E.** Changes in densities of *S. aureus* and PYO^{Sa} in serial transfer cultures initiated with PYO^{Sa} and single colonies of evolved (wild-type colony morphology) bacteria isolated from the 5th transfer of the cultures in panel B. **F.** Changes in the ratio of bacteria and phage at time 0 and 24 hours. Wild type *S. aureus* Newman (W), small colony variants (S), and evolved bacteria (E). Three independent replicas.

Based on the preceding results and interpretations, we postulate that the bacteria are of three states, the ancestral wild-type, small colony variants, and what we call the evolved state, which have wild-type or near wild-type colony growth rate and rise to high densities after serial passaging in the presence of phage. Both the wild-type

and the evolved are postulated to be capable of supporting phage growth whereas the small colonies type do not support phage growth.

The genetic basis of bacterial colony growth rate variation: To determine the genetic basis of the differences between wild-type *S. aureus* Newman, the small colony variants, and evolved states, colonies with a range of sizes were isolated from early and late in serial passaging experiments similar to those shown in Fig. 1B. Whole genome sequencing of several clones revealed a clear sequence of events during the passaging. The first event was the selection of mutations in *femA* which encodes a protein responsible for assembling the pentaglycine interpeptide bridges in the *S. aureus* cell wall (*SI Appendix*, Table S2). These mutants all have a small colony variant phenotype. The range of observed colony sizes is representative of the diversity of mutations identified in *femA*, and presumably indicates a direct correlation between the growth rate and the severity of the defect in FemA function. We observed in later transfers larger colonies that carried a *femA* mutation and an additional mutation (see below) suggesting that this was a compensatory mutation restoring growth rate and creating the evolved state. The small colony variant phenotype of *S. aureus* is known to be very unstable and subject to rapid suppression by a wide variety of compensatory mutations (27). To investigate the nature of evolved state, we chose several different *femA* mutants and used these to select faster-growing colonies. Fast-growers were easily selected and were observed on agar as larger colonies growing above the slower-growing parental small colony strains. Whole genome sequencing revealed an array of suppressing mutations were selected, including an internal suppressor in *femA*, mutations in a variety of genes affecting secondary messenger metabolism, and frequent mutations in the transcriptional regulator *sarA* (*SI Appendix*, Table S3). We concluded that the initial event upon exposure of wild-type *S. aureus* Newman to PYO^{Sa} is the selection of small colony variants associated with mutations in *femA*. These slow-growing mutants then evolve to the faster-growing evolved state by the acquisition of suppressor mutations that frequently affect global transcriptional regulators.

Phenotypic differences between wild-type, small colony, and evolved clones: The hypothesis above predicts that cultures derived from bacterial colonies of each state should respond differently when exposed to PYO^{Sa}.

To test this, we co-cultured high densities of each bacterial state (W, S, and E) with PYO^{Sa} and determined the relative change in densities of both bacteria and phage, respectively 10^8 and 10^7 cells and particles per ml, after 24 hours exposure (Fig. 1F). Each of the three states exhibited a unique dynamic. The density of the wild-type and evolved bacteria declined, with the wild-type declining to a much greater extent than the evolved state. In contrast, the density of small colony variant bacteria increased. PYO^{Sa} phage increased on the wild-type bacteria but declined on both small colony variant and evolved state bacteria. The decline in phage was greater on small colony variants than on the evolved state.

Measurement of the growth rates in liquid culture of the three bacterial states confirmed the growth parameters previously inferred from colony sizes (*SI Appendix*, Table S4). Mutations causing a small colony phenotype on agar also caused severe growth defects in liquid culture, while the evolved clones with secondary suppressing mutations showed partial restoration of growth rate toward wild-type levels.

The pentapeptide crosslinks that FemA synthesizes are notably the target of lysostaphin. FemA mutants resistant to lysostaphin have previously been observed to become hypersensitive to penicillin antibiotics (28, 29). To test for evidence of these phenotypes the MIC of the three states were measured against lysostaphin and oxacillin (*SI Appendix*, Table S4). We observed that all of the strains carrying *femA* mutations (both small colony and evolved state) became resistant to lysostaphin and hypersensitive to oxacillin. Accordingly, the compensatory evolution from small colony variant to evolved state does not phenotypically recreate a wild-type phenotype: wild-type and evolved are genetically and phenotypically distinct states. Since FemA is responsible for adding the 2nd and 3rd glycines to the interpeptide bridge, while FemB is responsible for adding the 4th and 5th residues, mutations in *femA* are expected to result in single glycine bridges between the cell wall peptides. To the degree that the *femA* mutants identified have different growth and susceptibility phenotypes, the cell wall defect in strains carrying these mutations is likely not complete, but rather represents a balance between full length pentapeptide crosslinks and single glycine crosslinks. FemA was recently reported to be essential (30) and it is notable that in our experiments no unequivocally *femA* null mutations were identified. Based on

the number of mutants we have screened, this indicates that *femA* null mutants are either non-viable or are counterselected in these experiments.

PYO^{Sa} does not replicate on stationary phase *S. aureus*. In infected hosts, many of the bacteria will not be replicating, and thereby, phage would be particularly effective for treatment if they, like some antibiotics (31), could kill non-replicating *S. aureus*. To determine whether PYO^{Sa} can kill and replicate on non-growing bacteria, three independent 48-hour stationary phase cultures were mixed with PYO^{Sa} for average initial densities of $\sim 4 \times 10^9$ *S. aureus* and 10^6 PYO^{Sa}. The bacteria and phage were incubated with shaking for 24 hours, and the viable cell and phage densities were estimated and compared to the initial densities. There was no evidence for the stationary phase bacteria being killed, the mean and standard error of the $N(24)/N(0)$ ratio was 0.96 ± 0.03 . Moreover and critically, there was a significant decline in the density of phage, $N(24)/N(0) = 0.043 \pm 0.006$. Thus, not only does PYO^{Sa} not kill stationary phase *S. aureus*, these non-replicating bacteria act as a sink and could reduce the density of PYO^{Sa} from treated hosts.

The results of experiments to determine whether the decline in the density of phage can be attributed to changes in the medium, such as a high pH, were negative. The density of PYO^{Sa} did not decline in sterile filtrates of 48-hour stationary phase cultures. There is, however, the suggestion that the bacteria must be viable to lead to the reduction in the viable density. When the *S. aureus* in the 48-hour stationary phase culture are killed with chloroform, the density of PYO^{Sa} does not decline

Accounting for the population dynamics presented in Fig. 1B: In the *SI Appendix*, Section IV, Fig. S2, using a mathematical model and numerical solutions, we present a hypothesis for the kill-recovery dynamics observed for the bacteria, and the maintenance of the phage in the serial transfer cultures depicted in Fig. 1B. In accord with this hypothesis, (i) the bacterial population recovers from its initial demise due to predation by PYO^{Sa} phage, by the generation and ascent of small colony variants which are immune to, and selected by, the phage,

and (ii) the phage are maintained because of the instability of the small colony variants which continuously generate the evolved state bacteria upon which the phage can replicate.

The joint action of PYO^{Sa} and antibiotics: To determine whether the action of antibiotics and PYO^{Sa} would be synergistic or antagonistic in killing *S. aureus* Newman and the effect of these drugs on replication of PYO^{Sa}, we followed the change in the densities of bacteria and phage over 24 hours of exposure to antibiotics and phage in combination, and to phage alone. For these experiments, we mixed growing cultures of *S. aureus* Newman and PYO^{Sa} in MHII at a density of 4×10^6 with 4×10^5 , respectively and super MIC concentrations of the antibiotics. The densities of bacteria and phage were estimated just before the antibiotics were added and 24 hours later, respectively $N(0)$ and $N(24)$, where N is either CFU or PFU. In these experiments, the antibiotics and phage were introduced into the growing cultures of *S. aureus* Newman in three different ways: (i) simultaneously, AB+PYO^{Sa}, (ii) antibiotics first and phage 30 minutes later, AB→PYO^{Sa}, and (iii) phage first and antibiotics 30 minutes later, PYO^{Sa}→AB. As controls, we also treated parallel cultures of *S. aureus* Newman with antibiotics only, AB, and with phage alone. In Fig. 2 (bacteriostatic antibiotics) and Fig. 3 (bacteriocidal antibiotics) we present $N(24)/N(0)$ ratios for the bacteria and phage for three independent experiments with each antibiotic and phage combination.

With the bacteriostatic antibiotics, tetracycline (TET), azithromycin (AZM), and linezolid (LZD), the greatest decline in the density of bacteria and increase in the density of phage obtained in the experiment where phage are used alone. There is clearly a negative synergy between these bacteriostatic antibiotics and the phage. Whether administered simultaneously or sequentially, at the concentrations used, these antibiotics prevent PYO^{Sa} from killing *S. aureus* Newman. When the phage are administered simultaneously with azithromycin and linezolid, the phage density declines.

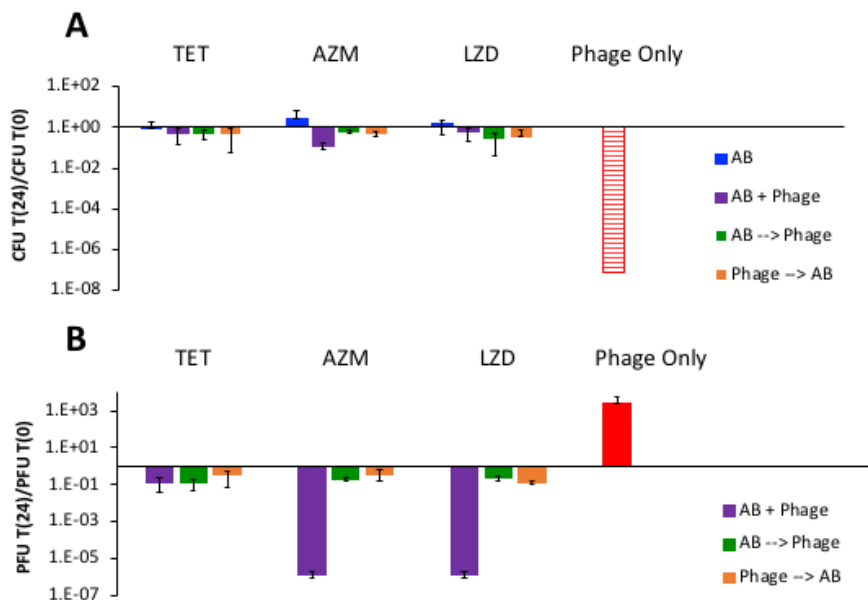


Fig. 2. Joint action of bacteriostatic antibiotics and PYO^{Sa}. The concentrations of these antibiotics are 10 µg/ml. **A.** The ratio of the change in density of *S. aureus* after 24 hours of exposure to antibiotics (blue), antibiotics plus phage (purple, green, orange, refers to order of addition as explained in the text) or phage alone (red). Hash red, the density of *S. aureus* recovered was below the detection limit, ~10² cells per ml. **B.** The ratio of the change in the density of PYO^{Sa} after 24 hours of confronting wild-type *S. aureus* in combination with antibiotics or alone.

In Fig. 3, we present the results of experiments with bactericidal antibiotics, rifampin (RIF), oxacillin (OXA), ciprofloxacin (CIP), vancomycin (VAN), daptomycin (DAP) and kanamycin (KAN). The data suggest that the simultaneous or sequential administration of PYO^{Sa} may modestly increase the rate at which bactericidal antibiotics kill *S. aureus* at the concentrations employed. However, as was observed for the parallel experiment with the bacteriostatic drugs (Fig. 2), the phage kill more *S. aureus* in the absence of antibiotics than with these drugs, an antagonistic interaction once again. The failure of rifampin to reduce the viable density of *S. aureus* can be attributed to rifampin resistance emerging. It should be noted however, that in one of the three treatments where PYO^{Sa} was used before adding rifampin, it prevented the ascent of resistance. Most

interestingly, while treatment with rifampin, oxacillin, and ciprofloxacin allowed PYO^{Sa} to replicate, this was not the case for vancomycin, daptomycin, and kanamycin, which appeared to suppress the replication of PYO^{Sa}.

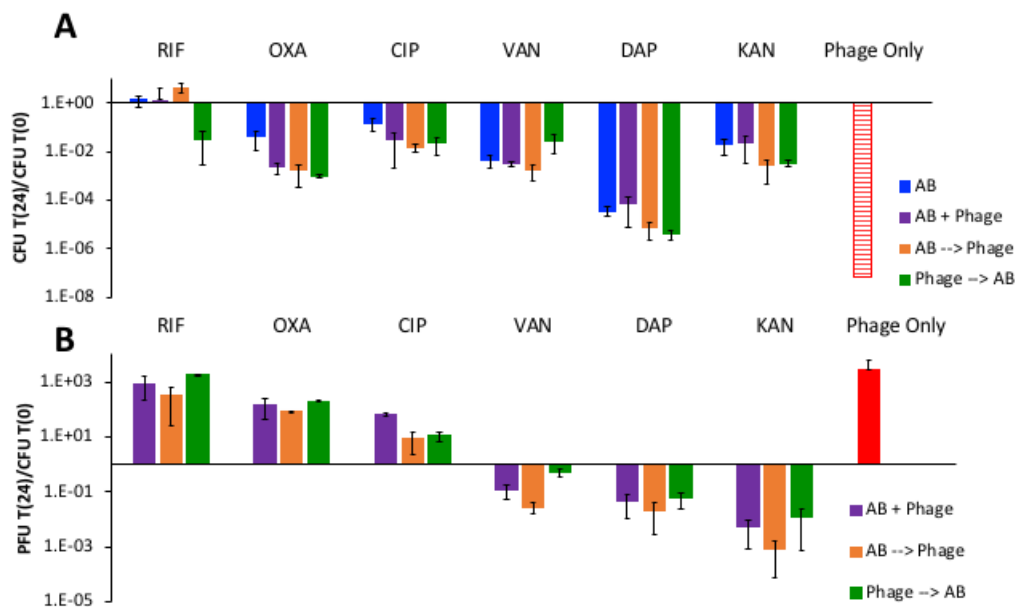


Fig. 3. The joint action of bactericidal antibiotics and PYO^{Sa}. Concentrations of the different antibiotics in $\mu\text{g/ml}$ (RIF 0.02, OXA 3, CIP 0.5, VAN 8, DAP 64, KAN 46), corresponding to minimum bacteriocidal concentrations. **A.** The ratio of the change in density of *S. aureus* after 24 hours of exposure to antibiotics, antibiotics and phage, or phage alone. Hash red, the density of *S. aureus* recovered was below the detection limit, $\sim 10^2$ per ml. **B.** The ratio of the change in the density of PYO^{Sa} after 24 hours of confronting *S. aureus* Newman in combination with antibiotics or alone.

Sequential treatment, phage followed by antibiotics: The serial transfer results presented in Fig. 1B indicate that as a consequence of the emergence and ascent of small colony variants, PYO^{Sa} by itself will not be able to control an *S. aureus* population for an extended time. Although the phage continue to be present, the density of the bacteria returns to levels similar to that of the phage-free control (Fig. 1B). We asked what result would be obtained if antibiotics were administered to these populations? To address this question, we performed the serial transfer experiments with the addition of bactericidal antibiotics following the phage-mediated reduction

in the density of wild-type *S. aureus* observed during the first 24 hours. The results of these experiments are presented in Fig. 4.

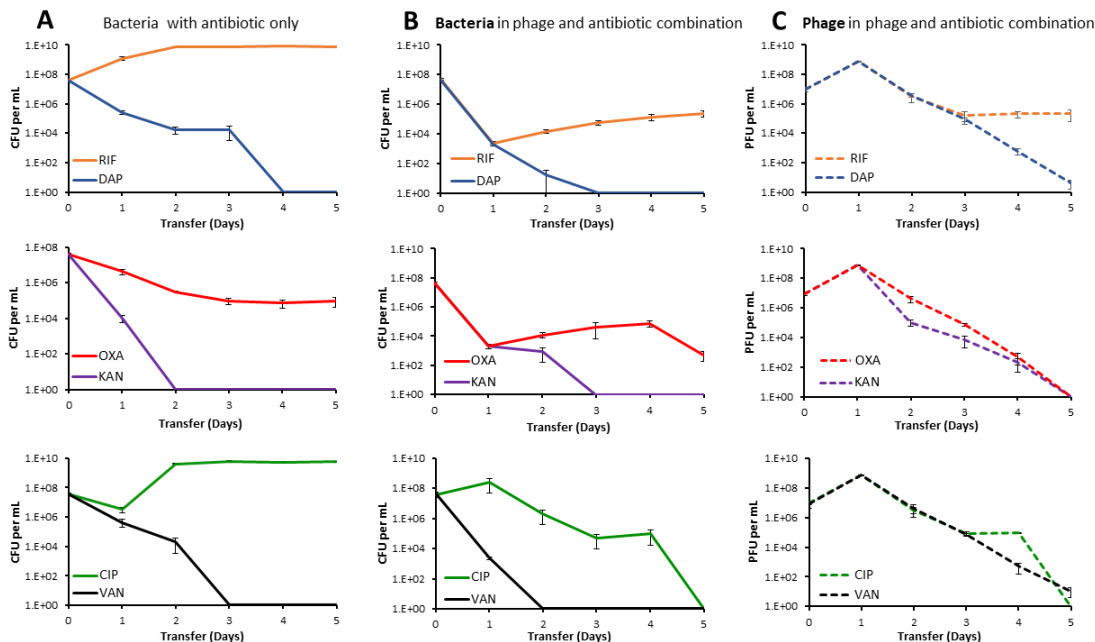


Fig. 4. Changes in the densities of bacteria and phage in serial transfer cultures treated with antibiotics alone, or in combination with phage. **Column A.** Bacteria treated with antibiotics alone. **Column B.** Bacterial densities in cultures containing both the antibiotic and the phage. **Column C.** Phage densities in cultures containing both the antibiotic and the phage. Mean and standard errors of 3 independent experiments. **Row 1.** Treatment with RIF and DAP, 0.02 and 64 $\mu\text{g}/\text{ml}$, respectively. **Row 2.** Treatment with KAN and OXA, 46 and 3 $\mu\text{g}/\text{ml}$ respectively, **Row 3.** Treatment with CIP and VAN, 0.5 and 8 $\mu\text{g}/\text{ml}$ respectively.

Three of the antibiotics, DAP, KAN and VAN, were alone sufficient to eliminate the *S. aureus* population (Fig. 4A). In contrast, with RIF by the second transfer the density of *S. aureus* in treated cultures reached a density observed for antibiotic and phage free cultures ($\sim 2 \times 10^9$ bacterial per ml). The reason for the failure of RIF to clear the culture was the emergence of mutants resistant to this drug. All six colonies tested from the 5th transfer were resistant to RIF. However, the viable cells recovered from the phage and RIF combination cultures were

as sensitive to RIF as the antibiotic-free controls. Neither OXA nor CIP alone cleared the cultures. In the case of OXA, the viable cell density declined but continued to persist at a density of approximately 10^5 cells per ml. The bacteria recovered from these cultures were sensitive to OXA. We postulate that this leveling off can be attributed to persistence (32); see *SI Appendix*, Section VI, Fig. S5. In the case of CIP, the initial exposure led to a substantial decline in the viable cell density of *S. aureus*, however, following the second transfer the bacterial population recovered and was sustained at densities similar to that in the antibiotic-free controls. The colonies of *S. aureus* recovered at the end of this experiment were susceptible to CIP. We postulate that these resurrection dynamics could be attributed to heteroresistance (33), see *SI Appendix*, Section VI, Fig S5.

Discussion

On first consideration, PYO^{Sa} seems to be an ideal phage for treating *S. aureus* infections. The results of this study provide evidence in support of three virtues of PYO^{Sa} as a therapeutic phage. 1) PYO^{Sa} is likely to kill virtually all methicillin-resistant as well as methicillin-sensitive *S. aureus*. 2) *S. aureus* are unable to generate classical surface-resistant mutants to PYO^{Sa}, thus, cocktails of multiple phages would not be needed to ensure coverage or prevent resistance. 3) *S. aureus* Newman has a high adsorption rate and burst size with PYO^{Sa} and, when first confronting growing populations of *S. aureus*, the bacteria are killed, and the phage replicate at a high rate.

On the downside, our experiments raise caveats about the use of PYO^{Sa} for treating *S. aureus* infections alone and suggest a possible liability as well. Not only is PYO^{Sa} unable to clear cultures of *S. aureus* Newman, it selects for potentially pathogenic small colony variants, (34-37) that are refractory to this phage. Through a “leaky resistance” mechanism (38), the phage continue to be maintained, and the bacterial population continues to persist at densities not much less than they do in the absence of PYO^{Sa}. Although not observed for the small colony variants tested here, at least some small colonies are more resistant to antibiotics than the bacteria from which they are derived (39, 27, 40).

For phage therapy to be a practical and acceptable enterprise, these viruses would have to be used in combination with antibiotics. Our results indicate that when administered simultaneously, or nearly simultaneously with antibiotics, PYO^{Sa} does worse in killing *S. aureus* than it does alone PYO^{Sa}. The ribosome-targeting bacteriostatic antibiotics, tetracycline, azithromycin, and linezolid, suppress the ability of PYO^{Sa} to kill *S. aureus* Newman. This observation is consistent with the failure of PYO^{Sa} to replicate on stationary phase populations of *S. aureus*. It is also consistent with the Numbers Game hypothesis for the action of bacteriostatic antibiotics (41) according to which, the number of free ribosomes is too low to support the protein synthesis needed for replication of the phage.

When administered simultaneously with bactericidal antibiotics, PYO^{Sa} is also less effective in killing *S. aureus* than it is in the absence of these drugs. We postulate that this can be attributed to pharmacodynamic and population dynamics of the joint action of antibiotics and phage; the antibiotics reduce the densities of the bacteria substantially and thereby lower the capacity of the phage to replicate (*SI Appendix*, Section IV).

Sequential treatment with PYO^{Sa} and antibiotics: Our experiments suggest a way to deal with the major caveat and potential liability of treatment with PYO^{Sa} alone, the recovery of the bacterial population due to the ascent of small colony variants. The administration of bactericidal antibiotics following the initial decline in the density of bacteria due to PYO^{Sa} prevents bacterial population recovery and eliminates or prevents the selection of small colony variants. The latter is not the case when the antibiotics are used alone. One interpretation of this is that sequential treatment, initially with phage, then with a bactericidal antibiotic may be more effective than treatment with antibiotics alone or phage alone.

Conclusion and Recommendation: We interpret the results of this *in silico* and *in vitro* study to suggest that PYO^{Sa} will be effective for treatment of *S. aureus* infections, but only if the administration of bactericidal antibiotics follows that of phage. The next step will, of course, be to test this sequential phage and antibiotic treatment hypothesis with *S. aureus* infections in experimental animals.

We suggest that the *in vitro* methods used to explore the potential efficacy of PYO^{Sa} would also be useful for evaluating other phages being developed for treating bacterial infections. Existing data suggested that PYO^{Sa} met all of the criteria desired for a phage to be effective for therapy; yet, the *in vitro* experiments performed here uncovered a limitation and potential liability of using this phage for therapy that would not have anticipated and they also subsequently revealed a way to deal with said limitation and liability.

Materials Methods

Unless otherwise noted, all experiments were performed from derivatives of the parent strain *S. aureus* Newman (ATCC 25904). The parent *S. aureus* Newman was obtained from Bill Schafer of Emory University. The small colony variant and evolved strains were obtained from PYO^{Sa} challenged *S. aureus* Newman by experiments performed in our lab. The investigation for classical resistance was performed in the following MSSA strains obtained from Abraham Moller in the Reid Lab at Emory University: NRS52, NRS102, NRS180, NRS110, NRS252, NRS253, NRS266, NRS109, NRS148, and NRS205.

Bacterial cultures were grown at 37°C in Mueller-Hinter II (MHII) Broth [275710, BD™] and on Luria-Bertani Agar (LB) Plates [244510, BD™]. PYO^{Sa} lysates were prepared from single plaques at 37°C in MHII broth alongside wild-type *S. aureus* Newman by plate lysis. Specifically, individual phage plaques were picked with a sterile stick, resuspended in 4ml of soft agar with 0.1ml of overnight bacterial culture and plated on top of phage plates. The plates were then incubated at 37°C overnight. The soft agar was scraped with a sterile iron scoop, resuspended in 10ml MHII with ~0.5ml of chloroform to kill the surviving bacteria. The lysates were then centrifuged to remove the agar, sterilized by filtration (0.2 µm) and stored at 4°C.

Sampling bacterial and phage densities

Bacteria and phage densities were estimated by serial dilutions in 0.85% NaCl solution followed by plating. The total density of bacteria was estimated on LB (1.6%) agar plates. To estimate the densities of free phage, chloroform was added to suspensions before serial dilutions. These suspensions were mixed with 0.1mL of overnight MHII grown cultures of wild-type *S. aureus* Newman (about 5×10^8 cells per mL) in 4 mL of LB soft (0.65%) agar and poured onto semi-hard (1%) LB agar plates.

Parameter estimations

The parameters critical for the interaction of the PYO^{Sa} phage and *S. aureus* Newman used in this study were estimated in independent experiments MHII broth. The maximum growth rate of different clones of *S. aureus* Newman was measured by Bioscreen, as described in (42). Phage burst sizes (β) were estimated with one-step growth experiments similar to (43). Adsorption of PYO^{Sa} to *S. aureus* was estimated as described in (43).

Serial transfer experiments

All serial transfer experiments were carried out in 10ml MHIII cultures grown at 37 C with vigorous shaking. The cultures were initiated by 1:100 dilution from 10-mL overnight cultures grown from single colonies. Phage was added to these cultures to reach the initial density of approximately 10^6 PFU/mL. At the end of each transfer, 0.1mL of each culture was transferred into flasks with fresh medium (1:100 dilution). Simultaneously, 0.1mL samples were taken for estimating the densities of colony-forming units (CFU) and plaque-forming units (PFU), by serial dilution and plating on solid agar.

Antibiotics and their Sources

Tetracycline, Oxacillin, Vancomycin, Kanamycin, Streptomycin (all from Sigma Aldrich), Azithromycin (Tocris), Daptomycin (MP Biochemicals), Rifampin (Applichem) and Linezolid (Chem- Impex International).

Whole-genome sequencing

For sequencing individual clones of *S. aureus*, genomic DNA was prepared using the MasterPure Gram-Positive kit, following the manufacturer's instructions (Epicentre, Illumina Inc., Madison, Wisconsin). Final DNA was resuspended in EB buffer. Genomic DNA concentrations were measured in a Qubit 2.0 Fluorometer (Invitrogen via ThermoFisher Scientific). DNA was diluted to 0.2 ng/ μ L in water (Sigma-Aldrich, Sweden), and the samples were prepared for whole genome sequencing according to Nextera® XT DNA Library Preparation Guide (Illumina Inc., Madison, Wisconsin). After the PCR clean up-step, samples were validated for DNA fragment size distribution using the Agilent High Sensitivity D1000 ScreenTape System (Agilent Technologies, Santa Clara, California). Sequencing was performed using a MiSeq™ desktop sequencer, according to the manufacturer's instructions (Illumina Inc., Madison, Wisconsin). The sequencing data were aligned and analyzed in CLC Genomics Workbench version 11.0 (CLCbio, Qiagen, Denmark).

Acknowledgements

We thank Melony Ivey and Esther Lee for superb technical help. We are grateful to our Staphylococcus maven, Abraham (Jon) Moller, for providing strains and sage advice. And, to Waqas Chaudhry, Andrew Smith, and the reviewers of an earlier incarnation of this report for helpful comments and suggestions. Funds for this research were provided by grants from the US National Institutes of General Medical Sciences, R01 GM091875 and R35 GM 136407 (Bruce Levin) and Vetenskapsrådet (the Swedish Research Council) (2017-03593) and from the Scandinavian Society for Antimicrobial Chemotherapy (SLS-693211, SLS-876451), Diarmaid Hughes. These funders had no role in study design, data collection and interpretation, or the decision to submit the work for publication.

References

1. F. D'Herelle, *The Bacteriophage and Its Behavior* (The Williams & Wilkins Company, Baltimore, MD., 1926), pp. 578.
2. M. Ansaldi *et al.*, "French Phage Network"-Third Meeting Report. *Viruses* **10** (2018).
3. G. Watts (2017) Phage therapy: revival of the bygone antimicrobial. (Elsevier).
4. K. E. Kortright, B. K. Chan, J. L. Koff, P. E. Turner, Phage Therapy: A Renewed Approach to Combat Antibiotic-Resistant Bacteria. *Cell Host Microbe* **25**, 219-232 (2019).
5. C. Schmidt, Phage therapy's latest makeover. *Nat Biotechnol* **37**, 581-586 (2019).
6. B. Martel, S. Moineau, CRISPR-Cas: an efficient tool for genome engineering of virulent bacteriophages. *Nucleic Acids Res* **42**, 9504-9513 (2014).
7. T. K. Lu, J. J. Collins, Engineered bacteriophage targeting gene networks as adjuvants for antibiotic therapy. *Proc Natl Acad Sci U S A* **106**, 4629-4634 (2009).
8. V. N. Krylov, [Phagotherapy in terms of bacteriophage genetics: hopes, perspectives, safety, limitations]. *Genetika* **37**, 869-887 (2001).
9. S. J. Labrie, J. E. Samson, S. Moineau, Bacteriophage resistance mechanisms. *Nat Rev Microbiol* **8**, 317-327 (2010).
10. Z. Moradpour, A. Ghasemian, Modified phages: novel antimicrobial agents to combat infectious diseases. *Biotechnol Adv* **29**, 732-738 (2011).
11. R. J. Dubos, J. H. Straus, C. Pierce, The Multiplication of Bacteriophage in Vivo and Its Protective Effect against an Experimental Infection with Shigella Dysenteriae. *J Exp Med* **78**, 161-168 (1943).

12. J. J. Bull, B. R. Levin, T. DeRouin, N. Walker, C. A. Bloch, Dynamics of success and failure in phage and antibiotic therapy in experimental infections. *BMC Microbiol* **2**, 35 (2002).
13. R. T. Schooley *et al.*, Development and Use of Personalized Bacteriophage-Based Therapeutic Cocktails To Treat a Patient with a Disseminated Resistant *Acinetobacter baumannii* Infection. *Antimicrob Agents Chemother* **61** (2017).
14. B. K. Chan *et al.*, Phage treatment of an aortic graft infected with *Pseudomonas aeruginosa*. *Evol Med Public Health* **2018**, 60-66 (2018).
15. R. M. Dedrick *et al.*, Engineered bacteriophages for treatment of a patient with a disseminated drug-resistant *Mycobacterium abscessus*. *Nat Med* **25**, 730-733 (2019).
16. G. Xia *et al.*, Wall Teichoic Acid-Dependent Adsorption of Staphylococcal Siphovirus and Myovirus. *Journal of Bacteriology* **193**, 4006-4009 (2011).
17. T. Suzuki, J. G. Swoboda, J. Campbell, S. Walker, M. S. Gilmore, In vitro antimicrobial activity of wall teichoic acid biosynthesis inhibitors against *Staphylococcus aureus* isolates. *Antimicrob Agents Chemother* **55**, 767-774 (2011).
18. G. Xia, T. Kohler, A. Peschel, The wall teichoic acid and lipoteichoic acid polymers of *Staphylococcus aureus*. *International Journal of Medical Microbiology* **300**, 148-154 (2010).
19. S. McCallin, S. A. Sarker, S. Sultana, F. Oechslin, H. Brussow, Metagenome analysis of Russian and Georgian Pyophage cocktails and a placebo-controlled safety trial of single phage versus phage cocktail in healthy *Staphylococcus aureus* carriers. *Environ Microbiol* **20**, 3278-3293 (2018).
20. S. O'Flaherty *et al.*, Genome of Staphylococcal Phage K: a New Lineage of Myoviridae Infecting Gram-Positive Bacteria with a Low G+C Content. *Journal of Bacteriology* **186**, 2862-2871 (2004).
21. Y. Sato'o *et al.*, Tailor-made gene silencing of *Staphylococcus aureus* clinical isolates by CRISPR interference. *PLoS One* **13**, e0185987-e0185987 (2018).

22. S. E. Hsieh, H. H. Lo, S. T. Chen, M. C. Lee, Y. H. Tseng, Wide host range and strong lytic activity of Staphylococcus aureus lytic phage Stau2. *Appl Environ Microbiol* **77**, 756-761 (2011).
23. E. Kutter *et al.*, Phage therapy in clinical practice: treatment of human infections. *Current pharmaceutical biotechnology* **11**, 69-86 (2010).
24. J. Dickey, V. Perrot, Adjunct phage treatment enhances the effectiveness of low antibiotic concentration against Staphylococcus aureus biofilms in vitro. *PLoS One* **14**, e0209390 (2019).
25. P. D. Fey *et al.*, A Genetic Resource for Rapid and Comprehensive Phenotype Screening of Nonessential Staphylococcus aureus Genes. *mBio* **4**, e00537-00512 (2013).
26. B. R. Levin, F. M. Stewart, L. Chao, Resource - limited growth, competition , and predation: a model and experimental studies with bacteria and bacteriophage. *American Naturalist* **977**, 3-24 (1977).
27. S. Cao, D. L. Huseby, G. Brandis, D. Hughes, Alternative Evolutionary Pathways for Drug-Resistant Small Colony Variant Mutants in Staphylococcus aureus. *mBio* **8** (2017).
28. A. M. Strandén, K. Ehlert, H. Labischinski, B. Berger-Bachi, Cell wall monoglycine cross-bridges and methicillin hypersusceptibility in a femAB null mutant of methicillin-resistant Staphylococcus aureus. *J Bacteriol* **179**, 9-16 (1997).
29. M. W. Climo, K. Ehlert, G. L. Archer, Mechanism and suppression of lysostaphin resistance in oxacillin-resistant Staphylococcus aureus. *Antimicrob Agents Chemother* **45**, 1431-1437 (2001).
30. J. M. Monteiro *et al.*, Peptidoglycan synthesis drives an FtsZ-treadmilling-independent step of cytokinesis. *Nature* **554**, 528-532 (2018).
31. I. C. McCall, N. Shah, A. Govindan, F. Baquero, B. R. Levin, Antibiotic Killing of Diversely Generated Populations of Nonreplicating Bacteria. *Antimicrob Agents Chemother* **63** (2019).

32. N. Q. Balaban *et al.*, Publisher Correction: Definitions and guidelines for research on antibiotic persistence. *Nat Rev Microbiol* **17**, 460 (2019).
33. H. Nicoloff, K. Hjort, B. R. Levin, D. I. Andersson, The high prevalence of antibiotic heteroresistance in pathogenic bacteria is mainly caused by gene amplification. *Nat Microbiol* **4**, 504-514 (2019).
34. B. Kahl *et al.*, Persistent Infection with Small Colony Variant Strains of *Staphylococcus aureus* in Patients with Cystic Fibrosis. *The Journal of Infectious Diseases* **177**, 1023-1029 (1998).
35. C. von Eiff *et al.*, A site-directed *Staphylococcus aureus* hemB mutant is a small-colony variant which persists intracellularly. *Journal of Bacteriology* **179**, 4706-4712 (1997).
36. P. Sendi, R. A. Proctor, *Staphylococcus aureus* as an intracellular pathogen: the role of small colony variants. *Trends in Microbiology* **17**, 54-58 (2009).
37. C. von Eiff, *Staphylococcus aureus* small colony variants: a challenge to microbiologists and clinicians. *International Journal of Antimicrobial Agents* **31**, 507-510 (2008).
38. W. N. Chaudhry *et al.*, Leaky Resistance and the conditions for the existence of lytic bacteriophage. *PLoS Biology* **16**:e2005971 (2018).
39. N. Baumert *et al.*, Physiology and Antibiotic Susceptibility of *Staphylococcus aureus* Small Colony Variants. *Microbial Drug Resistance* **8**, 253-260 (2002).
40. T. Norstrom, J. Lannergard, D. Hughes, Genetic and phenotypic identification of fusidic acid-resistant mutants with the small-colony-variant phenotype in *Staphylococcus aureus*. *Antimicrob Agents Chemother* **51**, 4438-4446 (2007).
41. B. R. Levin *et al.*, A Numbers Game: Ribosome Densities, Bacterial Growth, and Antibiotic-Mediated Stasis and Death. *MBio* **8** (2017).

42. J. Concepción-Acevedo, H. N. Weiss, W. N. Chaudhry, B. R. Levin, Malthusian parameters as estimators of the fitness of microbes: A cautionary tale about the low side of high throughput. *PLoS One* **10**, e0126915 (2015).
43. E. L. Ellis, M. Delbruck, The Growth of Bacteriophage. *J Gen Physiol* **22**, 365-384 (1939).

Supporting Information

I. Host range

In our report, we summarized the evidence that PYO^{Sa}'s host range included all 83 clinical isolates of *Staphylococcus aureus* tested. Much of those data are from LabCorp. The methods used are summarized in the following and the results obtained are summarized in Supplemental Table S1.

Methods

The methods LabCorp employed, as detailed below, to test the sensitivity of these strains to PYO^{Sa} were somewhat different than those we employed and presented in our report (See Results Section 1).

- (i) The *S. aureus* strains tested were streaked for single colonies on TSB agar.
- (ii) These single colonies were inoculated in 3 ml LB broth and grown overnight with shaking at 37°C.
- (iii) The overnight cultures were diluted by 1:30 in 3ml LB broth and grown with shaking at 37°C to an OD 600nm of between 0.3-1.0.
- (iv) 300ul of these cultures were added to 3ml LB soft (0.3% or 0.5%) agar supplemented with 3ul 1M CaCl₂ and 3ul 1M MgCl₂ which were spread onto LB agar plates to form a lawn.
- (v) 5μl of the PYO^{Sa} lysates were spotted onto the lawns and incubated overnight.
- (vi) Lysates were prepared from original spot plates and then re-spotted on the original spot plate host bacteria following the above conditions.

The Key to scoring the results of this assay follows:

Key	
-	No lysis
-/+	Weak lysis
+	Partial lysis (cloudy)
++	Complete lysis

Table S1 Assay for the susceptibility of *S. aureus* to phage PYO^{Sa}. Data provided by LabCorp.

Species	Strain	Spot	Re-spot
<i>Staphylococcus aureus</i>	27660	++	++
<i>Staphylococcus aureus</i>	RN6390	+	-/+
<i>Staphylococcus aureus</i>	502A	++	++
<i>Staphylococcus aureus</i>	6538	++	++
<i>Staphylococcus aureus</i>	25923	++	++
<i>Staphylococcus aureus</i> subsp. aureus	12600	++	++
<i>Staphylococcus aureus</i>	RN4220	++	++
Species	Strain	Spot	Re-spot

<i>Staphylococcus aureus</i> subsp. aureus	BAA-1721	++	++
<i>Staphylococcus aureus</i> subsp. aureus	14775	++	++
<i>Staphylococcus aureus</i>	AR0461	++	++
Methicillin-resistant <i>S. aureus</i>	017-243	++	++
Methicillin-resistant <i>S. aureus</i>	041-332	+	-/+
Methicillin-resistant <i>S. aureus</i>	045-188	++	++
Methicillin-resistant <i>S. aureus</i>	038-401	+	++
Methicillin-resistant <i>S. aureus</i>	049-841	++	++
Methicillin-resistant <i>S. aureus</i>	USA300	+	-
Methicillin-resistant <i>S. aureus</i>	002-639	+	+
Methicillin-resistant <i>S. aureus</i>	049-60	++	++
Methicillin-resistant <i>S. aureus</i>	026-485	++	++
Methicillin-resistant <i>S. aureus</i>	011-719	++	++
Methicillin-resistant <i>S. aureus</i>	045-696	++	++
Methicillin-resistant <i>S. aureus</i>	BAA-1707	+	-/+
Methicillin-resistant <i>S. aureus</i>	BAA-1717	+	+
Methicillin-resistant <i>S. aureus</i>	BAA-1720	++	++
Methicillin-resistant <i>S. aureus</i>	BAA-1747	+	-
Species	Strain	Spot	Re-spot

Methicillin-resistant <i>S. aureus</i>	BAA-1754	++	+
Methicillin-resistant <i>S. aureus</i>	BAA-1761	++	++
Methicillin-resistant <i>S. aureus</i>	BAA-1763	++	++
Methicillin-resistant <i>S. aureus</i>	BAA-1764	++	-/+
Methicillin-resistant <i>S. aureus</i>	BAA-1766	++	+
Methicillin-resistant <i>S. aureus</i>	BAA-1768	++	++
Methicillin-resistant <i>S. aureus</i>	BAA-41	++	++
Methicillin-resistant <i>S. aureus</i>	BAA-42	++	-/+
Multidrug-resistant resistant <i>S. aureus</i>	BAA-44	++	+
Methicillin-resistant <i>S. aureus</i>	BAA-1683	++	+
Methicillin-resistant <i>S. aureus</i>	BAA-2094	++	++
Methicillin-resistant <i>S. aureus</i>	BAA-2313	++	++
Methicillin-resistant <i>S. aureus</i>	33592	++	+
Methicillin-resistant <i>S. epidermis</i>	700583	-/+	-
Methicillin-resistant <i>S. haemolyticus</i>	700564	-/+	-
<i>Staphylococcus aureus</i> subsp. aureus	BAA-1718	++	++
Methicillin-resistant <i>S. aureus</i>	AR0462	++	-
Methicillin-resistant <i>S. aureus</i>	AR0463	++	++
Species	Strain	Spot	Re-spot

Methicillin-resistant <i>S. aureus</i>	AR0464	-/+	-/+
Methicillin-resistant <i>S. aureus</i>	AR0465	++	+
Methicillin-resistant <i>S. aureus</i>	AR0466	+	-
Methicillin-resistant <i>S. aureus</i>	AR0467	++	+
Methicillin-resistant <i>S. aureus</i>	AR0468	++	+
Methicillin-resistant <i>S. aureus</i>	AR0469	++	+
Methicillin-resistant <i>S. aureus</i>	AR0470	++	+
Methicillin-resistant <i>S. aureus</i>	AR0471	++	-
Methicillin-resistant <i>S. aureus</i>	AR0472	++	++
Methicillin-resistant <i>S. aureus</i>	AR0473	++	++
Methicillin-resistant <i>S. aureus</i>	AR0474	++	+
Methicillin-resistant <i>S. aureus</i>	AR0475	+	-
Methicillin-resistant <i>S. aureus</i>	AR0476	++	++
Methicillin-resistant <i>S. aureus</i>	AR0477	++	++
Methicillin-resistant <i>S. aureus</i>	AR0478	++	++
Methicillin-resistant <i>S. aureus</i>	AR0479	++	++
Methicillin-resistant <i>S. aureus</i>	AR0480	+	+
Methicillin-resistant <i>S. aureus</i>	AR0481	++	++
Species	Strain	Spot	Re-spot

Methicillin-resistant <i>S. aureus</i>	AR0482	++	++
Methicillin-resistant <i>S. aureus</i>	AR0483	++	++
Methicillin-resistant <i>S. aureus</i>	AR0484	++	++
Methicillin-resistant <i>S. aureus</i>	AR0485	++	++
Methicillin-resistant <i>S. aureus</i>	AR0486	++	++
Methicillin-resistant <i>S. aureus</i>	AR0487	+	-/+
Methicillin-resistant <i>S. aureus</i>	AR0488	+	-/+
Methicillin-resistant <i>S. aureus</i>	AR0489	+	-
Methicillin-resistant <i>S. aureus</i>	AR0490	++	++
Methicillin-resistant <i>S. aureus</i>	AR0491	-/+	-
Methicillin-resistant <i>S. aureus</i>	AR0492	+	-

II. Variation in the demise – resurrection population dynamics presented in Figure 1B.

To explore the generality of the PYO^{Sa} – *S. aureus* Newman serial transfer results presented in Figure 1B, we performed the experiments with ten 2 ml and six 10ml cultures. Both had effectively the same initial densities of phage and bacteria. The dynamics of only one of the ten 2 ml samples serially transferred were similar to the demise–resurrection dynamics observed from Figure 1B. While all six 10 ml serial transfer cultures were turbid by the 5th transfer, some did not become turbid until the 4th transfer. We interpret this observation to be consistent with the hypothesis that the resurrection of these phage-exposed bacteria is a stochastic process in *S. aureus* and thus is more likely to occur in the 10ml populations because the total number of bacteria is 5-fold greater than that in 2 ml cultures.

Also consistent with this stochastic hypothesis is that the time before the recovery of the *S. aureus* population due to the ascent of small colony variants, S, is variable. In Figure 1B, all three serial transfer populations started the recovery to high density by the second transfer. This was not the case for a repeat of this experiment. The recovery of one of the three populations (noted in red) started at the end of the first transfer (Figure S1A).

In Figure 1D, where the serial transfer cultures were initiated with *S. aureus* isolated at the end of serial transfer experiments with the PYO^{Sa}, the evolved bacteria, the phage were maintained in one of three cultures and were lost in two. In the repeat of this experiment with three independently evolved strains, the phage were lost in all three (Figure S1B).

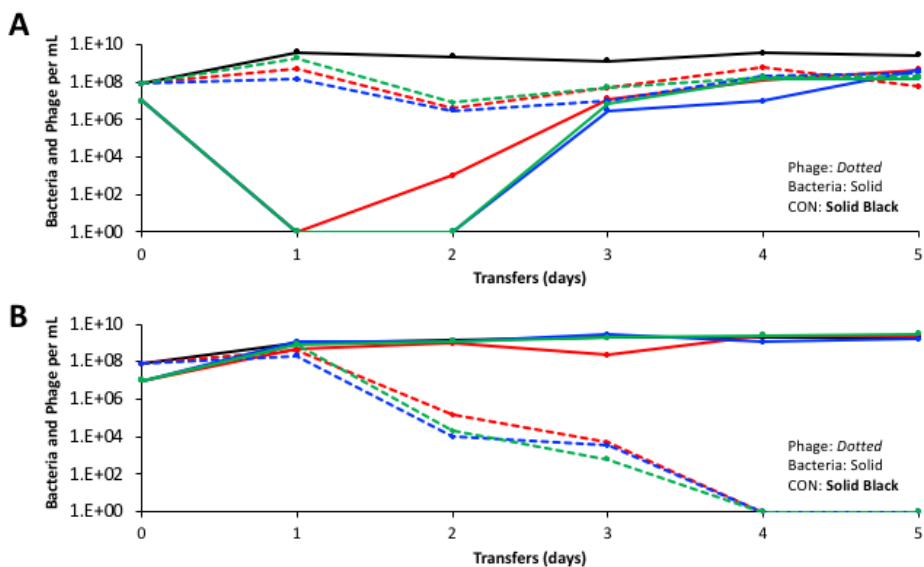


Figure S1 Changes in the densities of bacteria and phage in (1/100) 10 ml serial transfer cultures of *S. aureus* Newman and PYO^{Sa} and a phage-free control, CON. **A**) Three independent cultures initiated with *S. aureus* Newman (W) that had not previously been exposed to PYO^{Sa}. **B**) Three independent cultures initiated with *S. aureus* Newman (E) obtained from the 5th transfer of independent serial passage experiments with *S. aureus* Newman mixed with PYO^{Sa}.

III. Genotypes and phenotypes of *S. aureus* mutants selected in the presence of PYO^{Sa}

Table S2. Small colony variant (S) mutants selected by exposure to PYO^{Sa}

in experiments of the type shown in Fig. 1B.

Gene	Mutation
<i>femA</i>	G>T (nt -9)
<i>femA</i>	G>A (nt -12)
<i>femA</i>	M1I
<i>femA</i>	Δ G124 - A126
<i>femA</i>	I171AN
<i>femA</i>	Y327D
<i>femA</i>	72 bp Dup (nt 987-1058)
<i>femA</i>	G331D
<i>femA</i>	G368V

Mutations in *femA* were identified after whole genome sequencing of small colony mutants.

Table S3. Genotypes of evolved (E) mutants from 5 different small colony variant (S) mutants.

Primary Mutation	Compensatory mutation(s)	Annotated function of compensatory mutation(s)
<i>femA</i> nt(-9) G>T	<i>mgrA</i> W48*	HTH-type transcriptional regulator
<i>femA</i> Met1Ile	<i>csbA</i> Δ258bp	DEAD-box ATP-dependent RNA helicase
<i>femA</i> Met1Ile	<i>mgrA</i> Δnt 160-216	HTH-type transcriptional regulator
<i>femA</i> Met1Ile	<i>rpsL</i> G126D	30S ribosomal protein
<i>femA</i> Tyr327Asp	<i>clpX</i> G177fs	ATP-dependent Clp protease
<i>femA</i> Tyr327Asp	CNH36_00075 H326Q	Cyclic-di-AMP phosphodiesterase
<i>femA</i> Tyr327Asp	CNH36_06865 Δnt 1011-1058	2-oxoacid:acceptor oxidoreductase subunit alpha
<i>femA</i> Tyr327Asp	CNH36_12385 W117L	Lysostaphin
<i>femA</i> Tyr327Asp	<i>dacA</i> V78G	Diadenylate cyclase
<i>femA</i> Tyr327Asp	<i>femA</i> Q346R	<i>femA</i> internal suppressor
<i>femA</i> Tyr327Asp	<i>lpdA</i> E245*	Dihydrolipoyl dehydrogenase
<i>femA</i> Tyr327Asp	<i>nrnA</i> Q303*	Bifunctional oligoribonuclease PAP phosphatase
<i>femA</i> Tyr327Asp	<i>sarA</i> K72::IS1181	Transcriptional regulator
<i>femA</i> Tyr327Asp	<i>sarA</i> R84C, CNH36_04445 N3S	Transcriptional regulator, uncharacterized protein
<i>femA</i> Tyr327Asp	<i>sarA</i> Y51*	Transcriptional regulator
<i>femA</i> Gly331Asp	<i>lipL</i> V94fs	Octanoyl-[GcvH]:protein N-octanoyltransferase
<i>femA</i> Gly331Asp	<i>sarA</i> Inv (nt -51 to +78)	Transcriptional regulator
<i>femA</i> Gly331Asp	<i>sarA</i> R90K	Transcriptional regulator
<i>femA</i> Gly368Val	<i>rpoD</i> G77fs	RNA polymerase sigma factor

Secondary compensatory mutations associated with the evolved state were identified by whole genome sequencing.

Table S4. Relative growth rates and MICs of wild-type (W), small colony variant (S), and evolved (E) compensated mutants.

Genotype / Mutations		Growth Rate	MIC mg/L	
Primary	Compensatory	Relative	Lysostaphin	Oxacillin
Wild-type		1	≤ 0.008	2
<i>femA</i> M1I		0.53	1	0.25
<i>femA</i> I171N		0.48	4	0.125
<i>femA</i> Y327D		0.59	>4	0.125
<i>femA</i> Y327D	<i>femA</i> Q346R	0.76	0.125	0.063
<i>femA</i> Y327D	<i>sarA</i> K72::IS1181	0.93	>4	0.125
<i>femA</i> G331D		0.53	>4	0.063
<i>femA</i> G331D	<i>sarA</i> INV (nt -51- +78)	0.94	>4	0.125

Doubling time for wild-type is 25.8 min.

IV. A hypothesis to account for the population and evolution dynamics of the *S. aureus* and PYO^{Sa}.

In our article we postulated that the dynamics presented in Figure 1B can be attributed to the generation of small colonies from the wild-type *S. aureus* Newman and their ascent due to selection mediated by PYO^{Sa} phage. While the PYO^{Sa} phage adsorb to these small colony variants, they do not kill them, and the infecting phage are lost. The phage are maintained because the small colony variants are of low fitness and continually produce normal or near normal colony variants, an “evolved” state, that can support the replication of the phage. These evolved cells are not stable and continually produce small colonies. This hypothesis is illustrated in Figure S2.

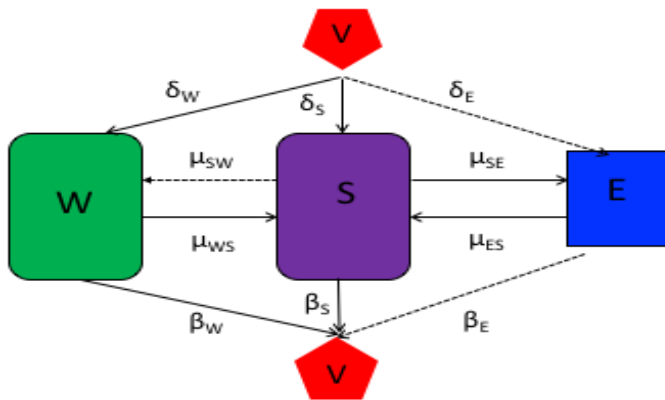


Figure S2 – A population dynamic model to account for the observed changes in the densities of bacteria and phage in Figure 1B. The variables, W, S and E are, respectively the wildtype *S. aureus* Newman, small colonies, and the evolved bacteria, cells per ml, and V the PYO^{Sa} phage, particles per ml. The parameters δ_w , δ_s and δ_e are the adsorption rate constants per cell per ml. The parameters β_w , β_s and β_e are the number of phage particles produced per infected cell burst. We assume that $\beta_s = 0$, the S are infected by PYO^{Sa} but the phage do not replicate or kill these bacteria. The parameters μ_{SW} , μ_{WS} , μ_{SE} and μ_{ES} are the transition rates, per cell per hour, between the different states.

The population is in liquid culture in which there is a limiting resource of concentration, r , $\mu\text{g/ml}$. The net growth rate of the bacteria is proportional to its maximum rate of growth and a hyperbolic function of concentration of the limiting resource, r , $\mu\text{g/ml}$ and a constant, k_i which is the concentration of the resource when the growth rate is half its maximum value., where the subscript i is W, S or E (1). We assume there is no latent period and upon adsorption, W and E are killed by the phage and instantly produce, β_W and β_E phage particles per cell (2). Although the phage adsorb to the small colonies, they are not killed. As the bacteria grow the concentration of the resource declines at a rate proportional to the net growth rates of the bacteria, and a conversion efficiency parameter, e_i $\mu\text{g/ml}$, the conversion efficiency, which is the amount of resource needed to produce a new cell of that type (3). To account for the declining physiological state of the bacteria as the bacteria approach stationary phase, $r=0$, we assume that the rates of phage adsorption and transitions between states is proportional to the net growth rate of that cell line. With these definitions and assumptions, the rates of change in the densities of the bacteria of different states, the density of free phage, and the concentration of the resource are given by the below set of coupled differential equations.

$$\begin{aligned} \frac{dr}{dt} &= -v_W \cdot \psi_W(r) \cdot e_W \cdot W - v_S \cdot \psi_S(r) \cdot e_S \cdot S - v_E \cdot \psi_E(r) \cdot e_E \cdot E \\ \frac{dW}{dt} &= v_W \cdot \psi_W(r) \cdot W - \delta_W \cdot W \cdot V \cdot \psi_W(r) + \mu_{SW} \cdot E \cdot \psi_S(r) - \mu_{WS} \cdot W \cdot \psi_W(r) \\ \frac{dS}{dt} &= v_S \cdot \psi_S(r) \cdot S + \mu_{WS} \cdot W \cdot \psi_W(r) - \mu_{SW} \cdot S \cdot \psi_S(r) \\ \frac{dE}{dt} &= v_E \cdot \psi_S(r) \cdot E - \delta_E \cdot E \cdot V \cdot \psi_E(r) + \mu_{SE} \cdot S \cdot \psi_S(r) - \mu_{ES} \cdot E \cdot \psi_E(r) \\ \frac{dV}{dt} &= \delta_W \cdot W \cdot V \cdot \psi_W(r) \cdot \beta_W + \delta_E \cdot E \cdot V \cdot \psi_E(r) - \delta_S \cdot V \cdot S \cdot \psi_S(r) \\ \text{where } \psi_W(r) &= \frac{r}{(r+k_W)}, \psi_S(r) = \frac{r}{(r+k_S)}, \text{ and } \psi_E(r) = \frac{r}{(r+k_E)} \end{aligned}$$

Numerical Solutions – Simulations: To solve this set of coupled differential equations and those for the models that follow we use Berkeley Madonna. The population growth and phage infection parameters employed for these numerical solutions, simulations, are of the range estimated for PYO^{Sa} and *S. aureus* Newman in MHII medium. To simulate a serial transfer mode of population maintenance every 24 hours there is a 100-fold reduction in densities of the bacteria and phage and the resource concentration is restored to its maximum level of 1000 μ g per ml. For copies of the program and instructions for it use write to blevin@emory.edu.

Simulation Results: In Figure S3, we follow the changes in the densities of the bacteria and phage in simulated serial populations. As observed in Figure 1B, the model predicts, as seen in Figure S3A, that upon the first encounter with the phage, V , the density of susceptible cells, W , and the total cell density of the bacteria, NT , will decline whilst that of the phage increase. In subsequent transfers, the population of bacteria recovers and becomes dominated by small colonies. As a consequence of the transitions between the different states of bacteria, the phage and all three bacterial populations are maintained with small colonies dominating the bacterial community. If we make the small colonies less efficient in the use of the resource, $e_c = 5 \times 10^{-6}$ rather than 5×10^{-7} , the total density of the small colony population is lower (Figure S3A). When cultures of just small colonies are started without the phage, they are ultimately diluted out due to their lower growth rate and low production rate in the absence of the phage and are overtaken by the evolved population being generated through reversion from small colonies (Figure S3B). When the evolved cells and phage are mixed, as observed in Figure 1D, the population recovers to full density more rapidly than when sensitive cells and phage are mixed (Figure S3C). However, in these simulations, the phage continue to be maintained, which was the case for only one of the two parallel experiments in the main body of the paper and in none of the parallel experiments presented in supplemental Figure S1B. This model can also account for why the mixture of the ancestral *S. aureus* Newman and small colony variants can maintain the phage (Figure 1E) with little effect on the density of bacteria (Figure S3D).

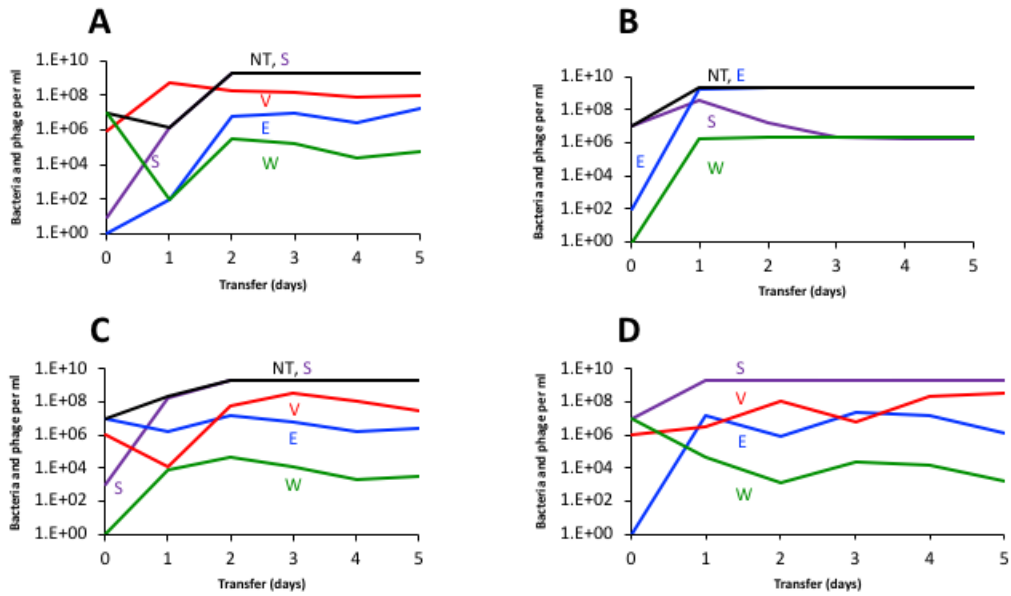


Figure S3 Simulated serial transfer populations. Changes in the densities of bacteria and phage in serial transfer culture. Standard parameters, $v_W = v_E = 1.7$, $v_S = 0.5$, $\delta_W = \delta_E = \delta_S = 2 \times 10^{-7}$, $\beta_W = \beta_E = 80$, $\beta_S = 0$, $e_w = e_e = 5 \times 10^{-7}$, $e_c = 5 \times 10^{-6}$, $C = 1000$, $k_W = k_E = 1$, $k_S = 10$, $\mu_{WS} = 10^{-6}$, $\mu_{SW} = 10^{-6}$, $\mu_{ES} = 10^{-3}$, $\mu_{SE} = 10^{-3}$. NT is the total density of bacteria. **A)** Serial transfer population with W and V and few S and E. **B)** Serial transfer population initiated with S and minority populations of W and E, but no phage. **C)** Serial transfer population initiated with E and phage and minority populations of S and W. **D)** Serial transfer populations initiated with a mixture of W, S, and V and a minority of E.

V – The joint action of bactericidal antibiotics and phage.

In our article, we postulate that the reason bactericidal antibiotics in combination with phage do worse than phage alone (Figure 4) can be attributed to the antibiotics reducing the density of bacteria and thereby the capacity of the phage to replicate. We illustrate this with the following model of the joint action of antibiotics and a bactericidal antibiotic.

Model of the joint action of antibiotics and phage: There are two populations of bacteria enumerated in cells per ml. The populations are respectively W (wild-type, which are sensitive to antibiotics) and P (persisters which are sensitive to the phage but phenotypically resistant to antibiotics). There is a single antibiotic of concentration A in $\mu\text{g/ml}$, a lytic phage of density V particles per ml, and a limiting resource r in $\mu\text{g/ml}$. The sensitive bacteria grow at a maximum rate, v_N , with the net growth/death rate $\psi(A,r)$ being proportional to the concentration of the antibiotic and the limiting resource voila,

$$\psi(A,r) = \left[v_{WMAX} - \left[(v_{WMAX} - v_{WMIN}) \cdot \left(\frac{\left(\frac{A}{MIC} \right)^\kappa}{\left(\left(\frac{A}{MIC} \right)^\kappa - \left(\frac{v_{WMIN}}{v_{WMAX}} \right) \right)} \right) \right] \right] \cdot \frac{r}{(r+k)}$$

Where v_{WMAX} (>0) is the maximum growth rate, v_{WMIN} (<0) is the minimum growth rate/maximum kill rate, MIC the minimum inhibitory concentration of the antibiotic, and a shape parameter, κ , such that the greater the value of κ the more acute the function.

The persisters, P, are non-replicating bacteria that are resistant to the antibiotic. The phage adsorb to the persisters but do not replicate on them. The rate constant of adsorption of the phage to sensitive cells is δ_w and that to the persisters δ_p . Infections of phage to sensitive cells produce β phage particles per cell. With a rate y per cell per hour, sensitive cells produce persisters, $W \rightarrow P$, and with a rate x per cell per hour, persisters produce sensitive cells, $P \rightarrow W$. With these definitions and assumptions, the rates of change in the densities of phage and the concentration of the resources are given by

$$\frac{dr}{dt} = -\psi(A,r) \cdot W \cdot e - v_{MAXW} \cdot \psi(r) \cdot W \cdot e$$

$$\frac{dW}{dt} = \psi(A,r) \cdot W - \delta_w \cdot W \cdot V \cdot \psi(r) - y \cdot W + x \cdot P$$

$$\frac{dP}{dt} = y \cdot W - x \cdot P - \delta_p \cdot P \cdot V \cdot \psi(r)$$

$$\frac{dV}{dt} = \delta_w \cdot V \cdot W \cdot \beta \cdot \psi(r) - \delta_p \cdot P \cdot V \cdot \psi(r)$$

where $\psi(r) = \frac{r}{(r+k)}$ and $e \mu g$ is the amount of the limiting resource need to produce a new cell

Numerical Solutions – Simulations: To solve these equations and simulate the dynamics, we use Berkeley Madonna. Copies of the programs are available from blevin@emory.edu.

Results

In Figure S4, we illustrate the rate of change in the total density of bacteria with a bactericidal antibiotic alone, with phage alone, and with the phage and antibiotic together. The rate of decline in the density of bacteria is lowest in the simulations where antibiotics are used alone. The highest rate of decline in the density of bacteria is obtained in the simulation where phage are used alone. When phage are used in combination with bactericidal antibiotics, they do not increase in density to the same extent that they do in the absence of the antibiotics. The leveling off in the density of bacteria is a consequence of persistence (4-6).

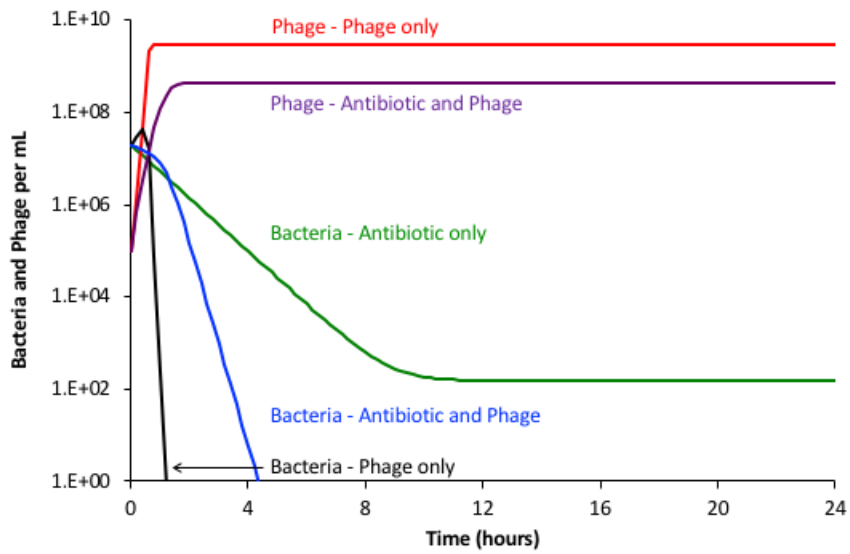


Figure S4 Simulation results: changes in the densities of bacteria and phage with different treatments.

Parameter values. $v_{S\text{MAX}}=2.0$, $v_{S\text{MIN}}=-2.0$, $\kappa=1.0$, $\text{MIC}=1.0$, $e=5 \times 10^{-7}$, $k=1.0$, $x=y=10^{-5}$, $\delta_p=10^{-8}$, $\delta_s=10^{-8}$, $\beta=50$,

$A = 2 \mu\text{g/ml}$, $r(0)=1000$.

VI. Persistence and heteroresistance

In the absence of phage in serial transfer culture, the super MIC concentration of oxacillin does not eliminate the bacteria but rather maintains the density at levels markedly lower than the antibiotic-free controls (Figure 4 A center). We postulate that this can be attributed to persistence in serial transfer culture. In the absence of phage, ciprofloxacin initially reduces the density of *S. aureus* but in subsequent transfers, the density of these bacteria return to levels within the range anticipated for antibiotic-free controls (Figure 4A bottom). We postulated that these pharmacodynamics can be attributed to heteroresistance (7). In the following, we present the evidence for persistence for oxacillin-treated cultures and heteroresistance for ciprofloxacin-treated cultures. Using a mathematical - computer simulation model, we illustrate how these postulated mechanisms can account for the observed pharmacodynamics of these drugs with *S. aureus* Newman.

A model for antibiotics in serial transfer culture with persistence and heteroresistance: There are three populations of bacteria, wild-type, heteroresistant, and persisters with designations and densities, W, H, and P cells per ml; a single antibiotic of concentration, A $\mu\text{g/ml}$; and a limiting resource of concentration r $\mu\text{g/ml}$. As in our model of the joint action of antibiotics and phage (II), we assume that the rate of growth, of bacteria of each of these states, $\psi_i(A,r)$ is a product of a Hill function for the antibiotic (4), and a Monod function for the resource (1).

$$\psi_i(A,r) = \left[v_{iMAX} - \left[(v_{iMAX} - v_{iMIN}) \cdot \left(\frac{\left(\frac{A}{MIC_i} \right)^k}{\left(\left(\frac{A}{MIC_i} \right)^k - \left(\frac{v_{iMIN}}{v_{iMAX}} \right) \right)} \right) \right] \right] \cdot \frac{r}{(r+k)}$$

The subscript i represents the bacterial population, W, H, or P. For strain i, v_{iMAX} (>0) is the maximum growth rate, v_{iMIN} (<0) the minimum growth rate/maximum kill rate, and MIC_i the minimum inhibitory

concentration of the antibiotic. Bacteria of the same state have the same Hill coefficient and Monod constant, respectively κ and k .

In these simulations, we assume the persisters can replicate, $v_{P_{MAX}} > 0$, and are resistant to the antibiotics, $v_{P_{MIN}} = 0$. As in (7), the MIC for the antibiotic of the heteroresistant cells is greater than the sensitive, $MIC_H > MIC_S$. There is a transition from W to P and from P to W respectively at rates, x and y per cell per hour, and a transition from W to H and H to W at rates, x_H , and y_H per cell per hour. Finally, we assume that the concentration of the antibiotic can decline at a rate d per hour. With these definitions and assumptions, the rates of change in the densities of the bacterial population and concentration of the antibiotic and resource are given by:

$$\begin{aligned}\frac{dr}{dt} &= -\psi(r) \cdot e \cdot (W \cdot v_{MAXW} + H \cdot v_{MAXH}) \\ \frac{dW}{dt} &= \psi_W(A, r) \cdot W - x \cdot W + y \cdot P - x_H \cdot W + y_H \cdot H \\ \frac{dP}{dt} &= v_{MAXP} \cdot \psi(r) \cdot P + x \cdot W - y \cdot P \\ \frac{dH}{dt} &= \psi_H(A, r) \cdot H + x_H \cdot W - y_H \cdot H \\ \frac{dA}{dt} &= -d \cdot A \\ \text{where } \psi(r) &= \frac{r}{(r + k)}\end{aligned}$$

Numerical Solutions: To solve these equations, we simulate the changes in the densities of the bacterial populations and changes in the concentration of the antibiotics with Berkeley Madonna. As in our experiments, in these simulations every 24 hours the density of the bacteria is reduced by a factor of 100, and new resources and antibiotics are added.

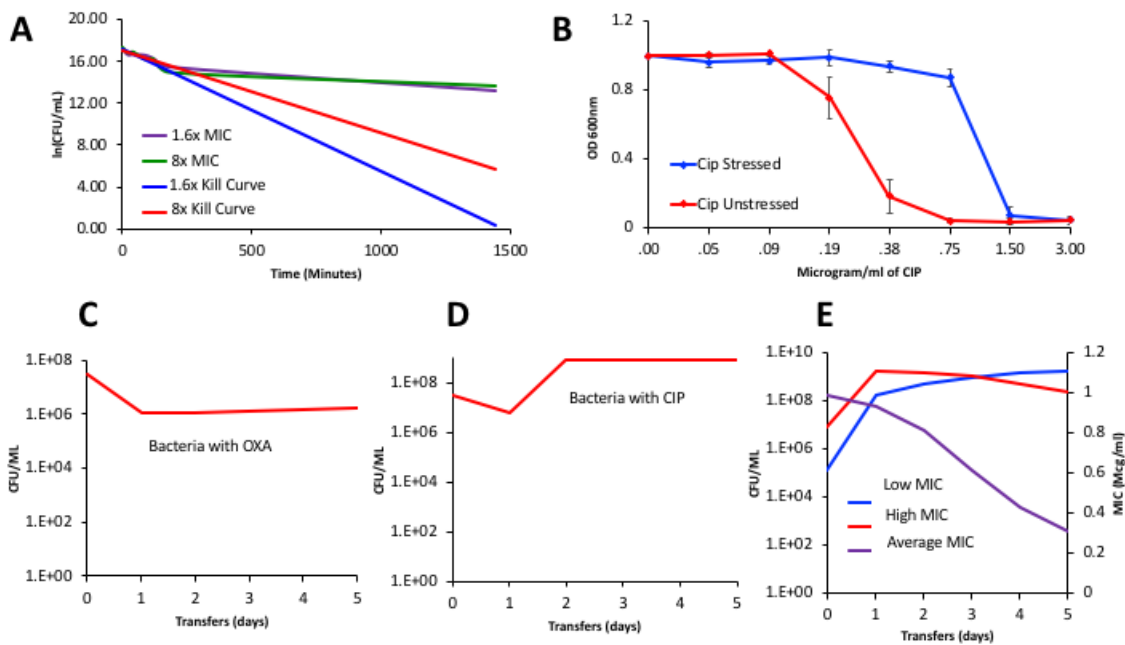


Figure S5 *S. aureus* antibiotic pharmacodynamics **A)** Natural log of the change in density of growing cultures of *S. aureus* Newman exposed to 1.6X and 8X MIC, low and high for 24 hours (1440 minutes). The green and purple lines are experimental changes in density estimated by plating; while the blue and red lines are the results of a linear regression of the changes in density estimated during the first 180 minutes of exposure. **B)** Changes in the optical density of experimental cultures of *S. aureus* Newman exposed to 5 µg/ml ciprofloxacin, mean and standard error of the ODs for three replicas. In red are cells that were treated with ciprofloxacin and then transferred without the presence of this drug for seven days before the MIC determination was performed. In blue are cells that were treated with ciprofloxacin for one week before the MIC was performed. **C, D, E)** Simulation Results Common parameters: $v_{MAXS}=1.5$, $v_{MINS}=-0.6$, $v_{MAXSR} = 1.2$, $v_{MINSR}=-3$, $k_s=1$, $k_h=1$, $k=1$, $e=5.0E-7$ **C)** Changes in the densities of bacteria in serial transfer culture with persistence with parameters in the range estimated for *S. aureus* in oxacillin. Specific parameters: $v_p=0.2$, $MIC_S= 1.8$, $x_p=1.0e-4$, $y_p=1E-3$, $A_{MAX}=3$. Exposure to oxacillin does not start until the second transfer (compare to Figure 4A center). **D) and E)** Heteroresistance for ciprofloxacin $MIC_S= 0.218$, $MIC_H=1$, $x=1E-6$, $y=1e-3$, $x_p=0$, $y_p=0$, $A_{MAX}=0.5$ Changes in the densities of bacteria in serial transfer culture with

heteroresistance with parameters in the range estimated for *S. aureus* in ciprofloxacin. Exposure to ciprofloxacin doesn't start until the second transfer (compare to Figure 4A bottom). **E)** Unique Parameters for E: $MIC_S = 0.218$, $MIC_H = 1$, $x = 1E-6$, $1E-3$ $x_P = 0$, $y_P = 0$. Simulation of the changes in the densities of bacteria and average MIC of the antibiotic mixture of the low MIC sensitive and the high MIC heteroresistant populations in serial transfer culture in the absence of the antibiotics.

In Figure S5A, we present the results of time-kill experiments with *S. aureus* Newman exposed to oxacillin. The observation that the rate of decline in the viable density of sensitive cells during the first few hours of exposure considerably exceeds the rate of decline later in the experiment is what would be anticipated for persistence. In Figure S5B, we present the evidence for heteroresistance; higher concentrations of ciprofloxacin are needed to kill cultures initiated with bacteria exposed to ciprofloxacin than to kill bacteria cultured in the absence of this drug. If we allow for persistence with parameters in the range estimated for oxacillin the predicted changes in the density of *S. aureus* Newman in serial transfer culture with oxacillin are similar to those observed (compare Figures S4A and S4C). If we allow for heteroresistance with the parameter in the range estimated for *S. aureus* Newman in serial transfer culture with ciprofloxacin the results are similar to those observed (compare figures S5B and S5D). One property of heteroresistance is that when the bacteria are removed from the drug, the resistant population will decline in frequency, and the average MIC will decline to levels similar to that of the original sensitive population (7), see Figure S5E.

Supplemental references

1. J. Monod, The growth of bacterial cultures. *Annual Review of Microbiology* **3**, 371-394 (1949).
2. B. R. Levin, F. M. Stewart, L. Chao, Resource - limited growth, competition , and predation: a model and experimental studies with bacteria and bacteriophage. *American Naturalist* **977**, 3-24 (1977).
3. F. M. Stewart, B. R. Levin, Resource partitioning and the outcome of interspecific competition: a model and some general considerations. *American Naturalist* **107**, 171-198 (1973).
4. R. R. Regoes *et al.*, Pharmacodynamic functions: a multiparameter approach to the design of antibiotic treatment regimens. *Antimicrob Agents Chemother* **48**, 3670-3676 (2004).
5. C. Wiuff *et al.*, Phenotypic tolerance: antibiotic enrichment of noninherited resistance in bacterial populations. *Antimicrob Agents Chemother* **49**, 1483-1494 (2005).
6. N. Q. Balaban *et al.*, Definitions and guidelines for research on antibiotic persistence. *Nat Rev Microbiol* **17**, 441-448 (2019).
7. H. Nicoloff, K. Hjort, B. R. Levin, D. I. Andersson, The high prevalence of antibiotic heteroresistance in pathogenic bacteria is mainly caused by gene amplification. *Nat Microbiol* **4**, 504-514 (2019).

Chapter 11

Chapter 11

The role of innate immunity, antibiotics, and bacteriophages in the course of bacterial infections and their treatment

Reprinted from: Brandon A. Berryhill, Teresa Gil-Gil, Christopher Witzany, David A. Goldberg, Nic M.

Vega, Roland R. Regoes, Bruce R. Levin. 2025. The role of innate immunity, antibiotics, and bacteriophages in the course of bacterial infections and their treatment. bioRxiv. <https://doi.org/10.1101/2024.08.23.609294>

Abstract

Critical to our understanding of infections and their treatment is the role the innate immune system plays in controlling bacterial pathogens. Nevertheless, many in vivo systems are made or modified such that they do not have an innate immune response. Use of these systems denies the opportunity to examine the synergy between the immune system and antimicrobial agents. In this study we demonstrate that the larva of *Galleria mellonella* is an effective in vivo model for the study of the population and evolutionary biology of bacterial infections and their treatment. To do this we test three hypotheses concerning the role of the innate immune system during infection. We show: i) sufficiently high densities of bacteria are capable of saturating the innate immune system, ii) bacteriostatic drugs and bacteriophages are as effective as bactericidal antibiotics in preventing mortality and controlling bacterial densities, and iii) minority populations of bacteria resistant to a treating antibiotic will not ascend. Using a highly virulent strain of *Staphylococcus aureus* and a mathematical computer-simulation model, we further explore how the dynamics of the infection within the short term determine the ultimate infection outcome. We find that excess immune activation in response to high densities of bacteria leads to a strong but short-lived immune response which ultimately results in a high degree of mortality. Overall, our findings illustrate the utility of the *G. mellonella* model system in conjunction with established in vivo models in studying infectious disease progression and treatment.

Significance statement

Central to our understanding of the course of bacterial infections and their treatment is the contribution of the innate immune system. We use the larvae of *Galleria mellonella* to test hypothesis about the role of the innate immune system on *Staphylococcus aureus* infections. We demonstrate that the innate immune system of these larvae can control the infection and be saturated by high bacterial densities. As a consequence of this innate immune system, bacteriostatic drugs and phages are as effective as bactericidal drugs, minority populations of bacteria resistant to antibiotics do not ascend, and excessive immune activation can result in increased mortality. Our findings illustrate the utility of *G. mellonella* as a model for studying infections dynamics and therapeutic strategies.

Introduction

The design of regimens for antibiotic therapy are based almost exclusively on studies of the pharmacodynamics of combinations of bacteria and antibiotics (1). These studies nearly always neglect the role of the host immune system in controlling infections, and thereby the synergy between antibiotics and the innate immune system to the course of treatment (2, 3). It is well known that an infected host's immune system plays a major role in the clearance of bacterial infections (4). The omission of the immune response also applies to studies with animal models that are specifically designed and intended to increase our knowledge of infections beyond what we learn from in vitro experiments. These animal model studies commonly rely on mice that have no innate immune system (5-8). Prior to infection and treatment these mice are treated with agents such as cyclophosphamide, thereby making them neutropenic (9). Consequently, studies with these mice do not further our understand of the contribution of the innate immune system to the course of treatment of infections with antimicrobial agents.

Theoretical studies suggest and a few experiments with non-immunocompromised animals have generated the following hypotheses: i) in the absence of chemotherapy, if the density of the infecting bacterial population is great enough to saturate the innate immune system, the infection will fail to be controlled (10); ii) bacteriostatic antibiotics and bacteriophages can be as effective as bactericidal drugs in controlling the infection (10, 11); and iii) minority populations of bacteria that are resistant to the treating antibiotic will not ascend (12).

To test these hypotheses and explore the role of the innate immune system in the control of bacterial infections and test the above hypotheses, we employ, in a quantitative fashion, the larvae of the Wax Moth, *Galleria mellonella* (13). These larvae have several qualities which make them amenable as a model system for this study: i) they have an innate immune system (14), primarily hemocytes (which are analogous to the neutrophils of mammals) and melanocytes; ii) the morbidity and mortality of these larvae is reflected by a change in melanization—which is to say a darkening of the larva, serving as a useful early indicator (15); iii) they are inexpensive and experiments can be highly replicated; iv) manipulation of this system is relatively facile and has

no bioethical constraints; v) the densities of infecting bacteria can readily be estimated; and vi) there is an extensive literature of using this model to discover new anti-infective compounds, particularly anti-fungals (16).

In this study we first confirm that those results obtained with *G. mellonella* mirror those obtained in other systems employed for studying the dynamics of infection, particularly those with non-neutropenic mice. Using these larvae and *Staphylococcus aureus*, we explore the appropriateness of this system for testing the above hypotheses. Lastly, we quantitatively characterize the dynamics of bacterial infection with a highly toxigenic strain of *S. aureus* (17). To explore an unanticipated result obtained from the dynamics of infection, we employ a mathematical computer-simulation model.

Results

Larvae Survival Is Dependent on the Density of Infecting Bacteria

Previous work in mice has shown that mortality is dependent on the initial bacterial inoculum (18). Critically, there appears to be a threshold effect under which mortality is mild, but once the inoculum exceeds that threshold density, mortality rises sharply. This result also obtains in *G. mellonella* when they are infected with *S. aureus*, where we find the critical threshold to be approximately 10^6 CFU/larva (Figure 1). Our experiments support the hypothesis that in the absence of chemotherapy, if the density of the infecting bacterial population is great enough to saturate the innate immune system, the infection will fail to be controlled.

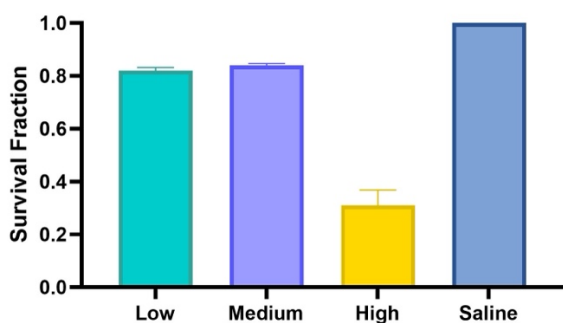


Figure 1. Larvae survival at 24 hours with different bacterial inoculum densities. Larvae were injected with *S. aureus* MN8 at 10^4 CFU/larva (turquoise), 10^6 CFU/larva (purple), 10^8 CFU/larva (yellow), or saline (blue). Mortality was assessed at 24 hours. Presented are means and standard deviations for the fraction of survival (N= 80 larvae). Low, medium, and high differ with saline at $p < .0001$ ****; low is statistically different from high at $p < .001$ ***; medium is different with high at $p < .001$ ***; and low and medium are not statistically different.

Treatment With Antibiotics and Phage Increases Larvae Survival

Theory predicts, and limited experiments confirm, that treatment of an infection with antibiotics will increase survival and that this outcome is independent of the type of antibiotic (19). To test these predictions in our *in vivo* system, we infected larvae of *G. mellonella* with a high density of *S. aureus* and treated immediately. All therapies tested increased survival to 90-100%, supporting the idea that bacteriostatic and bactericidal antibiotics are equally effective when the innate immune system is present (Figure 2A). Interestingly, treatment with a highly lytic bacteriophage, PYO^{Sa} (20), was able to replicate in these larvae (Supplemental Figure 1) and subsequently increase survival of the larvae by 10-fold, a result comparable to the antibiotics used.

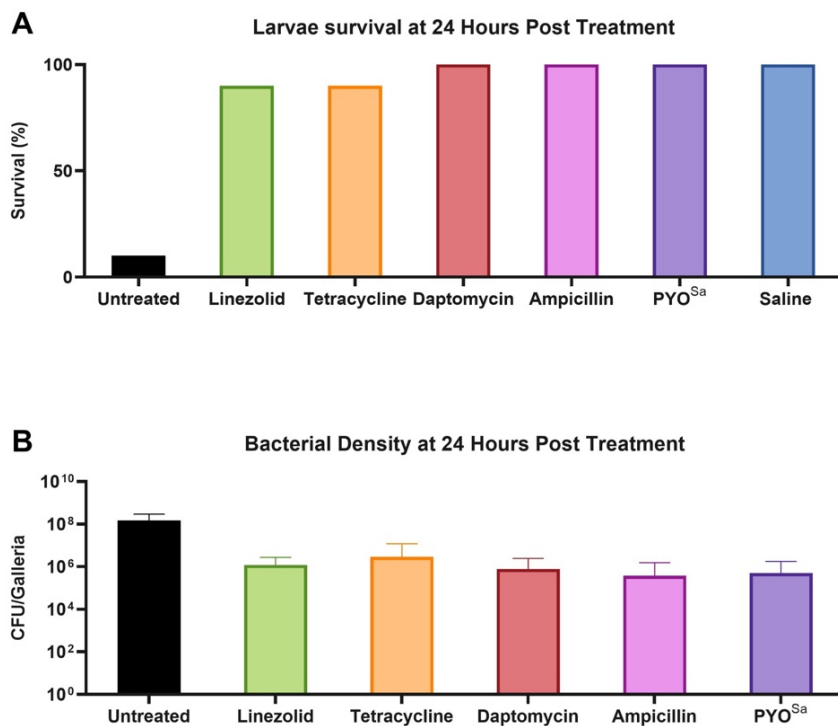


Figure 2. The effects of treatment on survival and bacterial density. Larvae were injected with 10^8 CFU/larva of *S. aureus* MN8 and either were untreated (black) or immediately treated with linezolid (green; a bacteriostatic drug), tetracycline (orange; a bacteriostatic drug), daptomycin (red; a bactericidal drug), ampicillin (pink; a bactericidal drug), or the phage PYO^{Sa} (purple). 24 hours after treatment, (A) mortality was assessed and compared to an uninfected saline injection control (blue) and (B) the final bacterial density was determined. Shown are means and standard deviations (N=20 larvae). All treatment conditions statistically differ from the saline in terms of survival and density ($p < .0001$ **** and $p < .0001$ ****, respectively).

All therapies, be they bacteriostatic antibiotics, bactericidal antibiotics, or lytic phage, decrease bacterial load to roughly the same level. While treatment drastically increases survival, it does not clear the infecting bacteria: however, all treatments decrease bacterial densities to around or below the critical threshold of 10^6 CFU/larva. This result is consistent with immune exhaustion being responsible for mortality during a bacterial infection. Of note, the strain of *S. aureus* used here, MN8, produces a beta-lactamase and has an ampicillin minimum

inhibitory concentration in excess of 256 $\mu\text{g}/\text{mL}$, demonstrating that the effective treatment can occur even when the underlying bacteria is resistant to the treating antibiotic.

Antibiotic-Resistant Bacteria do not Increase in Frequency Under Antibiotic Treatment

It has been postulated from mathematical modelling (21) and demonstrated using mice (12) that one role the innate immune system plays in controlling infections is preventing the increase in frequency of rare antibiotic resistant mutants. To explore if this result would be obtained with *G. mellonella*, larvae were infected with rifampin resistant and rifampin sensitive *S. aureus* MN8 at a ratio of 0.0001 to 1. Infected larvae were immediately treated with rifampin and the ratio of resistant to sensitive cells enumerated after 24 hours (Figure 3). As anticipated, the antibiotic resistant population did not substantially increase in the presence of antibiotic treatment.

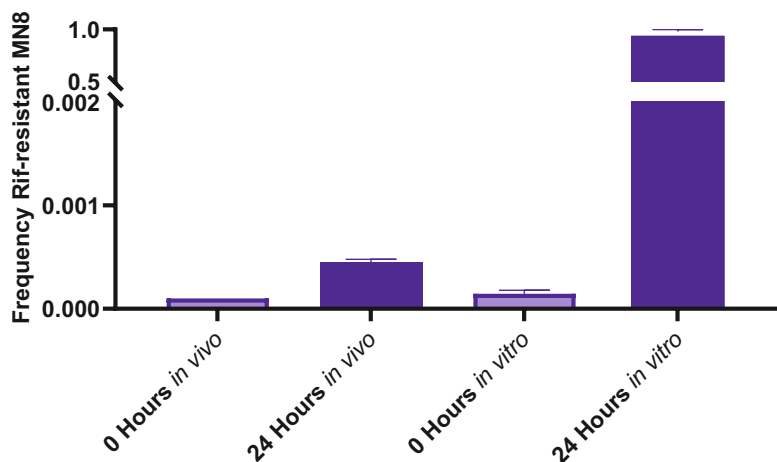


Figure 3. Invasion when rare of an antibiotic resistant subpopulation. At a ratio of 0.0001 to 1, rifampin-resistant *S. aureus* MN8 and rifampin-susceptible *S. aureus* MN8 were injected into 10 larvae which were immediately treated with rifampin. After 24 hours, larvae were sacrificed and the final ratio of rifampin resistant to rifampin sensitive cells in vivo determined. As a control for the in vivo invasion when rare, at a ratio of 0.0001 to 1, rifampin-resistant *S. aureus* MN8 and rifampin-susceptible *S. aureus* MN8 were mixed and immediately treated with rifampin. Flasks were grown overnight and the ratio of rifampin resistant to rifampin sensitive cells in vitro determined. Presented are means and standard deviations for each timepoint. The frequencies of Rif-resistant bacteria at 24 hours between the in vivo and in vitro conditions are highly statistically significant ($p < .0001$ ****)

The Innate Immune System Functions via ETosis

G. mellonella have three components to their innate immune response (22): i) antimicrobial peptides (AMP) and lytic enzymes, ii) melanocytes, and iii) hemocytes. Since *S. aureus* MN8 has many anti-AMP responses, this humoral response does not contribute to the dynamics of infection. Further, since the infections are systemic, the production of melanin by melanocytes is not able to sequester the *S. aureus*, thus this response plays little role in controlling the infection (14). This leaves only hemocytes as the main determinant of the immune response. These hemocytes, upon detection of lipopolysaccharides or wall teichoic acid, release their DNA

which forms an extracellular trap (ET) in a process called ETosis (23). Here, we show that the presence of a GFP labeled *S. aureus* is sufficient to cause ETosis (Figure 4A) and that these ETs can be degraded by DNase (Figure 4B).

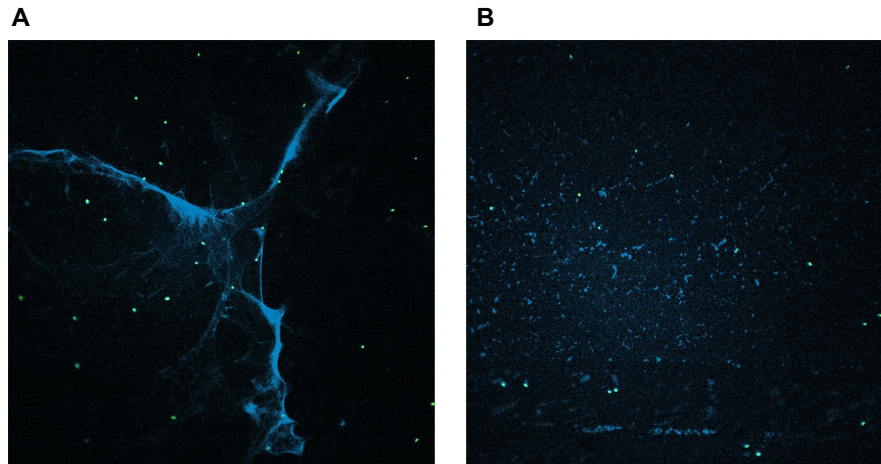


Figure 4. Hemocytes producing ETs. Hemocytes were incubated for 30 minutes with GFP producing *S. aureus* before being treated with either saline (A) or DNase (B) and then stained with DAPI.

Dynamics of Infection in *G. mellonella*

To understand the dynamics of how the immune system controls infections with *S. aureus* of differing initial densities, we infected 160 larvae with 10^4 , 10^6 , or 10^8 CFU/larva and sacrificed half of each condition at 4 hours (Figure 5A) and the other half at 24 hours (Figure 5B). Shown in Supplemental Figure 2 are the dynamics of each timepoint, and inoculum density separated. Of note, at 4 hours there is a convergence of all initial densities to around 10^5 - 10^6 (the critical density), illustrating that the immune system can control the infection in the short term regardless of initial infection density. However, at 24 hours, while the 10^4 CFU/larva and 10^6 CFU/larva initial inoculum infections are still controlled and around the same density as at 4 hours, the 10^8 CFU/larva initial inoculum infections have dramatically increased in density, corresponding with the high mortality seen in Figure 1. We hypothesize that the reason for the failure of the immune system to control the infection at 24

hours while it was readily capable of doing so at 4 hours is immune exhaustion. The hemocytes release their DNA in a density-dependent manner, thus, to control the high inoculum infection at 4 hours, a large number of the hemocytes had to release their DNA and ultimately die, leading to an exhaustion of these immune cells, leading to the infection not being controlled by 24 hours. To ensure that the results observed at 24 hours are the endpoints of the infection, rather than an intermediate stage, larvae were infected and maintained for 72 hours (Supplemental Figure 3). Notably, both survival and infection dynamics are qualitatively similar to that observed at 24 hours, with the exception that the average density of bacteria per larvae in the low inoculum group is several logs lower at 72 hours—showing a higher degree of infection control.

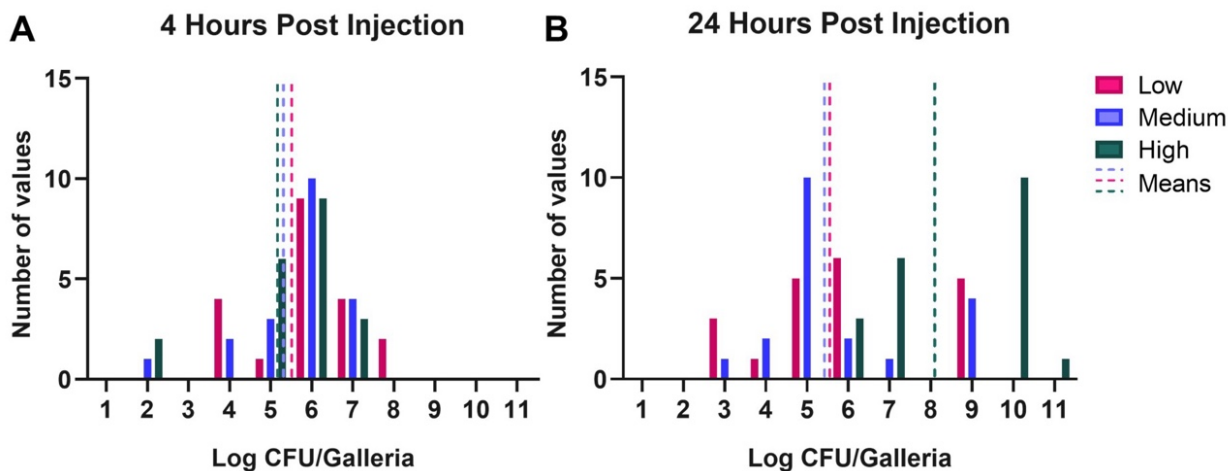


Figure 5. Dynamics of infection. Larva were infected with three different densities of *S. aureus* MN8: low (10^4 CFU/larva; pink), medium (10^6 CFU/larva; purple), or high (10^8 CFU/larva; green) and were sacrificed after (A) 4 or (B) 24 hours post infection. Shown are the number of larvae within each \log_{10} CFU. The mean of the CFU at each timepoint for each inoculum density is presented as a dotted line of the same color. For each condition $N=80$ individual larvae.

A Model of the Observed Infection Dynamics

We developed a mathematical population model that incorporates the innate immune system to explain the within-host dynamics of bacteria observed in the infected larva. By explicitly modeling both the bacterial population and the host immune response, we can evaluate how different initial bacterial population sizes affect infection dynamics and assess when the immune system is overwhelmed. We simulate the innate immune response under the assumption that immune effectors (E) need to be activated, then encounter (unprotected) bacteria (U), and subsequently take time to kill them (24). Further, our model accounts for persistent infections with low population sizes (as observed in Figure 2B) by incorporating a protected sanctuary site where bacteria evade the immune system (P). See Supplemental Information for model equations and detailed description.

Our simulations show that infection dynamics highly depend on the initial size of the inoculum (i.e., the starting population of bacteria U_0). For simulations with inoculum sizes above 10^5 cells, the total bacteria population grows to around 10^8 cells within 15 hours (Figure 6). This growth is mainly driven by the unprotected bacteria U and limited by the carrying capacity of the unprotected compartment (K_U , Table S1). Over the same time frame, the activated immune effectors E decline and ultimately reach zero. This decline shows that all E are engaged with bacteria U , but still cannot kill U faster than they are growing, hence the infection cannot be controlled, and the immune system gets overwhelmed.

For inoculum sizes below 10^5 we observe an initial drop in the total bacterial population, caused by the removal of U by E . Simultaneously, in response to the presence of U , more effectors get activated resulting in an increase in E until the total of available effectors is reached ($E_{tot} = 10^5$). The larger the initial population U the faster this activation happens. However, all simulations with inocula $<10^5$ quickly start to regrow after this initial decline. This recovery is not driven by U , but rather by growth of P in the protected compartment. A fraction of bacteria U migrates from the unprotected to the protected compartment before being removed by the immune system, where they grow protected from E until they reach capacity ($K_p = 1500$) – this occurs faster with larger initial inocula. Consequently, the infections become controlled and persistent, because E can keep in check the bacteria which migrate out of protection, stopping the total bacterial population from growing further, but E are unable to eradicate the bacteria P in the protected compartment.

In summary, our simulations show that there is a critical threshold inoculum size of around $\sim 10^5$ cells, at or above which infections quickly overwhelm the immune effectors, i.e. the immune effector population goes to zero, and bacteria grow to capacity in both the unprotected (U) as well as the protected compartment (P) (Figure S4). If the inoculum is below this critical threshold the infection can be controlled by the immune effectors, and the final total population size corresponds to the carrying capacity of the protected site (K_p). This critical threshold for the inoculum size, above which all infections become uncontrollable, exists for a wide range of parameters – and is primarily influenced by the immune effector killing rate (h_1) and effector engagement rate (h_2) (see Figure S5 and S6).

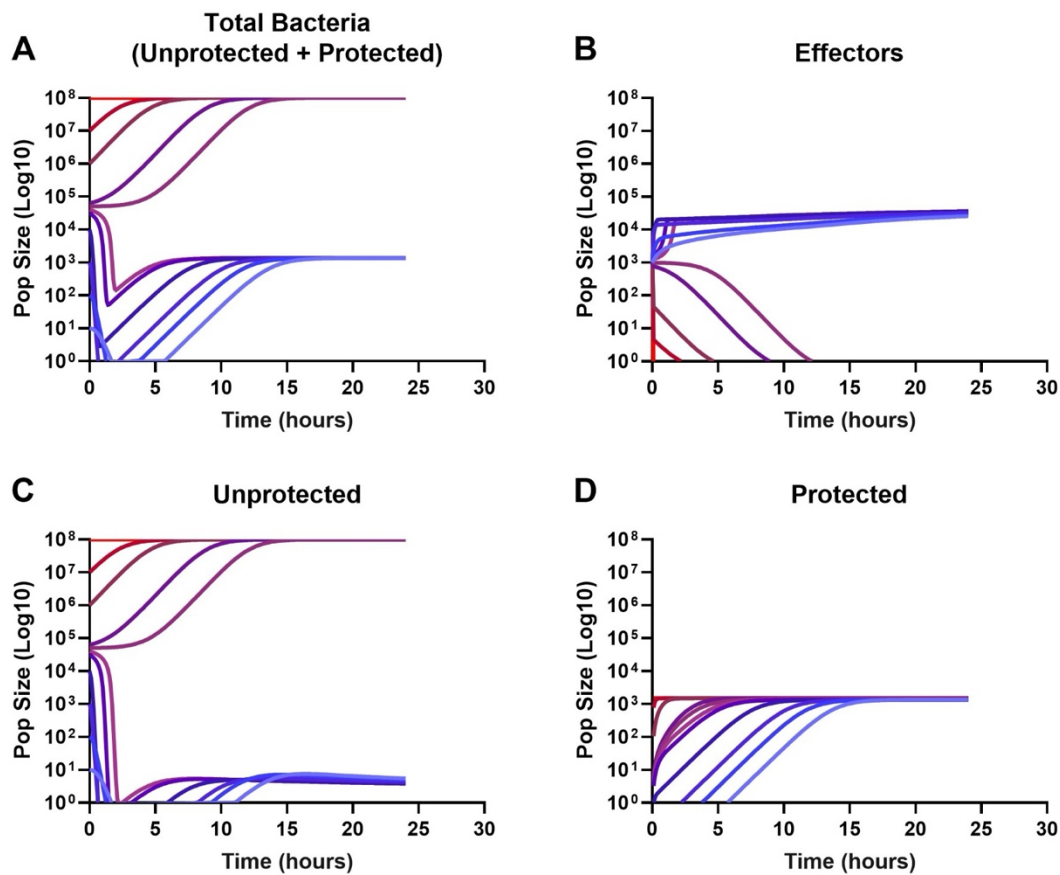


Figure 6. Simulated dynamics of within-host bacterial infections. Shown are the population sizes over time of (a) the total bacteria present within the host (sum of U and P), (b) the number of activated host immune effectors (E), (c) the number of bacteria in the unprotected site (U) and (d) the protected site (P). Each panel shows multiple-colored lines, with colors representing individual simulation runs with increasing inoculum sizes (blue to red). The following parameter values were used for this simulation: $r = 1$, $K_u = 10^8$, $K_p = 1.5 \times 10^3$, $f = 0.001$, $b = 0.1$, $E_0 = 10^3$, $E_{tot} = 10^5$, $h_1 = 0.001$, $h_2 = 0.001$, $d = 0.01$, $a = 0.01$, $g = 0.5$, and $s = 0.001$. See Methods and Table S1 for model and parameter descriptions.

Discussion

Critical to understanding both the course of an infection and how treatment changes that course is the innate immune system. Most in vivo systems traditionally used to study the treatment of bacterial infections purposefully ignore the immune response (5-8). In this study, we present a promising system that has an innate immune system which has elements which are analogous to those in humans, in that it works via ETosis, as neutrophils do. This highly tractable, inexpensive system with no animal biosafety considerations is the larva of the wax moth, *Galleria mellonella*. This system enabled us to test three major hypotheses about the functioning of the innate immune system during the course of an infection: i) in the absence of therapy, if the infecting bacteria is of sufficient density, the immune system will saturate and the infection will progress uncontrolled; ii) bacteriostatic antibiotics and phages will reduce mortality to the same degree as bactericidal drugs; and iii) minority antibiotic-resistant populations will not increase in frequency during antibiotic treatment.

While testing the above hypotheses with *G. mellonella*, we found support for each hypothesis that mirrors the previous results obtained in parallel experiments in mice. First, we demonstrated that the mortality is highly dependent on the initial inoculum such that initial densities above 10^6 CFU per larva results in mortality above 85%. Second, we found evidence that both bacteriostatic antibiotics and phages were as successful as bactericidal drugs in reducing mortality as well as in reducing the bacterial density after 24 hours. Interestingly, ampicillin was as effective as the other treatments even though this strain of *S. aureus* is highly resistant to beta-lactams. This result, while unintuitive, mirrors that seen in clinics where it has been observed that if the underlying bacteria is resistant to that antibiotic, treatment will still succeed 60% of the time (25, 26). Third, unlike in vitro experiments, when a larva is infected with a minority population of antibiotic-resistant bacteria, under treatment with the drug to which the minority population is resistant, this sub-population does not increase in frequency and invade when rare.

In addition to providing support to the above hypotheses, our results raise an interesting question about how the dynamics of infection underlie morbidity and mortality. When the initial inoculum is low ($\sim 10^4$ CFU per

larva) or medium ($\sim 10^6$ CFU per larva), the infection density will rise slightly at 4 hours but be controlled at a fixed density over 24 hours. More importantly, survival will be nearly 100%. When the initial inoculum is high ($\sim 10^8$ CFU per larva) the bacterial density will be brought down such that the density at 4 hours is the same as the low and medium inocula. In stark contrast to the other two conditions, by 24 hours, the density of bacteria in the larvae will not be controlled and often in excess of 10^8 CFU per larva, leading to a mortality of nearly 90%.

These dynamics were unexpected and suggest that the immune system responds very aggressively when there is a high inoculum, such that the host's cells responsible for the control of the infection are exhausted. This result is consistent with the mechanism by which these larvae control infections. When hemocytes detect lipopolysaccharides or (in this case) teichoic acids, they lyse and release their DNA in an effort to control the infection (27). Therefore, the higher the initial inoculum, the more immune cell death can be expected. Ultimately, the exhaustion of these cells leads to the failure of the immune system to control the infection by 24 hours. In support of this premise, we constructed a mathematical computer-simulation model. With biologically plausible parameters and assumptions, the model was able to recapitulate the above-described experimental results and found a critical inoculum above which the immune system will not control the infection.

In supporting the use of *G. mellonella* more broadly as a model system for infections, one needs to be able to manipulate the system, in particular, their innate immune response. Others have performed genetic manipulation of the system as well as chemical ablation of the innate immune system (28-30). We also performed this chemical procedure on the larvae to determine the effects that removing the immune response has on the infection dynamics (Supplemental Figure 7). First, in support that the immune ablation was successful, we lose the dose-dependent response of morbidity, mortality, and infection dynamics. However, *a priori* we expected mortality to trend to 0 and the infection densities to be extremely high. This is the opposite of what we saw. Generally, survival was high and the bacterial density in the surviving larvae was extremely low

(less than 10^1 CFU/larvae in most cases). On the other hand, the density of bacteria in the dead larvae was high. This provides another line of evidence that 10^6 CFU/larvae is this critical threshold for predicting survival. While we cannot currently experimentally explain these results, we do have a hypothesis we intend to test in the future. It is not currently clear where the *S. aureus* are located in the larva during an infection, however it is well known that Staphylococcus has an intra-phagocytic niche (31). As these larvae have an existing, stable microbiome, could it be that the only niche available for the infecting bacteria to fill is inside of these immune cells? Thus, when we ablate the immune response by killing the immune cells, the bacteria have nowhere to proliferate and thus are lost from the larvae. Supporting this hypothesis is the high density found in the dead larvae, in these cases due to technical error or some other uncontrolled variation, it is possible the chemicals were not able to fully ablate the immune system, thus leaving a niche for the bacteria to proliferate in, and now since the immune system is suppressed, the infection is fatal and the bacteria reach a high density.

While this study has focused on the dynamics of infection, future studies will seek to elucidate the conditions under which treatment with antibiotics and/or phages will be synergistic or antagonistic to the innate immune system dynamics observed here. This system, with its phenotypic marker for sickness, will enable us to treat infections not on a fixed timeline, but instead when the individual is displaying symptoms of morbidity. This allows a more realistic analogue to how humans are treated, as no one seeks medical attention when they become infected, but instead they wait until they are sick. Allowing this delay in treatment is vital to understanding the dynamics of infections under anti-infective therapy.

Materials and Methods

Growth media: All experiments were conducted in Muller Hinton II (MHII) Broth (90922-500G) obtained from Millipore. All bacterial quantification was done on Lysogeny Broth (LB) agar (244510) plates obtained from BD. E-tests were performed on MH agar plates made from MH broth (M391-500g) with 1.6% agar obtained from HiMedia. Overnights of GFP labeled *S. aureus* Newman were grown with 25 µg/mL of ampicillin.

Growth and infection conditions: All experiments were conducted at 37 °C.

Bacterial strains: All experiments were performed with *S. aureus* MN8 obtained from Tim Read of Emory University. *S. aureus* MN8 was marked with streptomycin resistance to enable differential plating from the larva microbiota. Green fluorescent protein labelled *S. aureus* Newman was obtained from Dr. Nic Vega of Emory University.

Antibiotics: Daptomycin (D2446) was obtained from Sigma-Aldrich. Tetracycline (T17000) was obtained from Research Products International. Ampicillin (A9518-25G) was obtained from Sigma-Aldrich. Linezolid (A3605500-25g) was obtained from AmBeed. All E-test strips were obtained from Biomérieux.

Bacteriophage: The bacteriophage PYO^{sa} was obtained from the Levin Laboratory's bacteriophage collection.

Bacteriophage preparation for injection: Lysates of PYO^{sa} were grown on *S. aureus* Newman such that the total volume exceeded 250 mL of media. These initial lysates were spun down and filtered through a 0.22 µm filter to remove cellular debris. From there, the lysates were run through a 100 kD tangent flow filtration (TFF) cassette (PAL 0A100C12) with a PAL Minimate TFF system. The volume was reduced during this process to 15 mL which was refiltered through a 0.22 µm filter. This lysate was incubated with shaking at 25 °C with equal parts octanol (Thermo Scientific 4345810000) for 24 hours. The non-organic fraction was then dialyzed with Thermo Scientific's 250 kD float-a-lyzer cassette (66455) against 60% ethanol and then again against saline. Finally, the lysate was refiltered through a 0.22 µm filter.

Sampling bacterial and phage densities: Bacteria and phage densities were estimated by serial dilutions in 0.85% NaCl solution followed by plating. The total density of bacteria was estimated on LB (1.6%) agar plates. To estimate the densities of free phage, chloroform was added to suspensions before serial dilutions. These

suspensions were mixed with 0.1 mL of overnight MHIII grown cultures of wild-type *S. aureus* MN8 in 4 mL of LB soft (0.65%) agar and poured onto semihard (1%) LB agar plates.

G. mellonella preparation: *G. mellonella* larvae were obtained from Speedy Worm (Minnesota, USA) and placed immediately at 4 °C for 24 hours as a cold shock. Larvae were then sorted such that only those that weighed between 180 and 260 mg.

G. mellonella infection and sampling: Larvae were allowed to acclimatize at 37 °C for 24 hours before the experiment. Overnight cultures of *S. aureus* MN8 were centrifuged for 20 min at room temperature at maximum speed, the supernatant discarded, and the pellet resuspended in saline. This process was repeated 5 times. The bacterial suspension was diluted in saline to the desired inoculum concentration. Groups of 10 larvae were injected with 5 µL of the desired bacterial suspension at the last left proleg. Larvae were incubated at 37 °C in the dark without food. After 4 or 24 hours the larvae were placed in 1 mL of saline and then homogenized. The homogenate was plated in LB agar plates containing 400 µg/mL of streptomycin.

G. mellonella treatment: Larva were treated by injection in the last right proleg. Antibiotic concentrations were analogous to those used for clinical treatment in humans and the amount of antibiotic determined by weight for a total final treatment amount of: LIN- 0.002 mg; TET- 0.01 mg; DAP- 0.002 mg; AMP- 0.04 mg.

G. mellonella immune system ablation: As in (28), larvae were injected in the right proleg with 20 µL of 10 µM cytochalasin b and nocodazole (note: this protocol does not work with 10 µL of 20 µM of each drug) and allowed to incubate in the dark at 37 °C for 4 hours. At 4 hours, larvae were infected as described above with a suspension that is 50% bacteria and 50% of the mixture of both of these drugs.

Antibiotic minimum inhibitory concentration: Resistance to ampicillin was determined by E-test on MHIII agar plates.

Hemolymph extraction and hemocyte isolation: Larvae were dipped in 100% ethanol and allowed to dry. After drying, larvae were stabbed in a proleg once an hour for four hours with a 30-gauge needle (BD, 305195) to stimulate the innate immune system (32). After the fourth timepoint, the larvae were stabbed in the central line and the hemolymph removed and placed in 1 mL of Insect Physiological Saline (IPS; 150mM Sodium Chloride, Fisher, S271; 5mM potassium chloride, Sigma, P-8041; 100mM Tris/HCl, Fisher, BP153; 10mM EDTA,

Promega, V4233; 30 mM sodium citrate, J.T. Baker, 3650) The lymph from 10-15 worms were pooled, the Eppendorf tube was centrifuged at 500 x g for 10 minutes. The pellet was washed twice with cold IPS then resuspended in a minimal amount of IPS.

Microscopy: GFP-marked *S. aureus* was incubated with 10^6 - 10^7 hemocytes for 30 minutes in an Eppendorf tube. After incubation with bacteria, 10 μ L of the cells were stained with 10 μ L of 0.4% trypan blue (Sigma, T8154), mounted and imaged on a Leica DMI8 motorized inverted microscope with motorized stage (Leica, 11889113) to ensure cells were viable. After ensuring hemocytes are viable, the sample was divided in half. Half of the sample was treated with PBS and the other half of DNase (MilliporeSigma, AMPD1) both samples were fixed with 4% paraformaldehyde (ThermoFisher, 043368.9M) and stained with 2-(4amidinophenyl)-1H-indole-6- carboxamide (DAPI, 1 μ g/mL; Invitrogen, D1306) and washed with Dulbecco's PBS. Afterwards, 2 drops of antifade mountant (Invitrogen, P36980) was applied and slides allowed to cure on benchtop for 24 hours. The cells were then imaged on a Nikon A1R HD25 confocal microscope system at 60x oil immersion lens with NA = 1.49.

Statistical analysis: All statistical analyses were performed in GraphPad Prism Version 8.0.1 using a two-tailed unpaired parametric t-test.

Mathematical Model: We model infection and immune response dynamics by the following ordinary differential equations:

$$\frac{dU}{dt} = \left(1 - \frac{U}{K_U}\right)rU - h_1EU - f\left(1 - \frac{P}{K_P}\right)U + b\left(1 - \frac{U}{K_U}\right)P$$

$$\frac{dP}{dT} = \left(1 - \frac{P}{K_P}\right)rP + f\left(1 - \frac{P}{K_P}\right)U - b\left(1 - \frac{U}{K_U}\right)P$$

$$\frac{dE}{dt} = (a + sU)\left(E_{tot} - E - \frac{h_2}{g}EU\right) - dE$$

U and P describe bacterial populations in compartments where they are either unprotected or protected from the active immune effector population E . Both, U and P grow at rate r , limited by the carrying capacities K_U and K_P , respectively. Bacteria migrate from U to P at rate f and from P to U at rate b , limited by the free capacity in the destination compartment, i.e., $1 - \frac{U}{K}$. Immune effectors E are activated from a limited pool E_{tot} at background activation rate a , or in response to bacteria sU , and deactivate at rate d . Unprotected bacteria U are removed by rate h_1 proportional to the product of U and E (h_1UE). Immune action is modelled as a two-step process: engagement at rate h_2 (akin to capture) and killing at rate g (akin to digestion). Assuming g is large, the total number of un-activated immune effectors can be described by $E_{tot} - E - \frac{h_2}{g}EU$, where $\frac{h_2}{g}EU$ reflects effectors currently engaged with U (24). See Supplemental Text for details.

Numerical solutions (simulations): All numerical simulations were implemented in R (version 4.3.1) using the deSolve package (33). Parameter sampling for the sensitivity analysis was done using Latin Hypercube sampling via the lhs package to efficiently maximize coverage of the parameter space (34). Global parameter sensitivity analysis was performed using the PAWN method implemented in the SAFER package (35). Briefly, the PAWN method evaluates parameter importance by the assessing the difference in output distributions if all parameters can vary compared to when one parameter is fixed. See Text S1 for equations and detailed description of the mathematical model, and Table S1 for parameter descriptions, values, and sampling ranges of the sensitivity analysis. All simulation code is available under https://gitfront.io/r/user-2939733/ruxwXHz8cVY9/galleria_immune/.

Acknowledgements

We thank our resident entomologist, Dr. Jason Chen, for his help in navigating the biology of this system. We are grateful to Speedy Worm for their supplying these larvae. Funds for this research were provided by a grant from the US National Institute of General Medical Sciences via R35GM136407. Roland R. Regoes was supported by the Swiss National Science Foundation (grant 31003A_179170). This work was supported by the Emory University Integrated Cellular Imaging Core Facility (RRID:SCR_023534). The content of this article is solely the responsibility of the authors and does not necessarily reflect the official views of the National Institute of Health or the Swiss National Science Foundation. The funders had no role in the design or execution of this research nor the decision to publish the results.

Data Availability

All data underlying this report can be found in the main text and its figures or the supplemental materials. Access to bacterial strains and phages can be had by contacting the corresponding author.

References

1. A. Berryhill Brandon *et al.*, What's the Matter with MICs: Bacterial Nutrition, Limiting Resources, and Antibiotic Pharmacodynamics. *Microbiology Spectrum* **11**, e04091-04022 (2023).
2. A. Berti, W. Rose, V. Nizet, G. Sakoulas, Antibiotics and Innate Immunity: A Cooperative Effort Toward the Successful Treatment of Infections. *Open Forum Infect Dis* **7**, ofaa302 (2020).
3. J. A. Galarza, L. Murphy, J. Mappes, Antibiotics accelerate growth at the expense of immunity. *Proceedings of the Royal Society B: Biological Sciences* **288**, 20211819 (2021).
4. M. G. Netea, A. Schlitzer, K. Placek, L. A. B. Joosten, J. L. Schultze, Innate and Adaptive Immune Memory: an Evolutionary Continuum in the Host's Response to Pathogens. *Cell Host & Microbe* **25**, 13-26 (2019).
5. R. Yedle *et al.*, Neutropenic Rat Thigh Infection Model for Evaluation of the Pharmacokinetics/Pharmacodynamics of Anti-Infectives. *Microbiol Spectr* **11**, e0013323 (2023).
6. W. A. Craig, Pharmacokinetic/pharmacodynamic parameters: rationale for antibacterial dosing of mice and men. *Clin Infect Dis* **26**, 1-10; quiz 11-12 (1998).
7. S. L. Preston *et al.*, Pharmacodynamics of levofloxacin: a new paradigm for early clinical trials. *Jama* **279**, 125-129 (1998).
8. P. G. Ambrose *et al.*, Pharmacokinetics-Pharmacodynamics of Antimicrobial Therapy: It's Not Just for Mice Anymore. *Clinical Infectious Diseases* **44**, 79-86 (2007).
9. A. F. Zuluaga *et al.*, Neutropenia induced in outbred mice by a simplified low-dose cyclophosphamide regimen: characterization and applicability to diverse experimental models of infectious diseases. *BMC Infect Dis* **6**, 55 (2006).
10. B. R. Levin, F. Baquero, P. Ankomah, I. C. McCall, Phagocytes, Antibiotics, and Self-Limiting Bacterial Infections. *Trends in Microbiology* **25**, 878-892 (2017).
11. E. Tacconelli, F. Foschi, C. Forstner, R. G. Finch, M. W. Pletz, "136 - Principles of Anti-infective Therapy and Surgical Prophylaxis" in *Infectious Diseases (Fourth Edition)*, J. Cohen, W. G.

- Powderly, S. M. Opal, Eds. (Elsevier, 2017), <https://doi.org/10.1016/B978-0-7020-6285-8.00136-2>, pp. 1145-1161.e1142.
12. W. Huo *et al.*, Immunosuppression broadens evolutionary pathways to drug resistance and treatment failure during *Acinetobacter baumannii* pneumonia in mice. *Nat Microbiol* **7**, 796-809 (2022).
 13. C. J. Tsai, J. M. Loh, T. Proft, *Galleria mellonella* infection models for the study of bacterial diseases and for antimicrobial drug testing. *Virulence* **7**, 214-229 (2016).
 14. T. C. Pereira *et al.*, Recent Advances in the Use of *Galleria mellonella* Model to Study Immune Responses against Human Pathogens. *J Fungi (Basel)* **4** (2018).
 15. M. Asai, Y. Li, S. M. Newton, B. D. Robertson, P. R. Langford, *Galleria mellonella*-intracellular bacteria pathogen infection models: the ins and outs. *FEMS Microbiol Rev* **47** (2023).
 16. S. Jemel, J. Guillot, K. Kallel, F. Botterel, E. Dannaoui, *Galleria mellonella* for the Evaluation of Antifungal Efficacy against Medically Important Fungi, a Narrative Review. *Microorganisms* **8** (2020).
 17. M. Su *et al.*, Genomic analysis of variability in Delta-toxin levels between *Staphylococcus aureus* strains. *PeerJ* **8**, e8717 (2020).
 18. O. Flores-Maldonado *et al.*, Dissemination of Gram-positive bacteria to the lung of newborn mice increases local IL-6 and TNF α levels in lethal bacteremia. *Microbes and Infection* **24**, 104984 (2022).
 19. N. Wald-Dickler, P. Holtom, B. Spellberg, Busting the Myth of "Static vs Cidal": A Systemic Literature Review. *Clin Infect Dis* **66**, 1470-1474 (2018).
 20. B. A. Berryhill, D. L. Huseby, I. C. McCall, D. Hughes, B. R. Levin, Evaluating the potential efficacy and limitations of a phage for joint antibiotic and phage therapy of *Staphylococcus aureus* infections. *Proceedings of the National Academy of Sciences* **118**, e2008007118 (2021).
 21. A. Handel, E. Margolis, B. R. Levin, Exploring the role of the immune response in preventing antibiotic resistance. *J Theor Biol* **256**, 655-662 (2009).
 22. N. Trevijano-Contador, O. Zaragoza, Immune Response of *Galleria mellonella* against Human Fungal Pathogens. *J Fungi (Basel)* **5** (2018).

23. R. Y. Chen, B. A. Keddie, *Galleria mellonella* (Lepidoptera: Pyralidae) Hemocytes Release Extracellular Traps That Confer Protection Against Bacterial Infection in the Hemocoel. *J Insect Sci* **21** (2021).
24. S. S. Pilyugin, R. Antia, Modeling immune responses with handling time. *Bull Math Biol* **62**, 869-890 (2000).
25. J. H. Rex, M. A. Pfaller, Has antifungal susceptibility testing come of age? *Clin Infect Dis* **35**, 982-989 (2002).
26. C. D. Doern, When does 2 plus 2 equal 5? A review of antimicrobial synergy testing. *J Clin Microbiol* **52**, 4124-4128 (2014).
27. Y. Hashimoto *et al.*, Identification of lipoteichoic acid as a ligand for draper in the phagocytosis of *Staphylococcus aureus* by *Drosophila* hemocytes. *J Immunol* **183**, 7451-7460 (2009).
28. N. Banville, J. Fallon, K. McLoughlin, K. Kavanagh, Disruption of haemocyte function by exposure to cytochalasin b or nocodazole increases the susceptibility of *Galleria mellonella* larvae to infection. *Microbes Infect* **13**, 1191-1198 (2011).
29. J. Pearce *et al.*, A microinjection protocol for the greater waxworm moth, *Galleria mellonella*. *bioRxiv* 10.1101/2024.09.17.613528, 2024.2009.2017.613528 (2024).
30. L.-L. Luo *et al.*, Efficient CRISPR/Cas9-mediated ebony gene editing in the greater wax moth *Galleria mellonella*. *Insect Science* **n/a**.
31. G. R. Pidwill, J. F. Gibson, J. Cole, S. A. Renshaw, S. J. Foster, The Role of Macrophages in *Staphylococcus aureus* Infection. *Front Immunol* **11**, 620339 (2020).
32. N. J. Senior, R. W. Titball, Isolation and primary culture of *Galleria mellonella* hemocytes for infection studies. *F1000Res* **9**, 1392 (2020).
33. R. R Core Team (2013) R: A language and environment for statistical computing. (R foundation for statistical computing Vienna, Austria).
34. R. Carnell, M. R. Carnell, Package 'lhs'. CRAN. <https://cran.rproject.org/web/packages/lhs/lhs.pdf> (2016).

35. F. Pianosi, T. Wagener, A simple and efficient method for global sensitivity analysis based on cumulative distribution functions. *Environmental Modelling & Software* **67**, 1-11 (2015).

Supporting Information

Text S1. Model Equations and Description

To investigate the within-host dynamics of bacterial infections in the experimental *Galleria mellonella* system, we developed a mathematical population model. The model is described by the following system of ordinary differential equations:

$$\frac{dU}{dt} = \left(1 - \frac{U}{K_U}\right)rU - h_1EU - f\left(1 - \frac{P}{K_P}\right)U + b\left(1 - \frac{U}{K_U}\right)P$$

$$\frac{dP}{dT} = \left(1 - \frac{P}{K_P}\right)rP + f\left(1 - \frac{P}{K_P}\right)U - b\left(1 - \frac{U}{K_U}\right)P$$

$$\frac{dE}{dt} = (a + sU)\left(E_{tot} - E - \frac{h_2}{g}EU\right) - dE$$

We assume that bacteria can be present in both an unprotected compartment (U), where they are exposed to the immune effectors (E), and a protected compartment (P), where bacteria are shielded from the immune effectors. Bacteria in both compartments, U and P , grow exponentially at rate r , with their growth limited by the carrying capacities K_U and K_P , respectively, where $K_P < K_U$. Bacteria migrate back and forth between the unprotected and the protected compartment at maximal rates f (U to P) and b (P to U). These rates are proportionally reduced as the destination compartment approaches carrying capacity.

In our model the innate immune system is described by a population of activated immune effectors (E). Following Pilyugin and Antia (2000)(1) we assume a fixed total number of immune effectors (E_{tot}). Un-activated immune effectors are described by the term $(E_{tot} - E - \frac{h_2}{g}EU)$, where $\frac{h_2}{g}EU$ represents the number of activated effectors currently engaged with unprotected bacteria (U , details below). The un-activated effectors activate with a background rate a or in response to bacteria as described by the term sU . Activated effectors (E) deactivate with rate d .

Mirroring the natural mode of action of immune systems, where pathogens are incapacitated upon contact with activated immune effectors, unprotected bacteria U are removed by E at rate h_1 according to mass action kinetics. Specifically, we assume that this interaction between E and U is a two-step process. First, E encounter U via mass-action kinetics by rate h_2 – this is analogous to how phagocytes capture bacterial cells. Then, they kill them at rate g – mirroring the enzymatic degradation that occurs within phagocytes. Therefore, the ratio $\frac{h_1}{h_2}$ describes how many bacteria an effector can simultaneously phagocytize.

Assuming that killing is relatively fast (i.e. g is large) allows us to make a quasi-steady state assumption for the dynamics of the engaged immune effectors and integrate the handling time via $\frac{h_2}{g}EU$ into the available number of activatable immune effectors (see (1) for details). Intuitively, the duration of killing by immune effectors results in a reduction of available effectors that could kill bacteria at a rate of $\frac{h_2}{g}EU$.

Table S1. Model parameter values.

Parameter	Description	Value	Range	Sampling
inoculum	Starting population size of bacteria	$10 - 10^{7.5}$	$10 - 10^{7.5}$	Log uni
r	Maximal growth rate in absence of antibiotics	1	1	/
K_U	Carrying capacity in protected site	10^8	10^8	/
K_P	Carrying capacity in unprotected site	1500	$10^2 - 10^4$	Log uni
f	Migration rate to protected site	0.001	$10^{-7} - 0.1$	Log uni
b	Migration rate to unprotected site	0.1	$10^{-7} - 0.1$	Log uni
E_0	Starting population size of activated immune effectors	1000	$1 - 10^5$	Log uni
E_{tot}	Total number of available immune effectors (2, 3)	10^5	$10^{4.5} - 10^{5.3}$	Log uni
h_1	Killing rate of bacteria by immune effectors	0.001	$10^{-7} - 0.1$	Log uni
h_2	Engagement rate of activated immune effectors with unprotected bacteria	0.001	$10^{-7} - 0.1$	Log uni
d	Deactivation rate of immune effectors	0.01	$10^{-4} - 1$	Log uni
a	Background activation rate of immune effectors	0.01	$10^{-4} - 1$	Log uni
g	Handling rate of immune effectors	0.5	$10^{-3} - 4$	Log uni
s	Activation rate of immune effectors in response to unprotected bacteria	0.001	$10^{-7} - 0.1$	Log uni

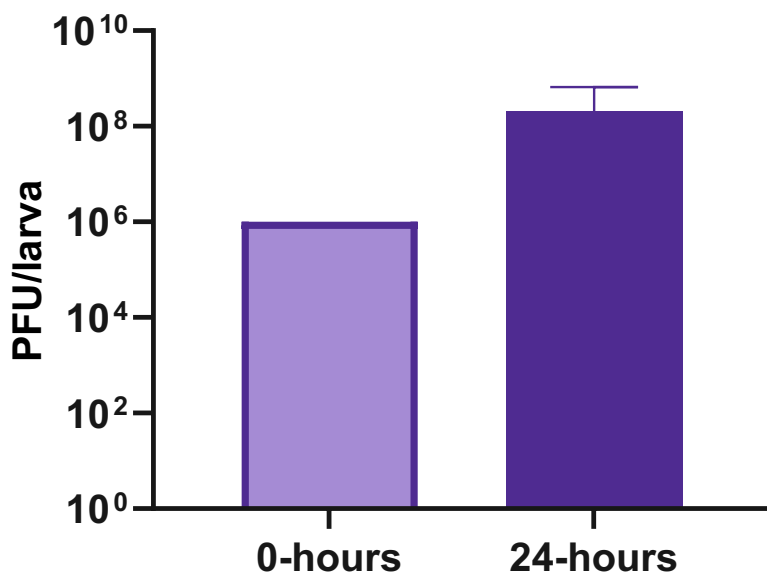


Fig. S1. Phage density before and after treatment. Larvae were infected with 10^8 CFU/larva of *S. aureus* MN8 and immediately treated with 10^6 PFU/larva of PYO^{Sa}. After 24 hours, larva were sacrificed and the phage density determined (N=20 larvae). Shown are means and standard deviations. The change in the phage density pre- and post-infection is highly statistically significant ($p < .0001$ ***).

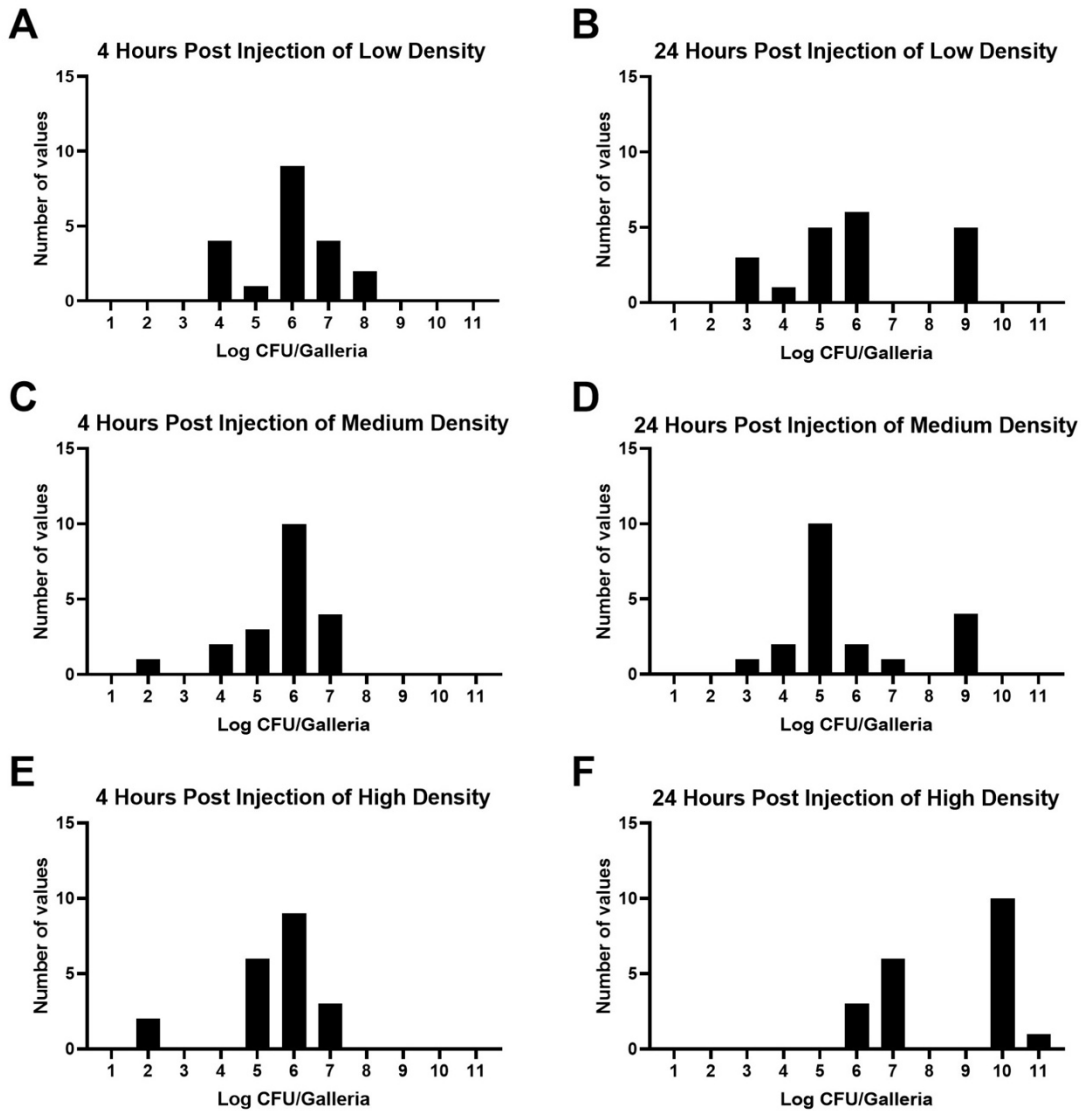


Fig. S2. Dynamics of infection. Larva were infected with three different densities of *S. aureus* MN8: low (10^4 CFU/larva; A, B), medium (10^6 CFU/larva; C, D), or high (10^8 CFU/larva; E, F) and were sacrificed after 4 (A, C, E) or 24 (B, D, F) hours post infection. Shown are the number of larvae within each \log_{10} CFU. For each condition N=80.

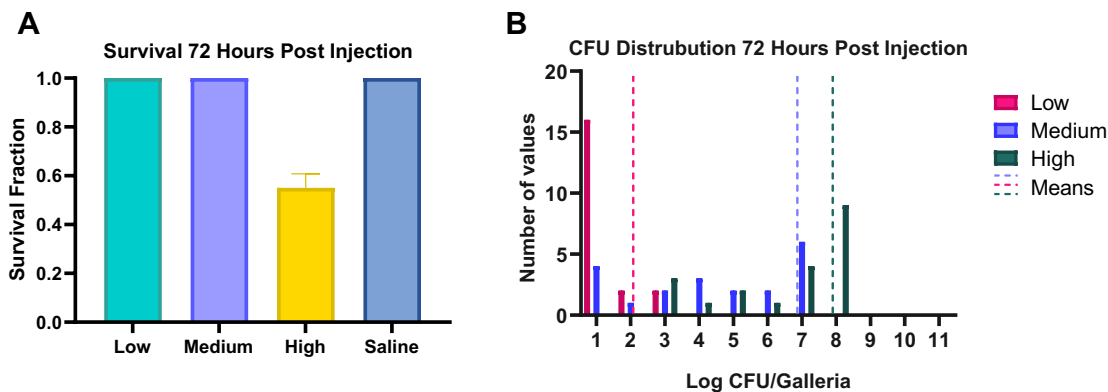


Fig. S3. Larvae survival and infection dynamics at 72 hours with different bacteria inoculum densities.

(A) Larvae were injected with *S. aureus* MN8 at 10^4 CFU/larva (turquoise), 10^6 CFU/larva (purple), 10^8 CFU/larva (yellow), or saline (blue). Mortality was assessed at 72 hours. Presented are means and standard deviations for the fraction of survival (N= 20 larvae). Low, medium, and high differ with saline at $p < .0001$ ****; low is statistically different from high at $p < .001$ ***; medium is different with high at $p < .001$ ***; and low and medium are not statistically different. (B) Larva were infected with three different densities of *S. aureus* MN8: low (10^4 CFU/larva; pink), medium (10^6 CFU/larva; purple), or high (10^8 CFU/larva; green) and were sacrificed after 72 hours post infection. Shown are the number of larvae within each \log_{10} CFU. The mean of the CFU at each timepoint for each inoculum density is presented as a dotted line of the same color. For each condition N=20 individual larvae.

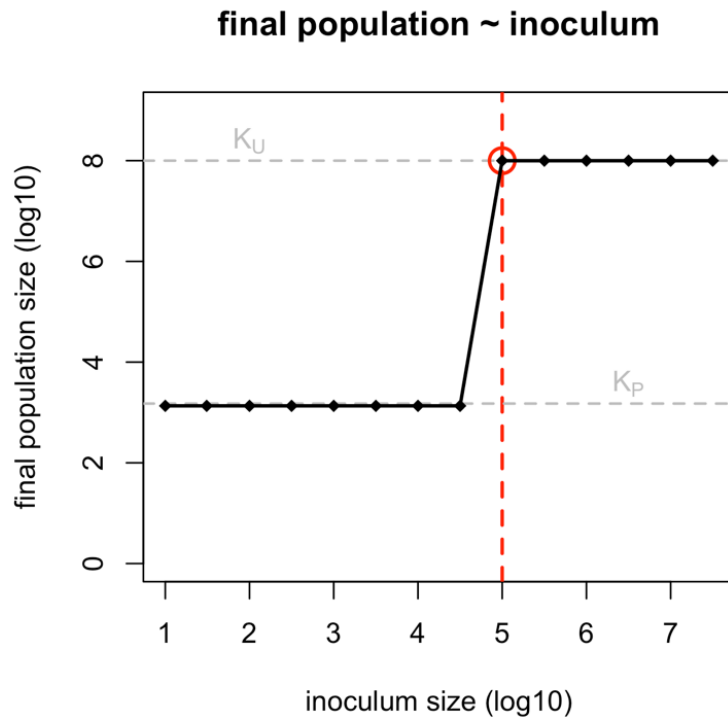


Fig. S4. High bacterial inoculum sizes overwhelm the immune system. Shown are the simulated total bacterial population sizes ($U + P$) at 72 hours after inoculation for different inoculum sizes (U_0). Grey, dashed lines show the carrying capacities of the unprotected (K_U) and the protected site (K_P). The critical inoculum threshold— the first size of inoculum that overwhelms the immune system – is highlighted in red. See Table S1 for parameter values used.

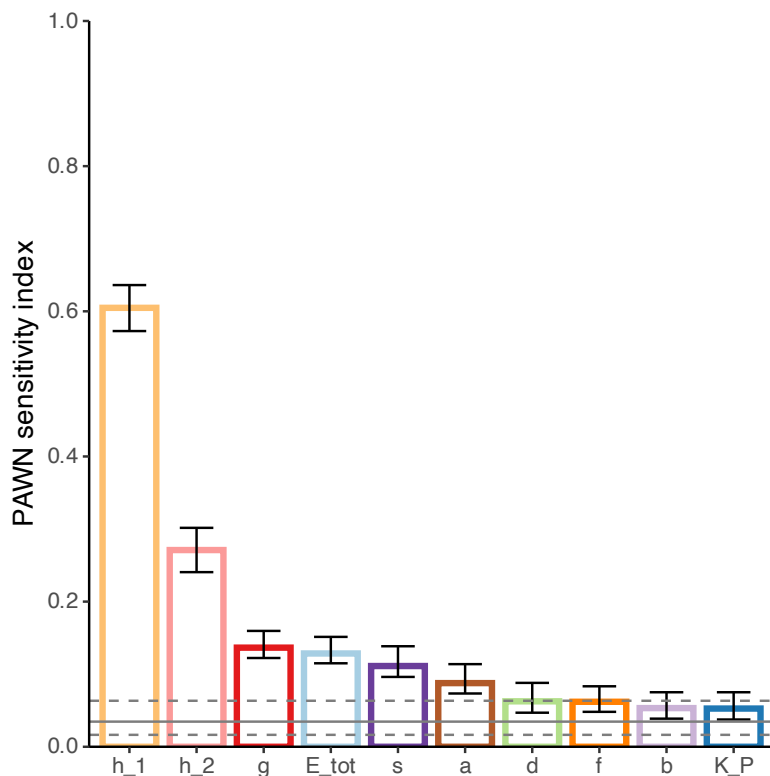


Fig. S5. Influence of model parameters on the critical inoculum threshold. We ran simulations for 10,000 randomly generated parameter sets to determine the critical inoculum thresholds – the first inoculum which overwhelms the immune system (highlighted in red in Fig. S4). For 1479 parameter sets, the immune system was not overwhelmed by any tested inoculum sizes. The remaining 8,521 parameter sets showed a clear critical inoculum threshold. For these 8,521 threshold values, we conducted a global sensitivity analysis by calculating PAWN sensitivity indices with bootstrapped 95% confidence intervals (CIs) to assess which model parameters most influence the threshold. The solid and dashed grey lines show the sensitivity index and CI of a dummy variable, i.e., a parameter which has no influence on the model output. The two immune parameters, h_1 and h_2 , are indicated to have the most influence on the critical inoculum threshold, whereas the non-immune parameters, i.e., b , K_P , and f , the least. See Material and Methods for details and Table S1 for parameter ranges sampled.

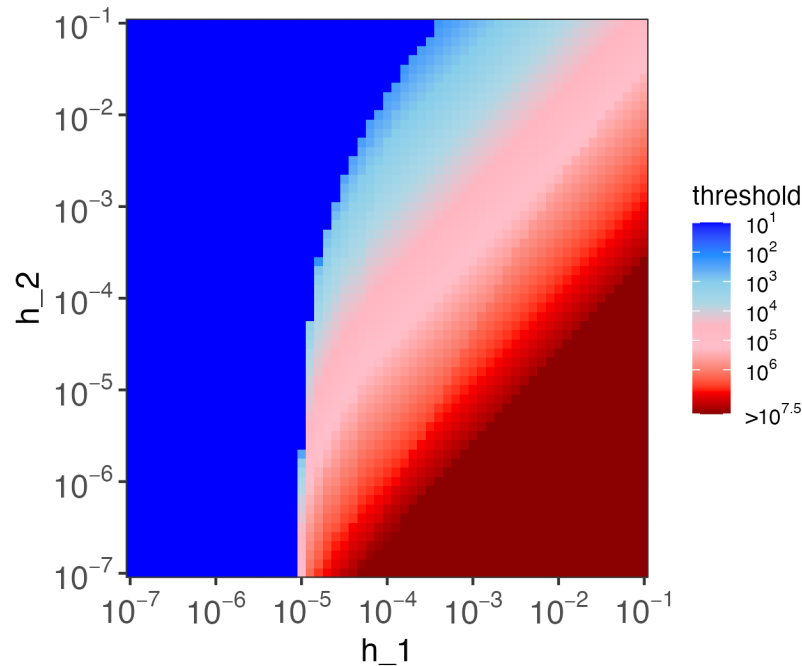


Fig. S6. Influence of the immune parameters, h_1 and h_2 , on the critical inoculum threshold. Shown is a heatmap of simulated inoculum thresholds – from low (blue) to high (red) – for pairwise combinations of effector killing rate (h_1) and effector engagement rate (h_2). All other model parameters are kept constant. For low values of h_1 ($<10^{-5}$) the immune system is overwhelmed with minimal bacterial inocula – irrespective of h_2 . When $h_1 >10^5$ and h_2 is at low to intermediate values of ($<10^{-4}$) the critical threshold increases to the point where no tested inocula can overwhelm the immune system (i.e. threshold $>10^{7.5}$). At high values of h_1 and h_2 the threshold is intermediate, ranging from 10^3 - 10^5 . See Table S1 for parameter values and Fig S4 for determination of the critical inoculum threshold.

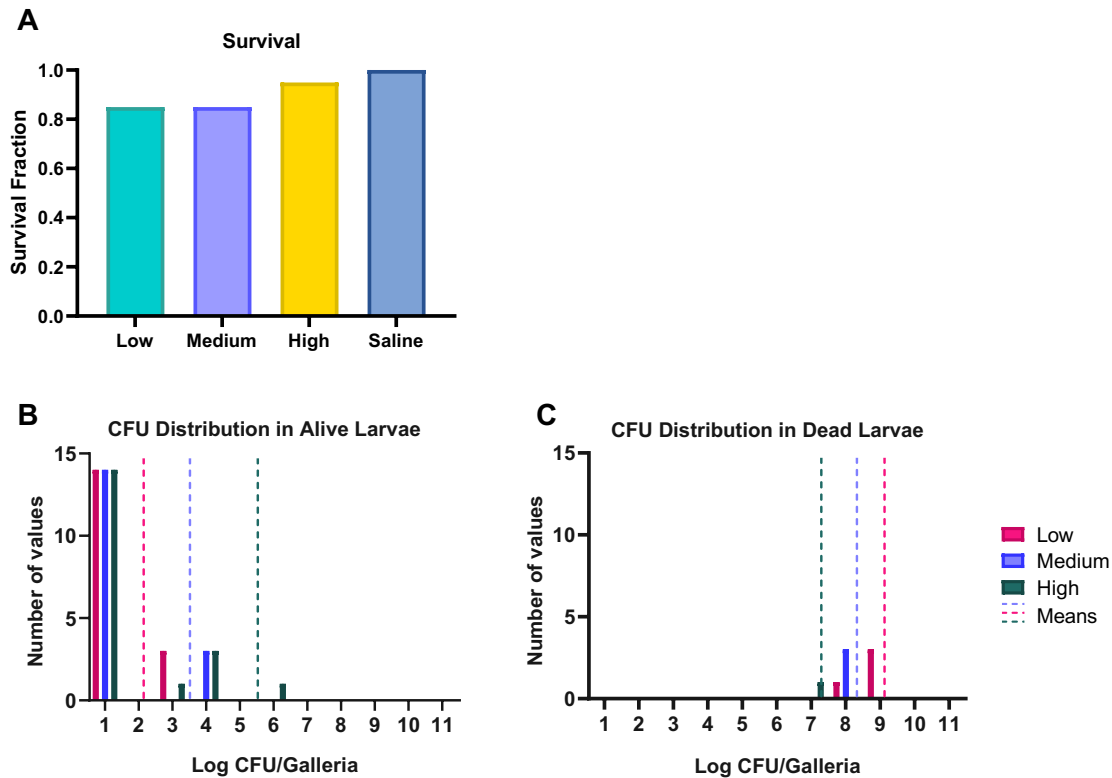


Fig. S7. Larvae survival and infection dynamics at 24 hours with different bacteria inoculum densities and ablated innate immune system. (A) Larvae were injected with *S. aureus* MN8 at 10^4 CFU/larva (turquoise), 10^6 CFU/larva (purple), 10^8 CFU/larva (yellow), or saline (blue). Mortality was assessed at 24 hours. Presented are means and standard deviations for the fraction of survival (N= 20 larvae). Low, medium, and high survival fractions are not statistically different. (B and C) Larva were infected with three different densities of *S. aureus* MN8: low (10^4 CFU/larva; pink), medium (10^6 CFU/larva; purple), or high (10^8 CFU/larva; green) and were sacrificed after 24 hours post infection. Shown are the number of larvae within each \log_{10} CFU. The mean of the CFU at each timepoint for each inoculum density is presented as a dotted line of the same color. For each condition N=20 individual larvae. (B) Larvae that were alive at 24 hours. (C) Larvae that were dead at 24 hours.

SI References

1. S. S. Pilyugin, R. Antia, Modeling immune responses with handling time. *Bull Math Biol* **62**, 869-890 (2000).
2. A. L. Jorjão *et al.*, From moths to caterpillars: Ideal conditions for *Galleria mellonella* rearing for in vivo microbiological studies. *Virulence* **9**, 383-389 (2018).
3. N. J. Senior, R. W. Titball, Isolation and primary culture of *Galleria mellonella* hemocytes for infection studies. *F1000Res* **9**, 1392 (2020).

Chapter 12

Chapter 12

Summary and Conclusions

Antibiotic resistance is one of the most pressing challenges facing modern medicine (1). Once readily treatable bacterial infections are becoming more difficult and costly to manage (2). Infections which were easy to treat 50 years ago are now impossible to cure (3, 4). The motivation of this dissertation, and my research at large, was the exploration of scientific questions that could help guide the future of infectious disease treatment, both by refining our understanding of antibiotics and bacteriophage (phage) and by offering tools that can inform clinical and public health practice for the treatment and prevention of bacterial infections. While the primary driver for this research has been clinical, the methodologies employed herein, and the contributions therefrom are interdisciplinary. These projects arise from population and evolutionary biology, ecology, pharmacology, molecular genetics, and clinical microbiology. In doing so, this dissertation embodies the growing recognition that overcoming the antibiotic-resistance crisis and improving therapeutic outcomes will require more than incremental changes to current practice. If, as anticipated, the trends of antibiotic resistance continue, we will require a fundamental rethinking of how we define drug efficacy, how we interpret susceptibility, and how we employ antimicrobial therapeutics.

One of the central themes that emerged throughout my studies is the inadequacy of minimal inhibitory concentration (MIC) as the sole pharmacodynamic parameter for evaluating antibiotic effectiveness (5). The first manuscript in this dissertation collection challenges the sufficiency of MIC-based assessments by demonstrating that nutrient limitation, a common feature of infected tissues and poorly vascularized sites, can dramatically alter the susceptibility of bacteria to antibiotics (6). These results question the ecological and clinical utility of current pharmacodynamic models and underscore the need to assess drug efficacy under physiologically relevant conditions. This concept is reinforced in several subsequent chapters, such as those which investigate the dynamics of treatment of bacterial populations at sub-MIC concentrations and the consequences of exposure to what would traditionally be called bacteriostatic agents.

Further complicating the interpretation of traditional, MIC-based antibiotic susceptibility assays is the phenomenon of heteroresistance (HR), which is explored in two chapters (7). In one, I use mathematical and computer-simulation models to examine two distinct forms of HR, revealing that the standard definitions and testing methods for HR are often insufficient to capture the dynamics of this clinically significant phenomenon (8). In a subsequent study, I show that prolonged exposure to ribosome-targeting bacteriostatic antibiotics can give rise to small colony variants (SCVs) that contribute to the evolution of HR. These SCVs not only demonstrate reduced susceptibility to multiple drugs but also rapidly revert to susceptible, highlighting a need to move beyond binary resistance metrics and toward a more dynamic framework of susceptibility that focuses on the outcome of treating a population with a drug over time, rather than just the MIC.

This demonstrated insufficiency of susceptibility metrics lends itself to questions about combination therapy and the pharmacodynamic of populations treated with multiple drugs. Traditionally, bacteriostatic antibiotics have been considered antagonistic to bactericidal antibiotics as the killing by the latter requires growing populations of bacteria (9). However, the findings presented in this dissertation challenge this assumption. My results demonstrate that sequential treatment with bacteriostatic followed by bactericidal agents will, under certain conditions, produce synergistic effects. These findings call for a reassessment of combination therapy guidelines and underscore the need for a more nuanced view of bacterial physiology during antibiotic treatment.

I also expand the discussion of antimicrobial treatment beyond antibiotics, focusing on the potential role of bacteriophage (phage) for the treatment of infections. I begin with a critical review of the history and current state of phage therapy and highlight both the promise and pitfalls of this therapeutic approach. Through both a perspective and experimental studies, my body of work on this topic emphasizes the need for rational, mechanistically informed design of phage-based therapies. One particularly distinction explored in the dissertation is the ecological and evolutionary difference between temperate and lytic (virulent) phages (10). Using a combination of theoretical and empirical methods, I show that natural populations of *Escherichia coli* harboring temperate phages in their genomes are often resistant as well as immune to their own prophages.

This is likely especially true when virulent phages sharing the same receptors are present in the environment. These results suggest that phage resistance should be understood not just because of evolution in the laboratory or as an unavoidable result of treatment, but instead as a trait selected for as part of a normal ecological interaction.

To further explore phage-bacteria dynamics in more naturalistic settings, I examined interactions between *E. coli* and phages from human gut microbiomes. My results indicate that most *E. coli* strains that comprise healthy enteric communities are resistant to phage due to express of the O antigen, nearly ubiquitously. However, phages persist in population of resistant hosts due to high rates of phenotypic switching between resistant and sensitive states. These findings suggest that phages may not strongly shape the bacterial strain composition in healthy microbiomes. Related to the ability of phage to shape communities of bacteria, I investigated a unique form of phage defense whereby infected bacterium destroys itself after the virus enters the cells but before more virions can be produced. My results demonstrate that retrons, which mediate this abortive infection response, can protect bacterial populations from predation by phage under broad conditions (11). However, the selective advantages of retrons are limited and these systems can only increase in frequency when rare in highly structured environments with the bacteria growing as colonies. This result emphasizes the importance of considering ecological context in evaluating the interactions between phage and their host bacteria.

The promise of phage therapy as a clinical intervention is directly addressed in a study evaluating the therapeutic potential of the broad host-range phage PYO^{Sa}, seemingly the perfect phage for therapy, for *Staphylococcus aureus*. Despite this, this virus fails to clear infections on its own due to the emergence of phenotypically diverse SCVs. However, sequential therapy combining PYO^{Sa} with bactericidal antibiotics yields substantially better outcomes, suggesting that rationally designed phage-antibiotic combination strategies may be a viable path forward for phage therapy. These results not only underscore the complexity of phage-bacteria interactions but also illustrate the utility of evolutionary and ecological thinking in improving the design of therapeutic regimens.

This dissertation also presents three practical tools, two of which are included as appendices and discussed here for their translational value. The first is the use of the larva of *Galleria mellonella* as an *in vivo* model system for quantitatively understanding infection and treatment (12). This report demonstrates that saturation of the innate immune system by infecting bacteria is the primary driver of mortality, and that bacteriostatic agents and phages are highly effective in controlling infection. Importantly, I also show that minority treatment-resistant populations do not necessarily ascend to dominance in the presence of a functioning immune response. Taken together, the results of this manuscript highlight the importance of incorporating immunological realism, in particular innate immunity, into models of infection and, ultimately, suggests that this larval model can serve as a bridge between *in vitro* experiments and mammalian model systems.

The second tool, presented as the first appendix, is a method for tracking pathogen transmission in healthcare settings using genetically marked phages. This technique provides a high-resolution view of how healthcare-associated infections may spread and allows for targeted interventions. By mimicking realistic contamination scenarios and mapping phage movement via healthcare worker contact, this method offers a standardized and adaptable way to investigate breakdowns in infection control and can allow for the implementation of policies and procedures to prevent nosocomial infections.

The second appendix details an empirical evaluation of doffing protocols for high-containment personal protective equipment (PPE), using traditional fluorescent markers and phages to identify contamination pathways that could lead to the infection of treating healthcare workers (13). This study led to revised protocols that eliminated the transmission of potentially pathogenic agents to medical staff, illustrating the importance of integrating microbiological tools into infection prevention and control practices. Together, these tools demonstrate the power of synthetic biology, microbiology, and creative study design in advancing both research and practical infection control strategies.

At a broader level, this dissertation argues for the integration of population and evolutionary biology and ecology into the development of infectious disease treatments. Concepts such as selection, trade-offs, phenotypic heterogeneity, and spatial structure are not just abstract ideas—they have direct implications for how infections establish and develop and how they can be treated. As the chapters in this dissertation

demonstrate, embracing these interdisciplinary thinking can lead to the generation of novel hypotheses, refinement of existing paradigms, and, ultimately, to better clinical outcomes.

Future research in the field of population and evolutionary microbiology should continue to focus on the concept of translational microbiology. The field stands to benefit from closer integration between experimental “basic science” microbiology, mathematical modeling, and clinical medicine. The most salient example of this is in personalized medicine, where adaptive treatment protocols that respond by modifying the treatment regimen in real-time to changes in pathogen population structure could be informed by the type of research developed in this dissertation.

Finally, this dissertation reflects a belief that meaningful progress against antibiotic resistance will require more than newer, better drugs. Progress will require better ways of thinking. Biology is inherently interdisciplinary; and we must be as well. The challenges before us are enormous, but so too are the opportunities.

References

1. M. M. Aljeldah, Antimicrobial Resistance and Its Spread Is a Global Threat. *Antibiotics (Basel)* **11** (2022).
2. A. N. Poudel *et al.*, The economic burden of antibiotic resistance: A systematic review and meta-analysis. *PLoS One* **18**, e0285170 (2023).
3. G. Mancuso, A. Midiri, E. Gerace, C. Biondo, Bacterial Antibiotic Resistance: The Most Critical Pathogens. *Pathogens* **10** (2021).
4. D. Chinemerem Nwobodo *et al.*, Antibiotic resistance: The challenges and some emerging strategies for tackling a global menace. *J Clin Lab Anal* **36**, e24655 (2022).
5. L. Zhang *et al.*, Pharmacodynamic Parameters of Pharmacokinetic/Pharmacodynamic (PK/PD) Integration Models. *Front Vet Sci* **9**, 860472 (2022).
6. A. A. Alagga, M. V. Pellegrini, V. Gupta, "Drug Absorption" in StatPearls. (StatPearls Publishing Copyright © 2025, StatPearls Publishing LLC., Treasure Island (FL), 2025).
7. D. I. Andersson, H. Nicoloff, K. Hjort, Mechanisms and clinical relevance of bacterial heteroresistance. *Nature Reviews Microbiology* **17**, 479-496 (2019).
8. O. M. El-Halfawy, M. A. Valvano, Antimicrobial heteroresistance: an emerging field in need of clarity. *Clin Microbiol Rev* **28**, 191-207 (2015).
9. P. S. Ocampo *et al.*, Antagonism between bacteriostatic and bactericidal antibiotics is prevalent. *Antimicrobial agents and chemotherapy* **58**, 4573-4582 (2014).
10. F. M. Stewart, B. R. Levin, The population biology of bacterial viruses: why be temperate. *Theor Popul Biol* **26**, 93-117 (1984).
11. A. Millman *et al.*, Bacterial Retrons Function In Anti-Phage Defense. *Cell* **183**, 1551-1561.e1512 (2020).
12. I. Wojda, B. Staniec, M. Sulek, J. Kordaczuk, The greater wax moth *Galleria mellonella*: biology and use in immune studies. *Pathog Dis* **78** (2020).

13. L. S. Munoz-Price *et al.*, Use of UV powder for surveillance to improve environmental cleaning. *Infect Control Hosp Epidemiol* **32**, 283-285 (2011).

Appendix 1

Appendix 1

Using Lambda phages as a proxy for pathogen transmission in hospitals

Reprinted from: Burke KB, Berryhill BA, Garcia R, Goldberg DA, Manuel JA, Gannon P, Levin BR, Kraft KS, Mumma J. 2023. A methodology for using Lambda phages as a proxy for pathogen transmission in hospitals. *The Journal of Hospital Infection*. <https://doi.org/10.1016/j.jhin.2023.01.004>

Abstract

One major concern in hospitalized patients is infections with pathogens borne on surfaces, patients, and healthcare workers. Fundamental to controlling healthcare associated infections is identifying the sources of pathogens, monitoring the processes responsible for their transmission, and evaluating the efficacy of the procedures employed for restricting their transmission. Here we present a method using the bacteriophage Lambda (λ) to achieve these ends. Defined densities of multiple genetically marked λ phages were inoculated at known hotspots for contamination on high-fidelity mannequins. Healthcare workers (HCWs) then entered a pre-sanitized simulated hospital room and performed a series of patient care tasks on the mannequins. Sampling occurred on the scrubs and hands of the HCWs, as well as previously defined high-touch surfaces in hospital rooms. Following sampling, the rooms were decontaminated using procedures designed and demonstrated to be effective. Following the conclusion of the simulation, the samples were tested for the presence, identity, and densities of these Lambda phages.

The data generated enabled the determination of the sources and magnitude of contamination caused by the breakdown of established infection prevention practices by HCW. This technique enabled the standardized tracking of multiple contaminants during a single episode of patient care. While our application of these methods focused on nosocomial infections and the role of HCW behaviors in their spread, these methods could be employed for identifying the sources and sites of microbial contamination in other settings.

Introduction

One of the greatest harms of being hospitalized is infections acquired from pathogenic microbes in treatment environments (e.g., catheter-associated urinary tract infections or catheter-associated bloodstream infections) (1). These pathogens can be unknowingly transmitted by healthcare workers (HCWs) to patients, thereby contributing to patient morbidity and mortality (2). Previous studies using mathematical models (3-5) have shown a solution to reducing the incidence of hospital-acquired infections is to increase the efficacy of measures for preventing the transmission of pathogens from HCWs to patients (e.g., hand hygiene and barrier precautions). Central to designing, implementing, and evaluating these measures is elucidating the sources of the pathogens responsible for infections and the pathways for transmitting those pathogens to patients.

As a patient care environment can harbor different sources of pathogens (6) and abounds in opportunities for their transmission, there is a need to simultaneously trace multiple transmission pathways. Existing approaches using non-biological or biological surrogates for pathogens do not satisfy the need for *in situ* evaluation of transmission events. Non-biological surrogates, such as fluorochrome-tagged body fluids, can be used to simulate different sources of contamination simultaneously but not the susceptibility of pathogens to disinfectants (7). Approaches using biological surrogates, including live viruses and viral DNA markers, are limited. Viruses, such as bacteriophage MS2, are susceptible to disinfectants (8) but can only be used to trace a single source of contamination at a time. Viral DNA markers, such as cauliflower mosaic virus DNA or silica nanoparticles with encapsulated DNA (9), can produce multiple unique markers (8)(10) but are unaffected by commonly used disinfectants (such as 70% ethanol ; (8)). Thus, a method is needed for tracing multiple transmission pathways simultaneously during patient care, each of which can be counteracted by common infection prevention and control measures, such as hand hygiene.

This report presents a methodology and preliminary results using genetically marked variants of the bacteriophage Lambda (λ) as a harmless surrogate for pathogen transmission. We then validate this method in a naturalistic setting by contaminating different surfaces prior to simulated patient care in a hospital environment.

Materials and Methods

Reagents and Equipment. The following reagents and equipment were used in this study: Luria-Bertani (LB) Broth Miller (Difco, USA, Product # 244620), Luria-Bertani (LB) Plates (Difco, USA, Product # 244510), 0.65% Agar Luria-Bertaini (LB) soft agar, LaboPlast Spray Bottle with Pump Vaporizor (Bürkle, Germany, Product # 10216-888), Self-contained 0.85% Saline Swab (Hardy Diagnostic, USA, Product # SRK35), RNase Away Reagent (Invitrogen, USA, Product # 10328-011), DNA AWAY (Molecular BioProducts, Mexico, Product # 7010), 70% ethanol solution (Decon Labs, USA, Product # 2716), Ruler, Disinfecting Wipes (Lysol, Alkyl (50% C14, 40% C12, 10% C16) Dimethyl Benzyl Ammonium Chloride - 0.26%. Other Ingredients: 99.74%, China, Product # 3168342), 138 oz. Whirl-Pak (Nasco, USA, Product # B01542), Sterile Saline Wipes (Hygea, USA, Product # C22370), Phusion Blood Direct PCR Master Mix (ThermoFisher, Lithuania, Product # F-175L), O'Gene Ruler DNA Ladder (Thermo Scientific, Lithuania, Product #SM1563), 10,000X GelRed Nucleic Acid Stain (Biotinium, USA, Product # 41003).

Strains. *Escherichia coli* strain C was acquired from Marie-Agnès Petit from INRAe, France. Bacteriophage λ (λ^{Temp}), Bacteriophage λ^{Chl} , Bacteriophage λ^{Kan} , and Bacteriophage λ^{Vir} was obtained from Maroš Pleška at The Rockefeller University.

Lysate Preparation. $1e^5$ PFU/ml of each phage were cultured with $1e^7$ CFU/ml log-phase *E. coli* C in 10ml of LB broth. These cultures were grown with shaking for six hours before being centrifuged and filtered through a 0.22 μm filter to generate sterile, high-titer lysates of each of the four bacteriophages. These lysates were serially diluted and plated on lawns of *E. coli* C to determine viral titers.

Phage Distribution. Ten milliliters of $1e^8$ CFU/ml of each type of λ phage lysate was loaded into their respective spray bottles. The spray bottles were stored at 4°C and transported on ice. Each bottle was primed by spraying five times into a waste container. Immediately after priming, each lysate was sprayed with one pump onto the target site from a distance of 10 cm. The spray dried clear, and nurses were unable to note that anything had been added to the surfaces. Contamination occurred no earlier than thirty minutes before the start of the simulation.

Phage Recovery. Immediately after the simulation, HCW hands were sampled by applying a saline hand wipe around both hands and forearms. The saline hand wipe was placed into a conical tube for storage. HCWs then placed their disposable scrubs into a Whirl-Pak for storage. High-touch surfaces (See Table I and Figure 1 (11)) were sampled with self-contained 0.85% saline swabs; each swab was removed from the saline, and the surface was swabbed in a progressive back and forth motion until the entire surface became damp from the saline. The swab was then returned to the saline solution. To liberate the phage from the saline hand wipe, the wipe was squeezed to remove the excess liquid and the extracted solution was used for testing. To recover phage from the disposable scrubs, 300mL of deionized water was added to the bags that contained the scrubs, shaken vigorously to ensure that all the scrubs got wet, and excess liquid was poured into a falcon tube for later processing.

Site Decontamination. After the phage recovery phase, a liberal coating of 70% ethanol was applied to all surfaces upon which the health care worker could have interacted. This alcohol was removed, and this cleaning step was repeated with DNA Away, RNA, and Lysol.

Phage Identification and Quantification. The samples were tested for the presence, identity, and densities of the four Lambda phages. Phage identification was performed by PCR, using Thermo Scientific's Phusion Blood Direct PCR Master Mix. Products were visualized on a 1% agarose/TAE gel with Biotium's 10,000X GelRed Nucleic Acid Stain. Band sizes of 800bp were called λ^{Temp} or λ^{Vir} , 1500bp called λ^{Chl} , and 1900bp called λ^{Kan} . Temperate phage (λ^{Temp}) and the virulent mutant (λ^{Vir}) were distinguished during the phage quantification step (Supplemental Figure A1).

The serum resistance lipoprotein (*bor*) gene (Gene ID: 2703532, NCBI) of the lambda phages was amplified by PCR using the following primers designed in PrimerBLAST (NCBI): Forward (*bor*RG1Fw) 5'-GCTCTGCGTGATGATGTTGC-3' and Reverse (*bor*RG1Rv) 5'-GCAGAGAAGTTCCCCGTCAG-3'. Using the double layer soft agar method, LB soft agar overlays containing 0.1 ml of a fully turbid *E. coli* C overnight were prepared and allowed to harden. 0.01 ml of serially diluted saline recovery solution was spotted on the overlay at four densities. These plates were grown overnight at 37°C, and plaques were enumerated the

next day. Based on the turbidity of the plaques, λ^{Vir} was distinguished from the other three temperate forms (see Supplemental Figure A2).

High-Fidelity Simulations. Across two pre-sanitized simulated hospital rooms, defined densities of genetically marked Lambda phages were inoculated at four plausible sources of pathogens on high-fidelity mannequins (e.g., simulated patient excrement, non-intact skin). After contamination, HCWs, comprising registered nurses (RNs) from the emergency department (ED), intensive care units (ICU), or medical/surgical (MS) floors, performed four tasks for two patients over the next hour. For each patient, two of the four tasks required the HCW to interact with a source of contamination: changing a dressing on simulated a stage-4 pressure ulcer (λ^{Temp} on Patient 1's wound), toileting a patient with a bedpan (λ^{Kan} on Patient 1's stool), inserting a Foley catheter (λ^{Chl} on Patient 2's groin), and collecting a stool specimen (λ^{Vir} on Patient 2's stool). HCWs knew that contamination may be present in the simulation but was unaware of the location of contamination and sampling sites. HCWs wore disposable scrubs over their clothing. Personal protective equipment (e.g., gloves and gowns) and medical-grade disinfectants (e.g., alcohol-based hand rub and disinfectant wipes) were available to every HCW during the simulation. Additionally, HCWs documented their work in an electronic medical record, accessed on a mobile "Workstation on Wheels" (WoW).

Table I. Surfaces sampled in each simulation

Type of Surface	Sampling Surface	Number in Figure 1
High Touch	Bedside Table	1,2 (Patient 1); 9,10 (Patient 2)
	Bedrails	3 (Patient 1); 11 (Patient 2)
	Bedrail Buttons	4 (Patient 1); 12 (Patient 2)
	Vital Signs Monitor	7 (Patient 1); 15 (Patient 2)
	Supply Cart	8 (Patient 1); 16 (Patient 2)
Healthcare Worker	Scrubs	19
	Bare Hands	20
WoW	Keyboard	17
	Table	18
Patient Critical Site	Wound	5
	Groin	13
Other Patient Site	Site of Stool Contamination	6 (Patient 1); 14 (Patient 2)

Figure 1. Sampling Design

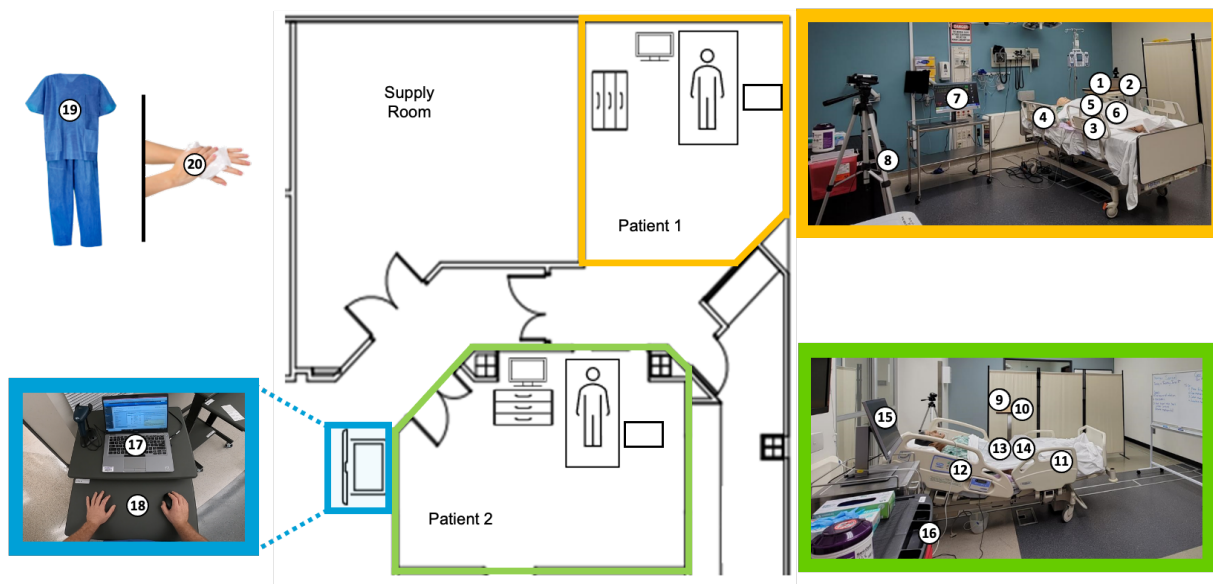


Figure 1. Sampling design. A diagram of the simulated hospital environment with the sampling sites numbered. **(Yellow Inset)** A picture of one simulated hospital room with sampling sites marked. **(Green Inset)** A picture of a second simulated hospital room with sampling sites marked. **(Blue Inset)** A picture of two sampling sites located on the health care worker's mobile workstation.

Results

Method Calibrations

Disinfectant Susceptibility To assess the effect of common hospital disinfectants (as well as disinfectants used in simulations; see High-Fidelity Simulations) on λ phages, we tested the ability of different cleaning agents to eliminate the phages independently and in combination and report changes in plaque forming units (Figure 2A). Each disinfectant was able to reduce the amount of bacteriophage by a minimum of three logs and a maximum of four logs. The combination of Ethanol 70%, DNA Away, RNA Away, and Lysol wipes used subsequently on the surface eliminated the phage so that it was undetectable by PCR. The lack of detectability by PCR shows that unlike other biological contamination proxies, such as cauliflower mosaic virus, our method responds to common hospital disinfectants. There was no difference in the reduction ratio to the disinfectants amongst the phages used. The HCW had access to a wide variety of commercially available disinfectants to use during the simulations, many of which were alcohol based. Three of those disinfectants were tested to see if the hospital based disinfectants had the same effect on the phage as the lab based disinfectants. The aloe wipes, saline spray, and purple wipes (get real names and add to material list) were able to reduce the amount of bacteriophage by a minimum of three logs and a maximum of four logs.

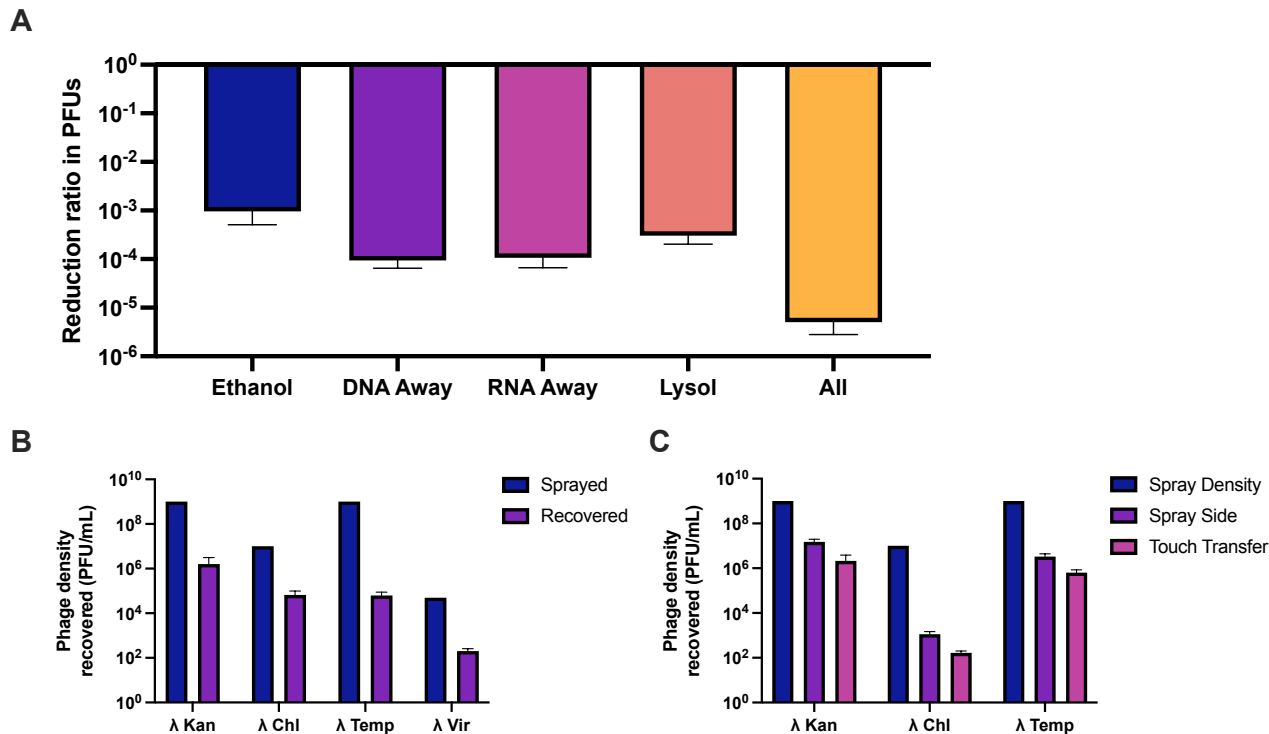


Figure 2: Phage recovery experiments. Experimental results of the effect of antiseptics, time, and surface transfer in sprayed bacteriophage recovery. **(A)** Reduction rate of the phage density on surfaces after exposure to sprayed antiseptics. **(B)** Phage density of the lysate (blue) and the recovery 2 hours post-spray on a surface (purple) at room temperature. **(C)** Phage density of the lysate (blue), the density of the residual phage left on the sprayed surface (purple) after being touched and transferred to a new surface, and the density of phage recovered from the new surface (pink).

Decay Over Time We estimated the rate of decay of each λ phage variant on a surface over time and from the changes in the density of plaque forming units over a given period (Figure 2B). The bacteriophages were sprayed on a surface and allowed to sit for two hours. The time of two hours was more than the allotted time that the bacteriophages would be sitting on a surface in the medical simulations. After the two hours, the surface was then swabbed and plated for recovery. There was a 2 to 3 log₁₀ rate of decay in recoverable PFUs

over time. This same rate of decay between lambda phages differentiates it from other bacteriophages used in medical simulations, such as Phi6 and MS2 (6).

Efficiency of Sampling To determine the efficacy of sampling, phages were sprayed at a known density on a defined area which was then sampled via swabbing. The recovered swabs were then plated on a lawn of *E. coli* C for PFU estimation. We evaluated the efficiency of swabbing recovery to be in excess of 80%.

Spray Bottle Variability We evaluated the variability between sprays in terms of volume and surface area from a given distance away. To ensure that the spray bottle was distributing a consistent and measurable volume, a weigh boat was placed in an analytical scale and tared. The weigh boat was sprayed with one full squeeze from a spray bottle, and the weight of the sample was recorded. It was assumed that the weight in grams was equivalent to the volume of phage sprayed. The average volume sprayed per pump was 0.215mL (± 0.00269). The phage suspension was sprayed from different distances of 5, 10, and 15cm above the bench, to modify the surface area covered. The spray was performed perpendicular to the bench, and the recorded diameter of the spray was defined as the outermost dark ring measured. The diameters for 5, 10, and 15cm away were 65(± 1), 80 (± 5), and 105 (± 10) mm, respectively.

Ability to Spread to Multiple Surfaces To determine the ability of our technique to track phages across multiple surfaces touched by gloved hands, we sprayed a surface with the marked λ phages, which were then touched, spread to other places via subsequent touches, and then sampled. Four subsequent touches from initial lysate. Two log reduction with each subsequent touch. Reported are the changes in plaque forming units between touched surfaces (Figure 2C). After subsequent touching, phage was recovered from the initial inoculation site as well as the site where the phage was transferred via touch. The initial inoculation side saw a one to three-log reduction in PFUs in comparison to the lysate used. The side that was subsequently touched,

which initially had no phage, saw a two to four-log reduction in PFUs in comparison to the lysate used. When comparing the initial inoculation side to the subsequently touched side, there was less than a one-log difference in PFUs that were recovered across all lambda phage strains.

PCR Sensitivity We evaluated the sensitivity of our PCR detection method by serially diluting a stock of the marked λ phages at known plaque forming units (PFUs)/mL, or number of infectious viruses, and performing PCRs at each dilution (Table I). All strains were 100% recoverable through the $1e^2$ PFU/mL, 58% recoverable (7/12) at $1e^1$ PFU/mL, 58% recoverable (7/12) at $1e^0$ PFU/mL, and 75% recoverable (9/12) at $1e^{-1}$ estimated PFU/mL. The difference in recovery rate is likely due to chance because of the small sample volume (1 μ L) used in the PCR processing.

Table II: PCR Sensitive for the Detection of Lambda Phage

Estimated PFU/mL	λKan^*	λChl^*	$\lambda Temp^*$	λVir^*	Positive PCR (%)
E ⁹	XXX	XXX	XXX	XXX	100
E ⁸	XXX	XXX	XXX	XXX	100
E ⁷	XXX	XXX	XXX	XXX	100
E ⁶	XXX	XXX	XXX	XXX	100
E ⁵	XXX	XXX	XXX	XXX	100
E ⁴	XXX	XXX	XXX	XXX	100
E ³	XXX	XXX	XXX	XXX	100
E ²	XXX	XXX	XXX	XXX	100
E ¹	XX	XXX	X	X	58
E ⁰	X	XX	XX	XX	58
E ⁻¹	XX	XXX	XXX	X	75

* An X is assigned for every positive PCR amplification out of 3 replicas

Method Validation with High Fidelity Simulations

As the high-fidelity simulations were conducted as part of a more extensive study, we present the results of a subset of ten randomly selected simulations performed in the manner described above. For each simulation and λ variant, we measured six binary outcomes: 1) whether transmission of a phage occurred within a patient room, 2) between patient rooms, 3) to the nurse, 4) to the WoW, 5) to a critical site on a patient or 6) to another (non-critical) patient site (Table III). We observed a total of 42 transmission events across the ten simulations, with a median of 5 transmission events (Range = 1 to 8 events) occurring per simulation. Transmission events occurred most frequently within patient rooms (29% of all events), to the nurse (19%), at similar frequencies between patient rooms (14%), to the WoW (14%), or to a critical site on a patient (14%), and least frequently to another (non-critical) site on a patient (10%).

Table III. Definition of transmission events

Transmission Event	Definition
Between-Room	A phage from one patient was recovered from at least one high touch surface in the other patient's room.
Within-Room	A phage from one patient was recovered from at least one high touch surface in the same patient's room.
Nurse	A phage was recovered from at least one surface on the nurse.
WoW	A phage was recovered from at least one surface on the WoW.
Patient Critical Site	A phage was recovered from a critical site on a patient, excluding phage introduced to the site as part of the simulation.
Other Patient Site	A phage was recovered from a non-critical patient site.

To illustrate the contribution of each source of contamination to these events, Figure 3 shows the percentage of each type of transmission event originating from each source. All five types of transmission events can be traced back to at least half of the sources of contamination. However, the sources varied in their involvement in transmission events; regarding involvement overall, 50%, 32%, 21%, and 18% of all transmission events originated from Patient 1's wound (λ^{Temp}), Patient 2's groin (λ^{Chl}), Patient 2's stool (λ^{Vir}), or Patient 1's stool (λ^{Kan}), respectively. Regarding involvement in types of transmission events, at least half of transmission events to the nurse (50%) or to the WoW (67%) originated from Patient 1's wound alone. Most transmission events within patient rooms (83%) originated from either Patient 1's wound or Patient 2's stool, and similarly, most transmissions between patient rooms (83%) originated from either Patient 1's wound or Patient 2's groin. Patient 1's stool alone contributed to half of the transmission events to a critical site on a patient. Lastly, phage was infrequently detected on another patient site (i.e., surfaces where the contaminated stool was applied to patients), often originating from another source of contamination on that same patient (e.g., wound or groin). Apart from transmission events, a median of 2 (Range: 1 - 3) of the 4 sources of contamination per simulation was positive for the phage with which they were inoculated, despite each source being cleaned or contained by the HCW.

Figure 3. Percentage of transmission event types originating from contamination sources

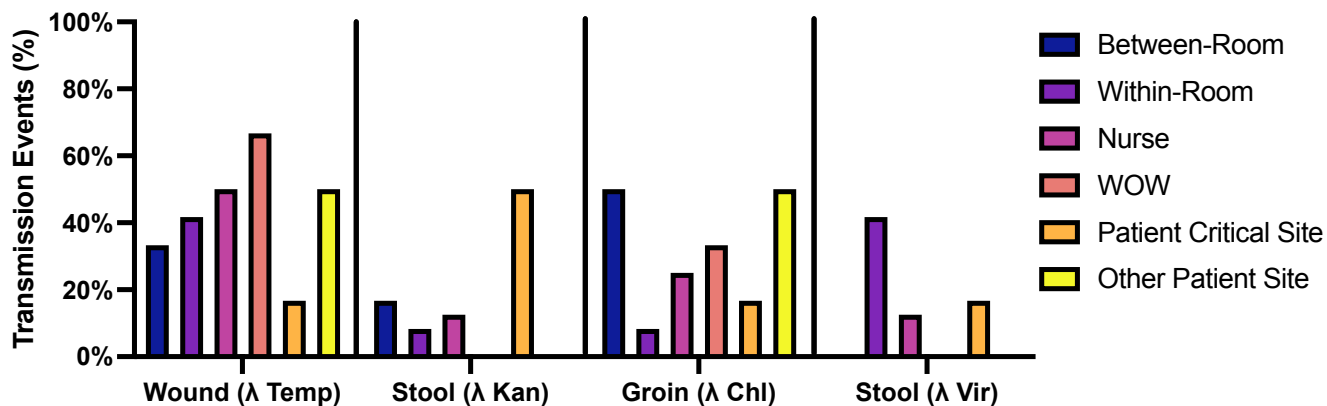


Figure 3. Percentage of transmission event types originating from contamination sources. Shown are data from ten randomly selected simulations. Bars in dark blue are transmissions between the two patient rooms, in orange are transmissions within the patient's own room, in grey recovery from the nurse, in yellow recovery from the workstation on wheels (WoW), and in light blue recovery of phage from a critical site on a patient. Bars of the same color sum to 100% across the four sources of contamination.

Discussion

In this report, we describe a method for using variants of bacteriophage λ as surrogates for pathogen transmission. These variants contain unique genetic markers, which permit the identification of the source and transmission path of each phage via PCR. We showed with our calibration experiments that the effect of disinfectants, decay after two hours, and transfer recovery had no difference among the four phages used in this project. The calibrations allow for the interchangeable ability of these viruses if used in different simulated environments and differentiate them from previous methods used to track contaminations.

To validate the transmission dynamics of λ phages in a naturalistic setting, each phage was inoculated onto a surface in a simulated hospital environment prior to simulated patient care. The patterns of dissemination observed in these simulations resemble those that occur during actual patient care; in the simulations, most transmission events involved the movement of phage from a patient to a high touch surface in that patient's room (e.g., to the bedrails, bedside table, or vital signs monitor). In clinical practice, frequent contact between a HCW, their patient, and the patient's immediate environment rapidly colonizes high-touch surfaces with a patient's own flora (12). Frequently, transmission events to the HCW (e.g., clothing or hands), which contribute to transmission between patients or their rooms (10). Among the least frequent events but most concerning was the transmission of phage to a critical site on a patient. These events are relatively uncommon during actual patient care (2) but increase the risk of a patient developing an infection (12).

An advantage of the present method is that it allows for transmission events to be traced back to different sources of contamination (e.g., patient care tasks). Demonstrating that the four phages were differentially involved in transmission events in the simulations provides further validation of their dynamics in naturalistic settings; for example, phage from Patient 1's wound (a simulated stage-4 pressure ulcer) was the variant most frequently involved in transmission events, particularly transmission to the WoW or the nurse. Wound care is considered a high-contact patient care task, which creates opportunities for pathogens to be transferred to

HCW hands or clothing (13). Consequently, in 2019, the Centers for Disease Control and Prevention began recommending the use of gowns and gloves when performing wound care in skilled nursing facilities (where multidrug-resistant organisms (MDRO) transmission is common), regardless of a resident's MDRO colonization or infection status (13). In accordance with this recommendation, the present method identified wound care as a frequent contributor to transmission events, particularly those that may disseminate pathogens between patients.

As calibration experiments demonstrated the equivalence of the λ variants, differences in how each variant was disseminated in simulated patient care reflect other factors, such as characteristics of tasks (e.g., amount of patient contact) or the infection prevention practices of HCWs. Consequently, this method is useful for identifying the sources of contamination that contribute most to transmission events, where sources could be located simultaneously in different rooms (e.g., to examine MDRO transmission between patients; (10)), body sites of a patient (e.g., to assess the role of endogenous microbes in hospital-acquired infections; (12)), or surfaces on a HCW (e.g., to evaluate the contribution of different items of PPE to HCW self-contamination during doffing;(7)). Lastly, unlike similar surrogates (9), λ phages are susceptible to common disinfectants like alcohol-based hand rub and surface disinfectants, so the effect of infection prevention practices on transmission may also be evaluated.

The present method is not without limitations. Unlike other surrogates, like fluorescent tracers, live viruses do not provide immediate feedback about the occurrence of transmission events. Although less useful for rapidly training HCWs in infection prevention practices (7), the ability to simulate multiple sources of pathogens simultaneously and realistically lends itself to rigorous research or quality improvement efforts (e.g., evaluating the effectiveness of the training program). Lastly, the number of available λ variants is limited, but any similar phages with detectable variation at one gene could be employed for future efforts.

Conclusions

Four variants of the bacteriophage λ were used as surrogates for pathogens to track transmission events in a simulated hospital environment. Analyses of the results from ten simulations in which healthcare workers performed common patient care tasks revealed that λ phages can identify the sources of pathogen transmission and assess their differential involvement in transmission events within and between patient rooms, to mobile surfaces, and to critical sites on patients. Whereas existing approaches using non-biological or biological surrogates for pathogens have succeeded in simulating multiple sources of contamination but not the susceptibility of pathogens to common disinfectants (e.g., alcohol-based hand rub), the present method is notable for achieving both. The applicability of the present method is broad but is particularly relevant to understanding the sources and pathways of MDRO transmission in healthcare settings.

Acknowledgements

We would like to thank Rebecca MacKay for her comments and support in the simulations, Jill Morgan, Golpar Ghassemian, and Lindsey Lee for their help designing the simulation scenario, and Ellen Jordan, Anagha Nair, and Marilyn Garcia for conducting the simulations. We would also like to thank the nurses who participated in the simulations.

BRL would like to thank the US National Institutes of General Medical Sciences for their funding support via R35 GM 136407.

Data Availability

The data supporting this study's findings are available in this manuscript and supplementary material. Further requests may be made to the corresponding author.

Strain Availability

All bacterial strains and bacteriophages used in this project are available upon request to Joel Mumma or Bruce Levin.

Conflict of Interest Statement

The authors have no competing interests to declare.

Funding Statement

This work is supported by the National Institute of General Medical Sciences (R35GM136407); This work is supported by the Centers for Disease Control and Prevention National Infection Control Strengthening Program (grant no. NU38CK000481).

References

1. Umscheid CA, Mitchell MD, Doshi JA, Agarwal R, Williams K, Brennan PJ. Estimating the proportion of healthcare-associated infections that are reasonably preventable and the related mortality and costs. *Infect Control Hosp Epidemiol*. 2011;32(2):101-14. Epub 2011/04/05. doi: 10.1086/657912. PubMed PMID: 21460463.
2. Clack L, Scotoni M, Wolfensberger A, Sax H. "First-person view" of pathogen transmission and hand hygiene - use of a new head-mounted video capture and coding tool. *Antimicrob Resist Infect Control*. 2017;6:108. Epub 2017/11/03. doi: 10.1186/s13756-017-0267-z. PubMed PMID: 29093812; PubMed Central PMCID: PMC5661930.
3. Grundmann H, Hellriegel B. Mathematical modelling: a tool for hospital infection control. *Lancet Infect Dis*. 2006;6(1):39-45. Epub 2005/12/27. doi: 10.1016/s1473-3099(05)70325-x. PubMed PMID: 16377533.
4. Wilson AM, Reynolds KA, Canales RA. Estimating the effect of hand hygiene compliance and surface cleaning timing on infection risk reductions with a mathematical modeling approach. *Am J Infect Control*. 2019;47(12):1453-9. Epub 2019/07/25. doi: 10.1016/j.ajic.2019.05.023. PubMed PMID: 31331717.
5. Lipsitch M, Bergstrom CT, Levin BR. The epidemiology of antibiotic resistance in hospitals: paradoxes and prescriptions. *Proc Natl Acad Sci U S A*. 2000;97(4):1938-43. Epub 2000/03/04. doi: 10.1073/pnas.97.4.1938. PubMed PMID: 10677558; PubMed Central PMCID: PMC26540.
6. Monegro AF, Muppidi V, Regunath H. Hospital Acquired Infections. *StatPearls*. Treasure Island (FL)2022.
7. Poller B, Hall S, Bailey C, Gregory S, Clark R, Roberts P, et al. 'VIOLET': a fluorescence-based simulation exercise for training healthcare workers in the use of personal protective equipment. *J Hosp*

Infect. 2018;99(2):229-35. Epub 2018/02/09. doi: 10.1016/j.jhin.2018.01.021. PubMed PMID: 29421340; PubMed Central PMCID: PMC7133760.

8. Alhmidi H, John A, Mana TC, Koganti S, Cadnum JL, Shelton MB, et al. Evaluation of Viral Surrogate Markers for Study of Pathogen Dissemination During Simulations of Patient Care. *Open Forum Infect Dis.* 2017;4(3):ofx128-ofx. doi: 10.1093/ofid/ofx128. PubMed PMID: 28752103.

9. Scotoni M, Koch J, Julian TR, Clack L, Pitol AK, Wolfensberger A, et al. Silica nanoparticles with encapsulated DNA (SPED) - a novel surrogate tracer for microbial transmission in healthcare. *Antimicrob Resist Infect Control.* 2020;9(1):152. Epub 2020/09/18. doi: 10.1186/s13756-020-00813-7. PubMed PMID: 32938493; PubMed Central PMCID: PMC7493369.

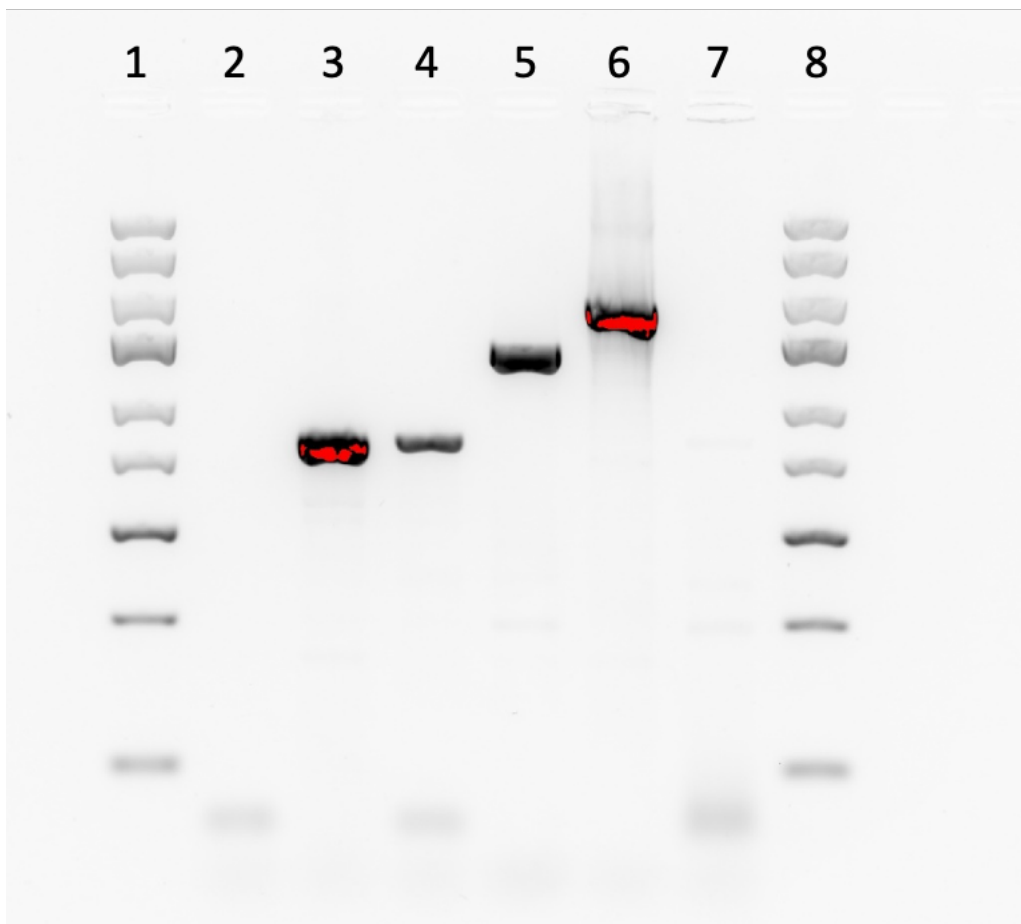
10. Thakur M, Alhmidi H, Cadnum JL, Jencson AL, Bingham J, Wilson BM, et al. Use of viral DNA surrogate markers to study routes of transmission of healthcare-associated pathogens. *Infect Control Hosp Epidemiol.* 2021;42(3):274-9. Epub 2020/10/01. doi: 10.1017/ice.2020.443. PubMed PMID: 32993827.

11. Huslage K, Rutala WA, Sickbert-Bennett E, Weber DJ. A quantitative approach to defining "high-touch" surfaces in hospitals. *Infect Control Hosp Epidemiol.* 2010;31(8):850-3. Epub 2010/06/24. doi: 10.1086/655016. PubMed PMID: 20569115.

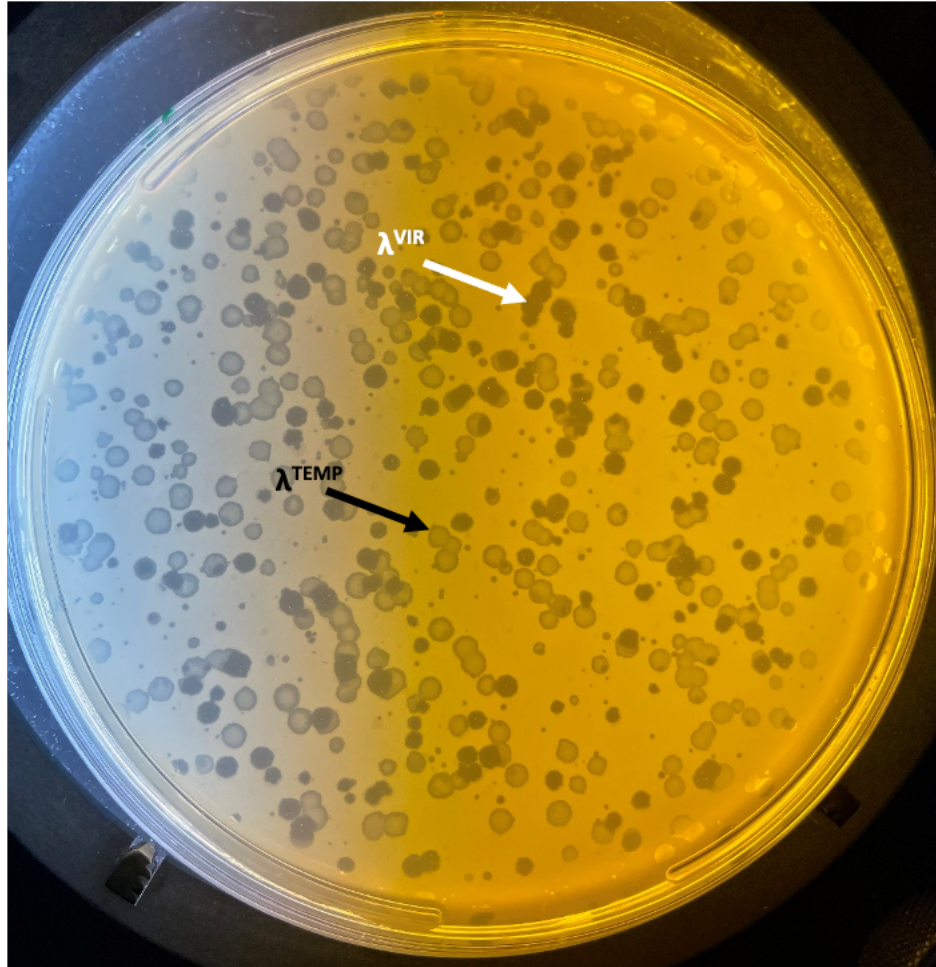
12. Sax H, Allegranzi B, Uçkay I, Larson E, Boyce J, Pittet D. 'My five moments for hand hygiene': a user-centred design approach to understand, train, monitor and report hand hygiene. *J Hosp Infect.* 2007;67(1):9-21. Epub 2007/08/28. doi: 10.1016/j.jhin.2007.06.004. PubMed PMID: 17719685.

13. Siegel JD, Rhinehart E, Jackson M, Chiarello L. Management of multidrug-resistant organisms in health care settings, 2006. *Am J Infect Control.* 2007;35(10 Suppl 2):S165-93. Epub 2007/12/11. doi: 10.1016/j.ajic.2007.10.006. PubMed PMID: 18068814.

Supporting Information



Supplemental Figure A1. PCR Differentiation of Lambda phage variants. Shown from left to right are the (1) Standard Ladder, (2) a water control, (3) λ^{Temp} , (4) λ^{Vir} , (5) λ^{Chl} , (6) λ^{Kan} , an (7) *Escherichia coli* bacterial host control, and a (8) O'GeneRuler Express DNA Ladder (5kb).



Supplemental Figure A2. Plaque morphology difference in λ^{Temp} and λ^{Vir} . Shown is a double-layer soft agar lawn of *E. coli* C containing both λ^{Temp} (turbid plaques) and λ^{Vir} (clear plaques).

Appendix 2

Appendix 2

A Bacteriophage-based Validation of a Personal Protective Equipment Doffing Procedure to be Used with High Consequence Pathogens

Reprinted from: Brandon A. Berryhill, Kylie B. Burke, Andrew P. Smith, Jill S. Morgan, Jessica Tarabay, Josia Mamora, Jay B. Varkey, Joel M. Mumma, Colleen S. Kraft. 2024. A Bacteriophage-based Validation of a Personal Protective Equipment Doffing Procedure to be Used with High Consequence Pathogens. *Infection Control & Hospital Epidemiology*. <https://doi.org/10.1017/icc.2024.84>

Abstract

Objective To determine if the high-level personal protective equipment used in the treatment of high consequence infectious diseases is effective at stopping the spread of pathogens to healthcare personnel (HCP) while doffing.

Background Personal protective equipment (PPE) is fundamental to the safety of HCPs. HCPs treating patients with high-consequence infectious diseases use several layers of PPE, forming complex protective ensembles. With high-containment PPE, step-by-step procedures are often used for donning and doffing to minimize contamination risk to the HCP, but these procedures are rarely empirically validated and instead rely on following infection prevention best practices.

Methods A doffing protocol video for a high-containment PPE ensemble was evaluated to determine potential contamination pathways. These potential pathways were tested using fluorescence and genetically marked bacteriophages.

Results The experiments revealed existing protocols permit contamination pathways allowing for transmission of bacteriophages to HCPs. Updates to the doffing protocols were generated based on the

discovered contamination pathways. This updated doffing protocol eliminated the movement of viable bacteriophages from the outside of the PPE to the skin of the HCP.

Conclusions Our results illustrate the need for quantitative, scientific investigations of infection prevention practices, such as doffing PPE.

Introduction

To protect healthcare personnel (HCPs) caring for patients with communicable diseases, protocols have been established to mitigate the risk of transmission [1]. Central to these protocols is personal protective equipment (PPE). The PPE used to minimize exposure to high consequence infectious diseases (HCIDs), such as Ebola virus disease, utilizes layers of barrier precautions including fluid-resistant coveralls, impervious aprons or gowns, fluid-resistant footwear, powered air-purifying respirators (PAPRs), and gloves. Protocols that outline proper donning and doffing of the PPE are fundamental to mitigating self-contamination for HCPs and preventing the transmission of contaminants outside patient rooms [2]. However, PPE protocols are often based on manufacturer recommendations of individual products and infection prevention best practices. Accordingly, ensembles of PPE and their corresponding protocols usually have not been empirically validated.

Previous studies have demonstrated that adherence to PPE doffing protocols is challenging and variable among HCPs [2]; previous studies have quantitatively examined and discovered high rates of deviations from established protocols [3]. Doffing protocols would optimally be safe even considering this high underlying variability. Moreover, rigorous risk assessments of PPE ensembles should consider this factor in evaluating PPE safety.

This study explores contamination risks of an established doffing protocol. To validate this protocol's efficacy, we applied a quantitative analysis of the PPE ensemble to test for self-contamination. This investigation consisted of two phases: 1) examination of the original PPE ensemble and its doffing protocol with fluorescence and bacteriophages; and 2) determination if an amended protocol decreased self-contamination.

This study highlights the need for infection prevention protocols, such as high-containment PPE doffing, to be evaluated in a quantitative, experimental fashion. We present results from both phases of our investigation below.

Methods

Investigational Procedures

Movie analysis

Doffing protocols were captured on video. Each movie was analyzed by authors BAB, KBB, APS, and JSM who viewed and stopped the movie and recorded comments when potential hazards were observed.

For each doffing trial, footage was taken from four camera angles using camcorders (Canon, Japan, Model #HF R80) supplied by the Healthcare and Human Factors Lab at Emory. Comments were made for possible contamination during the Phase 1 phage trial and deviations from the protocol in the Phase 2 phage trial (Supplementary Table 1).

Fluorescent testing

To verify the contact we observed in the movie described above, we used a 0.5% fluorescein solution (Millipore Sigma, USA, Catalogue #F6377) and Glo Germ powder (Glo Germ, USA, #GGP10) to visualize contamination and identify the steps where spread of contaminant may occur. To conduct this test, a trained HCP donned a complete high-containment PPE ensemble and was then sprayed with the fluorescein solution. The solution was sprayed to coat surfaces of the PPE that may be exposed to contact with patients (patient-facing surfaces). The HCP then doffed according to the protocol. Pictures were taken from multiple angles to record how fluorescein transfer; ultraviolet flood lights (Onforu, China, #UFLAU004102) were used to emphasize fluorescence. A separate test was performed for aerosolization risk where the heavy-loading filter on top of the PAPR hood was laden with Glo Germ powder. After the filter was removed, pictures were taken with ultraviolet to capture results of the experiment.

Phage testing

Using a previously validated procedure [4], we sprayed with small spray bottles (Bürkle, Germany, #10216-888) high densities (approximately 10^8 phages per mL) of three genetically distinct λ phages on HCP

volunteers to reflect densities of pathogens found in patient samples (Supplementary Table 2). 2mL of λ phages were sprayed onto three locations, and each site was sprayed with a different variant of λ : one marked with a kanamycin resistance gene was sprayed on the wrists; one marked with a chloramphenicol resistance gene was sprayed on the back of the hood; and one lacking an antibiotic marker at the critical triangle, described below. HCPs then doffed, after which their hands, forearms, and PAPR were swabbed and scrubs were collected and tested for bacteriophage presence and identification.

Materials and Technical Methods

Strains

Escherichia coli strain C was acquired from Marie-Agnès Petit from INRAe, France. Bacteriophages λ (λ^{Temp}), λ^{Chl} , and λ^{Kan} was obtained from Maroš Pleška at The Rockefeller University.

Bacteriophage Lysate Preparation and Distribution

Each type of λ phage lysate were inoculated, shaken, centrifuged, and filtered per the methods in Burke et al. [4] to create high-titer lysates (PFU/mL between 1×10^8 and 1×10^9). These lysates were stored in spray bottles, transported, and primed per the methods in Burke et al. [4]. Immediately after priming, each lysate was sprayed with one pump from a distance of 10 cm onto the target sites for initial contamination. The spray dried clear and were unidentifiable to the naked eye. Contamination occurred no earlier than five minutes before the start of the doffing.

Bacteriophage Recovery

Immediately after the doffing procedure, skin was sampled by applying a saline wipe (Hygea, USA, #C22370) around the hands and a wipe around the forearms; these wipes were stored in conical tubes (Corning, USA, #352070). Disposable scrubs were then stored in a Whirl-Pak (Nasco, USA, #B01542). Four sites of interest were swabbed with self-contained saline swabs (Hardy Diagnostic, USA, #SRK35) using a progressive back-and-forth motion until the entire surface appeared damp. To liberate phage from the saline wipe, the wipe was squeezed to remove excess liquid and the extracted solution was tested. To recover phage from the scrubs, 300mL of deionized water was added to the bags that contained the scrubs and shaken vigorously to ensure scrubs were fully saturated. Excess liquid was poured into a conical tube for testing. To recover phage from the swabs, the saline containers were vortexed vigorously.

After bacteriophage recovery, all surfaces with possible phages were sprayed with 70% ethanol (Decon Labs, USA, #2716) and wiped with Sani-Cloth Disposable Wipes (Professional Disposables International, Inc., USA, #Q55172).

Bacteriophage Identification and Quantification

Phage identification was performed by PCR, using the methods and materials used in Burke et al. [4]. Band sizes of 800bp were called λ^{Temp} , 1500bp called λ^{Chl} , and 1900bp called λ^{Kan} . The PCR was performed with an O'Gene Ruler DNA Ladder (Thermo Fisher Scientific, USA, #SM1563).

The serum resistance lipoprotein (*bor*) gene (Gene ID: 2703532, NCBI) of the λ phages was amplified by PCR using the following primers designed in PrimerBLAST (NCBI): Forward (borRG1Fw) 5'-GCTCTGCGTGATGATGTTGC-3' and Reverse (borRG1Rv) 5'-GCAGAGAAGTTCCTCCGTCAG-3'. Using the double layer soft agar method [5] LB soft agar overlays containing 0.1 mL of a turbid *E. coli* C overnight were prepared and allowed to harden. 0.01 mL of serially diluted saline recovery solution was spotted on the overlay at four densities. These plates were grown overnight at 37°C, and plaques were enumerated the next day.

If samples were determined to be PCR positive but negative via spot testing, 100 μ L of sample were cultured with 1×10^7 CFU/mL log-phase *E. coli* C in 10mL of LB broth. These cultures were grown with shaking for six hours, centrifuged, and filtered through a 0.22 μ m filter to generate boosted lysates. 300 μ L of these lysates were plated on *E. coli* C lawns to determine viable bacteriophage presence.

Process Documentation (Videography and Still Photography)

For the fluorescein and Glo Germ experiments, pictures were taken with an iPhone under ultraviolet illumination in a dark room; footage was recorded with one camcorder. During doffing trials, pictures and footage were recorded under standard room lighting.

Results

Initial protocol analysis

Analysis of initial doffing movie

The investigation of the initial protocol (detailed in Supplementary Table 3, 4, 5) began with a movie analysis.

Table 1 notes observations of potential sources of contamination to the HCP during the doffing protocol displayed in Movie 1. Steps can be correlated to the steps of the original protocol in Supplementary Table 3.

Table 1: Events of concern noted during annotation of the PPE doffing movie.

Event Description	Step Number
When removing the outer gloves, the sleeves of the coverall may come into contact with the front surface of the PAPR hood.	17
Removing the heavy-loading PAPR filter creates a high risk of aerosolization.	19
The tie at the neck of the PAPR is not fully covered by the apron and could potentially contaminate the gloves when it is broken.	21
Incidental contact to the inside of the PAPR hood may occur when reaching in to unzip the coverall.	27
When the coverall is being pulled down the PAPR hood is free to move about and may contact skin of participant.	28
When marching in place to remove coverall, incidental contact with the PAPR hood occurs.	30

Event Description	Step Number
When marching in place, the PAPR hood is free to move around, potentially generating aerosols.	30
When the coverall is removed from the legs, one is instructed to “keep your hands together.” Forearms came in contact with the front of the PAPR hood that is not covered by the apron (henceforth referred to as the PAPR hood Critical Triangle).	31
When disposing of the coverall, there is a risk of incidentally interacting with patient-facing surfaces should care not be taken when picking the coverall off the ground.	32*
When removing the PAPR hood, the back of the hood is pulled forward from the back of the head to cover the face shield. The corner of the PAPR hood can fold out so that the PAPR hood Critical Triangle is exposed and the HCP removing the PAPR has no way of seeing this.	37
When the PAPR hood is flipped forward, the back of the PAPR can contact the front of one’s scrubs.	38
While reaching back and grabbing the hood, there is a large amount of contact between bare forearms, scrubs, and the PAPR hood Critical Triangle.	37
When locating the edges of the visor, incidental contact with the face may occur.	38
General Procedural Notes	
The alcohol sanitation is only being performed on gloves and not the forearms or wrists.	

*This step in the movie deviated from the written protocol.

Evaluating contamination via fluorescence testing

In Figure 1 we present several pictures of testing with fluorescence that illustrate the concerns raised by the movie. We note that the protocol as performed in our trials, including this one, follows the written protocol and differs slightly from Movie 1; Movie 2 accurately portrays the written doffing protocol. There are six pairs of pictures: The left (L) panes show areas of concern, and the right (R) panes show the spread of fluorescence from those events.

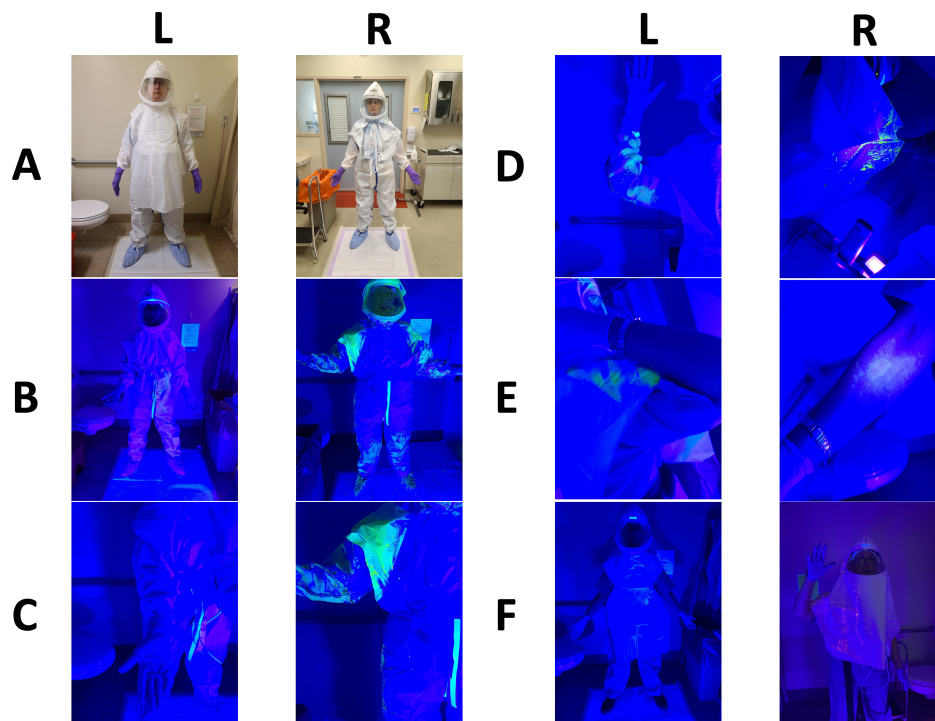


Figure 1: Fluorescent visualization of areas and actions of concern during doffing. Experimental results of doffing with fluorescent markers present for specific actions of concern or highlighting areas of concern, as found during review of the doffing protocol movie. **Left (L):** Before; shows areas that may be of concern. **Right (R):** After; shows potential concerns by transfer of fluorescence. **(A)** The original PPE ensemble in natural light, both with the apron and with the apron removed. **(B)** Patient facing surfaces of the PPE not covered by the apron which could become contaminated. **(C)** Critical Triangle area of the PAPR. **(D)** Interaction of the coverall sleeves with the inside of the PAPR hood. **(E)** Transfer of contaminate from the PAPR hood to the forearm that can occur during doffing. **(F)** Aerosolization of fine powder trapped on the heavy-loading filter.

The fluorescein reveals the materials in the complete PPE ensemble that are patient-facing. 1AL shows a complete ensemble, and 1AR shows the ensemble without the apron. 1BL shows the ensemble under blacklight, and 1BR shows contamination not covered by the apron. 1CL and 1CR highlight the “Critical Triangle”, which includes parts of the shoulder, the side of the abdomen, and the arm.

The movement of the fluorescein demonstrated in Figure 1 reveals how contamination can move from the outside of the PPE ensemble to an intermediate location, then ultimately to the HCP. These contamination pathways are demonstrated in 1D, 1E, and 1F. 1DL shows how contamination may reach the arm or Critical Triangle of the coveralls. From here, contamination could transfer to the underside of the shroud (shown in 1DR) which could then move to scrubs. 1E shows a second pathway, where contamination on a patient-facing shoulder (1EL) transfers to arms when reaching up to roll up the PAPR hood, with that contamination demonstrated in 1ER. 1F demonstrates how aerosolized pathogens land on skin, scrubs, and footwear.

Using these results, three initial locations on the PPE were determined to pose a high contamination risk. These locations are (i) the PAPR hood Critical Triangle, located to the left and right of the apron and near shoulders, (ii) the wrist/lower forearm area of the protective coverall, and (iii) the back of the PAPR hood near the filter and shoulders.

Doffing in the presence of a bacteriophage proxy

To more accurately mirror pathogenic contamination, we inoculated three genetically marked variants of λ on the three sites above to determine both the origin and final location of each virus. Presented in Figure 2 are the results of doffing performed by four HCPs with varying heights and body types and varying experience in performing the protocol.

HCW1-1		Recovery Location			
		Scrubs	Hands	Forearms	Inside PAPR
Origin	Critical Triangle*	---	---	2.5×10^3	5.4×10^4
	Coverall Cuffs	---	---	---	---
	Back Hood	---	1×10^3	---	5.4×10^4

HCW2-1		Recovery Location			
		Scrubs	Hands	Forearms	Inside PAPR
Origin	Critical Triangle	---	---	---	4×10^2
	Coverall Cuffs	---	---	---	---
	Back Hood	---	---	5.6×10^3	---

HCW3-1		Recovery Location			
		Scrubs	Hands	Forearms	Inside PAPR
Origin	Critical Triangle	---	---	---	---
	Coverall Cuffs	---	---	1.8×10^3	---
	Back Hood	---	---	---	---

HCW4-1		Recovery Location			
		Scrubs	Hands	Forearms	Inside PAPR
Origin	Critical Triangle	3.6x10 ⁴	---	---	---
	Coverall Cuffs	---	---	---	---
	Back Hood	3.6x10 ⁴	1x10 ³	1.9x10 ³	---

*Critical Triangle = The side of the PAPR hood, coveralls, and arm, which may be exposed and facilitate contamination

Figure 2: Phage recovery after doffing PPE. Experimental results of doffing protocols performed by four HCPs with three bacteriophages initially inoculated on the PAPR Critical Triangle, coverall cuffs, and the back of the PAPR hood. Numbers inside each square represents the number of PFU/mL recovered from that location.

Figure 2 demonstrates that phages moved to the four locations we had hypothesized could become contaminated. Moreover, we found these phages to be viable and present at high densities. All four HCPs demonstrated contamination.

These four HCPs were recorded from multiple angles while performing the doffing procedure. We present in Table 2 behaviors noted during our analysis of the movies which would increase the risk of contamination.

Table 2: Concerns noted while reviewing movie of four HCPs doffing.

*Critical Triangle = The side of the PAPR hood, coveralls, and arm, which may be exposed and facilitate contamination

Event Description	Step Number
When removing the heavy-loading filter, people tend to not be conscious of where it is and have a tendency to either swing it around, aerosolizing particles, or touch it to their PAPR hood.	19
During the stomping to remove the coverall, the PAPR hood moves around substantially, often coming into contact with the scrubs and in the forearms.	30
One HCP misinterpreted how they should hold their hands in front of their body when removing the coverall and put their clasped hands against the front of the PAPR hood.	31
Clasping the hands in front of the body when removing the coverall often results in the bare forearms interacting with the front and/or Critical Triangle* of the PAPR.	31
Any manipulation above the head post coverall removal puts the HCP's forearms in contact with the PAPR hood Critical Triangle.	37-39
The PAPR hood repeatedly bunches up or flips over near the shoulders.	
On short HCPs, the front of the PAPR hood folds in on itself easily.	
On particularly tall HCPs, the apron does not cover nearly as much of the coverall and PAPR as it does on shorter individuals.	

Updated protocol analysis

Changes to the Protocol

Our analysis and experiments of the first protocol revealed insufficiencies that led to contamination of the HCP. We aimed to eliminate viable phage recovery by limiting the observed contamination pathways. Accordingly, we altered the protocol in both equipment and doffing steps (Movie 3; Supplementary Table 3; Supplementary Table 4; Supplementary Table 5). Below is a table detailing changes made to the PPE ensemble and procedure.

Six amendments were made to the protocol. Adjustments were made based largely upon concerns raised by the phase one analysis, but amendments were also incorporated for ease of doffing. Of the six changes, three were changes in equipment; one was an additional step made for added equipment; and two were reordered steps.

Table 3: Updates to the protocol.

Protocol Amendments			
Old Protocol	New Protocol	Revision	Comment
No inner shoe liner	Calf-high shoe liner over shoes and pant legs	Add inner shoe cover	Makes doffing coverall easier
Regular length inner gloves	Extended cuff inner gloves	Change length of inner gloves	Reduces risk of exposed skin at wrist
Outer gloves donned before PAPR	Outer gloves donned last	Move step for donning outer gloves	Outer gloves are worn over sleeve of gown
Apron	Gown	Replaced apron with gown	Improved coverage of PAPR hood at shoulders and Critical Triangle
Heavy-loading filter removed after apron	Heavy-loading filter removed first	Move step for heavy-loading filter removal	Removes higher-contaminated items earlier in doffing protocol
No gown	Gown sleeves freed from outer gloves	Insert step to pull gown sleeve out of the outer glove cuff	Facilitates gown removal

Phage Testing with Updated Protocol

We next evaluated the updated protocol with the phage testing described previously. Nine HCPs doffed using the updated protocol. The results of these doffing trials are presented in Figure 3.

HCW1-2		Recovery Location			
		Scrubs	Hands	Forearms	Inside PAPR
Origin	Critical Triangle*	---	---	X	---
	Coverall Cuffs	---	---	X	X
	Back Hood	X	---	---	---

HCW2-2		Recovery Location			
		Scrubs	Hands	Forearms	Inside PAPR
Origin	Critical Triangle	---	---	---	---
	Coverall Cuffs	---	---	X	X
	Back Hood	---	---	---	---

HCW3-2		Recovery Location			
		Scrubs	Hands	Forearms	Inside PAPR
Origin	Critical Triangle	---	---	---	---
	Coverall Cuffs	---	X	---	X
	Back Hood	X	---	---	---

HCW4-2		Recovery Location			
		Scrubs	Hands	Forearms	Inside PAPR
Origin	Critical Triangle	---	---	X	---
	Coverall Cuffs	X	---	---	---
	Back Hood	X	X	---	---

HCW5-2		Recovery Location			
		Scrubs	Hands	Forearms	Inside PAPR
Origin	Critical Triangle	---	---	---	---
	Coverall Cuffs	---	---	---	---
	Back Hood	---	X	---	X

HCW6-2		Recovery Location			
		Scrubs	Hands	Forearms	Inside PAPR
Origin	Critical Triangle	---	---	---	---
	Coverall Cuffs	---	---	---	---
	Back Hood	X	---	---	X

HCW7-2		Recovery Location			
		Scrubs	Hands	Forearms	Inside PAPR
Origin	Critical Triangle	X	---	---	---
	Coverall Cuffs	X	---	---	---
	Back Hood	X	X	X	X

HCW8-2		Recovery Location			
		Scrubs	Hands	Forearms	Inside PAPR
Origin	Critical Triangle	---	---	---	---
	Coverall Cuffs	---	---	---	X
	Back Hood	X	---	---	---

HCW9-2		Recovery Location			
		Scrubs	Hands	Forearms	Inside PAPR
Origin	Critical Triangle	---	---	---	---
	Coverall Cuffs	---	---	X	---
	Back Hood	---	---	---	X

*Critical Triangle = The side of the PAPR hood, coveralls, and arm, which may be exposed and facilitate contamination

Figure 3: Bacteriophage recovery after doffing PPE with the altered protocols. Experimental results of the altered doffing protocols performed by nine HCPs with three bacteriophages initially inoculated on the PAPR Critical Triangle, coverall cuffs, and the back of the PAPR hood. An X denotes that the phage DNA from the origin location was found at that sampled location at the end of doffing via PCR. To test for viable phages below the limit of detection (1×10^2 PFU/mL) samples were incubated with a susceptible bacteria host and no viable phages were recovered from any HCP.

Following the updated protocol, no viable phages were recovered. Phage DNA was found via PCR from several locations (indicated by an X) but viable phages were unable to be recovered from these PCR-positive samples even after providing a bacterial host. This indicates that the phages moved during doffing, but these phages were likely inactivated by the alcohol-based sanitizer during hand hygiene. Even if a contamination pathway was not eliminated, the updated protocol limited those pathways to contamination on gloves where sanitation could deactivate the bacteriophages.

Deviations from the doffing protocol by HCPs could contribute to variability in the results shown in Figure 3. We analyzed footage of each HCP doffing and noted deviations from the protocol which may lead to the spread of bacteriophages (Supplementary Table 1). Several HCPs deviated from the procedure. However, these deviations did not increase contamination per the results in Figure 3.

Discussion

PPE forms the cornerstone of safety for HCPs, but for HCPs working with HCIDs, satisfactory high-containment PPE is especially important [6]. Hundreds of HCPs experienced near-miss events, infections, or death from Ebola virus disease [7, 8]. Although individual pieces of equipment receive National Institute for Occupational Safety & Health approval, PPE ensembles and their doffing protocols do not. Indeed, Koh et al. wrote over twenty years ago that PPE needed to be evaluated for efficacy against infection from SARS – this is a problem that has needed addressal for decades [9], and later, the same call to action was issued for empirical review of Ebola PPE and ensembles [10].

This PPE ensemble had not been assessed by empirical means. Our goal was to evaluate the ensemble and doffing protocol for possible contamination pathways and offer interventions to mitigate potential contamination. Even a slight contamination of an HCID could be a threat to HCPs (Supplementary Table 2). Thus, the aim of our interventions was to prevent viable self-contamination. We note that although other methods exist for analyzing the antiviral and disinfection qualities of PPE and its ensembles [11, 12], we elected to focus exclusively on how this ensemble performed in the transfer of pathogens.

Our first phase of this study began with an examination of a movie depicting the original protocol. The original protocol followed infection prevention best practices and was designed with disease containment in mind, but an in-depth evaluation revealed potential contamination pathways. We found from the fluorescence testing that contamination moved through the pathways we had hypothesized onto scrubs and skin.

Fluorescence experiments, however, carry limitations [13]. Fluorescence does not reflect sanitation measures and can be visually tracked by participants. Contamination experiments with phages resolve both failings. The viruses are visually undetectable and can be inactivated via alcohol-based sanitation but pose no appreciable risk [4, 14]. With the original doffing protocol, all participants had at least one contamination with at least

1800 virions present – an amount far greater than the minimum infective dose of many HCIDs (Supplementary Table 2).

We next offered an assortment of interventions. Modifications were made not only to reduce contamination by contact, but also to make doffing easier. Reducing discomfort for HCPs may reduce deviations from a protocol, reducing contamination. The result of these changes manifested in the phage experiment with the updated protocol. In the second phage experiment, we did not recover a viable population of phage on any of the nine HCPs. Through PCR, we found phage DNA in several locations, indicating that the phages were inactivated by the use of alcohol-based sanitizer during the doffing. Phages that may have contaminated several locations were routed through pathways that included successful hand sanitation. Moreover, updates to the protocol eliminated intermediate contamination locations present in the original doffing protocol, which would have re-contaminated the HCP at later doffing steps. These results were observed despite deviations from the protocol by the HCPs during their doffings. The protocol, built to include redundancies and reduce events of contamination, allowed for small deviations without self-contamination.

This study does contain limitations. The original contamination was deliberately placed according to the fluorescent test with the intention of revealing contamination pathways. Thus, we cannot wholly capture contamination that would occur in a clinical setting – instead, we show how specific contamination can be tracked and eliminated through specific procedures. Further studies are needed to capture how contamination may move throughout a clinical environment, on PPE and otherwise. We further note that phages are only proxies. Using HCIDs for studies such as this is not ethical, but accordingly, we are closely approximating how they would function in a clinical setting through phages.

With the initial PPE ensemble and doffing protocol, contamination occurred that would have endangered the individual HCP and the community at large had it occurred with a dangerous pathogen. Through modifications of both protocol and equipment, the doffing protocol was successfully improved from initially

incurring dangerous amounts of contamination to eliminating viable contaminants in all cases. These tests did not pose a great financial burden. Excluding PPE costs, each trial cost less than \$45 USD, and our interventions were modest. Based on our results, validation of other healthcare PPE protocols by quantitative methods such as those we employed here is both logistically feasible and informative. No hospital procedure is designed for failure, but with empirical validation, those procedures can ensure they provide necessary protection.

Acknowledgements

We thank the other members of the Levin Lab, particularly Joshua Manuel and Bruce Levin, for their advice and assistance. We also Jessica Carag and Darryl Grant for their help with revising this manuscript.

Financial Support

This work was supported by funds from the US National Institute of General Medical Sciences [grant number R35GM136407 to Bruce R. Levin]; the US National Institute of Allergy and Infectious Diseases [grant number U19AI158080-02 to Bruce R. Levin]; and the Centers for Disease Control and Prevention [grant number NU38CK000481 to Joel M. Mumma]. The funding sources had no role in the design of this study and will not have any role during its execution, analysis, interpretation of the data, or drafting of this report. The content is solely the responsibility of the authors and do not necessarily represent the official views of the Centers for Disease Control and Prevention.

Potential Conflicts of Interest

The authors have no potential conflicts of interest to declare.

Data Availability

All data generated for this manuscript are available in the manuscript or its supplementary material.

References

1. Centers for Disease Control and Prevention NCFEaZIDN, Division of Healthcare Quality Promotion (DHQP). Guidance on Personal Protective Equipment (PPE) To Be Used By Healthcare Workers during Management of Patients with Confirmed Ebola or Persons under Investigation (PUIs) for Ebola who are Clinically Unstable or Have Bleeding, Vomiting, or Diarrhea in U.S. Healthcare Settings, Including Procedures for Donning and Doffing PPE. Accessed 25 April.
2. Casanova LM, Erukunuakpor K, Kraft CS, et al. Assessing Viral Transfer During Doffing of Ebola-Level Personal Protective Equipment in a Biocontainment Unit. *Clin Infect Dis* **2018**; 66(6): 945-9.
3. Kwon JH, Burnham CD, Reske KA, et al. Assessment of Healthcare Worker Protocol Deviations and Self-Contamination During Personal Protective Equipment Donning and Doffing. *Infect Control Hosp Epidemiol* **2017**; 38(9): 1077-83.
4. Burke KB, Berryhill BA, Garcia R, et al. A methodology for using Lambda phages as a proxy for pathogen transmission in hospitals. *J Hosp Infect* **2023**; 133: 81-8.
5. Kropinski AM, Mazzocco A, Waddell TE, Lingohr E, Johnson RP. Enumeration of bacteriophages by double agar overlay plaque assay. *Methods Mol Biol* **2009**; 501: 69-76.
6. MacIntyre CR, Chughtai AA, Seale H, Richards GA, Davidson PM. Uncertainty, risk analysis and change for Ebola personal protective equipment guidelines. *Int J Nurs Stud* **2015**; 52(5): 899-903.
7. World Health O. EBOLA RESPONSE ROADMAP SITUATION REPORT: World Health Organization, **2014**.
8. Houlihan CF, McGowan CR, Dicks S, et al. Ebola exposure, illness experience, and Ebola antibody prevalence in international responders to the West African Ebola epidemic 2014-2016: A cross-sectional study. *PLoS Med* **2017**; 14(5): e1002300.
9. Koh D, Lim MK, Chia SE. SARS: health care work can be hazardous to health. *Occup Med (Lond)* **2003**; 53(4): 241-3.
10. Sprecher AG, Caluwaerts A, Draper M, et al. Personal Protective Equipment for Filovirus Epidemics: A Call for Better Evidence. *J Infect Dis* **2015**; 212 Suppl 2(Suppl 2): S98-s100.

11. Xue X, Coleman CM, Duncan JD, et al. Evaluation of the relative potential for contact and doffing transmission of SARS-CoV-2 by a range of personal protective equipment materials. *Sci Rep* **2022**; 12(1): 16654.
12. Pfuderer L, Stark WJ, Grass RN. Synthetic Microbial Surrogates Consisting of Lipid Nanoparticles Encapsulating DNA for the Validation of Surface Disinfection Procedures. *ACS Applied Bio Materials* **2023**; 6(3): 1252-9.
13. Hall S, Poller B, Bailey C, et al. Use of ultraviolet-fluorescence-based simulation in evaluation of personal protective equipment worn for first assessment and care of a patient with suspected high-consequence infectious disease. *J Hosp Infect* **2018**; 99(2): 218-28.
14. Burke KB, Berryhill BA, Garcia R, et al. Using Lambda phages as a proxy for pathogen transmission in hospitals. *medRxiv* **2022**: 2022.09.09.22279770.
15. Franz DR, Jahrling PB, Friedlander AM, et al. Clinical recognition and management of patients exposed to biological warfare agents. *Jama* **1997**; 278(5): 399-411.
16. Vetter P, Fischer WA, 2nd, Schibler M, Jacobs M, Bausch DG, Kaiser L. Ebola Virus Shedding and Transmission: Review of Current Evidence. *J Infect Dis* **2016**; 214(suppl 3): S177-s84.
17. Suess T, Remschmidt C, Schink SB, et al. Comparison of shedding characteristics of seasonal influenza virus (sub)types and influenza A(H1N1)pdm09; Germany, 2007-2011. *PLoS One* **2012**; 7(12): e51653.
18. Yezli S, Otter JA. Minimum Infective Dose of the Major Human Respiratory and Enteric Viruses Transmitted Through Food and the Environment. *Food Environ Virol* **2011**; 3(1): 1-30.
19. Musisi E, Sessolo A, Kaswabuli S, et al. High Mycobacterium tuberculosis Bacillary Loads Detected by Tuberculosis Molecular Bacterial Load Assay in Patient Stool: a Potential Alternative for Nonsputum Diagnosis and Treatment Response Monitoring of Tuberculosis. *Microbiol Spectr* **2022**; 10(1): e0210021.
20. Sakamoto K. The Pathology of Mycobacterium tuberculosis Infection. *Veterinary Pathology* **2012**; 49(3): 423-39.

21. SeyedAlinaghi S, Karimi A, Mojdeganlou H, et al. Minimum infective dose of severe acute respiratory syndrome coronavirus 2 based on the current evidence: A systematic review. *SAGE Open Med* **2022**; 10: 20503121221115053.
22. Oh M-d, Park WB, Choe PG, et al. Viral Load Kinetics of MERS Coronavirus Infection. *New England Journal of Medicine* **2016**; 375(13): 1303-5.
23. Frey SE, Newman FK, Yan L, Belshe RB. Response to Smallpox Vaccine in Persons Immunized in the Distant Past. *JAMA* **2003**; 289(24): 3295-9.
24. Price PA, Jin J, Goldman WE. Pulmonary infection by *Yersinia pestis* rapidly establishes a permissive environment for microbial proliferation. *Proceedings of the National Academy of Sciences* **2012**; 109(8): 3083-8.
25. Kolodziejek AM, Hovde CJ, Minnich SA. *Yersinia pestis* Ail: multiple roles of a single protein. *Front Cell Infect Microbiol* **2012**; 2: 103.

Movie Legends

Movie 1: Original Training Video. The basis for Table 1. Slight deviations occur between this video and Supplementary Table 3.

Movie 2: Original Doffing Protocol. A demonstration of the original doffing protocol. The steps performed are detailed in Supplementary Table 3.

Movie 3: Updated Doffing Protocol. A demonstration of the updated doffing protocol. The steps performed are detailed in Supplementary Table 3.

Supporting Information

Supplementary Table 1: Analysis of Movie – Adherence to Doffing Protocol

HCP	Deviations
HCP 1	Did not take off outer gloves before undoing PAPR ties
HCP 2	Poor hand sanitization (duration)
HCP 3	Poor hand sanitization (duration and technique)
	Excessive contact with PAPR hood at most steps
	Skipped hand sanitization at multiple steps
HCP 4	None
HCP 5	Poor hand sanitization (duration)
	Poor gown rolling
	Excessive contact with PAPR hood
HCP 6	None
HCP 7	Folding gown near body
	Unzipping coverall while touching PAPR
HCP 8	None
HCP 9	Gown touched PAPR

Supplementary Table 2. Critical densities for pathogens of concern

Pathogen	High Limit of Pathogen Density Commonly Found in Patient Samples	Reported Minimum Infective Dose
<i>Ebolavirus spp.</i> [8, 9]	1x10 ⁷ PFU/mL	1 to 10 Virions
<i>Alphainfluenzavirus sp.</i> [10, 11]	5x10 ⁵ PFU/mL	4 Virions
<i>Mycobacterium tuberculosis</i> [12, 13]	5x10 ⁵ CFU/mL	1 to 200 Bacteria
<i>Betacoronavirus MERS-CoV</i> [14, 15]	1x10 ⁷ PFU/mL	200 to 1000 Virions
<i>Orthopoxvirus Variola virus</i> [8, 16]	5x10 ⁵ CFU/mL	10 to 100 Virions
<i>Yersinia pestis</i> [17, 18]	1x10 ⁹ CFU/mL	1 to 10 Bacteria

Supplementary Table 3. Donning Stepwise Procedure

Steps written in bold font indicate updated steps in the new donning procedure.

Step Number	Original Donning Procedure	Updating Donning Procedure
1	Qualified monitor is present.	Qualified monitor is present.
2	Set up cart for donning and doffing.	Set up cart for donning and doffing.
3	Remove personal effects (phone, keys, badges, pens, etc.).	Remove personal effects (phone, keys, badges, pens, etc.).
4	Put on inner gloves.	Put on inner gloves.
5	Secure belt snug around waist with clip facing up. Place excess belt into clip and loop.	Don clear inner boot liners over shoes and pants.
6	Secure the battery on the left side of the belt.	Secure belt snug around waist with clip facing up. Place excess belt into clip and loop.
7	Connect helmet to battery.	Secure the battery on the left side of the belt.
8	Check that 3 LED lights are green to ensure battery is fully charged.	Connect helmet to battery.
9	Adjust temple holder (top hole for larger head, 2nd hole works for most though).	Check that 3 LED lights are green to ensure battery is fully charged.
10	Put helmet on head and size to fit by turning ratchet knob to adjust the headband.	Adjust temple holder (top hole for larger head, 2nd hole works for most though).

Step Number	Original Donning Procedure	Updating Donning Procedure
11	Bend over to ensure helmet is tight enough to stay on without slipping.	Put helmet on head and size to fit by turning ratchet knob to adjust the headband.
12	Ensure long hair is in a low bun or ponytail is above shoulders.	Bend over to ensure helmet is tight enough to stay on without slipping.
13	Adjust fan speed to comfort.	Ensure long hair is in a low bun or ponytail is above shoulders.
14	Disconnect the battery.	Adjust fan speed to comfort.
15	Open the hood bag.	Disconnect the battery.
16	Set aside outer heavy loading filter.	Open the hood bag.
17	Orient the hood so markings face you and are in upward direction and flat edge is at top.	Set aside outer heavy loading filter.
18	Hold the upper corners and shake the hood until it fully unfolds.	Orient the hood so markings face you and are in upward direction and flat edge is at top.
19	Connect the center hole of the hood to the center hook on the front of the helmet. Once you are hooked, keep pushing until you hear a snap.	Hold the upper corners and shake the hood until it fully unfolds.
20	Connect the right and left sides of the hood to the helmet in the same way until you hear a snap.	Connect the center hole of the hood to the center hook on the front of the helmet. Once you are hooked, keep pushing until you hear a snap.

Step Number	Original Donning Procedure	Updating Donning Procedure
21	Grab the bottom of the hood and pull it back and over the helmet until it fits.	Connect the right and left sides of the hood to the helmet in the same way until you hear a snap.
22	Take the heavy loading filter and fit it fully over the top of the hood.	Grab the bottom of the hood and pull it back and over the helmet until it fits.
23	Set assembled PAPR hood aside.	Take the heavy loading filter and fit it fully over the top of the hood.
24	Put on coveralls outside room. Feet in first. Open-end faces your front. Do not zip up yet.	Set assembled PAPR hood aside.
25	Ensure proper mobility of arms and legs within coveralls.	Put on coveralls outside room. Feet in first. Open-end faces your front. Do not zip up yet.
26	Tape coverall and wrist of the gloves, forming a release tab at end of the loop.	Ensure proper mobility of arms and legs within coveralls.
27	Put on pair of extended cuff outer gloves.	Tape coverall and wrist of the gloves, forming a release tab at end of the loop.
28	Don booties.	Don booties.
29	Sanitize gloves and touched dispenser.	Sanitize gloves and touched dispenser.
30	Insert PAPR power cord connector into the battery.	Insert PAPR power cord connector into the battery.

Step Number	Original Donning Procedure	Updating Donning Procedure
31	Put the helmet on, letting the hood drape around your shoulders over the coveralls. Last chance to adjust the helmet.	Put the helmet on, letting the hood drape around your shoulders over the coveralls. Last chance to adjust the helmet.
32	Tuck the cord into your coverall.	Tuck the cord into your coverall.
33	Zip up the front of the coveralls.	Zip up the front of the coveralls.
34	Insert fingers into facial liner and tug it around your face until it tucks under your chin.	Insert fingers into facial liner and tug it around your face until it tucks under your chin.
35	Find both neck ties and bring them to the front and tie a shoelace knot close to neck.	Find both neck ties and bring them to the front and tie a shoelace knot close to neck.
36	Grab both torso ties off of back, bring them around and insert them through the front of the hood insertion holes, then tie into shoelace knot.	Grab both torso ties off of back, bring them around and insert them through the front of the hood insertion holes, then tie into shoelace knot.
37	Tear neck loop of apron.	Don gown.
38	Tie apron on around neck. Hood should be underneath apron.	Secure neck of gown, making sure neck tie of hood is covered.
39	Tie apron around waist.	Tie gown at waist in back.
40	Monitor completes 360° check of PP.	Put on pair of extended cuff outer gloves, securing gown sleeve inside of the extended cuff glove.
41	Sanitize gloves and touched dispenser.	Monitor completes 360° check of PP

Step Number	Original Donning Procedure	Updating Donning Procedure
42	Enter room. Do not enter room without proper fit of the PAPR system.	Sanitize gloves and touched dispenser.
43	Do not touch or re-adjust PAPR system inside the room.	Enter room. Do not enter room without proper fit of the PAPR system.
44		Do not touch or re-adjust PAPR system inside the room.

Supplementary Table 4. Doffing Stepwise Procedure

Steps written in bold font indicate updated steps in the new donning procedure.

Step Number	Original Doffing Procedure	Updating Doffing Procedure
1	Check that your partner outside of the room is aware you are preparing to doff.	Check that your partner outside of the room is aware you are preparing to doff.
2	Inspect PPE for obvious soiling or contamination. Have your partner inspect your back through the window on the door.	Inspect PPE for obvious soiling or contamination. Have your partner inspect your back through the window on the door.
3	Wipe away contamination with EPA-approved disinfectant wipes.	Wipe away contamination with EPA-approved disinfectant wipes.
4	Place a non-slip chuck pad in front of the door.	Place a non-slip chuck pad in front of the door.
5	Ensure that you have sanitizer and trash can within reach of pad.	Ensure that you have sanitizer and trash can within reach of pad.
6	Sanitize gloves and touched dispenser.	Sanitize gloves and touch dispenser.
7	Grab the apron under the arms at the base of each tie.	With one hand, reach up to back of helmet and remove heavy loading filter from top of PAPR hood, throw into trash.
8	Pull forward until back ties break.	Sanitize gloves and touched dispenser.
9	Pull apron down until neck ties break.	Gently pull the sleeves of the gown free from each outer glove cuff.

Step Number	Original Doffing Procedure	Updating Doffing Procedure
10	Bring your hands together until the apron folds vertically.	Sanitize gloves and touched dispenser.
11	Roll up while keeping arms extended.	Grasp gown at sides over waist tie, pull forward to break tie.
12	Discard apron into trash.	Cross your arms to grasp gown at upper arm/ shoulder, avoid touching P APR hood.
13	Sanitize gloves and touched dispenser.	Uncross your arms slowly, inverting the gown and extending your arms outward until they are outstretched. Keeping arms extended away from your body, bundle the gown and discard.
14	Choose one hand to remove one bootie. As you remove it, step with that foot onto pad. Throw bootie away.	Sanitize gloves and touched dispenser.
15	Use same hand to remove other bootie, if you can balance properly. Use CPR stand or tall trash can to aid in balance and step onto pad. Throw bootie away.	Choose one hand to remove one bootie. As you remove it, step with that foot onto pad. Throw bootie away.
16	Sanitize gloves and touched dispenser.	Use same hand to remove other bootie, if you can balance properly. Use CPR stand or tall trash can to aid in balance and step onto pad. Throw bootie away.

Step Number	Original Doffing Procedure	Updating Doffing Procedure
17	Remove outer gloves using beaking technique and throw away.	Sanitize gloves and touched dispenser.
18	Sanitize gloves and touched dispenser.	Remove outer gloves using beaking technique and throw away.
19	Remove the heavy loading filter into the trash can.	Sanitize gloves and touched dispenser.
20	Sanitize gloves and touched dispenser.	Untie the necktie of the PAPR hood, gathering it together, and discard.
21	Undo or break just the neck ties and throw into trash.	Sanitize gloves and touched dispenser.
22	Sanitize gloves and touched dispenser.	Grab torso ties of hood and undo or break those ties and throw into trash.
23	Grab torso ties of hood and undo or break those ties and throw into trash.	Sanitize gloves and touched dispenser.
24	Sanitize gloves and touched dispenser.	Remove tape from both wrists using tabs and throw into trash.
25	Remove tape from both wrists using tabs and throw into trash.	Sanitize gloves and touched dispenser.
26	Sanitize gloves and touched dispenser.	Zip down coveralls.
27	Zip down coveralls.	Grasp coveralls around lower back area and pull down.

Step Number	Original Doffing Procedure	Updating Doffing Procedure
28	Grasp coveralls around lower back area and pull down.	Remove coveralls from shoulders and pull down below knees, touching only inside to inside.
29	Remove coveralls from shoulders and pull down below knees, touching only inside to inside.	March and stomp out of the coveralls. Do not use your hands to remove.
30	March and stomp out of the coveralls. Do not use your hands to remove.	Step off and leave coverall for next person to pick up.
31	Step onto leg of coverall and slowly kick backwards to get each foot out.	Sanitize gloves and touched dispenser.
32	Step off and leave coverall for next person to pick up.	Observer opens door.
33	Sanitize gloves and touched dispenser.	Exit patient room.
34	Observer opens door.	Sanitize gloves and touched dispenser.
35	Exit patient room.	Place both hands under the PAPR hood at the shoulders. Grasp the back portion of the PAPR hood and gather the material by rolling it together, touching the inside only.
36	Sanitize gloves and touched dispenser.	Continue to roll the hood material up across the back and top of the helmet until you reach the top of the head, in line with the ears.

Step Number	Original Doffing Procedure	Updating Doffing Procedure
37	Grab shoulders of the hood, pull back, and lift over head.	Move fingers to the edge of the face shield and unsnap the hood and shield from the PAPR visor, folding the shield away from the PAPR.
38	Find edges of the visor and pop out the sides.	Do not touch your face.
39	Tilt head down and pull visor up and away from you and throw it away.	Sanitize gloves and touched dispenser.
40	Do not touch your face.	Remove inner gloves (beak method).
41	Sanitize gloves and touched dispenser.	Sanitize hands and touched dispenser.
42	Remove inner gloves (beak method).	Observer holds battery.
43	Sanitize hands and touched dispenser.	Observer unbuckles belt.
44	Observer holds battery.	Observer removes helmet motor from behind, avoiding the face.
45	Observer unbuckles belt.	Wash hands and arms thoroughly with soap and water.
46	Observer removes helmet motor from behind, avoiding the face.	Talk with your infection prevention team about showering protocols.
47	Wash hands and arms thoroughly with soap and water.	
48	Talk with your infection prevention team about showering protocols.	

Supplementary Table 5. PPE Ensemble and Purpose

Item	Ref Number	First/ Second/ Both Protocols	Purpose
Disposable Scrubs	Halyard, USA, Pants: 47790, 47791, 47792, 47793; Tops: 47786, 47787, 47788, 47789	Both	Disposal of potentially hazardous outer garments
Shoe Covers	MedLine, USA, #NON31859	Both	Prevent bodily fluids from contaminating shoes of HCP
Shoe Liners	ULine, USA, S-19250	Second	Facilitate easier removal of coveralls from shoes
Inner Gloves	Halyard, USA, GLV2304	First	Exam gloves, prevent contamination from spreading to hands of HCP
	Halyard, USA, #55095	Second	Long cuff gloves, provide additional protection to forearms of HCP

Item	Ref Number	First/ Second/ Both Protocols	Purpose
Outer Gloves	Halyard, USA #53141,	Second	Long cuff gloves, prevent contaminants from reaching inner cuff of coveralls
	Halyard, USA, 50602	First	Long cuff gloves, prevent contaminants from reaching inner cuff of coveralls
Tape	Grainger, USA #H6195	Both	Seal outer gloves to coveralls
Gown	Life Science Products, USA, #GO-633VPE,	Second	Provide complete coverage to outer layer of protection to patient-facing surfaces
Apron	Halyard, USA, #A7779	First	Provide a front outer layer of protection to patient-facing surfaces
Coveralls	International EnviroGuard, USA, W2501	Both	Complete body covering
PAPR Belt Pack	MaxAir, USA, Belt: 2000-76; Battery: 2500-36TSC Li-Ion Battery	Both	Hold PAPR battery to supply power to respirator

Item	Ref Number	First/ Second/ Both Protocols	Purpose
PAPR Helmet	MaxAir, USA, 2084-03 Helmet - Helmet, Liner, Power Cord	Both	Provide shape and mount for PAPR hood
PAPR Hood	MaxAir, USA, 2281PR- 100	Both	Prevent contamination to head and mucosal membranes of HCP
PAPR Heavy Loading Filter	MaxAir, USA, 2172-97	Both	Provide an additional filtration to PAPR